The Role of PAR2 in the Myeloid Compartment and the Regulation of Osteoclastogenesis

Sarah McGrath
BSc. (Hons)

Thesis submitted in fulfilment of the requirements for the degree of Doctor of Philosophy

College of Medical, Veterinary and Life Sciences

Institute of Infection, Immunity and Inflammation

University of Glasgow

October 2019

Abstract

Protease activated receptor 2 (PAR2) is one member of a family of G-protein coupled receptors. A defining feature of this family of receptors is their protease mediated activation. An emerging role for PAR2 in both the immune system and also in bone biology suggests a potential function for this receptor in osteoimmunology and its associated pathologies. Inflammatory arthritic conditions such as rheumatoid arthritis (RA), are pathologies that include both inflammation and bone destruction, making them a prime model for osteoimmunological studies. Previous murine studies identified that loss of PAR2 results in protection from inflammatory adjuvant-induced arthritis. These animals experienced an attenuated form of arthritis, with significantly reduced joint inflammation and damage. In addition, PAR2 is known to be upregulated in both macrophages (from tissue biopsies) and peripheral blood monocytes in patients with RA. However, the functional impact of protease signalling via PAR2 in monocytes in RA and how this receptor influences joint destruction via monocytes and their tissue differentials is still unknown.

The central aim of this doctoral study was to understand the function of PAR2 in monocytes and how protease signalling via PAR2 would influence the differentiation potential of these cells. Specific focus was placed on osteoclasts (OCs), and how protease signalling may further contribute to bone erosion through the action of PAR2 on these bone resorbing cells.

Initial work confirmed the expression of the PAR2 on the plasma membrane of monocytes, with the highest expression consistently found on classical monocytes that have the highest osteoclastogenic potential. In order to study the impact of PAR2 signalling on OC formation and activity, *in vitro* OC differentiation assays were set up using both WT and *par2*$^{-/-}$ cells. Both standard homeostatic and inflammatory TNF enhanced OC assays were utilised. These studies revealed that during homeostatic OC formation PAR2 contributed to the regulation of OC formation and prevented excessive fusion of precursors (OCPs) into giant cells. The PAR2 mediated regulation of OC formation was found to be important both via OCPs directly, and via the stromal compartment. An absence of PAR2 in osteoblast (OB) -like cells resulted in a more osteoclastogenic stroma and contributed to enhanced OC formation. However, during inflammatory-

driven OC formation, the role of PAR2 in osteoclastogenesis was reversed, and protease signals via PAR2 enhanced the formation of OCs. The observations made in murine *in vitro* systems were replicated in human cell cultures when monocytes were exposed to PAR2 inhibitors during the process of OC differentiation.

Combined, this work indicates that PAR2 has an impact on the process of osteoclastogenesis. Whether PAR2 signalling regulates or enhances OC formation is dependent upon the environment and the combination of signals received by precursor cells.

Table of Contents

List of Tables

List of Figures

Acknowledgements

First and foremost, I would like to thank my supervisors Carl Goodyear, John Lockhart, and Leif Hultin; your input and support throughout my PhD has been invaluable. As my primary supervisor special thanks goes to Carl, it has been your guidance through the last 4 years that has helped me to develop into the scientist I am now, and for that I am very grateful.

I would also like to thank (enormously) the past and present members of the Goodyear lab. I have made such great friends and been truly lucky to work amongst so many kind and helpful people. Tremendous thanks goes to Simone, Louise, and Aysin, you taught me everything I needed to know when I first started. Thanks to Lewis, Heather, Hussain, Shiny, Caitlin, Katy, Flavia, Kieran, and Lauren. At some point along the way you've all helped me out (on occasions saved me from a science crisis), and definitely assisted with some pints (Friday pub?)! Of course thanks goes to Cecilia, you introduced me to the world of osteoclasts and helped me get through my initial clueless-ness, thank you!

I would also like to thank all of those who helped me get through this PhD at the CMS – without your PAR2 knowledge I would have been lost. Carmen you are a bone genius, your input into my project was invaluable. Lynette, thank you for all of the hours you have helped me with protocols and animal models, you're the perfect teacher. And of course special thanks to Kendal! Thanks for all the help; from the crazy mice to writing our review. And of course even greater thanks for being such a brilliant travel partner (even when I dragged you to some questionable hostels).

Special thanks to Caroline, you've been the perfect room-mate, friend, and cousin. Thank you not only for reading my thesis but for being the best company to come home to from late nights in the lab! Chris, thank you for all of your support and your unbeatable ability to boost my confidence when the science was getting me down. Very special thanks goes to my mum and my sister Catherine. You have been my most vital support, without which I would never have gotten to where I am today.

I would like to dedicate this thesis to my dad, Jim McGrath.

Author's Declaration

I declare that this thesis is the result of my own work. No part of this thesis has been submitted for any other degree at The University of Glasgow, or any other institution.

Signature_____ Printed name Sarah McGrath

Abbreviations

AA	Ascorbic acid
ABD	Ascorbic acid, glycerol-2-phosphate, dexamethasone
ACPA	Anti-citrullinated peptide antibody
ACR	American College of Rheumatology
AF488	Alexa Fluor 488
AF647	Alexa Fluor 647
Akt	Protein Kinase B
ALP	Alkaline Phosphatase
ATP	Adenosine Tri-Phosphate
AZ	AstraZeneca
BM	Bone Marrow
BMP	Bone Morphogenetic Proteins
BMU	Basic Multicellular Unit
BSP	Bone Sialoprotein
BV	Brilliant violet
C3a	Complement Component 3a
Ca^{2+}	Calcium
CCL	C-C motif ligand
CCP	cyclic-citrullinated peptides
CCR	C-C motif receptor
CD	cluster differentiation
CDP	Common DC Progenitor
CIA	Collagen induced arthritis
cMoP	Committed Monocyte Progenitor
CMP	Common Myeloid Progenitors
CNS	central nervous system
COX	cyclooxygenase
CRP	C reactive protein
CSB	Cell Separation Buffer
Cthrc1	Collagen triple helix repeat containing 1
CXCL	C-X-C motif ligand
CXCR	C-X-C motif receptor
DAP12	DNAX-activating protein 12
DAPI	4', 6-diamidino-2-phenylindole
DAS	Disease activity score
DBA-1	Dilute Brown Non-Agouti 1
DC	Dendritic Cell
Dex	Dexamethasone

DMARD	Disease modifying anti-rheumatic drug
DMEM	Dulbeccos Modified Eagle Medium
DNA	Deoxyribonucleic acid
EMP	Embryonic Erythron-myeloid Progenitor
ERK	Extracellular signal-regulated kinase
ESR	erythrocyte sedimentation rate
F2RL1	FR2 like Trypsin Receptor 1
FACS	Fluorescence-activated cell sorting
FADD	Fas associated death domain
FBS	Foetal Bovine Serum
FCA	Freunds Complete Adjuvant
FcRγ	Fc receptor common γ subunit
FGF	Fibroblast Growth Factor
FITC	Fluorescein isothiocyanate
FLS	Fibroblast-like Synoviocytes
FRET	Forster resonance energy transfer
FSC	Forward scatter
FZD	Frizzled
g	Grams
Gab2	Grb2-associated binder 2
GAPDH	Glyceraldehyde 3-phosphate dehydrogenase
GDP	Guanosine diphosphate
GFP	Green Fluorescent Protein
GLI	Glioma-associated Oncogene
GM-CSF	Granulocyte macrophage colony stimulating factor
GMP	Granulocyte Macrophage Progenitors
GPCR	G-protein Coupled Receptor
GTP	Guanosine triphosphate
GWAS	Genome Wide Association Studies
h	Human
HCl	Hydrochloric Acid
hi	high
HLA-DR	Human leukocyte antigen - DR isotype
HRP	Horseradish Peroxidase
HSC	Hematopoietic Stem Cell
HUVECs	Human Umbilical Vien Endothelial Cells
ICAM-1	Intracellular adhesion molecule 1
IF	Immuno-fluorescence
IFN-γ	Interferon gamma
IHC	Immuno histo chemistry
IHH	Indian Hedgehog
IKK	I kappa B Kinase

IL	Interleukin
ITAM	Immunoreceptor tyrosine-based activation motif
JIA	Jouvinile Idiopathic Arthritis
JNK	c-Jun N-terminal kinase
Kb	Kilobase
kDa	killo dalton
KO	Knock out
LBP	LPS binding protein
lo	low
LPS	Lippopolysaccharides
M	Molar
m	Murine
M alone	M-CSF
M-CSF	Macrophage - colony stimulating factor
MAPK	Mitogen-activated protein kinases
MDP	Monocyte/Macrophage Dendritic Cell Progenitors
MFI	Mean Fluorescence Intensity
MITF	Microphthalmia-associated Transcription Factor
MPS	Mononuclear Phagocyte System
MR	M-CSF + RANKL
mRNA	messenger RNA
MRT	M-CSF + RANKL + TNF
MSC	Mesenchymal Stem Cells
MTX	Methotrexate
MyD88	Myeloid differentiation primary response 88
n	Nano
NA	Non-adherent
NA-BM	Non-adherent bone marrow cells
NFATc1	Nuclear Factor for Activated T cells c1
NFkB	nuclear factor kappa B
NSAIDs	Non-steroidal Anti-inflammatory Drugs
OA	Osteoarthritis
OB	Osteoblast
OC	Osteoclast
OCP	Osteoclast precursors
OPG	Osteoprotegrin
OSCAR	Osteoclast -associated Receptor
OSP	Osteopontin
OSX	Osterix
PAR	Protease Activated Receptor

PB	Peripheral Blood
PBMC	Peripheral Blood Mononuclear cells
PBS	Phosphate Buffered Saline
PBST	Phosphate Buffered Saline 1% Tween
PCR	Polymerase Chain Reaction
PE	Phycoerythrin
PGE	Prostaglandin E2
PI3K	Phosphoinositide 3 Kinase
PIP2	phosphatidylinositol 4,5-bisphosphate
PKC	Protein Kinase C
PLC	Phospholipase C
PMA	phorbol 12-myristate 13-acetate
PTCH1	Patched Homologue 1
PTH	Parathyroid Hormone
PTHrP	Parathyroid Hormone-related Protein
PV	Porstaglandin E2, and 1α,25-Dihydroxyvitamin D3
PVDF	Polyvinylidene difluoride
RA	Rheumatoid Arthritis
RANK	Receptor activator of nuclear factor kappa-B
RANKL	Receptor activator of nuclear factor kappa-B ligand
RF	Rheumatoid Factor
RIPA	Radioimmunoprecipitation assay buffer
RNA	Ribonucleic acid
ROS	Reactive oxygen species
ROX	Reactive oxygen species
RPMI	Roswell Park Memorial Institute
RUNx2	Runt-related Transcription Factor – 2
S1P	Sphingosine 1-phosphate
SH2	Src homology 2
SMO	Smoothened
SNBTS	Scottish National Blood Transfusion Service
SSC	Side scatter
SYK	Spleen Tyrosine Kinase
TACE	TNF-a convertase
TGF-ß	Transforming Growth Factor-beta
Th	T helper cell
TLR4	Toll-like receptor 4
TNF	Tumour Necrosis Factor
TNFR	Tumour Necrosis Factor Receptor
TRADD	TNFR1-associated death domain protein
TRAF	TNF Receptor Associated Factor
TRAP	Tartrate-resistant acid phosphatase
Tregs	Regulatory T cells

UK	United Kingdom
VitD	1α,25-Dihydroxyvitamin D3
Wnt	Wingless-related Integration Site
WT	Wildtype
βGP	glycerol-2-phosphate

1 Introduction

1.1 The Myeloid Compartment

1.1.1 The Myeloid Lineage and Monocyte Development

The myeloid compartment is comprised of cells of the innate immune system including monocytes, dendritic cells (DCs), granulocytes (such as neutrophils), erythrocytes, and platelets. After physical boundaries such as the skin, innate immune cells are the first line of defence against pathogens, and this system is responsible for initiating adaptive immune responses against invaders. In addition, the cells of the innate immune system maintain homeostasis, and aid in tissue healing. Monocytes are a primary cell of the myeloid system, found circulating in the peripheral blood (PB). These cells migrate into tissues when called upon, during states of inflammatory or infectious stress[1]. While DCs, another staple of the myeloid system, are located in tissue sites, gathering antigen in order to migrate and present it to adaptive immune cells (T cells) in secondary lymphoid organs. Together the myeloid lineage components, monocytes, DCs, and macrophages, form the mononuclear phagocyte system (MPS).

Traditional dogma of the MPS proposed that monocytes were PB circulating precursors of tissue macrophages, which when required enter into the tissue and replenish the macrophage population, or supply macrophages to sites of infection or inflammation[2]. However, recent developments in our understanding of the MPS have indicated that this traditional dogma does not accurately represent the development of the myeloid system. It is now appreciated that a pool of resident macrophages exist within the tissue which arise from the embryonic yolk-sac[3] and the neonatal liver[4]; these cells are self-renewing, lasting throughout life and replenish themselves through local proliferation, independent of adult haematopoiesis[5,6]. These cells are not derived from bone marrow (BM) residing hematopoietic stem cells (HSCs) but instead arise from an embryonic erythron-myeloid progenitor (EMP)[3]. Resident macrophages maintain homeostasis within the tissue, primarily phagocytosing apoptotic cells[7]. Each tissue environment drives a “differentiation” of resident macrophages, to develop tissue specialised functions, for example microglia of the brain have

very different functions from Langerhans cells of the skin, in order to maintain tissues appropriately[8]. Their life span can be variable dependent on the tissue in which they reside, with monocytes replenishing macrophage populations more frequently in some tissues, such as the gut, and very rarely in others such as the brain[9]. Monocytes do enter the tissue sites, especially during inflammation and infection, where they develop phagocytic functions, as well as driving the immune response and promoting further infiltration of innate immune cells. However, the phagocytes originating from monocytes are recognised to be a different cell, in both phenotype, and ontogeny, from tissue macrophages. In addition, DCs arise from an independent PB progenitor, not from monocytes as was previously proposed. These cells are independent of the monocyte compartment in both phenotype and function. In order to take into account this new appreciation of the development of the MPS a new nomenclature was proposed by Guilliams et al, which was based primarily on the ontogeny (where the cellular pre-cursor originates) and then cellular function[10]. In brief, all mononuclear phagocytes within the tissue that originate from the embryonic foetal liver are termed macrophages. DCs originate from the BM, and differentiate into subsets of conventional DCs, and plasmacytoid DCs from the common DC progenitor (CDP). These cells have a more stellate morphology and are primarily responsible from presenting antigen to adaptive immune cells such as T cells. Finally, monocytes are classified separately; these cells originate from the BM, but not the CDP, and primarily circulate in PB until they receive signals to enter into the tissue where they can develop pro-inflammatory and phagocytic functions. Their tissue state is termed monocyte-derived cell, in order to differentiate these cells from resident macrophages.

Unlike resident self-renewing innate immune cells such as resident macrophages, monocytes are short-lived. These cells are only maintained within the PB for 1-6 days. Consequently, monocytes are regularly replenished from pluripotent, self-renewing HSCs located within the BM niche throughout adult hemopoieses. HSCs are the quintessential stem cell for the generation of all immune cells; self-renewing but also differentiating into multipotent progenitors for both the lymphoid and myeloid lineage of the immune system. For the purposes of this thesis the myeloid lineage, specifically monocytes and osteoclast precursors

(OCPs) will be the focus. OCPs also originate from myeloid BM precursors, this will be discussed in a subsequent section (1.2.1)

The pioneering transcription factor and master regulator that drives HSC differentiation towards a myeloid route, and development into the Common Myeloid Precursor (CMP) is PU.1. This factor is so essential in the development of the myeloid system, that PU.1 null mice have no detectable monocytes or macrophages, while retaining T and B cell development, and delayed neutrophil development[11]. Successive commitment continues from the CMP, into granulocyte/macrophage committed progenitor (GMP), which can give rise to both granulocytes and myeloid progenitors. From GMP these can further differentiate into macrophage/DC progenitors (MDPs)[12]. MDPs maintain self-renewing capabilities and are retained within the BM, largely via CXCL12 – CXCR4 chemokine interactions. Recent research has identified a subsequent progenitor commitment stage derived from MDPs, which commits these cells to a monocyte lineage, without the capability of generating DCs. This subsequent progenitor stage is known as the committed monocyte progenitor (cMoP)[13]. Monocytes differentiate from this progenitor, and egress the BM into the peripheral blood upon requirement, mediated by chemokine receptor CCR2 signals[14]. Monocyte development within the BM and into the PB is shown in Figure 1.1.

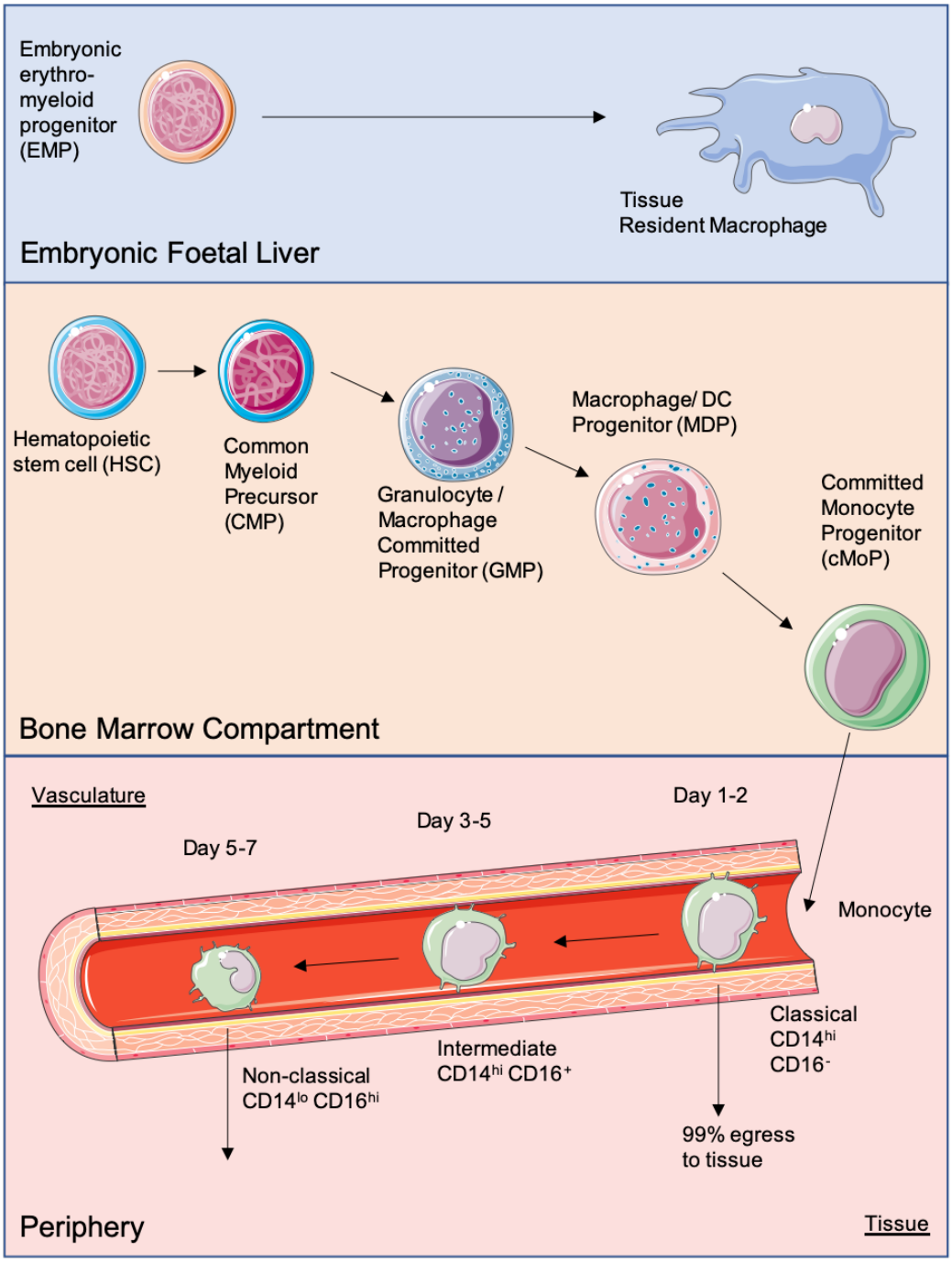

Figure 1.1 Monocyte Development and Maturation
Tissue resident macrophages appear developmentally prior to the establishment of the hematopoietic BM niche. These cells derive from the EMP in the embryonic yolk sac, or foetal liver. These phagocytes are self-renewing and maintain themselves within the tissue. While PB monocytes derive from HSCs in the BM. To begin differentiation to a myeloid lineage HSCs become the common myeloid progenitor (CMP). From this point they further differentiate into GMPs which have the capacity to develop into granulocytes, monocytes, or DCs. To further the differentiation process to monocytes these GMPs specialise to MDPs which can no longer become granulocytes. MDPs then loose the capacity to develop into DC and commit to a monocyte lineage through differentiation into the cMoP. This maturation process all takes place in the BM. Monocytes then derive from cMoPs and migrate into the PB. The first stage of blood monocytes is the classical stage where monocytes express high levels of the surface TLR4 co-receptor CD14, and lack expression of CD16. Most of these cells egress the blood into tissue to respond to infection, inflammation, or to support the resident macrophage populations. Classical monocytes which do not leave the blood within 2 days then develop into intermediate monocytes, where they express both CD14 and CD16. This stage lasts 1-3 days before the final maturation step of blood monocytes into non-classical $CD14^{-}$ $CD16^{hi}$ cells. These are known as luminal patrollers.

1.1.2 Monocyte Heterogeneity

Monocytes do not exist as a homogenous population, instead upon leaving the BM for the PB they further mature into subsets that are morphologically and functionally distinct. Differential surface expression markers are gained, which delineate monocytes with diverse functional capabilities. Human monocytes were initially identified through their expression of the Toll like receptor 4 (TLR4) co-receptor known as CD14. These can be further subdivided based on expression levels of FcγRIII, also known as CD16[15]. Monocytes with high CD14 expression and low/no CD16 expression are termed "classical" monocytes ($CD14^{hi}CD16^{lo}$), which make up around 90% of the PB human monocyte populations. While CD14 low, CD16 high expressing monocytes are termed "non-classical" ($CD14^{lo}CD16^{hi}$) and only make up around 5-10% of the PB monocytes. In addition to the classical and non-classical subsets, intermediate monocytes express both CD14 and CD16 ($CD14^{+}CD16^{+}$)[16], this is summarised in Figure 1.1.

Further differentiation of these subsets can be made based on chemokine receptor expression[17], with classical monocytes expressing high levels of CCR2, which decreases in intermediates and decreases further in non-classical monocytes. Non-classical monocytes express high levels of CX_3CR1 chemokine receptor, compared to lower expression in classical monocytes[17]. The ligand for CCR2, CCL2 plays a crucial role in monocyte recruitment. $CCL2^{-/-}$ mice have normal levels of resident macrophages but completely lack monocyte-derived tissue phagocytes[18]. These mice are also less capable of fighting bacterial infection, demonstrating the requirement for classical monocyte-derived tissue phagocytes in anti-bacterial defence[19,20]. While loss of CX_3CR1 chemokine receptor and its ligand CX_3CL1 in murine models shows a specific loss of non-classical monocytes in the PB[21].

The classical and intermediate populations of monocytes are largely considered to possess pro-inflammatory functions, and these cells infiltrate into sites of inflammation or infection within the tissue[22,23], whereas non-classical monocytes are recognised to have an alternate functional role (Fully reviewed in [24]). These cells adopt a luminal patrolling phenotype, whereby they monitor and maintain vascular homeostasis[25]. Non-classical monocytes do not contribute to an inflammatory state within the tissue like their classical counterparts, and are

instead thought to play a more immune-regulatory role. Using a new method of *in vivo* deuterium cell labelling in human subjects, Simon Yona and colleagues identified that human monocyte subsets exist in a continuum. Upon release from the BM all monocytes are in a classical monocyte state, and around 99% of these cells migrate into tissue after 1 day of PB migration. The monocytes that are maintained within the PB after 1 day mature into intermediate monocytes ($CD14^+$ $CD16^+$). All of these intermediate monocytes then begin to mature again after 2 days into non-classical, luminal patrolling monocytes, which survive in the circulation for a further 3-4 days[26].

This heterogeneity is reflected in the murine system, where classical and non-classical monocytes are also represented. The CD14 and CD16 markers from the human system however, do not hold true in the murine system. Chemokine receptors CCR2 and CX_3CR1 are maintained in this species. Similar to the human system classical monocytes express both CCR2 and CX_3CR1 and are able to migrate by either CCL2 or CX_3CL1 chemokine drivers. “Non-classical” monocytes do not express CCR2 and have higher expression of CX_3CR1, making them dependent on CX_3CL1 for survival and migration. In addition to differential expression of chemokine receptors, these subsets can also be defined by their expression of Ly6C, a membrane protein with unknown function. Classical murine monocytes express high levels of Ly6C on their surface while non-classical cells are $Ly6C^{lo}$ [27].

This standard identification of monocyte subsets based on surface markers is now recognised as a potentially simplified model. Advancements in technology have enabled single cell sequencing analysis of blood myeloid cells to identify differences within this population using non-bias analysis. Notably, studies utilising this technology have identified that there is heterogeneity within currently defined monocyte populations[28]. This new data has demonstrated that monocytes can be clustered into 4 populations, and highlighted that the intermediate population may be more heterogeneous than previously appreciated[29].

1.2 Osteoimmunology

Osteoimmunology is the interdisciplinary research field studying the interactions between the immune and skeletal systems. Initial observations that the immune system influenced the function of skeletal cells were first made over 40 years ago, when supernatant isolated from activated peripheral blood mononuclear cells (PBMCs) was shown to increase bone resorption in explant cultures[30].

This marriage of 2 specialties coined the new interdisciplinary field of "osteoimmunology", a term first proposed in 2000[31]. An understanding of each system is required to interrogate the complex crosstalk between these organs and thus, appreciation of the field as a whole. Overlap of both disciplines is evident in their shared cellular ontogeny; shared transcription factors, driving both immune and bone cell development and action; and finally shared ability to respond to immune mediators. A striking example of the interaction of these fields is observed in pathologies relating to either system. Chronic immune pathologies that have symptoms of severe bone erosion include chronic inflammatory diseases such as inflammatory arthritis, periodontal disease[32,33], or leukemic malignancies such as multiple myeloma[34]. This further emphasises how dysregulation of one system can substantially impact the other.

The cellular ontogeny of the bone resorbing osteoclast (OC) is a major bridge between these disciplines. OCs are derived from the hematopoietic lineage and precursors of myeloid/monocytic cells. The hematopoietic origin of these cells was initially recognised through the use of parabiosis[35] and BM chimeras[36,37], which rescued the osteopetrotic phenotype of grey lethal (*gl*/*gl*) mice with WT infusion. Further definition of the OC precursors (OCPs) as cells of myeloid origin was then made in the 1980s, where *in vivo* transfer of thymidine labelled monocytes were traced to OCs[38], with further conformation through observation of monocyte fusion into OCs *in vitro* [39]. In addition, mutation of the M-CSF gene results in abnormal formation of both macrophages and OCs, indicating these cells are closely linked and dependent on this growth factor[40]. Overall, the shared precursor of both monocyte-derived phagocytes and bone resorbing OCs intimately links the bone and immune systems. Alterations to monocyte migration, and activity, can and does have an impact on OC formation.

In addition to bone cell development from the immune system, interaction between bona fide immune cells such as T cells and macrophages, and OCs, OCPs, and stromal bone compartments such as osteoblasts (OBs), also has an impact on bone formation and resorption. Activated T cells are a key immune cell known to promote the development and activity of OCs[41]. Activation of T cells drives the upregulation of receptor activator of nuclear factor κ-B ligand (RANKL) [42,43], an essential driver of OC formation [44,45]. In addition cytokines from activated T cells and macrophages such as TNF[46], IL-6[47], and IL-17[48] are known drivers of OCP fusion to OCs. While alternate cytokines of an immune source can regulate OC development and inhibit OC formation such as IFN-γ[49], IL-4[50], IL-10[51], or IL-12[52]. Depending upon the type of immune response that is mounted, bone resorption can be promoted or controlled. Cytokines with known capabilities to drive OC formation such as TNF and IL-6 [53], are also highly expressed in erosive inflammatory arthritic conditions. In addition to driving excessive OC formation, or regulating OC differentiation, cytokines can also control bone formation through direct action on OB stromal cells. TNF inhibits the development and activity of OB cells; suppressing bone formation and thus promoting further bone erosive pathology[54].

Development of the skeleton precedes immune system maturation, as the skeleton creates the space to host haemopoietic stem cells (HSCs). HSCs give rise to cells of the immune system and reside in the bone marrow (BM) compartment. Providing an appropriate niche for HSCs and immune precursors is an essential function of the skeleton, and thus normal bone development is required for normal immune development. OC activity is essential to carve out the space for niches that are essential for BM development[55]. OBs are also a key producers of survival factors such as BMPs which maintain HSCs [56].In addition, RANKL, which drives OC formation, is an essential driver of secondary lymphoid organ development and thus crucial for immune cell development [45,57].

Overall these systems are intimately linked, both during developmental stages and throughout life in homeostasis and maintenance of these organs. Perturbation of one system leads to disturbance within the other. Therefore, an understanding of both of these systems is essential in treating conditions such as

RA, whereby both immune overactivity and bone erosion drive pathology and tissue destruction.

1.2.1 Osteoclast Precursors

Osteoclasts have been confirmed as a terminal differentiation point for myeloid/monocyte cells since the publication of work conducted by Tinkler and colleagues (discussed above, 1.2). This understanding came in 1981[38], however the exact precursor cells of OCs within the myeloid lineage has been somewhat elusive. Despite ongoing research in this field, multiple suggestions and possibilities have been proposed. Whether OC have a specific precursor that is divergent from that of the tissue monocyte-derived phagocytes has been a subject of research for the last 20 years. Studies conducted in murine systems have provided the wealth of our understanding in this field and proposed specific monocyte populations that could contribute to the OC pool.

Flow cytometric and FACS techniques were employed to identify a population of myeloid cells with a high osteoclastogenic potential *in vitro* and *in vivo* from murine BM. In brief, myeloid cells from the murine BM, identified as CD115+ and thus M-CSF responsive, were further subdivided based on expression levels of other myeloid associated markers, such as Ly6C, CD11b, CD117 (c-kit), and chemokine receptors CCR2, and CX_3CR1. Collectively these studies identified that while multiple populations of myeloid cells had limited OC differentiation potential, $Ly6C^{hi}CD11b^{lo}CD117^{+}CD115^{+}CX3CR1^{hi}Ly6G^{-}$ cells had the highest OC differentiation capacity[58-60]. The OCPs defined here differ from circulating monocytes in their expression of CD11b. Monocytes express high levels of this integrin subunit and it contributes to multiple fundamental functions of this cell type such as migration, and phagocytosis[61]. The requirement for a lack of this integrin is confirmed by the negative regulation of CD11b-β2 integrin heterodimer signalling in OC differentiation[62]. However, aside from CD11b the OCPs do share many of the cell surface markers of monocytes, such as Ly6C and chemokine receptors, therefore lack of CD11b is one method of identifying these cells from the alternative monocyte populations. OCPs also maintain the capacity to differentiate in phagocytic “macrophage” or “DC” like cells dependent on the stimuli and growth factors provided, indicating plasticity of this precursor. As well as osteoclastogenic tendencies, subsequent studies

identified that this population of monocytic BM OCP cells had myeloid suppressor functions including suppression of T cell expansion [63]. This subset of BM myeloid cells was expanded in the BM during active disease in inflammatory models of arthritis[63]. The authors of this study propose that while the OCP population identified with the above mentioned Ly6C^{hi} CD11b^{lo} phenotype confer both OCP and myeloid suppressor capabilities, this population may still be mixed and whether single cells have the plasticity to develop into both OCs or monocyte-derived suppressor cells is still unknown. A single cell analysis approach may provide more insight into this question.

Recently studies investigating the origin of the OC have taken a systematic approach, utilising multiple reporter mice, with various cell transfer models and imaging techniques, in order to follow OC formation from foetal development of the skeleton, to bone maintenance in adulthood [64]. A conditional knock out of *csf1r* (CD115 gene), and *tnfrsf11a* (RANKL gene) in the hematopoietic lineage resulted in normal skeletal development, with normal OC numbers, successful tooth eruption, and BM cavity formation at birth and throughout early life. However, these rodents began to lose OCs over time, developing increased bone density and a loss of the BM cavity which became observable at 16 weeks and continued to deteriorate to 22 weeks. This was the first indication that OC formation during developmental stages was not dependent on cells of BM hematopoietic origin, while simultaneously demonstrating that myeloid cells of the BM were necessary for the maintenance of the OC compartment in adulthood. This observation has similarities with macrophage development and maintenance, discussed above (1.1.1). The authors further explored this phenomenon using alternate conditional knock out animals which would provide a CD115 knock out primarily in EMPs over HSCs (tnfrsf11a^{cre};csf1r$^{fl/fl}$). These animals failed to develop a normal skeleton, which supported the hypothesis that OC formation during skeletal development in foetal and early life stages was dependent upon embryonic macrophage precursors, EMPs.

This study provides a whole new perspective on OC development which appears to closely mirror macrophage development. The authors of this continued using fluorescent reporter mice to show that OCs formed during development are long lived, but also fuse with HSC derived precursors of the monocyte lineage to

support their maintenance over time. Overall, from this study it can be determined that like macrophages, OC are dependent upon EMPs for early development and OC formation, but throughout life maintenance of the bone and OC differentiation becomes increasingly dependent upon monocyte-derived precursors. These HSC derived adult pre-cursors are likely those identified previously with $Ly6C^{hi}CD11b^{-}$ surface identification. This thesis will focus on later stage, hematopoietic, myeloid-dependent osteoclastogenesis, and the development of these cells in both health and disease states.

Identification of OCPs as circulating in the PB, prior to migration to the bone, as well as the dependence on chemokine receptors for osteoclast formation, demonstrates the requirement of OCP migration for OC differentiation. In addition, one of the first observations that led to the hypothesis that OC were of hematopoietic origin was their motile appearance[65,66]. Collectively these initial observations of OCP phenotype, location, origin and surface markers support the possibility that these cells are reliant upon appropriate and controlled migration to direct their differentiation into OCs. Despite the origin of adult OCPs within the BM compartment, where the requirement for OC is largely located, these cells appear to first circulate in the PB before returning to the bone and BM area for local OC differentiation. Evidence of circulating OCPs first came from observations that cells from the PB could be differentiated into OCs [67-69]. OCP leave the BM and enter the PB via a sphigosine-1-phosphate (S1P) mediated mechanism[70,71]. The exact trafficking of OCPs after they have left the BM (and if all precursors leave the BM environment) is still unknown. However, the lack of OC present in CCR2 and CX_3CR1 KO rodents indicates that OCPs are actively trafficked to the bone site for differentiation.

Advancement in murine systems has given us a clear insight to the cellular origins of OCs. The technologies that can be applied to murine *in vivo* systems such as genetic knock out, and monitoring of labelled cell trafficking etc, cannot be applied to human *in vivo* systems. For this reason, the exact profile of human OCPs are still elusive. Circulating human monocytes isolated from PB have established *in vitro* OC differentiation potential in co-culture with osteoblastic cell lines [72], with $CD14^{+}$ monocytes identified as a possible OCP[73]. All subsets of human monocytes (classical, intermediate and non-classical) have OC

differentiation potential. However, the response to some OC enhancing factors can differ between subsets, indicating that the route to OC differentiation and the resulting OC generated from different monocyte precursors are slightly different[74]. Human *in vitro* OC assays still regularly use total PBMC populations or isolated $CD14^+$ monocytes.

Murine *in vitro* assays for experimental investigation of OC consistently use cells isolated from the BM of the long bones. Aside from this one consistency, these assays vary greatly in how they are conducted. Some studies utilise the whole BM to generate OC[75], which includes hematopoietic stem cells, matured immune cells, and mature/precursor stromal cells. Using this mixed culture system, cells of the stromal compartment can be stimulated to become OC driving cells, or OCPs can be directly stimulated using M-CSF and RANKL stimulation. Alternatively, total BM can be incubated overnight and non-adherent cells removed for further differentiation into OC[76-79]. This method aims to limit the stromal contribution to the culture, leaving behind the adherent stromal cells. Even within this method there is variation in how OC differentiation is conducted between studies. The length of M-CSF stimulation varies with some studies first differentiating cells into a "macrophage-like" phenotype and then stimulating with RANKL to drive OC formation[76,77]. While other studies use short M-CSF stimulation (24 hours) to drive RANK expression and then stimulate with RANKL immediately after this pre-incubation[78]. Overall, methods of murine BM OC cultures have large levels of variation throughout the literature, making comparison between *in vitro* OC studies difficult. A standardised approach to murine *in vitro* osteoclastogenesis cultures is urgently required. In contrast, human OC cultures have less variation, with most studies isolating $CD14^+$ monocytes from peripheral blood and culturing in M-CSF and RANKL, with variation largely in concentrations of growth factors and duration of cell culture[80]. Some studies still utilise whole PBMC populations, and these mixed cultures will be influenced by the presence of other cell types[80].

1.2.2 Osteoclast Differentiation

The process of mononuclear OCP differentiating into mature OC is termed osteoclastogenesis. The process of multinucleated OC formation is multistep requiring; 1) the recruitment of OCPs, 2) attraction and migration of these cells

to the bone surface where they can interact with bone lining stromal cells, 3) induction of OC-associated genes in mononuclear cells, and finally, 4) fusion of pre-OCs to multinucleated OC. Multinucleated OC have traditionally been identified via histological staining of Tartrate-resistant acid phosphatase (TRAP) enzyme, a marker of OCs[81]. Resorbing bone results in the release of chemotactic factors, primarily from active OCs and OBs, which is thought to drive migration of peripheral OCP to sites of bone remodelling[82]. Upon arrival at the active bone sites, OCPs come into contact with stromal OB bone lining cells. From *in vitro* co-culture assays it was established in 1988 that OB and OC interaction was required for OC formation[83]. Various signals are supplied from stromal OB cells to co-ordinate the induction of OC-associated transcription factors and gene expression. The transcription of these genes into functional proteins, along with active adhesion and migration of OCPs and pre-OCs, enables the fusion of mononuclear myeloid precursors into catabolically active syncytia.

Two essential factors for the process of osteoclastogenesis have been identified; M-CSF and RANKL. While other cytokines and soluble mediators can influence the process (as mentioned above in section 1.2), these factors cannot drive the process alone. The presence of M-CSF and RANKL is always required for this differentiation process.

Commitment to the myeloid lineage (discussed in section 1.1.1) is the first step in the differentiation process of hematopoietic OC differentiation. The commitment to this lineage through the expression and action of transcription factor PU.1 enables these precursors to be responsive to M-CSF via CD115. Mice lacking M-CSF (*op/op* mice) have an extreme osteopetrotic phenotype, as the result of complete failure to differentiate OCs (both EMP and BM origin) [40]. M-CSF is a vital survival signal for precursor cells and the first essential signal to further differentiate OCP[84]. M-CSF signalling via CD115 initiates expression of microphthalmia-associated transcription factor (MITF). In conjunction with PU.1, MITF initiates the transcription of RANK, the surface receptor responsive to RANKL.

1.2.2.1 M-CSF

M-CSF is a soluble growth factor essential for the proliferation and survival of myeloid precursors, monocytes and macrophages. Its only receptor is known by a variety of nomenclatures such as CSF-1, c-FMS, and CD115[85]. It is one member of a large family of tyrosine kinase receptors. Upon engagement with M-CSF these receptors dimerise and self-phosphorylate[86]. The phosphorylated elements of the C terminal of this receptor act as binding sites for SH2 domain containing proteins and amplify the signal[87]. CD115 signals via 2 primary pathways; activation of the mitogen-activated protein (MAP) kinase pathway, specifically extracellular signal regulated kinase (ERK) [88], and activation of the phosphoinositide 3 kinase (PI3K) Akt pathway[89]. Collectively these signals promote proliferation by driving entry into the cell cycle via expression of D cyclins[90]. In addition to survival and proliferation signals M-CSF also drives the expression of RANK making them responsive to RANKL [60].

1.2.2.2 RANKL

RANKL is a type II membrane protein of the tumour necrosis factor (TNF) family. It is commonly expressed within the bone on the surface of stromal OB cells, and can be induced in inflammatory environments to be expressed on immune cells. RANKL can be shed from the cell surface via proteolytic cleavage mediated by TNF convertase (TACE) [91]. The receptor for this ligand is RANK, a type I membrane protein expressed by OCs and their precursors in response to M-CSF. RANKL – RANK interactions are indispensable for OC differentiation, as demonstrated by *rank*$^{-/-}$ murine models that experience severe osteopetrosis attributed to a lack of OCs[45]. Both transmembrane and soluble forms of RANKL contribute to homeostatic OC formation[92].

RANK – RANKL interaction results in receptor trimerization, which initiates activation and recruitment of signalling adaptor proteins. TNF receptor associated factor (TRAF) 6 binds the intracellular portion of RANK upon activation and mediates OC associated RANK signalling [45,93]. This is not the only mediator to associate with active RANK, Grb2-associated binder 2 (Gab2) is a scaffold signalling adaptor protein that also mediates RANKL signalling[94]. Multiple signalling cascades are initiated by active RANK; which in turn

orchestrate a selection of nuclear transcription factors to drive OC formation. These signalling cascades include; both canonical and non-canonical NFκB activation and translocation to the nucleus, activation of AP-1 transcription factor via c-Jun N terminal kinase 1 (JNK1), activation of the Src pathway, and MAPKinase activation of p38 pathway driving MITF transcription factor and ERK1/2 (Reviewed further in [95]).

The master transcription factor responsible for OC differentiation was identified as Nuclear Factor for activated T cells c1 (NFATc1) [96]. This transcription factor is induced early in OC differentiation and is driven by RANK mediated calcium signalling and NFκB activity. In addition, NFATc1 can drive its own expression post induction, in a process known as auto-amplification[97]. NFATc1 trans-locates into the nucleus where alongside other OC associated transcription factors; PU.1, MITF, and Fos, it binds promotor regions of osteoclast-associated genes, promoting their transcription. This includes *ctsk* (Cathepsin K), *acp5* (Tartrate-resistant acid phosphatase – TRAP), *dcst* (Dendritic cell-specific transmembrane domain – DC-STAMP), *Oscar* (Osteoclast-associated receptor), and β3 integrins[98-100].

Regulation and inhibition of the RANK-RANKL interaction is mediated by RANKL decoy receptor osteoprotegerin (OPG)[101]. This decoy receptor binds any free RANKL and prevents binding to RANK on OCP surface in order to control/inhibit further OC differentiation and activation.

1.2.2.3 ITAM Signals

The role of ITAM signalling is essential, in concert with RANKL signalling cascades, to induce osteoclastogenesis. This signalling transduction from phosphorylated ITAMs activates phospholipaseCγ (PLCγ), releasing calcium (Ca^{2+}) into the cytoplasm and providing the necessary Ca^{2+} signal for NFATc1 induction (an essential osteoclast transcription factor). Two immune cell associated membrane adaptors have been shown to be involved in this process: Fc receptor common γ subunit (FcRγ) and DNAX-activating protein 12 (DAP12) [102]. $FcR\gamma^{-/-}$ $DAP12^{-/-}$ mice have been shown to exhibit severe osteopetrosis due to a lack of osteoclasts, demonstrating that M-CSF and RANKL signalling alone is not sufficient for osteoclastogenesis[102]. Osteoclast associated receptor (OSCAR), is a

relatively novel leukocyte receptor present on pre-osteoclasts, and mediate Ca^{2+} signalling via FcRγ, through binding to its collagen ligand[103]. This receptor can rescue the osteopetrotic phenotype of $DAP12^{-/-}$ mice, and thus can contribute the required Ca^{2+} signal to mediate osteoclastogenesis[103]. The collective signals required for osteoclast differentiation and OC associated gene transcription are shown in Figure 1.2.

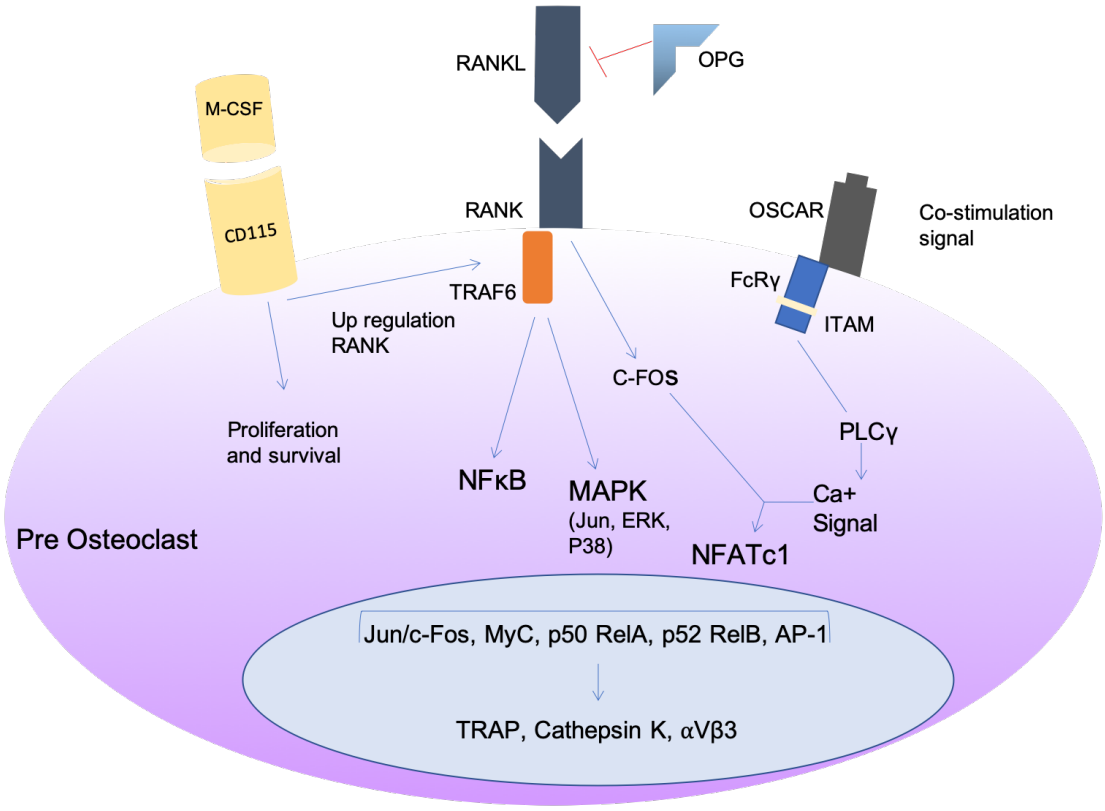

Figure 1.2 Signals which Drive Osteoclast Differentiation
M-CSF signalling via CD115 drives the proliferation and survival of OCPs, as well as driving the upregulation of RANK, making these cells more receptive to RANKL. RANKL signals through NFκB, MAPKinase to mediate the translocation of NFκB and AP-1 to the nucleus. In addition RANKL signals drive c-Fos activation which in combination with Ca^{2+} from OSCAR signalling pathways mediates the activity of master regulator of OC differentiation NFATc1. These signals all work in combination to drive OC-associated gene transcription such as TRAP, Cathepsin K, and integrin expression.

1.2.2.4 Fusion

The signals discussed above co-ordinate the transcription of genes necessary for OC differentiation and function. A fundamental process differentiating pre-OCs must then co-ordinate is cell fusion. This process is still not fully understood but

is known to require a series of co-ordinated events to enable pre-OC fusion. This firstly involves directional chemotaxis of OCPs towards each other via chemokines, with CCL-2 thought to contribute to this stage of fusion[104,105]. Once cells have been brought into close proximity with one another they must adhere. The process of cell-cell adhesion relies upon the expression and activation of cadherins and integrins. E-cadherin participates in mediating early pre-cursor interactions, which enables cellular fusion. By blocking this cadherin, the formation of multinuclear osteoclasts is significantly diminished[106]. In addition, an essential integrin involved in the fusion of OCPs is $\alpha V\beta 3$[107]. While cellular adherence via integrins is required to enable close contact of cells to mediate their fusion, integrins also act to enable fusion through cytoskeletal re-organisation within the cell. Integrin mediated signalling via SYK enacts to promote skeletal rearrangement through microtubules and actin[108]. This promotes the formation of cellular extensions formed of f-actin known as podosomes. The formation of these f-actin structures is essential for the process of macrophage fusion[109].

In addition to the migration, adhesion and cytoskeletal re-organisation discussed above, two surface receptors have been identified as essential mediators of fusion in osteoclastogenesis; DC-STAMP[110] and OC-STAMP[111]. However, the mechanism by which these surface receptors mediate this process is still unknown. Similarly, the ligands for these receptors during OC fusion is still not known. However, their importance in this process is evident in DC-STAMP KO animals, which fail to generate multinucleated OCs, leading to osteopetrosis[110].

1.2.3 Osteoclast Function

The primary function of an OC is the controlled degradation of calcified tissue for the purpose of resorbing old and damaged bone[112]. In order to perform this unique function, OCs must both generate and direct bone eroding enzymes and acids onto the bone surface without causing any collateral damage to surrounding cells, tissue, or microenvironment. Acids such as hydrochloric acid (HCl) are released via ion channels and H^+ATPase proton pumps[113]. In addition to acidic breakdown of inorganic calcified tissue, proteases are released to breakdown the extracellular organic matrix. The central protease released by OCs is cathepsin K[114]. The activity of both acidic components and proteases is

essential for the function of OC, and a lack of either of these components results in osteopetrosis [115,116]. However high concentrations of acidic and proteolytic material can be damaging not only to bone but also to surrounding cells and tissues. Thus, the release of this material is targeted specifically to the bone surface below the cell. In order to do this a seal is created between the bone surface and the OC cell via the sealing zone and a structure known as the ruffle border. Adhesion and cytoskeletal re-organisation are fundamental processes that enable the formation of the sealing zone and ruffle border.

The sealing zone is created by the formation of actin filament rich podosomes. Adhesion molecules mediate binding of OC cells to bone and the formation of these podosomes. Cell surface glycoprotein CD44 is at the core of the podosomes, directing the formation of actin filaments surrounding it. In addition, other OC-associated integrins are also present in the periphery of the podosomes, maintaining interaction between OCs and the bone surface in a low affinity state[117]. Podosomes begin to combine, eventually amalgamating to form an actin ring around the periphery of the OC. This "actin ring" structure is a principle phenotype in recognising formed OCs *in vitro*[118]. Integrins are also essential in the adhesion of OC to the bone surface and the organisation of the cytoskeleton. Integrin heterodimer $\alpha V\beta 3$ is the primary integrin that enables the mediation of bone resorption. Expressed by OCs, $\alpha V\beta 3$ recognises proteins that reside on the bone surface such as osteopontin (OSP) and bone sialoprotein (BSP). Attachment and spreading of OC cells on the bone surface is dependent upon $\alpha V\beta 3$ interaction with these bone proteins, demonstrated by competitive ligands of this integrin resulting in the arrest of bone resorption[119-121]. In addition, $\beta 3$ subunit knock out mice have an osteopetrotic bone phenotype attributed to dysfunctional OCs[107]. Outside-in signalling through $\alpha V\beta 3$ integrins enables co-ordination of cytoskeletal actin rearrangement[122]. In addition to mediating adhesion, signals received from $\alpha V\beta 3$ also enhance OC differentiation signals[123]. Through adhesion of OCs to the bone surface and formation of the sealing zone, OCs become polarised, which enables directional exocytosis to occur.

While formation of the sealed zone is important for efficient OC function, the formation of the ruffle border is still required in order to complete resorption

functions. The ruffle border is enclosed within the sealed zone and all of the organelles responsible for resorption functions are contained within this ruffle border. This is therefore known as the hallmark of active resorption in OC cells. As indicated by its title “the ruffle border”, it is the complex folding of the plasma membrane that borders the bone surface, creating a ruffled appearance. This was first observed using electron microscopy demonstrating the folded membrane[124]. Within the ruffle border and sealing zone, proteases such as cathepsin K and acids are secreted onto the bone surface. These compounds mediate the breakdown of the bone below and the degraded fragments are then endocytosed in the centre of the ruffled border region for further degradation and removal. The process of OC differentiation from HSC to endpoint functional resorbing OC and the signals which drive this process at each stage are summarised in Figure 1.3.

Multinucleated OC have traditionally been identified via histological staining of Tartrate-resistant acid phosphatase (TRAP) enzyme, a marker of OCs [81]. The exact role of this enzyme in OC function is still not fully understood. However it is known to be secreted by during active resorption, with its release positively correlating with resorptive behaviour[125]. This enzyme hydrolyses a number of substrates, including osteopontin (OSP), a protein component of bone tissue which mediates OC binding. The TRAP dependent dephosphorylation of OPN results in a loss of binding to OC[126]. TRAP is essential for normal bone development as demonstrated with trap-/- mice. These animals had abnormal skeletal formation (long bones were shorter, wider, with thicker cortices), and increased bone density indicative of mild osteopetrosis and failed resorption phenotype[127]. Overall, this indicates a role for the TRAP enzyme in OC function and bone resorption.

The process of releasing high quantities of proteolytic and acidic material in a polarised manner consumes a huge amount of energy. The proton pumps which delivered acidic HCl material to the bone surface require ATP for their function. In order to complete these functions OCs are highly metabolic cells and require glucose consumption for glycolysis. It is thought that the process of glycolysis is the central metabolic driver of osteoclast resorption function[128].

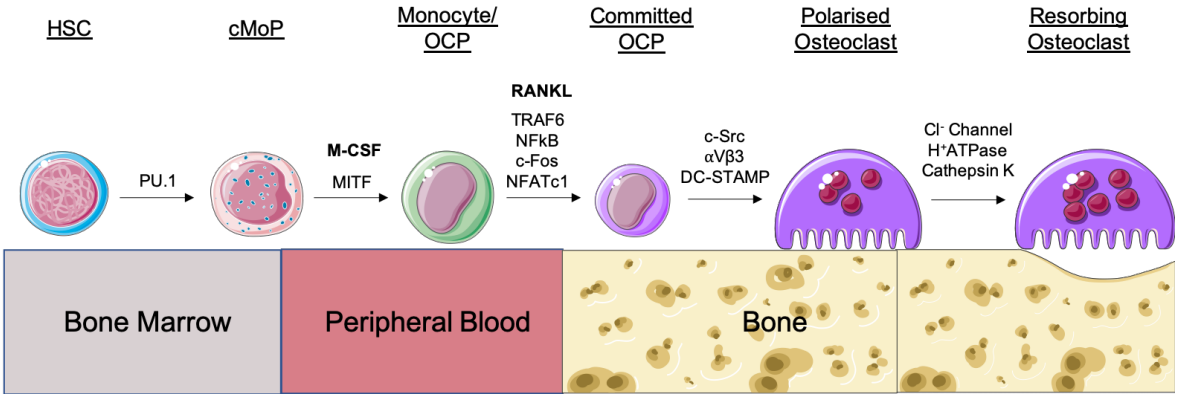

Figure 1.3 Osteoclast Differentiation
Osteoclasts originate from immune precursors in the BM, HSCs. These cells give rise to cMoP through upregulation of PU.1, which in turn give rise to monocytes/OCPs through MITF activation via M-CSF. Monocytes and OCPs circulate in the peripheral blood. These cells migrate to bone surfaces through chemokine receptors CCR-2, and CX_3CR1. Initial signals received via M-CSF results in upregulation of RANK. Stimulation of monocytes at the bone via RANKL initiates signalling molecules and transcription factors; TRAF6, NFκB, c-Fos, and NFATc1 driving commitment to the osteoclast lineage. Committed OCPs then upregulate integrin αvβ3 and DC-STAMP which mediates fusion of OCPs into multinucleated polarised osteoclasts bound to the bone surface. Polarised OCs form ruffle borders and through upregulation of Cathepsin K and active secretion of acids these cells begin to resorb bone. (Adapted from [129])

1.2.4 Osteoblasts

Osteoblasts (OBs) produce the organic basis of the bone tissue and are responsible for its mineralisation, and thus are the “bone forming” cell type. OBs are found lining the bone, especially at newly synthesised areas of bone, and are cuboidal in morphology. As the sole producers of all organic components of the bone tissue and inorganic calcification, these cells are highly anabolic, with large mitochondrial capacity and golgi apparatus in order to mediate the production of high amounts of protein.

OBs are derived from mesenchymal stem cell progenitors (MSCs), which have the capacity to differentiate into adipose cells, chondrocytes, or OBs, dependent upon the signals received and active transcription factors. Many extracellular signalling factors drive and regulate osteogenic differentiation of MSCs, including; Indian hedgehog (IHH), bone morphogenic proteins (BMPs), notch ligands, fibroblast growth factors (FGFs), parathyroid hormone-related protein (PTHrP), transforming growth factor β (TGF-β), the Wnt signalling family, and integrin ligands. Hedgehog signalling pathways initiated by IHH via patched homologue 1 (PTCH1), Smoothened (SMO), and zinc finger protein glioma-

associated oncogene (GLI) drive the master transcription factors of OB differentiation RUNX2 (runt-related transcription factor – 2), and OSX (osterix) [130]. In addition, Wnt signalling via frizzled (FZD) through either β-catenin canonical signalling or non-canonical pathways with PKC[131], also drives increased levels of both RUNX2 and OSX. The signals which drive MSC differentiation into OBs are outlined in Figure 1.4.

These transcription factors drive the transcription of OB-associated genes and enable the differentiation of this cell type. OB differentiation occurs across a period of time, which can be broken down into stages that are loosely defined by what proteins are being produced and the cells activities. In the earliest stage of differentiation (stage 1) these cells will be producing fibronectin, collagen type I, osteopontin, and expressing TGF-β receptors. This reflects the primary role of secreting and forming osteoid at this stage, laying down the organic bone matrix. This extracellular matrix also enables the adherence of OBs and OCs via fibronectin and osteopontin, which are both integrin ligands. Once OB differentiation reaches stage 2, these cells are still producing collagen I but will also begin to produce alkaline phosphatase (ALP). This enzyme hydrolyses phosphate, thus providing inorganic phosphate to promote mineralisation. As such; the expression of ALP is an important step in the process of initial mineralisation. Finally, mature OBs will be defined by their fully mineralising phenotype. These cells will produce osteocalcin and calcium phosphate, which enables the complete mineralisation of the organic matrix formed earlier in development[132]. Once fully mature osteoblasts have generated new mineralised bone, they can then either become enveloped within the mineralised tissue and develop into osteocytes, or they can become quiescent bone lining cells.

During development, the skeleton can be formed by 2 methods, dependent on the location and type of bone formation. Long bones of the extremities and some of the axial skeleton are formed by a process of endochondral ossification, while cranial bones are formed by a process of intramembranous ossification. Essentially endochondral ossification is the process by which growing cartilage is systematically replaced by bone in order to form the calcified skeleton. Chondrocytes form the cartilage anlage, which will eventually become future long bones. During this process chondrocytes are proliferative and produce

matrix, increasing the size of the cartilage anlagen. Chondrocytes in the centre of this structure become hypertrophic, and begin to differentiate into more OB-like cells, secreting a distinct selection of matrix components, this is termed the primary ossification centre. These hypertrophic chondrocytes direct cells in the surrounding membrane (termed the perichondrium, which contains OB precursor cells) to differentiate into OB and mineralise. This begins the formation of cortical bone, the dense, compact layer of bone which will provide long bones with strength and rigidity. At this point the primary ossification centre becomes perfused with blood vessels, hypertrophic chondrocytes either develop into mineralising OBs[133,134] or undergo apoptosis, and the centre of the structure becomes mineralised. Secondary points of ossification also form at the bulbous ends forming the metaphysis. Remaining cartilage is driven away from the diaphysis (shaft of the long bone) until it meets the ossified metaphysis, where this cartilage/bone interface remains, bordering the 2 regions. This band of chondrocytes remains post-natal and is traditionally known as the "growth plate". It is from this point that the length of the long bone can be extended throughout growth until adulthood (bone development reviewed in [135]). OCs also control this mineralisation process, by resorbing some of the new bone formed, maintaining the trabecular bone structure and providing space for BM formation.

Intramembranous ossification, which occurs primarily in the cranial and facial bones, differs from endochondral ossification in that there are no cartilage intermediates[135]. Mesenchymal precursors aggregate in areas where bone formation will occur and then once these have reached a high enough density they will begin to differentiate directly into OBs. These cells secrete the osteoid and then subsequently mineralise this to form the cranial skeleton.

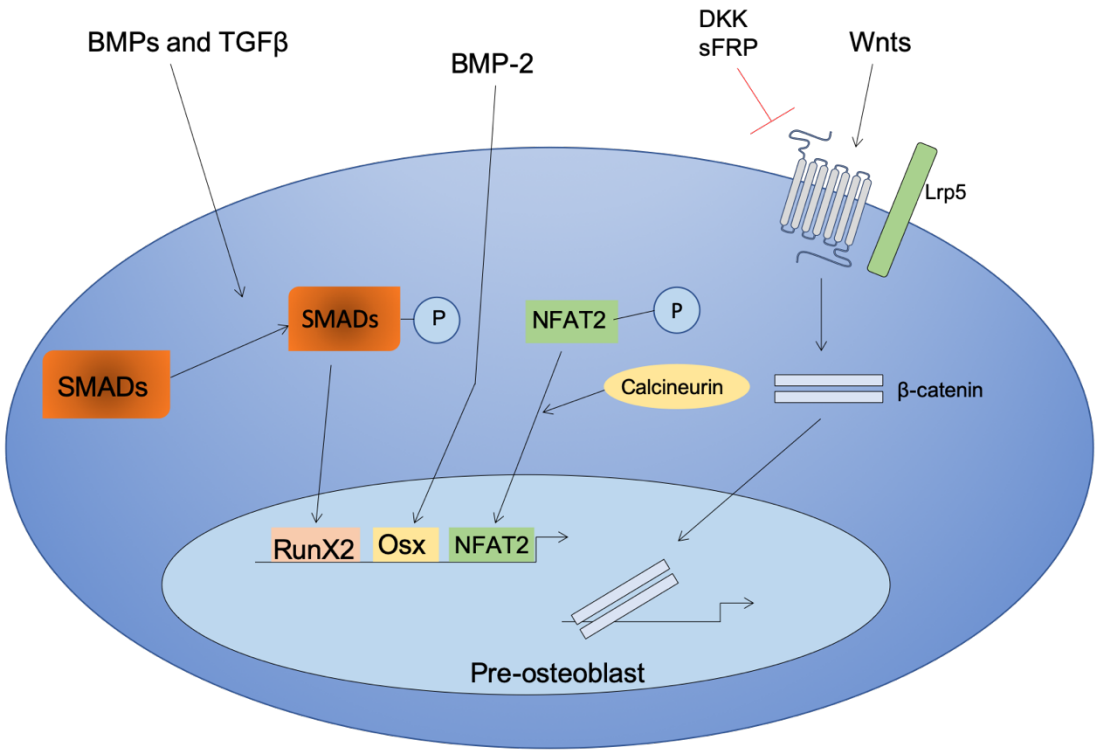

Figure 1.4 Signals which Drive Osteoblast Differentiation
MSCs can differentiate into chondrocytes, adipocytes, or osteoblasts. Signals received from BMPs, TGF-β, and calcineurin drive RunX2, OSX, and NFAT2, all master regulators of osteoblast differentiation. In addition, wnt signalling drives β-catenin mobilisation to the nucleus and also drives OB specific gene transcription.

1.2.5 Bone Remodelling

Bone remodelling is a healthy, homeostatic process by which the quality, quantity and integrity of the bone is maintained throughout life, as well as maintaining mineral homeostasis by regulating calcium liberation into the circulation[136]. The cell types discussed above; OBs and OCs, are the mediators of this process and work closely together within what is known as the basic multicellular unit (BMU), in order to mediate the removal of old bone and laying down of new bone. The BMU is named based on a concentration of multiple OBs in close proximity to multiple OCs, each regulating and enabling the function of the other group. These cells perform the same individual functions as they did during skeletal development. In this instance these functions are performed as more of a marathon than a sprint. The remodelling of bone is stimulated by

weight bearing, microscopic bone fractures, and the requirement to release calcium into the circulation; an essential requirement for cellular processes and signalling.

In order to maintain the skeleton but also avoid excess bone resorption or bone formation, the molecular communication between OCs and OBs, or these bone cells and cells of the BM and immune system, is a fundamental mechanism that regulates this physiological process with remarkable precision. It is essential that the quantity of bone formation and resorption is tightly balanced. However, in addition to this, the process of bone formation and resorption also requires spatial and temporal regulation to ensure sites of old bone removal are quickly replaced by new bone. A subtle loss in the tight regulation of this process is apparent in many bone pathologies.

Tight regulation of the BMU is what maintains the structure of the bone, and coupling of bone formation to the preceding action of bone resorption is thought to be primarily dictated by OC / OB interaction. These regulate the activity of one another, via cell-cell interactions or soluble mediator production. Active OBs are able to initiate the action of OCs, through production of OC attractants and differentiation promoting factors [23]. Hormone activated OBs produce CCL-3, a chemoattractant cytokine that mediates the movement of myeloid osteoclast precursor cells to the bone area[137]. Expression of osteoclastogenic factors such as, M-CSF, RANKL[138], and OSCAR ligand[139] are up-regulated on PTH stimulated osteoblasts in order to drive bone resorption. However, in order to prevent over-active bone resorption mature OB then produce RANKL decoy receptor OPG[25] to stop the effect of RANKL.

As well as control of OC formation by OBs, mediators produced by OCs can also act as OB attractants and activators or induce their differentiation[140]. Some examples of this arm of the cross-talk are OC production of complement component 3a (C3a) [141], collagen triple helix repeat containing 1 (Cthrc1) [142] and Sphingosine 1-phosphate (S1P) [143], which all attract, activate, or promote the survival of neighbouring OBs. In addition to the role of RANK-RANKL signalling in the promotion of OC formation, it has been recently demonstrated that this system can signal in reverse via surface RANKL on OB cells. This reverse RANKL signal promotes OB differentiation through activation of RUNx2. A mouse model

expressing a mutant RANKL that can still enable a forward RANK signal but cannot signal in reverse (RANKLp29A), has defective bone formation in comparison to WT counterparts[144]. The process of bone resorption (presence and activation of OCs), there in stimulates bone formation by initiating OB migration and maturation and vice versa.

The process of bone remodelling in a region of the skeleton can take a few weeks to complete and is achieved in distinct stages. These can be split into 5 processes, namely, initiation of bone remodelling, the resorption phase, the reversal phase, bone formation phase, and finally termination of bone remodelling [145]. The initiation of bone remodelling can be triggered by mechanical stimuli received by osteocytes via mechano-transduction[146] or through bone damage such as micro-cracks[147]. Osteocyte cell death caused by bone damage can result in a loss of OC inhibitory signal TGF-β and thus trigger bone remodelling [148]. In addition, a requirement for calcium liberation can be detected and PTH is released from the parathyroid gland, which acts upon OBs and promotes the production of factors to promote OC activity[149]. Therefore, during the initiation stage signals are generated to initiate remodelling from either local osteocyte activity or at a hormonal level, which drives OB activation.

This leads into the second stage of remodelling; the resorption phase. OBs activated during the initiation phase produce chemokines (e.g. CCL-3, mentioned above) which promote the recruitment OCP and promote their differentiation[150]. At this stage mature OBs produce M-CSF, RANKL and reduce OPG release in order to drive the differentiation and activity of OC at the site of bone remodelling[138]. The maturation of OC and maintenance of their activity lasts the duration of the resorption stage where they are responsible for the removal of old bone tissue. In order to prevent excessive resorption, the next stage of bone resorption is the reversal stage, where catabolic resorption is stopped, and the process is switched to anabolic formation. At this stage clearance of resorbed bone is completed by OCs themselves, and possibly with the aid of macrophages resident at the bone periosteum (termed osteomacs) [151,152]. During the removal of the matrix debris, OBs are recruited to the site by factors produced by OC during the resorption phase such as SP1 (mentioned

above 1.2.5, page 39). Factors released or expressed on the OC surface promote mesenchymal pre-OB migration and maturation, and prevent OC activity, leading to the bone formation stage. A coupled signal between EphB4 ephrin-B2 expressed on OC and its receptor EphB4 receptor on osteoblastic cells can generate bi-directional signalling that simultaneously inhibits OC activity and promotes OB differentiation and maturation[153].

OB are matured at the site of bone remodelling, initially producing osteoid and then reaching full maturity where they mineralise the osteoid matrix and form new bone (see section 1.2.4). The final stage of this process is the termination phase, when equal quantities of new bone have been created in place of the old resorbed bone, the process comes to a halt. The specific signals that drive the termination of the bone remodelling process and thus in turn prevent excessive bone formation, are still not fully understood. However, it is now thought that osteocytes may play a role in this process, potentially through the production of sclerostin, an OB inhibitory factor[154,155]. The interactions between OCs and OBs which drive and regulate the activity of these cells to co-ordinate bone remodelling are summarised in Figure 1.5.

As well as known factors produced by either OCs or OBs that initiate or inhibit their activities, recent work using intravital imaging techniques has identified that the dynamic regulation of the OC/OB spatial relationship also regulated function[156]. This research identified that OB and OCs largely remain in distinct areas of the bone, ensuring there is no active resorption or active formation at the same time and same place. Notably, when OC and OB came into contact this was highly inhibitory for resorptive activity, and thus this process may be part of the reversal phase. Therefore, direct cell–cell communication is essential in preventing excessive resorption. This may be linked to the bi-directional signalling of the EphB4 pathway mentioned previously (see section 1.2.5, page 40).

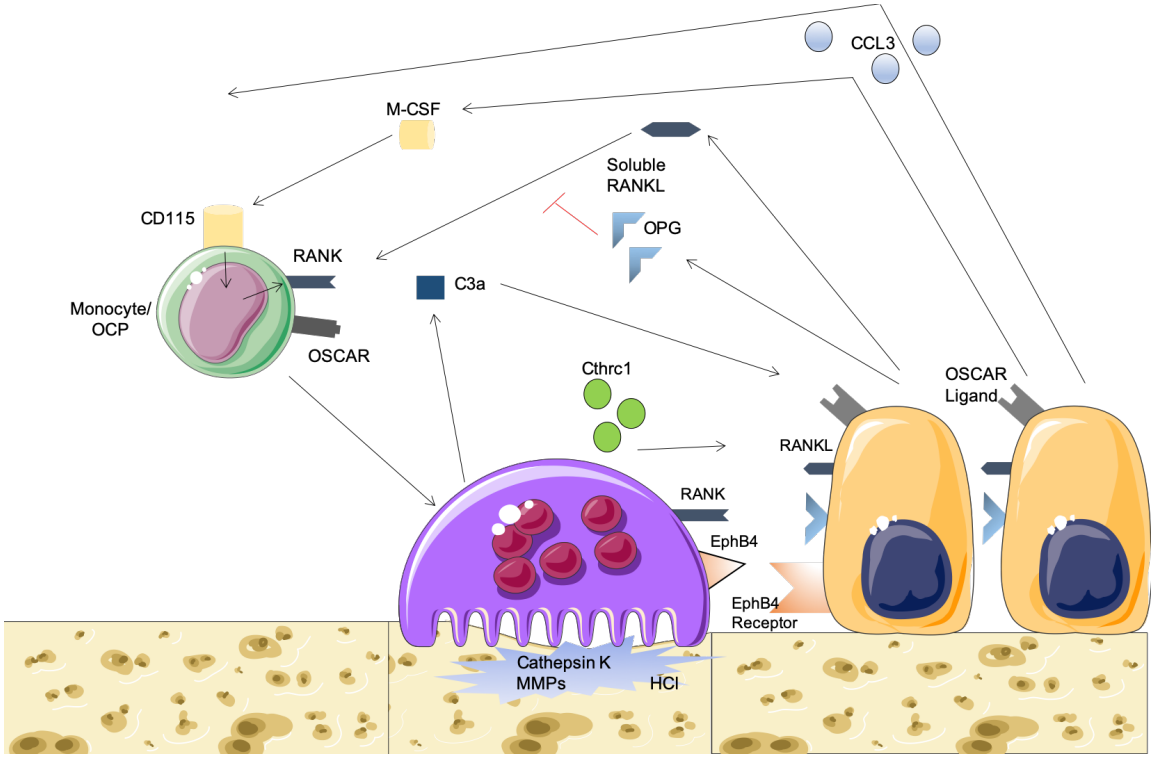

Figure 1.5 Dynamic Regulation of Bone Remodelling Conducted By Osteoblasts and Osteoclasts.
OB receive signals to initiate the process of bone remodelling. This drives expression of monocyte/OCP chemo-attractants CCL3 to promote the migration of OCPs to the site. OBs then increase expression of OCP survival factor M-CSF, and osteoclastogenic RANKL (as both cell surface ligand or in soluble form) and OSCAR ligand. Simultaneously they reduce expression of RANKL decoy receptor OPG. In turn driving OC formation and promoting the resorption phase. Active OC then resorb old bone through production of acidic and proteolytic mediators. This phase is constrained to prevent excessive resorption again through interaction with OBs. OBs initiate the reversal phase which stops OC activity and promotes OB activity. Interaction of OCs and OBs via EphB4 (OCs) and EphB4 receptor (OBs) drives bi-directional signals – simultaneously suppressing OC activity while promoting OB maturation. In addition, OC produce C3a driving OB migration and cthrc1 promoting OB survival and maturation. This initiates the formation phase of active bone formation and replacement of the old bone with newly synthesised bone.

1.2.6 Bone Pathologies

Several pathologies are associated with dysregulated OB/OC balance, resulting in excessive bone formation (osteosclerosis) or excessive bone resorption (osteopenia). Pathologies can be either systemic, affecting the whole skeleton in diseases such as osteoporosis or osteopetrosis, or be specifically localised to the joints such as arthritic conditions. In many of these conditions dysregulated OC drive pathology.

Osteoporosis is a condition characterised by systemic low bone mass and deterioration of the bone microarchitecture, which consequently increases bone fragility and susceptibility to fracture[157]. This most commonly affects

postmenopausal women, with approximately 30% of postmenopausal women in the United States (US) and Europe experiencing osteoporosis[158]. Increased resorption via OCs and limited bone formation by OBs results in systemic loss of bone. As such 2 therapeutic approaches have been taken to tackle this condition, anti-resorptive to directly target OC activity, and anabolic treatments to promote remodelling and bone formation through OBs. In addition, to osteoporosis another condition characterised by an increased rate of bone resorption is Pagets disease. The enhanced OC activity and resorption results in localised areas of destruction. Subsequently a compensatory increase in bone formation is then induced at the eroded sites, which results in an accelerated deposit of disorganised hyper-vascularised bone rather than the linear pattern formed in healthy bone remodelling. Overall the process results in skeletal deformity[159].

Bisphosphonates are the most common anti-resorptive treatment that has been historically prescribed for diseases characterised by hyper-resorption of bone. These compounds mimic the structure of endogenous inorganic pyrophosphates (PPi), a by-product of many reactions within the body and found endogenously in the blood and urine. These PPi's are known to be capable of inhibiting calcification and hydroxyapatite breakdown, via direct binding to hydroxyapatite crystals within the skeleton, where they are retained[160]. In doing this they effectively suppress the process of bone resorption and are thus great tools in the treatment for conditions of overactive OCs, such as osteoporosis and Pagets disease.

In contrast osteopetrosis is a heterogeneous group of conditions where there is a defect in the process of bone resorption. These heritable conditions are generally caused by mutations in genes essential to OC formation or action, thus patients fail to form functioning OCs. The most common osteopetrotic mutations occur in the H+ ATPase proton pump, and the *CLCN7* OC-specific chloride channel[161]. These mutations cause defects in the acidification action of OCs. As these conditions are primarily genetic in nature, the only current form of treatments available are bone marrow transplant, which would replace the HSC pool with cells which do not carry these mutations and can differentiate into functional OCs. In addition gene therapy methods to correct these null mutations

are in development currently, with moves to enter into human clinical trials in the near future[162].

In addition to systemic imbalance of OC and OB activity, localised imbalance within this system is also found at the joint site in arthritis conditions. Exacerbated OC formation in inflammatory arthritis contributes to bone erosion as discussed in detail in section 1.3.4. Osteoarthritis (OA) is also characterised by bone remodelling dysfunction at the joint site, however this is not comprised of erosion based deformity found in inflammatory arthritis. Instead this pathology is associated with abnormal bone formation in the form of bony spurs (osteophytes) [163], and subchondral bone formation[164]. While the exact mechanisms that drive the bone pathology associated with OA are not fully understood, it is thought that one contributing factor is the altered biomechanics of the OA joint which could drive dysfunctional bone formation through mechano-transduction mechanisms[165]. These abnormalities and deformities of the OA bone cannot currently be treated.

1.3 Rheumatoid Arthritis

1.3.1 Introduction

The arthritides are a heterogeneous group of conditions with a common endpoint of structural joint degradation. Rheumatoid arthritis (RA) is the most prevalent overtly inflammatory condition of this group. This chronic, autoimmune disorder affects around 1% of the UK population [166] and is characterised by swelling, fatigue, pain, and loss of joint mobility. In addition to join pathology, RA is also characterised by a range of co-morbidities such as cardiovascular disease, mental health conditions, osteoporosis, and cancer, all of which may be associated with systemic inflammation. RA more predominantly affects women with onset age most commonly between 30 and 50 years of age. Therapeutic management of this condition is primarily through immunosuppressive agents such as; non-steroidal anti-inflammatory drugs (NSAIDs, ie., naproxen), disease modifying anti-rheumatic drugs (DMARDs, i.e., methotrexate), or specific immuno-pathway targeting biologics (i.e., anti-TNF, or anti-CD20) (Fully reviewed by [167]).

1.3.2 Immunopathology

A number of immune-related pathways have been highly associated with RA through Genome Wide Association Studies (GWAS) from both the innate and adaptive arms of the immune system. For example, the HLA-DR locus has the highest association with this pathology[168]. Thus, highlighting the importance of presentation of antigen (possibly self-antigen) and both the innate and adaptive immune compartments in this pathology. In addition to underlying genomic risk factors for RA, the possibility of developing RA is also highly associated with a number of environmental risk factors. For example, smoking is the highest lifestyle associated risk factor that increases the likelihood of developing this pathology[169]. The exact mechanisms linking smoking and RA are still not fully understood but the enhanced modification of self-antigens induced by smoking may drive the recognition of these as foreign and drive an increased likelihood of a break in immune tolerance.

Therefore, this disease manifests as a result of a break in immune tolerance towards antigens associated with articular joints in genetically susceptible individuals. This leads to an adaptive driven immune response to self-antigens, such as IgG (rheumatoid factor, RF) [170] or post-translationally modified proteins (anti-citrullinated protein antibody, ACPA) [171]. Interestingly, self-reactive antibodies such as ACPAs present prior to disease symptom onset [172]. The RA inflammatory synovial infiltrate consists of auto-reactive B and T cells, inflammatory monocytes, mast cells, and neutrophils, which together produce a network of pro-inflammatory cytokines (TNF-α, IL-6) [173] chemokines (CCL2, CXCL8), proteases, and reactive oxygen species (ROS), creating a hypoxic, inflammatory environment.

The synovial membrane in healthy individuals is 1-2 cells thick and comprised of fibroblast-like synoviocytes (FLS) and tissue resident macrophages. However, during pathology, this expands, creating a hyperplastic expansion of the membrane[174]. In addition, increased inflammatory mediators (e.g. IL-6), and catabolic proteases are produced by active pro-inflammatory FLS of the membrane. This aggressive phenotype is maintained [175] through epigenetic imprinting, creating an almost “transformed” synovial membrane [176]. FLS hyperplasia creates structural damage due to thickening of the synovial membrane, creating an invasive pannus which can erode neighbouring tissue[177]. Structural damage is also caused by immune cell infiltrate invading the juxta-articular bone and calcified cartilage, led by excessive osteoclast activity (derived from infiltrating myeloid cells e.g. monocytes) and TNF-α driven mechanisms [178].

In addition, adaptive immune mechanisms also drive the chronicity of this disease. Pathogenic populations of CD4+ T helper Th17 and Th1 cells have been identified. Regulatory T cells (Tregs) are also abundantly present, however, their function has been shown to be attenuated, limiting their ability to regulate chronic inflammation[179]. The presence of ectopic lymphoid follicles at the RA joint is a hallmark of uncontrolled disease pathology. This is the site of active T cell and B cell communication that closely resembles germinal centres present in active lymph nodes[180]. T cells provide aid for driving B cell differentiation and somatic hypermutation at these follicle sites, which then become a large source

of auto-antibody[181]. The presence of elevated levels of B cell survival factors within the synovium maintains their survival, and promotes further chronicity[182].

1.3.3 Monocytes in RA

The innate immune system is integral in the pathogenesis of RA (see section 1.3.2). Monocytes are altered during chronic RA, with these cells expressing a TNF skewed transcriptional signature[183]. Their importance in disease pathogenesis is highlighted in that their heightened cell number correlates with disease activity and also indicates responsiveness to drugs such as anti-TNF[184]. Frequencies of monocyte populations are altered in RA patients, skewing towards a more prominent intermediate population than in healthy controls. Moreover, this expanded intermediate population is thought to drive pathogenic T cell population expansion[185]. Systemic inflammation is a hallmark of RA and while elevated cytokine levels impact the phenotype of PB monocytes, the chronic inflammation also drives early release of monocytes from the BM [186]. This early release phenotype is thought to be driven by increased demand and turnover of monocytes, due to their constant recruitment to the joint. Research looking at monocytes in RA is somewhat limited as more focus has been given to their tissue differentiated states within the joint (monocyte-derived macrophages).

1.3.4 Inflammatory Bone Erosion

Chronic RA is characterised by generalised osteopenia (a reduction in the protein and mineral content of bone), resulting in overall increased fracture risk[187]. Measurements of osteopenia and bone mineral density correlate with disease activity in RA patients[188]. In addition to general bone loss, a hallmark of uncontrolled RA is localised bone loss and focal bone erosions at the inflamed joint. These erosions are evident in radiographic imaging of the joint, with erosions most commonly localised to the “marginal areas”. These are the periarticular regions of the joint not covered or protected by the articular cartilage. Focal bone erosions are the end point of structural damage, most commonly found in patients who experienced uncontrolled disease for some time.

Peri-articular bone erosion usually occurs in joints that display active inflammation. These focal bone erosions at the pannus/bone interface contain OCs at their forefront. This has been demonstrated in both RA and juvenile idiopathic arthritis (JIA) joint tissue where $TRAP^+$ cells are clearly evident[189]. The presence of OCs is essential in mediating bone erosion, as demonstrated in the K/BxN murine serum transfer model. When the serum of this mouse is transferred to another background the host develops arthritis. Notably, when K/BxN serum was transferred to a *rankl* knock out mouse, although they developed inflammatory arthritis, there was no evidence of any bone erosion[190]. The evidence above indicates that, even in a highly inflammatory environment, bone erosion cannot occur independently of RANKL-mediated OC formation. However, some contradicting work has suggested that RANKL independent osteoclastogenesis can occur during inflammatory arthritis. Many different mechanisms of RANKL independent osteoclastogenesis have been proposed. Some studies have demonstrated TNF driven osteoclastogenesis independent of RANK/RANKL [191,192], indicating potential non-RANKL driven osteoclastogenesis during TNF dominant inflammatory arthritis. In addition to inflammatory cytokine driven OC formation, bacterial toxins such as pasteurella multocida toxin[193], and hypoxia associated lysyl oxidase[194] as potent inducers of osteoclastogenesis independent of RANK/RANKL signals. However, time and again the reports of RANKL independent osteoclastogenesis have been disputed, demonstrated as irreproducible and are generally considered controversial[195-197]. Overall, the field still does not fully accept the possibility of RANK independent osteoclastogenesis even in the extreme circumstances of cancer and chronic inflammation.

RANKL is upregulated not only in experimental rodent models of disease [198], but also in human inflammatory joint diseases such as RA[199,200], and psoriatic arthritis [201]. Direct inhibition of OC activity and formation in human disease through the use of clinical treatment with anti-RANKL (denosumab) is effective in preventing bone erosion, however, it has no other clinical benefits. Supporting the concept that inflammatory OC formation is still dependent on RANKL in human disease. Also indicating that this mechanism does not contribute to any other clinical manifestation, such as joint space narrowing or cartilage degradation[202].

While the formation of OCs and thus the presence of bone erosions in still dependent upon the basic mechanisms of OC development and activity, i.e., RANK / RANKL interaction, the increase in number and activity of these cells is driven by a combination of inflammatory factors. The RA joint is a location of high monocyte trafficking (see 1.3.3), these cells are capable of differentiating into OC with the right combination of signals. The inflamed synovium is an environment rich in OC promoting factors, such as osteoclastogenic cytokines (TNF, IL-17, and IL-6), and RANKL, providing a wealth of signals to drive the excessive formation of these multinuclear cells. Within the RA synovium various cell types are responsible for promoting their differentiation, 2 primary cells involved in this process are FLS of the invasive pannus, and activated T cells within the synovium. Active and aggressive RA FLS are a primary source of RANKL, and can thus drive OC formation[199], which provides an in-road into the bone, where the pannus follows to further invade this tissue. Active T cells, especially Th17 cells, also provide a source of RANKL, in combination with other OC promoting cytokines such as IL-17[203]. While both of these cells are known RANKL producers, the primary source of RANKL during inflammatory arthritis was identified as synovial fibroblasts. Through a series of conditional *rankl*$^{-/-}$ murine models of inflammatory disease T cells, chondrocytes, and synovial fibroblasts were all selectively depleted of RANKL, which demonstrated the highest dependence of RANKL from the fibroblast[204]. In addition to pro-inflammatory cytokines, auto-antibodies have also been implicated in driving OC formation in RA. Within *in vitro* cultures of OC assays and auto-antibodies isolated from RA patients, the enhancement in OC formation was shown to be dependent upon chemokine IL-8[205]. Thus, antibody driven OC enhancement is most likely dependent on cellular migration. It was initially suggested that specific polyclonal ACPA isolated from RA patients enhanced the formation of OC. However, subsequent follow up determined that the citrullinated peptide binding capacity of these antibodies had not fully been elucidated and therefore this may not be an ACPA specific phenomenon[206].

Another key mediator that drives RA bone erosion and OC formation is the pro-inflammatory cytokine TNF, which is prominent factor in disease pathogenesis. This is noted as one of the most important enhancers of OC formation in RA and will be discussed in more detail below (1.3.4.1).

It should also be appreciated that bone erosion in RA patients is not repaired, resulting in irreversible joint damage. This could be the result of a failure in the bone formation pathways driven by this disease. Inflammation, also reduces osteoblast differentiation potential, prohibiting their maturation into a mineralising state and thus their bone forming capacity[207]. Thus, taken together, in RA there is a loss of regulation in the homeostatic bone remodelling process. Bone resorption via OC is enhanced, while bone formation pathways and OBs are inhibited, preventing any repair of excessive bone erosion.

1.3.4.1 TNF in Osteoclastogenesis

TNF is a pro-inflammatory cytokine. Un-detectable in healthy individuals but enhanced and detectable during inflammation related to both sterile and infectious pathologies. RA patient serum levels of TNF are significantly enhanced[53]. This enhancement of serum TNF also positively correlates with disease activity [208]. In addition TNF is also prevalent within the inflamed synovia[209]. This cytokine is a central driver of RA disease pathogenesis, and inhibitors for TNF were the first biologic approved to treat RA patients[210]. Activated macrophages are the central producers of TNF. However, it is also produced by activated helper T cells[211], neutrophils[212] and fibroblasts[213]. Similarly to RANKL, this cytokine can be found anchored to the cell surface, in a membrane bound form, or it can be cleaved from the cell membrane to a soluble state via TNF-α converting enzyme (TACE)[214]. Both forms of the cytokine are active. It is a well-known driver of inflammation, especially innate immunity, and has high association with innate immune driven conditions, for example in bacterial infections where macrophage activation is crucial for bacterial clearance. This is highlighted by the increased risk of bacterial infections during anti-TNF therapy[215].

In addition to the success of anti-TNF in regulating inflammation in patients, this treatment has been demonstrated to reduce the risk of developing radiographic evidence of bone erosions[216]. Most likely, the reduction in the likelihood of bone erosion with anti-TNF therapy is due to the potent pro-osteoclastogenic action of TNF. TNF was first identified as a potent enhancer of RANKL mediated osteoclastogenesis in 2000, in a study conducted by Jonathan Lam. This study determined that in conditions of reduced RANKL expression TNF was able to

drive excessive osteoclast differentiation *in vitro*. This effect was lost if TNF was added to the culture system too early in the differentiation phase[46]. Thus, the effect was based on enhancing an already committed progenitor post-RANKL exposure. Since this publication, the TNF OC enhancement has been further demonstrated in murine model both *in vitro*[191] and *in vivo*[217,218], and also in human cell culture systems of monocyte / OC differentiation. Some publications have reported that TNF can drive OC without RANKL, however, this idea is not widely accepted. Double genetic manipulation murine models with *rankl*$^{-/-}$, and TNF-overexpression maintain osteopetrosis, as the overexpression of TNF fails to rescue OC deficiency in these animals[219]. Therefore, it is commonly recognised that TNF does not drive OC differentiation alone but instead enhances RANKL-mediated OC differentiation.

TNF has 2 cognate receptors, tumour necrosis factor receptor 1 (TNFR1) and tumour necrosis factor receptor 2 (TNFR2). These receptors can each signal via distinct pathways but can also overlap through TRAF2 mediated NFκB and MAPKinase signals. Both of these receptors are expressed by OCPs. TNFR1 can couple with TRADD, which can subsequently couple to FADD (fas associated death domain) to drive apoptotic signals. Alternatively, TRADD can couple with RIP which in turn activates the NFκB pathway via IKKs and IκB phosphorylation. Driving NFκB translocation to the nucleus and inflammatory-associated gene transcription. Finally, TNFR1 coupled TRADD can also activate the MAPKinase signalling cascade via JNK1, driving the AP-1 transcription factor. In comparison, activation of TNFR2 leads to engagement of multiple TRAFs (TRAF 1, 2, 3, 5, and 6) and subsequent MAPKinase JNK signalling and AP-1 assembly, or NFκB activation[220,221].

The exact mechanisms by which TNF drives enhanced OC formation are still not fully understood. It is thought that this cytokine can promote enhanced expression of both RANK[222] and RANKL. Furthermore, the signalling mechanisms of TNF share many similarities to that of RANKL, and it was therefore originally thought that this signal may be contributing to the RANKL signal[223]. However, it is now recognised that the TNF driven OC enhancement is dependent upon RANKL expression but driven by pathways independent of RANK/RANKL[191]. Even

though OCP express both TNFR1 and TNFR2[191], the OC stimulatory signal from TNF is thought to be driven primarily via TNFR1[223,224].

1.4 Protease Activated Receptors (PARs)

1.4.1 PAR Family of Receptors

Protease activated receptors (PARs) 1-4 are a small family of transmembrane, G-protein coupled receptors. The unique aspect of these receptors is their lack of traditional ligand. All members of the PAR family are activated via cleavage of their N terminus by serine proteases, unveiling a novel N terminus, which in turn can bind the second extracellular loop as a "tethered ligand" to induce activation. This results in an inability to dissociate the bound ligand and re-use the receptor, therefore, post-activation PARs are internalised and degraded. In 1991, PAR1 (a thrombin responsive receptor) was the first family member to be cloned [225]. Following this, the trypsin-responsive receptor PAR2 was cloned[226,227], and then in 1997 a second thrombin responsive receptor, PAR3, was identified via a PCR-based approach to complementary DNA of PAR1[228]. PAR4, the final receptor family member to be identified, was cloned in 1998[229]. PARs 1, 3 and 4 play important roles in vascular physiology, the coagulation pathway and the immune system, and are primarily cleaved by thrombin [230]. PAR2, however, is activated by a number of serine proteases such as trypsin[231], mast cell tryptase[232], neutrophil proteinase 3 [233] and matriptase[234], many of which are generated and released during tissue injury or inflammation. Thus, PAR2 (also known as FR2 Like Trypsin Receptor; F2RL1) serves slightly different physiological roles from the other family members. And in the last decade a strong link has emerged between this receptor and innate and adaptive immunity.

Located on chromosome 5[227], the FR2 Like Trypsin Receptor (F2RL1) gene is 2.9Kb in length[235]. This is translated into a 394 amino acid sequence to form the PAR2 protein, with a predicted molecular weight of around 44kDa. The structure of this receptor includes 7 transmembrane domains, and a 74 amino acid N terminal sequence that during activation is irreversibly cleaved. The standard trypsin cleavage site is 36 amino acids from the N-terminus, which when dissociated exposes a novel N terminal with a SLIGKV sequence[227]. This tethered sequence is then capable of self-binding the second extracellular loop of the receptor to induce signal transduction[236].

1.4.2 PAR2 Activation and Signalling

The unconventional method by which this receptor is activated via protease cleavage results in irreversible changes to the receptor structure. The self-anchored ligand does not dissociate so in order to end signalling from the activated receptor it is internalised. Many other G protein coupled receptors are also internalised post activation, and within the endosome ligands are removed and the receptor is recycled to the cell surface ready to be activated again[237]. However, the structural modifications undergone for protease activation leave the PAR receptors unable to be activated again. Thus, post endocytosis these receptors are trafficked to lysosomes for complete degradation. Endocytosis of the receptor is mediated by β-arrestins, which are recruited after G protein signalling. PAR2 action is regulated by appropriate trafficking around the cell, thus enabling it to only be expressed on the surface when required and to end irreversible signalling via receptor internalisation and degradation.

Once activated via protease cleavage of the N terminus, the binding of the novel N terminus to the second extracellular loop of the receptor[238] induces a conformational change and activation of PAR2, initiating G protein signalling. Canonical PAR2 signalling is initiated by conventional PAR2 activating proteases that all cleave the receptor at the same point exposing the SLIGKV activating N-terminus. This includes; trypsin, tryptase, granzyme A, coagulation factor VIIa and Xa, and kallikrein 2, 4, 6, and 14. While all of these proteases cleave the same section of the PAR2 N terminus, they all differ in terms of their potency for PAR2 cleavage. In addition to conventional protease mediated cleavage, in order to study the function of PAR2, without cleaving any other PARs or surface proteins, activating peptides were produced. These activating peptides mimic the tethered ligand, such as SLIGKV in human cells, and have been further modified (furoylation) to improve potency [239].

Canonical PAR2 activation initiates multiple signalling pathways, associated with diverse groups of G protein α subunits, such as calcium mobilisation, MAPKinase ERK phosphorylation, and GTPase associated Rho signalling. In addition to G protein mediated pathways, PAR2 also directs β-arrestin-mediated signalling via structurally independent regions of the C-terminus[240,241]. The activating peptides that mimic the conventional tethered ligand for this receptor function in largely

the same way as direct protease activation. They also activate canonical G protein signalling pathways, β-arrestin interactions and drive internalisation of the receptor.

Canonical PAR2 signalling involves activation of multiple G protein α subunits, such as Gαq[118,119], Gα12/13[242], Gαs [243]. Utilising a cell line system with transfected flag-tagged human PAR2 in COS-7 cells, activation of these G protein α subunits was confirmed in response to PAR2 activating peptide, and the α subunits that drive or are associated with independent signalling pathways were elucidated[243]. The $G\alpha_{12/13}$ family initiates the Rho signalling pathway, an essential pathway involved in cytoskeletal organisation. The Gαs pathway activation has been suggested to stimulate the adenylyl cyclase pathway (cAMP) which can in turn activate cAMP dependent protein kinases and amplify the signal. It is also known to regulate and inhibit Rho activation. Activation of $G\alpha_{q/11}$ was associated with the activation of phospholipase C (PLC), mediated hydrolysis of phosphatidylinositol 4,5-bisphosphate (PIP2) driving Ca^{2+} mobilisation, inositol 1, 4, 5 triphosphate and protein kinase C (PKC) signalling pathway activation[240]. Downstream of this, PKC activates the NFκB pathway, increasing IKKα and IKKβ, which subsequently translocate to the nucleus. This process can be inhibited with PKC inhibitors [241]. Through activation of RasGTPase, PAR2 is also able to signal via MAPkinase signalling elements ERK, p38, and JNK[241,244]. Activation of NFκB, and MAPkinase are principal signalling pathways involved in inflammatory responses, which result in the survival and proliferation of immune cells, and drive the induction of inflammatory associated genes e.g. pro-inflammatory cytokine production. In addition pathways such as Rho activation via PAR2 drive cytoskeletal rearrangement, and actin polymerisation that drive immune cell migration and adhesion[245].

Activation of the PLC pathway also aids in directing signalling regulation via phosphorylation of the intracellular C terminus, resulting in uncoupling of G proteins, thus preventing continued signalling in an irreversibly activated receptor. G-proteins are un-coupled from the PAR2 C terminus by β-arrestins, which themselves become associated with the C terminus. Not only do β-arrestins stop G-protein association with the C-terminus they also mediate clatherin-dependent endocytosis of the activated receptor. A study by Bohm and

colleagues in 1996[246] used calcium flux monitoring and microscopy imaging techniques to greater understand and visualise PAR2 signalling and cellular trafficking. They demonstrated that within 15 minutes of PAR2 activation there is a diminished surface expression but increased PAR2 presence in small vesicles close to the cell surface. By 30 minutes $PAR2^{+}$ vesicles appeared larger and localised to the cytoplasm. Through visual co-localisation with an endosomal marker (transferrin receptor) the group identified that PAR2 enters endosomes and then through subsequent co-localisation with GM10, a lysosomal marker, they concluded that the receptor is degraded within lysosomes[246].

In addition to driving the trafficking of activated receptors away from the membrane for degradation, β-arrestin is also an essential signalling mediator that drives non-G protein signalling from PAR2. During β-arrestin driven internalisation of PAR2, in the early endosome there is formation of the β-arrestin signalling complex. This includes recruitment of Raf which activates ERK, and initiates cell membrane ruffling, and filopodia formation to drive cellular motility[247-249]. In addition to its association with Raf-ERK signalling, PAR2-β-arrestin also complexes with cofilin, a protein that interacts directly with actin in the cytoskeleton. By binding the cofilin activating protein chronophin, the PAR2-β-arrestin complex activates cofilin, which induces actin polymerisation at the cells leading edge and thus drives cellular motility[250,251]. Overall, the signalling complexes created with β-arrestin during receptor internalisation are key drivers of cell migration. The signals initiated during canonical PAR2 activation are shown collectively in Figure 1.6.

Studies conducted with various adherent cell lines transfected with human PAR2 tagged proteins have been invaluable in teasing apart the intricacies of the expansive signalling cascades that are induced by canonical PAR2 activation, outlined above. However, it must also be considered that while these signal mediators have been connected in PAR2 transfected cell lines, such findings do not always directly translate to primary cells. It is possible that cell type may drive some bias with regards to the signalling pathways initiated by canonical PAR2 activation, and certainly the functional outcomes of these signalling pathways may differ between cell type. Further exploration of PAR2 signalling in primary cells with endogenous PAR2 expression has only been minimally explored

and would undoubtedly be valuable in further understanding the role of this receptor in specific cell types and settings.

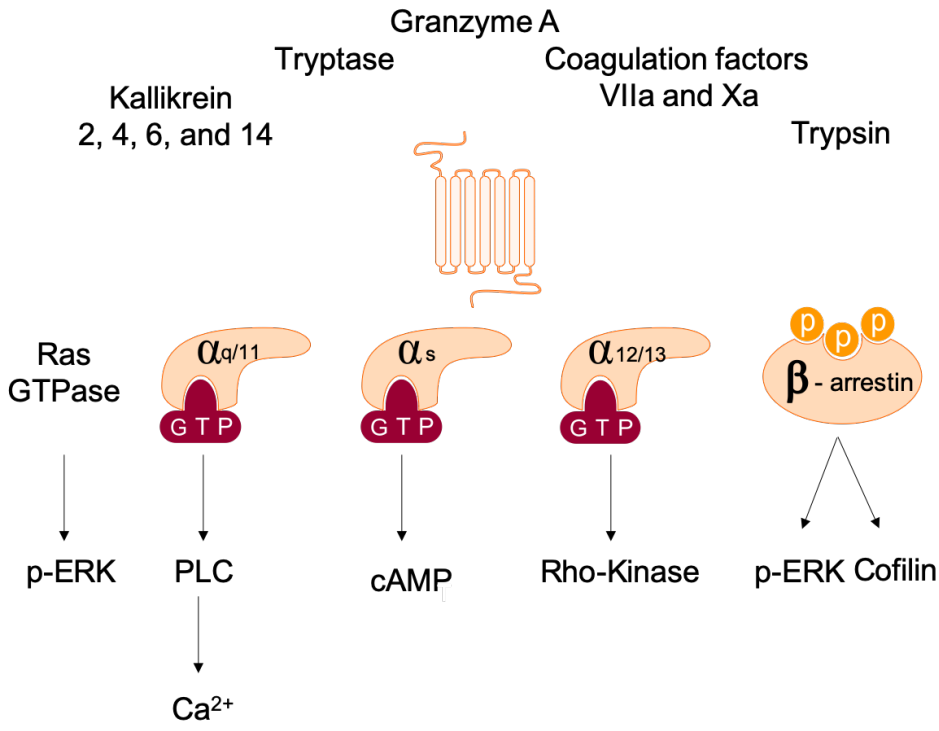

Figure 1.6 PAR2 Canonical Signalling Pathways
Various serine proteases are known to cleave PAR2 at the N-terminus to reveal the activating novel N-terminus SLIGKV (SLIGRL in mice), including Trypsin, Granzyme A, Tryptase, Kallikrein 2, 4, 6, and 14, and Coagulation factors VIIa and Xa. This novel N terminus binds the second extracellular loop of the receptor to initiate canonical PAR2 signalling. Canonical signalling can drive the activation of multiple Gα proteins and β-arrestin. This includes; activation of Gαq/11 which drives signalling via PLC and Ca2+ mobilisation, activation of Gαs which drives signalling via cAMP, and activation of Gα12/13 which drives signalling via Rho-kinase to mediate cellular migration. In addition, canonical PAR2 activation results in receptor association with β-arrestin which mediates receptor internalisation, but also signals via MAPKinase phospho-ERK and cofilin to drive actin rearrangement. Finally, canonical activation can also result in Ras GTPase activity to mediate MAPKinase signalling through phospho-ERK as well.

1.4.2.1 PAR2 Bias Signalling

In addition to canonical PAR2 cleavage, which provides the novel N terminus of SLIGKV in the human or SLIGRL in mice, other proteases can cleave PAR2 at alternate sites. When this was first discovered it was thought that this alternate cleavage was only intended to disarm available receptors, making them unresponsive to their canonical activation[252]. However, it is now apparent that alternate cleavage can drive PAR2 activation in a limited form, also known as bias signalling. These distinct sites of alternative PAR2 cleavage cannot initiate

all of the signalling pathways driven by canonical activation, and instead they selectively activate specific pathways in a bias manner, driving alternative or selective actions of this receptor.

This concept of bias signalling in PAR2 and the PAR family in general is a relatively new finding and our knowledge of this is still somewhat limited. As more research is conducted more proteases have been found that can drive a bias activation of PAR2. Many of these bias proteases are also abundantly sourced from activated immune cells, such as neutrophil elastase, proteinase-3, and cathepsin G, all of which are released by activated neutrophils[253,254]. Neutrophil elastase cleaves PAR2 at a distinct site, beyond the canonical trypsin site, much closer to the first transmembrane region. Cleavage by this proteinase drives $G\alpha_{12/13}$ activation, without any other G protein involvement. This drives MAPKinase ERK activation via Rho kinases, with no β-arrestin recruitment, and thus no signalling via β-arrestin, nor receptor internalisation[255]. The cleavage site results in a very short tethered ligand in this case. Moreover, the peptide mimic for this novel elastase-generated N-terminus cleavage does not activate PAR2. Suggesting that this mechanism leads to a tethered ligand independent PAR2 activation. The mechanism of activation has not been fully explored but cleavage of the N-terminus at this site could possibly induce an active conformation of the receptor.

Cathepsin S is a cysteine protease with known production by specific macrophage populations, i.e. alveolar macrophages. It also has capacity to cleave PAR2 at a non-canonical site and is capable of driving alternate PAR2 activation. Unlike elastase, cathepsin S drives Gαs driven cAMP accumulation, but does not trigger Ca^{2+} signalling or ERK phosphorylation[256]. As such, this drives yet another form of signalling bias, distinct from elastase. The physiological responses associated with this bias signal have been associated with pain reception. The known routes of PAR2 signalling bias are presented in Figure 1.7.

These findings indicate that during inflammatory responses, the release of neutrophil and macrophage associated proteinases could drive alternative PAR2 activation during inflammatory assault. PAR2 is able to dynamically respond to diverse proteinase signatures within the environment to trigger precise

intracellular pathways that will drive distinct cellular responses. This may provide some insight as to why PAR2 sometimes appears to drive opposing actions in different disease states. A greater understanding how to drive specific actions of PAR2 by promoting signalling bias could also be a valuable therapeutic tool[257]. By driving PAR2 activity in a particular direction, this could eliminate the pathogenic actions of this receptor in some disease settings without losing its valuable actions.

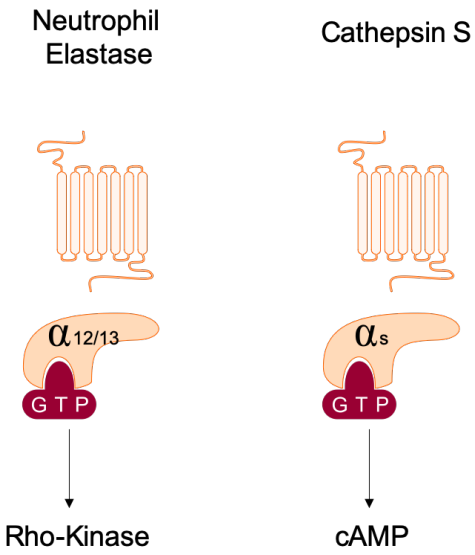

Figure 1.7 Known PAR2 Bias Signalling Pathways
Unlike canonical activators, some proteases cleave PAR2 N terminus at an alternate site. This can sometime still initiate receptor activity but only drive activation of particular Gα subunits and signalling pathways. Two identified proteases that can drive a bias non-canonical activation of PAR2 are neutrophil elastase and cathepsin S. Neutrophil elastase can only mediate Gα12/13 signalling via PAR2, which drives Rho-Kinase signals. While cathepsin S can only drive Gαs activity and cAMP actions through PAR2. Neither protease mediates β-arrestin recruitment to PAR2.

1.4.3 PAR2 Expression and Function

Upon discovery of PAR2, initial investigation of the expression patterns of PAR2 throughout the body were crudely performed. In 1995, Nystedt and colleagues performed northern blot techniques with RNA isolated from various human organs and blotted for PAR2 mRNA. Organs that contained large amounts of PAR2 mRNA included the liver, kidneys, pancreas, prostate, small intestine, and colon. A lot of these organs were high producers of proteases and involved in metabolism or digestion in some form. As a protease activated receptor this

made physiological sense for this receptor to be localised to environments with high levels of protease expression. Since this initial observation it has been established that PAR2 does play a substantial role in digestion and specifically in stimulating exocrine secretion in the pancreas[258], intestinal cells[259,260], and the release of saliva from salivary glands [261]. PAR2 also stimulates gut motility through smooth muscle contraction and relaxation, an essential function mediating the peristaltic movement through the GI tract[262]. In addition to homeostatic functions in mediating secretion and motility, PAR2 has also been established to drive pain reception in the intestine[263], as well as association with immunological functions within the gut, playing a role in chronic inflammatory intestinal conditions[264]. Overall, it is clear PAR2 plays fundamental roles in GI tract health, homeostasis and in disease[265].

In addition to expression in GI associated organs the initial crude analysis of organ-associated PAR2 transcript expression identified lower, but still evident levels of PAR2 mRNA in leukocytes, and the spleen[227] (see 1.4.4).

Subsequently, expression was then confirmed in endothelial cells (Human umbilical vein endothelial cells - HUVECs) [266]. Furthermore, PAR2 transcript levels were enhanced in response to inflammatory stimuli IL-1α, TNF, and LPS[266]. Importantly, this enhanced expression was limited to PAR2, as the same responses were not found in PAR1 transcript; a clear discriminator between these receptors and their potential functions[266]. In addition to this, a further study identifying a key role for PAR2 in HUVECs was conducted by Plevin and colleagues. Demonstrating that TNF, and IL-1β cytokine stimulation, and LPS stimulation of TLR4, resulted in PAR2 upregulation both at the mRNA and functional protein level. Through the use of adenoviruses to inhibit specific points in the MAPkinase and NF-κB signalling pathways, they also found that PAR2 upregulation post-cytokine stimulation was dependent on p38 MAP kinase protein[40]. This study also identified self-regulation of PAR2 expression. Stimulation with PAR2 activating peptides also resulted in increased PAR2 expression. As the cell type responsible for the recruitment of immune cells to sites of tissue inflammation from the peripheral blood, the increased PAR2 expression during inflammatory responses in this cell type gives a further indication of a role for this receptor during inflammation.

Overall PAR2 has a clear association with digestion, the GI tract, and the immune system. The functions of this receptor within these systems are diverse and very much cell type specific. The focus of this thesis was to investigate the role of PAR2 in bone turn over and inflammatory bone erosion and thus the role of PAR2 in the immune system will be further expanded upon below.

1.4.4 Immunological Functions of PAR2

In the last decade PAR2 research has demonstrated a strong link between this receptor and innate and adaptive immunity. The connection between these has been established in a number of leukocyte populations from both innate and adaptive arms of the immune system. Protein and mRNA expression of PAR2 has been identified on human eosinophils[267], neutrophils[268], mast cells[269], monocytes[270], macrophages[271,272] and T cells[273]. Non-hematopoietic cells with a close relationship to leukocytes and relevant roles in leukocyte migration and activation, such as endothelial cells (as mentioned previously in section 1.4.3) and fibroblasts also express PAR2[274,275]. It is also of note that in most of these cell types' qPCR and western blotting techniques were employed to identify the presence of this receptor, and while these techniques provide evidence of the presence of this receptor in these cells, they do not provide information regarding the location within the cell (e.g. cell surface or cytoplasmic). By adopting flow cytometry approaches Rachel Steven and colleagues[271], identified PAR-2 receptors in human monocyte-derived macrophages, discriminating between intracellular (70% of cells) versus cell surface PAR2 expression (~20% of cells). Subsequent investigation of this intracellular expression in peripheral blood monocytes confirmed that intracellular stores of PAR2 are present and can be trafficked to the cell surface in response to stimulation[270]. Indicating that PAR2 responses could be a form of early response mechanism, which may be relevant to many immune cells, especially those of the innate arm that already have established fast response mechanisms to inflammatory cues.

As well as expression, a functional role for this receptor in these cell populations has also been reported. In order to identify the functional role of this receptor a PAR2 deficient mouse was generated. Using homologous recombination, a null allele of the PAR2 gene was created in embryonic stem cells creating a homozygote KO[276]. Through the use of *par2*$^{-/-}$ mice and PAR2 agonists (SLIGKV-

NH2), and inhibitors (ENMD-1068, SAM-11), the functional role of this receptor in inflammation has been interrogated in both *in vivo* models and *in vitro* cell culture systems. Agonist-mediated activation of PAR2, on leukocyte populations has been shown to induce cytokine production; such as IL-6 in T cells[277], IL-6 and IL-8 release from endothelial cells[278], increased LPS driven TNF production in macrophages[271], and interestingly drive IL-1β, IL-6, and IL-8 production in human peripheral blood monocytes[270]. In addition, PAR2 activation has been shown to drive the release of reactive oxygen species (ROS) and generation of prostaglandins via cyclooxygenase (COX) activation[279]. It has also been associated with increased vascular perfusion[280], a trait characteristic of inflammation, which aids in leukocyte infiltration. The interaction between endothelium and leukocytes is also a key relationship in initial inflammatory responses for leukocyte migration and both of these cell types express PAR2. A study conducted by Bernstein and colleagues (2000) found that *par2*$^{-/-}$ mice exhibited delayed inflammatory response to surgical trauma, characterised by delayed leukocyte rolling, adhesion, and extravasation into tissue[281]. This was not an isolated finding; a study prior to this demonstrated that topical administration of the rodent PAR2 agonist (SLIGRL-NH2) to murine mesentery induced a 3 fold increase in leukocyte adherence to the venule and a significant increase in polymorphonuclear leukocyte extravasation into the peritoneal cavity[282]. Therefore, it is clear that PAR2 activation is able to promote trans-endothelial migration of leukocytes via activation of endothelium, leukocytes, or both. However, this process has not been fully explored and it would be interesting to investigate how elements of the leukocyte recruitment process are altered by PAR2 activation, for example chemokine receptor and adhesion molecule upregulation. These studies collectively confirm that PAR2 plays a role in early and acute inflammatory responses.

The use of *par2*$^{-/-}$ mice has also given us a clear indication that this receptor does not only contribute to acute inflammation but is also crucial in chronic inflammation. Multiple murine inflammatory disease models fail to establish or were significantly abrogated in *par2*$^{-/-}$ mice. This included neuroinflammation[283], and atopic skin models[284], where a significant reduction in infiltrating immune cells to the skin was observed. The most well-defined association between PAR2 and chronic inflammation, however, comes from models of rheumatoid arthritis;

a classic, chronic inflammatory condition characterised by swelling and destruction of the synovial joints (see section 1.4.6).

1.4.5 Role of PAR2 in Bone Biology

PAR2 has reported expression on cells of the skeletal system, such as OBs[285], skeletal stromal cells (pre-OB)[75], and monocytes [286](OCP). There are currently no studies confirming the presence of PAR2 protein on OCs, however, it has been shown that the PAR2 transcript is increased in RAW264.7 upon RANKL incubation[75]. Skeletal cells, such as OBs, OCs, or osteocytes, themselves are not known producers of PAR2 activating proteases. However, OCs are highly proteolytic in nature, and some of the proteases these cells produce could potentially activate PAR2. A study comparing the production of proteases within *in vitro* cultures of BM-derived macrophages and OC, outlined a panel of proteases produced by OC but not by macrophages. This list did not contain any confirmed PAR2 activating proteases, but did contain serine proteases and various cathepsins. It is therefore possible that some of these identified proteases may be unidentified PAR2 activators. In addition, there may be PAR2 activating proteases produced by both BM-derived macrophages and OCs, which were not identified due to non-differential expression [287]. While there have been no confirmed PAR2 activating proteases produced by OCs or OBs, there has been reported expression of PAR2 activating proteases in BM cells[76]. Total BM cell isolates contained trypsin, matriptase, acrosin, and kallikrein 4, indicating that the skeletal environment will contain PAR2 activating proteases. During inflammation that is associated at or near the bone site, such as that observed in osteomyelitis, septic arthritis, or chronic autoimmune conditions such as RA, the influx of active immune cells could result in the release of alternative PAR2 activating proteases. Cells such as neutrophils, mast cells, and macrophages will be active at these sites. These cells are known producers of canonical and non-canonical PAR2 activating peptides, such as matriptase, neutrophil elastase, and cathepsin G. This change in the microenvironment is likely to influence the PAR2 signals received.

Numerous studies of the functional role of PAR2 in the skeleton have been conducted. However, this research has often identified contradictory roles for this receptor within the skeleton. Thus, the fundamental role of PAR2 in bone

biology is still not fully understood. Gross analysis of the skeleton of *par2*$^{-/-}$ mice, does not reveal any overt abnormalities. For example, observable phenotypes include; a slight enhancement in tibial length in young *par2*$^{-/-}$ males, which is normalised by 90 days; an increase in bone volume, including enhanced cortical thickness, and trabecular area in young (50 days old) *par2*$^{-/-}$ animals which subsequently resolved by 90 days old[76]. Combined, this data provides an indication that there are subtle bone phenotypes as the result of a lack of PAR2. This could suggest that the absence of PAR2 results in reduced or enhanced rates of bone turn over, which may not result in an overt phenotype of the skeleton but does impact the activity of OCs and OBs. In support of this, the observation of a reduced number of both OBs and OCs in *par2*$^{-/-}$ trabecular bone, may indicate a reduced rate of bone turn over in these animals[76]. Overall, during homeostasis *par2*$^{-/-}$ animals do not present with overt skeletal abnormalities. However, subtle changes in architecture and cell number in the skeleton of KO animals indicates a minor influence of a lack of this receptor in this system, the impact of which may be more overt during disease states.

The first studies interrogating the role of PAR2 in OCs employed whole BM osteoclastogenesis *in vitro* assays. In these studies, the whole BM was stimulated with OB survival and differentiating factors such as PTH and VitD. This is known to drive the expansion and differentiation of OBs, which produce OC stimulatory factors such as M-CSF and RANKL, and in turn stimulates BM OCPs to differentiate into OCs. This *in vitro* culture system is a classical OB/stromal-driven OC differentiation assay. With this experimental procedure the authors found that PAR2 stimulation via activating peptides of the whole BM culture inhibited the differentiation of OCs. The proposed mechanism of this was that PAR2 activating peptide inhibited RANKL expression, as demonstrated with decreased tnfsf11 transcript levels and unaffected OPG expression[75]. They concluded that PAR2 activation prevented OC differentiation by suppressing transcription of OC activating RANKL. A complementary study was also conducted looking at the impact of PAR2 alone. PAR2 activation of OB stimulated enhanced transcription of collagen type 1. Thus, together this data suggests that PAR2 prevents bone resorption and enhances the production of osteoid components, so overall promoting bone formation and inhibiting bone resorption.

Subsequent osteoclastogenesis assays were conducted in 2012, using a culture system that directly promoted OC formation in BM cells using M-CSF and RANKL. This study found that BM macrophages isolated from *par2*$^{-/-}$ animals had a reduction in osteoclast formation, as measured by the number of TRAP^{+} OC formed. Indicating that in this context PAR2 was stimulating OC formation, which contradicted previous thoughts on the role of this receptor in bone turn over. Overall, the research conducted suggests that PAR2 activity in OB suppresses their capability to form OCs, while PAR2 activity in macrophage/OC cells appears to enhance OC differentiation. All of this work was conducted in homeostatic conditions, however, the proteases present during inflammation may change the way this receptor operates during inflammatory assault, or indeed during alternative less inflammatory bone pathologies such as OA.

Murine models of OA conducted in *par2*$^{-/-}$ animals have demonstrated that this receptor plays a key role in pathogenic bone formation in this context. For instance, *par2*$^{-/-}$ animals are protected from both osteophyte formation, with a reduction in the size and number of osteophytes formed, and also from osteosclerosis[288]. OB isolated from OA patients have enhanced PAR2 expression and in response to PAR2 activating peptides they produced increased levels of MMPs and IL-6, as well as increasing expression of membrane bound RANKL[289]. This enhanced RANKL expression translated into an enhanced capability to stimulate OC differentiation when OA osteoblasts were co-cultured with PBMCs. These studies indicate that in OA and OA-like models PAR2 contributes to both pathogenic bone formation, and also pathogenic bone resorption. This contrast in conclusions demonstrates a contradicting literature with regards to PAR2 and pathogenic bone biology.

1.4.6 PAR2 in Murine Experimental Models of Arthritis

The first ‘proof of concept’ that PAR2 has a direct role in chronic inflammatory arthritis was demonstrated via PAR2 deficient mice. Using these animals Ferrell and colleagues developed an adjuvant (Freund’s complete adjuvant) induced mono-arthritis model in WT, *par2*$^{-/-}$ homozygote and through backcrossing of homozygotes, *par2*$^{-/+}$ heterozygote mice. This innate immune mediated arthritis model revealed almost complete ablation of arthritis in the *par2*$^{-/-}$ compared to WT mice, with the heterozygotes demonstrating an intermediate phenotype[276].

This paper also demonstrated via PAR2 agonist treatment, that direct stimulation of PAR2 in the joint resulted in a significant pro-inflammatory effect with prolonged joint swelling and increased synovial blood perfusion. Using β-galactosidase incorporation into the PAR2 gene region this group also demonstrated that in the articular tissue from the adjuvant-induced arthritis model in WT mice, PAR2 was substantially upregulated in extravascular tissue unlike the uninflamed model in which PAR2 expression was limited to the endothelium[276]. This was the first study to find a direct link between PAR2 and a chronic arthritis, demonstrating both correlation between inflamed tissue and a functional role in induction of an inflammatory pathology. This opened many possibilities for the role of PAR2 in the innate system and warranted further investigation of its mechanistic role in inflammatory disease. In addition to the mentioned findings, this study also provided a proof of concept that isolated PAR2 depletion could inhibit inflammatory disease and confirmed its potential as a therapeutic target. However, it should also be appreciated that when an alternatively generated *par2*$^{-/-}$ mouse was used for further investigation in various innate and adaptive murine models of arthritis by Busso and colleagues in 2007, they found no significant alteration in inflammatory response in the equivalent innate immune model they induced[290], contrary to the pro-inflammatory role in innate immunity theory proposed by the Ferrell group. Instead they proposed that PAR2 was possibly only relevant in antigen-specific, adaptive models of chronic inflammation. There were multiple variables that differed between the 2 studies that make their results possibly non-comparable. Firstly it could be argued that the genetic addition of ß-galactosidase[276], not present in the Busso murine model may alter PAR2 expression or action in some way. Perhaps a more likely explanation was that the differences in model induction between the 2 papers resulted in a more severe model in the Ferrell paper compared to Busso et al., which in turn may give a more obvious difference between wild type and *par2*$^{-/-}$. Importantly, subsequent studies of the role of PAR2 in murine arthritis models have further indicated a pro-inflammatory role for this receptor in inflammatory arthritis models.

The immunological role of PAR2 in murine RA models was further investigated by Ferrell and colleagues using the collagen induced arthritis (CIA) model in DBA/1 mice[291]. This is considered a gold standard, reliable model of inflammatory RA

that activates the murine adaptive immune responses against type II collagen. Due to a lack of PAR2 KO on the CIA susceptible mouse strain DBA-1, prophylactic treatment of PAR-2 inhibitors (both small molecule ENMD-1068, and monoclonal antibody SAM-11) were employed prior to model induction[291]. The result of this PAR2 inhibition was a highly significant reduction in arthritis score compared to the vehicle-treated models, and lymph node cell suspensions isolated from PAR2 inhibited mice had significantly reduced IL-17 and IFNγ levels. Trending inhibition of TNF, IL-1β, IL-6, IL-12, CCL3, and GM-CSF was also observed, and titres of anti-collagen antibodies were significantly reduced in PAR2 inhibited models[291]. This study provided evidence in support of PAR2's immunological role in inflammatory disease, pinpointing reductions in key inflammatory associated cytokines and linking a role for PAR2 to the induction of adaptive antibody responses.

As the inflammatory role of PAR2 became more evident, the source of its activating proteases in the context of inflammatory joint disease models gained interest. Mast cells present one potential source of PAR2 activating proteases. The ability of mast cell granules to activate PAR2 was demonstrated using KO animals. Administration of compound 48/80 to induce mast cell degranulation in mice induced significant vasodilation in WT animals, but failed to exert these actions in *par2*$^{-/-}$ [292]. Mast cells significantly contribute to the murine collagen induced arthritis model (CIA) of RA. Pre-clinical depletion of these cells in CIA reduces inflammation and inflammatory cytokine expression in this model[293]. In addition, mice that lack the dominant mast cell tryptase also experience attenuated forms of inflammatory arthritis models, however this is not dependent upon PAR2[294].

Overall it is evident from studies conducted in mouse models that PAR2 plays a significant role in arthritis and inflammation models; the mechanistic role of this receptor in the immune system and within this inflammatory disease is still under scrutiny. The immune cell types that mediate the pro-inflammatory effects of PAR2 activation in inflammatory arthritis, and the mechanism by which these PAR2 activated cells induce inflammation, are still unclear. Accordingly, ongoing work is investigating the cellular mechanisms of this

relatively new inflammatory associated receptor in the pursuit of a potential new therapeutic target for arthritic disease.

1.4.7 PAR2 in RA

Work on murine models established proof of concept that PAR2 influences the inflammatory aspect of murine models of arthritis and enabled *in vivo* investigation of the immune influence of PAR2. However, it is important to be able to translate these findings into human systems and find relevance for in human disease. Using immunohistochemistry (IHC) for protein detection and transcript analysis via PCR, enhanced expression of PAR2 was identified in RA articular biopsies compared to osteoarthritic (OA) tissue[290]. This provided the first indication that PAR2 upregulation during inflammatory disease was not isolated to mice but also found in human tissue. This led onto further studies of human articular samples which demonstrated that PAR2 expression also positively correlated with synovitis scores in human patients[295]; further implicating this receptor in RA pathology. This could potentially be either as a by-product of the inflammatory environment or directly contributing to the chronic inflammation.

In addition to enhanced expression of PAR2 in RA tissue, there is also increased levels of serine proteases which activate this receptor in this disease setting. A substantial increase in the number of synovial mast cells in RA patients has been previously established[296] and their role in promotion of inflammation in the joint has been linked to the release of granule stored mediators such as histamine, heparin and proteases. These cells therefore represent a possible source of PAR2 activating proteases. As mentioned above (see section 1.4.6), mast cell degranulation activates PAR2. In RA patients, mast cells are in high abundance and co-localise with PAR2 expressing cells in inflamed articular tissue; mast cells in these tissues were also found to possess PAR2, suggesting possible self-activation[292]. This evidence supports further investigation of the hypothesis that mast cells contribute to the pathogenesis of inflammatory arthritis via PAR2 activation induced by release of proteases.

This enhanced expression in human diseased tissue provoked further mechanistic studies to dissect the pathways influenced by this receptor's activation in RA

patients. Crilly and colleagues investigated PAR2 cell surface expression on circulating $CD14^+$ cells (identified as monocytes) in both RA patients in remission or in those flaring. They found that PAR2 expression on patient monocytes positively correlated with classic signs of disease flare such as erythrocyte sedimentation rate (ESR) and C reactive protein levels (CRP). Furthermore, this study also identified that high PAR2 expression in circulating monocytes from RA patients was subsequently inhibited post-NSAID treatment [270,297]. This direct correlation between receptor expression and circulating PB monocytes is interesting as it goes beyond expression at the primary site of inflammation in this chronic disease. As mentioned previously (section 1.3.1) RA is a systemic inflammatory environment, so this enhancement of PAR2 expression could be a reflection of a response to inflammatory mediators within the blood. It could also indicate that monocytes are primed either within the PB or prior in the BM, driving this enhanced expression. Suggesting that these cells may have the potential to respond differently, or have a greater response to proteases present within the swollen joint. The functional effect of PAR2 activation in human monocyte-derived macrophages gave an indication of the role of upregulated PAR2 in active disease monocytes[271]. Human macrophages were treated with PAR2 agonist SLIGKV *in vitro* and subsequent phenotypic analysis of the cells found an altered cytoskeleton and enhanced TNF production with and without LPS stimulation[271], confirming that enhanced PAR2 expression on monocytes reported by Crilly et al. [297] translates to a functional impact on the cells.

The importance of altering macrophage activity in the inflamed RA joint should not be underestimated. Many of the biologic treatments currently in trials or being used clinically target macrophage activating factors or their pro-inflammatory products. Monocyte-derived macrophages are a large proportion of the inflammatory infiltrate in the inflamed synovium, and embryonically-derived macrophages are resident within the synovial membrane. These immune cells contribute to the inflammatory milieu through production of cytokines such as TNF, IL-6, and IL-12, as well as promoting leukocyte infiltration through chemokine production (CCL-2 and CCL-3). Successful RA treatment also correlates with reduced macrophage infiltrate to the synovium, to the extent that it is considered a robust biomarker of treatment responsiveness[298]. Therefore, targeting a receptor that activates these and potentially other cells

of the immune system is a very attractive small molecule approach to inhibiting inflammation in RA patients. As such, PAR-2 represents a possible therapeutic target which encompasses macrophages and other innate cells to inhibit the cytokine network.

1.5 Hypothesis and Aims

The family of protease activated receptors were discovered throughout the 1990's. These receptors respond dynamically to the protease environment and have highlighted a novel function of proteases acting as hormone-like mediators to influence cellular function. Of this family PAR2 has the strongest associations with the immune system and inflammation. PAR2 is activated by a different group of proteases compared to its counterpart PAR1, with most if not all of the proteases being more highly associated with immune function. Moreover, PAR2 is prominently expressed on immune and stromal cells that commonly interact with each other. In addition, this receptor has been linked to inflammatory disease, with *par2*$^{-/-}$ animals experiencing milder symptoms of disease models. Human tissue samples from people experiencing chronic inflammatory diseases such as asthma, and RA also have enhanced expression of this protease receptor. This heightened expression is most prominent in the monocyte compartment where RA patients have increased PAR2 surface expression on their monocytes that is further enhanced when patients are hospitalised in a flare episode.

The mechanisms that drive enhanced PAR2 expression in human monocytes during inflammatory stress is not known. Moreover, the function of PAR2 in monocytes and it's effect on their potential to differentiate into osteoclasts, remains poorly defined. Monocytes are a key cell type trafficked to the inflamed RA joint. Upon arrival at the inflamed articular tissue these cells receive signals to differentiate into osteoclasts; the drivers of irreversible bone destruction in RA. Finally, osteoclasts are a proteolytically active cell, required to produce an abundance of proteases in order to complete their functions in bone resorption.

In light of this, we hypothesise that systemic inflammatory mediators within the PB of RA patients enhances the expression of PAR2 in circulating monocytes of these patients. Upon entering the inflammatory joint these monocytes will receive signals to undergo differentiation into bone resorbing osteoclasts within a proteolytically active inflammatory joint. The heightened expression of PAR2 on these cells and the protease rich environment may influence the differentiation of monocytes into osteoclasts.

The aim of this thesis was to test this hypothesis. In order to do so the following questions were proposed:

- Do inflammatory mediators enhance surface expression of PAR2 in human monocytes?
- What impact does the loss of PAR2 have on osteoclastogenesis?
- Does an inflammatory environment influence the impact of PAR2 on osteoclastogenesis?

Using murine PAR2 knock out mice, this thesis attempted to understand the function of PAR2 in the process of osteoclast differentiation from monocyte precursors during both homeostasis and inflammation. This was then translated to human cells through the use of PAR2 activating peptides and inhibitors during *in vitro* OC differentiation assays.

2 Materials and Methods

2.1 Human Study Methodology

2.1.1 1321N1 Cell line

2.1.1.1 Cell Culture

Human astrocyte cell line 1321N1 was transferred from collaborators at AstraZeneca. This cell line was originally obtained from European Collection of Authenticated Cell Cultures (Public Health England; UK) and was stably transfected with human PAR2 (hPAR2) and antibiotic resistance to Geneticin (G418) at AstraZeneca. The founder cell line was also maintained as a negative control for the hPAR2 stable transfection. These cells were seeded at $2x10^6$ cells per $75cm^2$ flask and cultured in complete Dulbeccos Modified Eagle Medium (DMEM, Invitrogen; UK, see appendix) and split twice weekly. Transfected cells were also cultured in the presence of 600ug/ml of G418 antibiotic (Thermofisher Scientific; UK) to select for successfully transfected cells. When 1321N1 cells reached 70-80% confluency they were split 1:5, or used for downstream applications.

2.1.1.2 PAR2 expression via Western Blot

1321N1-hPAR2 and naïve 1321N1 cells were harvested from $75cm^2$ tissue culture flasks using TrypLE. In brief, cells were washed with PBS to remove remaining media, before incubation at 37°C in 5ml of trypsin replacement cell dissociation buffer TrypLE (ThermoFisher Scientific; UK. #12605010). This buffer was selected as an alternative to trypsin in order to limit trypsin dependent PAR2 activation. Cells became detached from the plastic surface after 5-10 minutes of incubation and were transferred to 50ml falcons and topped up with 5ml media to limit any further protease activity of the dissociation buffer. These cells were counted manually using a haemocytometer with trypan blue (Sigma-aldrich; UK) dead cell exclusion, and $2x10^6$ cells were washed twice in PBS and resuspended in 200μl of RIPA buffer (see appendix). Lysates were incubated for 30 minutes on ice and centrifuged at 17,000g for 10 minutes. The protein lysate was aspirated and stored at -20°C (short term) or at -80°C if for long term storage; the pellet was discarded.

Protein concentration was measured using the Pierce BCA Protein assay kit (Thermo Scientific, UK) according to manufacturers' instructions. In brief, reagent A and B were mixed 50:1, and a standard curve of known concentrations (25-2000μg/ml) of BSA protein in RIPA buffer prepared. The BCA reagent (200μl) was mixed with 25μl of each sample and the standard curve. This reaction was incubated for 30 minutes at room temperature and the colour change measured on a colorimetric plate reader at 562nm. From this the standard curve was plotted against the detected wavelengths and a line of best fit applied. The equation of the line was applied to sample wavelengths and the concentration of protein contained in each sample determined.

The volume of lysate required for 30μg of protein was calculated and this was taken forward for gel electrophoresis. Protein was reduced using NuPAGE Sample Reducing agent (Thermo Fisher;UK #NP0004) and denatured using NuPAGE LDS sample buffer (Invitrogen; UK #NP00007) and brought to 95°C for 5 minutes. Samples and 5μl of a broad range pre-stained protein marker were loaded onto a 12 well Novex Bis-Tris 4-12% poly-acrylamide gel (Invitrogen; UK #NP0322BOX) and run at 120 volts for approximately 1 hour. Gels were transferred to PVDF membranes using the iBlot2 dry transfer system (Invitrogen; UK) and the presence of protein on the membrane checked using Ponceau S. Briefly, Ponceau S. was poured onto the membranes after protein transfer; this rapidly stains available protein, presenting as bands of pink/red dye. The stain is easily reversible. Washed in water and with gentle agitation the stain is removed. After checking for successful protein transfer the blots were washed (PBS-T) and incubated in blocking buffer (PBS-T 5% milk) at room temperature for 1 hour. Anti-PAR2 antibodies listed in Table 2.1 were diluted in PBS-T 5% BSA at differing concentrations dependent on manufacturers guidance (see Table 2.1). Blocking solution was removed and membranes were incubated with diluted antibodies overnight at 4°C with gentle shaking. Membranes were subsequently washed in PBS-T 5 times, each wash 10 minutes on a shaker. Secondary antibodies, anti-rabbit HRP (Cell Signalling Technology; UK #7074S) and anti-mouse HRP (Santa Cruz; USA #sc-2371), were diluted in PBST 5% BSA (for dilution concentrations see Table 2.1). Membranes were incubated in secondary antibody for 2 hours at room temperature. Following this a series of 5 washes was repeated as above. West Femto substrate (Thermofisher Scientific; UK #34095) was add to the

membrane surface and incubated for 1 minute in the dark. Bands were visualised using the LI-COR Chemi-luminescence detection system (LI-COR Biosciences, UK). The pre-stained ladder bands were marked with the WesternSure Pen (LI-COR Biosciences; UK #P/N 926-910000) to be visualised at the same time. Further quantitative analysis of blots was performed using ImageJ.

Table 2.1 Western Blot Antibodies

Specificity	Clone	Concentration (µg/ml)	Supplier	Dilution (v/v)
PAR2	SAM-11 D61D5 Polyclonal	200 250 600	Santa Cruz Biotechnology Cell Signalling Technology Alomone Labs	1:500 1:1000 1:500
Phospho-ERK(1/2) (Thr202/Tyr204)	D13.14.4E	500	Cell Signalling Technology	1:2000
ERK (1/2)	137F5	80	Cell Signalling Technology	1:1000
Rabbit IgG (HRP)	Polyclonal	Unknown	Cell Signalling Technology	1:1000
Mouse IgG (HRP)	Polyclonal	400	Santa Cruz Biotechnology	1:5000

2.1.1.3 1321N1 Fluorescent Microscopy

Naïve and stably transfected 1321N1 cell lines were cultured on 8 well glass chamber slides (Thermofisher Scientific; UK #154534PK) for 2 days to allow adherence while preventing over confluence. Medium was aspirated and cells were fixed with 4% paraformaldehyde in PBS for 10 minutes at room temperature, then washed 3 times for 5 minutes each. Cells were permeabilised with PBS 0.2% Triton X-100 for 5 minutes at room temperature and washed as above. Samples were blocked using 1X PBS 5% goat serum 0.1% Tween 20 for an hour at room temperature. The primary antibodies were prepared in antibody dilution buffer (1x PBS 1%BSA 0.1% Tween) at the following concentrations; D61D5 1:25 (Cell Signalling Technology; UK #6976), SAM-11 1:50 (Santa Cruz; USA #sc-13504), Alomone polyclonal 1:200 (Alomone Labs; Israel #APR-032); blocking solution was aspirated and antibodies incubated with the cells overnight at 4°C. The following day AF488 fluorochrome-conjugated secondary antibodies (anti-

rabbit and anti-mouse) were prepared in antibody dilution buffer at 1:500 dilution. Samples were washed in 1xPBS 0.1% Tween three times for 5 minutes each and secondary antibody incubated for 1 hour at room temperature. Washing was repeated as above and chambers removed from slides. DAPI mounting media (Vector Laboratories; UK. Vectasheild #H-1200-10) was used to mount coverslips to the glass slides and cells were imaged using EVOS FL Auto. Control wells that contained secondary only antibody or isotype antibody were used to confirm specific staining.

2.1.1.4 PAR2 detection via Flow Cytometry

1321N1 cells were either left untreated or treated with FLIGRL (2μM, Tocris; UK) for 20 minutes and then removed from the cell culture plastic surface using TrypLE (Thermofisher Scientific #12605010), as described in section 2.1.1.2. Immediately post dissociation, cells were washed in PBS, and incubated with DAPI live dead stain (CyStain DNA 2 Step, Sysmex; UK) in PBS for 15 minutes, some cells were heat killed at 65°C for 5 minutes as a positive control for staining. Cells were washed and maintained in suspension in FACS buffer (1% FBS, 1mM EDTA, 0.5% sodium azide) and incubated with 1μl of D61D5 (CST; UK) or 2μl SAM-11 PE (Santa Cruz; US) for 45 minutes on ice. Cells were washed again in FACS buffer and samples which had been stained with D61D5 clone were incubated with 1μl of secondary anti-rabbit AF647 for a further 45 minutes on ice. Further washes in FACs buffer were conducted and samples were fixed in Cell Fix (BD Biosciences; UK #340181) for 20 minutes before running samples on the LSR II.

Intracellular PAR2 stains were also conducted in these cells. In this instance live/dead stain was not performed and cells were permeabilised with Cytofix/CytoPerm (BD Biosciences; UK #554714) for 20 minutes at 4°C. Cells were washed in perm/wash buffer before intracellular staining of D61D5 (1μl) or SAM-11 PE (2μl) was conducted in perm/wash buffer for 1 hour on ice. Samples were washed in perm/wash buffer and secondary staining conducted on the D61D5 stained samples, samples were incubated in 1μl anti-rabbit for 45 minutes on ice in perm/wash buffer. All samples were washed again in perm/wash and

then reconstituted in FACs buffer to run on the LSRII (BD; UK). All Flow Cytometry samples were analysed using FlowJo software.

2.1.2 Primary Human Cells

2.1.2.1 RA patients and healthy donors

Human blood samples were acquired from buffy coat obtained directly from the Scottish National Blood Transfusion Service (SNBTS) from healthy volunteers who had granted informed consent at the transfusion service. Alternatively, healthy volunteer samples were collected fresh at the Glasgow Biomedical Research Centre (GBRC); with informed consent from a trained phlebotomist. Rheumatoid arthritis patient samples were collected from the peripheral blood of individuals attending rheumatology clinics within Greater Glasgow and Clyde; with informed consent taken by trained physicians. Recruitment of these individuals was conducted by trained medical professionals in the Great Glasgow and Clyde district, primarily by Dr. James Robertson. RA patients with both active disease and those in remission were recruited for this study, patients were also on a variety of treatments with most patients on DMARDS but not on biologics. All samples were obtained after written consent, with appropriate ethical approvals in place.

2.1.2.2 PBMC Isolation from Human Blood

Human Peripheral Blood Mononuclear Cells (PBMCs) were isolated from buffy coat or fresh blood samples via density gradient centrifugation. In brief, 9ml of freshly isolated blood was carefully layered directly onto 3ml of ficoll (Sigma-aldrich; UK), avoiding mixing. Buffy coat was diluted 1:1 in PBS (Gibco; UK) prior to layering and then the same protocol was followed for both. Layered blood samples were centrifuged at 400g for 30 minutes with no brake in order to separate each blood fraction; this results in erythrocytes at the bottom, followed by a layer of ficoll, PBMCs are less dense and thus form a layer above the ficoll, and finally this is topped with plasma. All centrifugation steps were conducted at room temperature, with a swing out rotor unless stated otherwise. Using a Pasteur pipette the serum upper layer was removed to within 1cm of the PBMC layer and discarded. The buffy coat layer was then isolated by eye, again using a Pasteur pipette and transferred into a fresh 50ml falcon tube (Corning, UK), and red blood cells were discarded. The PBMCs were washed twice in PBS, first with a low centrifugal force of 200g for 10 minutes in order to wash off any remaining serum from the cells, then a second faster spin at 400g for 5 minutes.

At this point cells were counted using the traditional haemocytometer method with trypan blue (Sigma-aldrich; UK) dead cell exclusion and resuspended at $1x10^7$ cells/ml in FACs buffer or cell culture media (RPMI, 10% FBS, 1% Penicillin/streptomycin, 1% L-glutamine). To perform a cell count 50 μl of cells (currently in 10ml of PBS) were mixed with 200μl of PBS and then 50μl of this 1:5 diluted cell solution was mixed with 50μl Trypan blue, giving a final dilution of 1:10. 10μl of this cell dilution was added to a haemocytometer and a light microscope used to count (EVOS, Thermofisher Scientific; UK).

2.1.2.3 Flow Cytometry

PBMCs were washed in PBS and a sample of cells were heat killed at 65°C for 5 minutes for a positive control for a live/dead stain. All samples, excluding an unstained control of PBMCs were then stained with DAPI dead cell stain (CyStain DNA 2 Step, Sysmex; UK) for 15 minutes on ice. Cells were washed in FACS buffer and Fc receptors were blocked using 1:10 dilution of human FcR Blocking Reagent (Miltenyi Biotech; UK. #130-059-901) and incubated on ice for 10 minutes. Surface marker staining to discriminate monocytes from other PBMC cells was employed and the cocktail of antibodies used for this are listed in Table 2.2. In addition to cell markers, cells were also stained with the D61D5 clone for PAR2 detection, keeping one sample for each donor negative for this stain. Surface stain was conducted on ice for 45 minutes and samples are washed in FACS buffer. A secondary antibody stain was conducted with anti-rabbit AF647 (Biolegend; UK), 1:50 dilution in FACS buffer, again for 45 minutes on ice. Samples are again washed in FACS buffer and finally fixed in Cell Fix (BD; UK) for 20 minutes before acquiring on the LSRII. Intracellular stains were also conducted in these cells, for this the live dead was not conducted, surface stains for cell markers were still performed and permeabilization and intracellular staining procedure was conducted from here. This protocol is outlined in 2.1.1.4.

Peripheral blood samples were collected over an extended period of time, however, the samples were processed and run on the flow cytometer immediately. The flow cytometer fluctuates subtly over time meaning that using the same settings (voltage and compensation set up) may actually result in different detection levels over time. In order to allow comparison between samples processed at different times and to limit the impact of machine

fluctuation over time, an application settings method of experimental set up was adopted. Thus, initial set up of voltages and compensation are subtly adjusted by the machine over time so that for example, the mean fluorescence intensity (MFI) that would have been detected for sample 1 on day 1 would be the same if sample 1 were run on day 135. Thus limiting the technical impact of long term sample collection.

Samples were prepared in the same way to run on the ImageStream (Luminex; USA). All Image Stream samples were analysed using "IDEAS" software (Merck Millipore; UK).

Table 2.2 Antibody Panel for PAR2 Detection in Human Monocytes.

Specificity	Fluorescent label	Clone	Concentration (μg/ml)	Supplier	Catalogue Number	μl/sample
CD14	BV605	M5E2	150	BioLegend	301834	2
CD16	V500	3G8	Unknown	BD Horizon	561394	2
HLADR	PE Cy7	G46-6	Unknown	BD Pharmingen	560651	2
CD3	FITC	UCHT1	Unknown	BD Pharmingen	555332	10
CD19	FITC	HIB19	Unknown	BD Pharmingen	555412	10
CD56	FITC	B159	Unknown	BD Pharmingen	561905	2
CD15	FITC	HI98	50	BioLegend	301903	2
PAR2	N/A	D61D5	250	Cell Signalling Technologies	6976S	1
Rabbit IgG	AF647	Poly4064	100	BioLegend	406414	1

In addition, human PBMCs were also stained for integrins in conjunction with PAR2. In this instance isolated PBMCs were resuspended at $1x10^6$ cells/ml in complete RPMI and 1ml of cells put into 6ml lidded FACS tubes. PBMCs were left unstimulated, stimulated with 100ng/ml of LPS (Salmonella ? source; Invivogen; UK), 100ng/ml PMA (Abcam; UK), 2μM FLIGRL, or 3μM AZ8838 for 90 minutes at 37°C and then immediately put on ice to prevent modulation of surface proteins.

The same staining procedure was followed as above, with a live/dead DAPI stain, followed by FcR block, followed by the antibody cocktail found in Table 2.3. No intracellular staining was conducted with the integrin staining procedure. Cells were left unfixed in FACS buffer and ran on the LSRII within 2 hours.

Table 2.3 Antibody Panel for Integrin and PAR2 Detection in Human Monocytes.

Specificity	Fluorescent Label	Clone	Concentration (μg/ml)	Supplier.	Catalogue Number	μl/sample
CD14	BV605	M5E2	150	BioLegend	301834	2
CD16	V500	3G8	Unknown	BD Horizon	561394	2
HLADR	PE Cy7	G46-6	Unknown	BD Pharmingen	560651	2
CD3	FITC	UCHT1	Unknown	BD Pharmingen	555332	10
CD19	FITC	HIB19	Unknown	BD Pharmingen	555412	10
CD56	FITC	B159	Unknown	BD Pharmingen	561905	2
CD15	FITC	HI98	50	BioLegend	301903	2
PAR2	N/A	D61D5	250	Cell Signalling Technologies	6976S	1
Rabbit IgG	AF647	Poly4064	100	BioLegend	406414	1
CD18	PerCP Cy5.5	TS1/18	200	BioLegend	302119	2
CD11a	PerCP	TS2/4	200	BioLegend	350608	2
CD11b	PE TR	ICRF44	100	BioLegend	301347	2
CD11c	AF700	Bu15	200	BioLegend	337220	2
αVβ3	PE	23C6	200	BioLegend	304406	2

2.1.2.4 Protein Lysis, Quantification, and Western Blot

PBMC samples were maintained in suspension in complete RPMI (10% FBS, 1% L-glutamate, 1% Penicillin/Streptomycin) at 37°C and stimulated with FLIGRL (2μM, Tocris Bioscience; UK), PMA (100ng/ml), or left unstimulated. Stimulations were conducted in a time course ranging from 2 to 90 minutes (2, 5, 15, 30, 60, 90 minutes) of FLIGRL exposure, and PMA stimulation for 15 minutes. Stimulations were stopped with 8% paraformaldehyde (PFA) diluted 1:1 in cell

suspensions. Fixed cells were then centrifuged at 500g for 5 mins and the fixative discarded. From this point onwards the same protocol was followed as described in 2.1.1.2. Instead of incubation with anti-PAR2 antibodies, membranes from the PBMC stimulation experiments were incubated with antibodies against phopho-ERK and total ERK protein. These antibodies were diluted in PBS-T 5% BSA, details and working concentrations of these can be found in Table 2.1.

2.1.2.5 Monocyte Isolation

PBMCs isolated from blood samples were counted, using trypan blue exclusion of dead cells, and resuspended in cell separation buffer (CSB, PBS 1% FBS, 2mM EDTA) at a concentration of $1x10^8$ cells/ml. The volume of cells expected for the required number of monocytes needed for each assay (with expected frequency of around 10%) was put into sterile 6ml plastic FACS tubes (Falcon, Corning; UK). EasySep human CD14 positive selection Kit II (STEMCELL Technologies; UK) was used to enrich CD14+ cells from the PBMCs, following manufacturer's instructions. In brief, 100μl of CD14 positive selection cocktail was added per ml of PBMCs and incubated at room temperature. After 10 minutes, 100μl of magnetic nanoparticles per ml of PBMCs was added to the sample and incubated for a further 3 minutes. Sample volumes were then topped up to 2.5ml total with CSB and the samples were incubated in a purple EasySep Magnet (STEMCELL Technologies; UK). After 3 minutes incubation the tube, whilst still inside the magnet, was inverted over a discard bottle to remove the unlabelled negative fraction. The remaining cells were resuspended in 2.5ml of CSB inside the same 6ml FACS tube. This was placed back inside the magnet and incubated for a further 3 minutes. Again, the negative fraction is poured off and this process was repeated once more. The cells that remain in the 6ml FACS tube were the purified fraction of CD14+ monocytes and these were resuspended in complete α-MEM media, counted, centrifuged for 5 minutes at 400g and finally resuspended at $1x10^6$ cells/ml in complete α-MEM for downstream cell cultures.

In order to check the purity of this monocyte isolation a small sample of purified CD14+ cells, the negative (discarded) fraction, and the whole PBMC fraction were kept for flow cytometry analysis. These samples were initially washed and then incubated in a 1:5 diluted FcR block (Miltenyi Biotech; UK) at room

temperature for 10 minutes. A cocktail of antibodies against cell surface markers which identify cell populations present in the PBMC fraction, listed in Table 2.4, was added to the cells without washing off the FcR block. This antibody cocktail was incubated for 30 minutes at room temperature. Cells were washed in FACS buffer (centrifugation at 400g for 5 minutes). These samples were then acquired on the LSRII and analysis conducted on FlowJo software.

Table 2.4 Antibody Cocktail for Human Monocyte Isolation Purity Check

Specificity	Fluorescent label	Clone	Concentration (μg/ml)	Supplier	Catalogue Number	μl / sample
CD3	V450	UCHT1	Unknown	BD Horizon	560365	1
CD20	APC	2H7	Unknown	BD Pharmingen	559778	5
CD14	BV605	M5E2	150	BioLegend	301834	1
CD56	AF488	B159	Unknown	BD Pharmingen	557699	2

2.1.2.6 Human Osteoclast Culture

The enriched CD14+ monocytes suspended in complete α-MEM at $1x10^6$ cells/ml were treated with 25ng/ml of Macrophage Colony Stimulating Factor (M-CSF; Peprotech, UK). These cells were then plated in flat bottom 96 well cell culture plates, 100μl per well; resulting in $1x10^5$cells/well, and incubated overnight at 37°C, 5% CO_2. After approximately 16 hours of incubation, 50μl of cell culture medium was removed and replaced with 50μl fresh media containing 50ng/ml recombinant human soluble receptor activator of nuclear factor kappa-B ligand (RANKL; Peprotech, UK), and 50ng/ml of M-CSF – which are diluted 1:1 in the original media for a final concentration of 25ng/ml of both cytokines. M-CSF alone was used as a negative control of osteoclastogenesis. Media was refreshed on day 4, applying the same 50% media change method used above. After 7 days of culture cells were fixed with 4% acetone buffered formalin and stained for osteoclast associated enzyme, tartrate-resistant acid phosphatase (TRAP), the protocol for this is detailed below in section 2.1.2.7.

In some experiments, a TNF-enhanced inflammatory osteoclastogenesis method was adopted. For these experiments, on day 1 media was changed to contain a final concentration of only 1ng/ml RANKL, and when cell media was refreshed on

day 4 this included 10ng/ml of TNF (Peprotech, UK). These cultures were fixed and TRAP stained on day 7 (see section 2.1.2.7).

2.1.2.7 TRAP Stain of Human Osteoclast Cultures

Media was removed from osteoclast cultures after 7 days of culture and cells were fixed with the addition of acetone buffered 4% formalin (For 100ml; 25ml citrate solution, 10ml 37% formaldehyde, and 65ml acetone). Wells were washed in distilled water 3 times. TRAP staining solution was made up as per manufacturer's instructions (Sigma-aldrich; UK #387A). In brief, a fast garnet solution is prepared first, this is formed of a 1:1 ratio of Fast Garnet and Sodium Nitrate, mixed by inversion for 30 seconds and incubated at room temperature for 2 minutes. In order to make 5ml TRAP staining solution 50μl of this Fast Garnet solution is added to 4.5ml H_20, along with 50μl napthol, 200μl acetate, and 250μl of Tartrate solution. The TRAP solution is then added to the fixed osteoclast cultures, 70μl per well, and incubated at 37°C for 20 minutes. This stain is washed off, using 3 washes of distilled water. The stained cultures are left to dry before imaging. Digital images of the entire wells at 10x magnification were acquired post TRAP stain using the EVOS FL Auto Cell Imaging System (Life Technologies; UK). Mature OCs were identified as TRAP+ cells with 3 or more nuclei, quantified by manual counting using ImageJ software. TRAP positive cells will appear purple.

2.2 Murine Study Methodologies

2.2.1 Murine Colonies

2.2.1.1 Murine Colony Maintenance

All mice used in this study were on the C57Bl/6 background. Mice were housed in standard plastic bottom cages with food and water available to them freely. Animals were bred and maintained in the Biological Procedure Unit at Strathclyde University or the Joint/Central Research Facility at the University of Glasgow in accordance to the Home Office regulations. All procedures carried out were in accordance with the Animal (Scientific Procedures) Act 1986.

PAR2 deficient mice were generated prior to the commencement of this study, the methods of this were previously published from this group and can be found in the 2003 publication by Ferrell et al in the Journal of Clinical Investigation[276]. Colonies were maintained from a colony originally established by Professor Robin Plevin at the University of Strathclyde. Heterozygote crosses; which result in wild type (WT), *par2*$^{-/-}$, and heterozygote offspring; provide homozygote breeders for homozygote WT and *par2*$^{-/-}$ colonies in order to prevent genetic drift. Ear punch samples were taken to identify mice and the samples acquired from this event were used to isolate DNA and ascertain the genotype of the heterozygote colony. All breeding of genetically modified murine colonies was conducted under protocol 1 of project license: P989A202D.

2.2.1.2 Genomic PCR

In order to genotype animals from heterozygote colonies, genomic DNA was isolated from ear punch sections and PCR detection of PAR2 gene, F2RL1. DNA extraction was conducted using the Phire tissue direct kit (Thermo Scientific; UK). In brief, DNA extraction buffer was prepared by mixing 20μl of diluent buffer and 0.5μl of DNA release for each sample and ear tags were submerged in 20μl of DNA extraction buffer and vortexed to disrupt. Samples were heated to 98°C for 2 minutes. After this incubation, samples were vortexed again and the DNA extract buffer now contained extracted DNA from the ear tag. This DNA was used for the detection of the F2RL1. PCR master mix was prepared which included 10μl PHIRE, 6μl nuclease free H_2O and 1μl (100μM) of each primer

(Primer 1: 5'-AAGGCAGAGGGCTATCCGA –3', Primer 2: 5'-CCTGGAGAACTTGTTGGAGC –3', Primer 3: 5'– GACCGCTTCCTCGTGCTTTA –3'). In 200μl thermostable PCR tubes (Starlab; UK) 1μl of genomic DNA extract was added to 19μl of PCR master mix and these samples were subjected to the following cycling protocol in a Thermocycler; 5 minutes at 98°C; then 25 cycles of 10 seconds at 98°C, 10 seconds at 67°C, and 30 seconds at 72°C; with a final extension of 5 minutes at 72°C. Samples were then stored at -20°C or immediately taken forward for gel electrophoresis. Both a ladder of known DNA weights (10μl, 50μg O'GeneRuler Express DNA Ladder, Thermo Fisher) and samples (15μl) were loaded onto a 2% agarose ethidium bromide gel that was prepared by adding: 2.6g agarose (Bio-rad; UK) and 2μl ethidium bromide (10mg/ml stock solution, ThermoFisher; UK), 55g of Boric acid (Fisher Scientific, UK), 9.3g ethylenediaminetetraacetic (EDTA, Fisher Scientific, UK) and made up to 1 litre with distilled water. The gel was run at 150 volts for 30 minutes. Gels were then visualised under UV light (Cleaver Scientific, UK) in order to display DNA bands and captured using a Canon PowerShot G16 camera (Canon; Japan). Due to the method of cassette insertion knock out, the genomic product post amplification of F2RL1 will be larger in *par2*$^{-/-}$ mice compared with the wild type counterpart. The product sizes for each genotype are as follows: Homozygous WT – 302bp, homozygous KO- 482-512bp, with heterozygotes containing both bands. An example genotyping gel containing WT, *par2*$^{-/-}$, and heterozygous samples shows a clear distinction between each genotype (Figure 2.1).

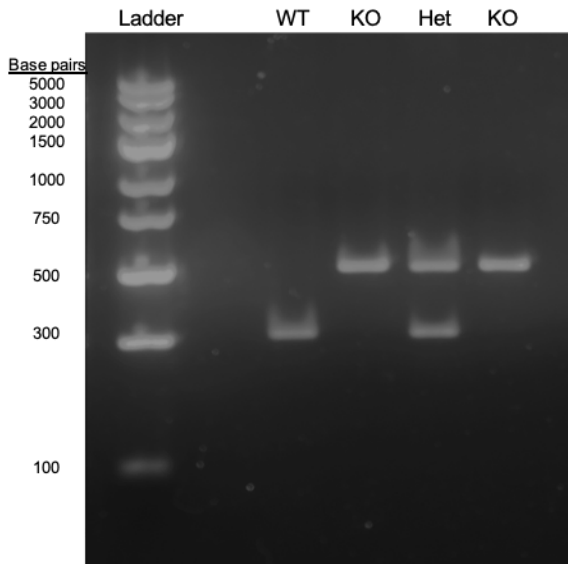

Figure 2.1 DNA PCR Products of FR2LR1 gene from WT, *par2*$^{-/-}$, and Heterozygote Mice. Post amplification with FR2LR1 primers, genomic products were run by gel electrophoresis and separated by size. The genomic products from the unchanged FR2LR1 found in WT animals is 302 base pairs long, which can be seen in lane 1. While the PCR product of FR2LR1 gene with cassette insert from KO animals measures around 482-512 base pairs, as can be seen in lane 2 and 4. Heterozygote animals possess one copy of each gene, found in lane 3.

2.2.2 *In Vitro* Cultures

2.2.2.1 Murine Bone Marrow Extraction from Long Bones

Freshly isolated Bone marrow (BM) cells were used for murine *in vitro* cultures. In order to obtain BM cells, mice from WT and *par2*$^{-/-}$ between 6-10 weeks old were culled under a schedule 1 procedure. The tibias and femurs were dissected from these animals and in a tissue culture hood, using sterile technique the epiphyseal ends of the bones were removed. The bone marrow was flushed out of the long bones with α-MEM complete media using a 10ml syringe and 25 gauge needle (0.5 x 16mm, BD Microlance 3; UK). Cells were dissociated into a homogenous solution by repeated pipetting.

2.2.2.2 Flow Cytometry

Flow cytometric analysis of WT and *par2*$^{-/-}$ BM cells was conducted to check the cellular composition of these genotypes. Freshly isolated BM cells were washed in PBS and then live dead staining was conducted using CyStain DNA 2 Step DAPI stain (Sysmex; UK) diluted 1:2 in PBS, incubated for 15 minutes at room temperature. The samples were topped up with FACS buffer and centrifuged at

400g for 5 minutes at room temperature. Cells were incubated with 1:10 dilution of CD16/32 block (BD Pharmingen; UK) in order to prevent non-specific binding of antibodies via Fc regions for 10 minutes at room temperature. Following this, an antibody cocktail against markers used to identify BM cell populations in mice (Table 2.5) was added to the samples for 30 minutes at room temperature. Samples were subsequently washed in FACS buffer (centrifugation at 400g for 5 minutes) and either fixed for post analysis at a later date, or maintained in FACS buffer and acquired on the LSRII analyser immediately. Data analysis was subsequently completed using FlowJo software.

Table 2.5 Antibodies for Murine Bone Marrow Analysis

Specificity	Fluorescent label	Clone	Concentration (μg/ml)	Supplier	Catalogue Number	μl/sample
CD3	PE	145-2C11	200	BD Pharmingen	553064	2
B220	PE/Cy7	RA3-6B2	200	eBioscience	25-0452-81	2
Ly6C	PerCP/Cy5.5	HK1.4	200	BioLegend	128012	2
Ly6G (Gr-1)	AF700	RB6-8C5	200	Invitrogen	56-5931-80	2
CD11b	APC/Cy7	M1/70	200	BD Pharmingen	557657	2
CD16/32	N/A	2.4G2	500	BD Biosciences	553141	1

2.2.2.3 Bone Marrow Osteoclast Cultures

Freshly isolated BM was used to obtain osteoclast precursors for culture. In brief, total BM was cultured in a 75cm^2 tissue culture flask overnight (12-16 hours) in 37°C and 5% CO_2. Post overnight incubation the non-adherent bone-marrow cells (NA-BMCs) were collected; this population should be depleted of adherent stromal cells and enriched for monocyte populations. The NA-BMCs were counted manually by haemocytometer using trypan blue for dead cell exclusion and resuspended at 1x10^6 cells/ml in complete α-MEM (see appendix). These cells were cultured in flat bottom 96 well plates, at a concentration of 1x10^5 cells/well in the presence of 30ng/ml of recombinant murine M-CSF overnight (approximately 18 hours). The following day media was half changed by

removing 50μl of media and adding 50μl of α-MEM containing 100ng/ml of both murine M-CSF and RANKL (to give a final concentration of 50ng/ml of each). Cells were checked daily to monitor progress and after 4 days media was refreshed again by half changing. Negative control for OC formation was NA-BM cultured in M-CSF alone, with no RANKL. The following day (day 5 of the culture) media was removed, cells were fixed, and TRAP stained as detailed in 2.1.2.7.

An inflammatory osteoclastogenesis protocol was also adapted, in which BM was isolated in the same way, cultured overnight and NA-BMCs were again put into culture with M-CSF (30ng/ml) the same as above. Media was also half changed the following day, however, on this occasion a reduced concentration of RANKL was used (10ng/ml), with 50ng/ml M-CSF. After 2 days of RANKL treatment (day 3 of the culture), 10μl of 400ng/ml of TNF was added to the appropriate sample wells, diluting to a final concentration of 40ng/ml of TNF. Media was half changed on day 4 of the culture, again maintaining 10ng/ml RANKL, 50ng/ml of M-CSF, and 40ng/ml of TNF. Samples without TNF were maintained for comparison to TNF enhancement, as well as negative M-CSF alone controls for osteoclast formation. Cultures were maintained for a total of 9 days with media change every 3 days. These cultures were finally fixed and TRAP stained as described in section 2.1.2.7.

Analysis of whole well images of TRAP stained murine cultures was conducted with ImageJ software. Analysis included counting total osteoclast numbers (TRAP+, 3 or more nuclei), as well as quantification of the area of each well that contains TRAP+ multinucleated osteoclasts, used as a surrogate of osteoclast size. OC area was investigated by manually outlining OC cells on ImageJ and calculating the percentage of the total well area covered by outlined OCs.

As well as TRAP staining of murine osteoclasts, activity of these cells was also measured by conducting the same culture as above but on osteo-assay surface plates (Corning; UK). These plates are coated with a calcium phosphate micro-crystalline scaffold that mimics native bone. Thus allowing direct assessment of osteoclast functionality by enabling quantification of resorption and pit formation. Culture for this particular assay was extended to 12 days, with culture media half changed every 3 days. On day 12, the media was removed and

60μl of 10-15% sodium hypochlorite solution (Sigma-aldrich; UK) added to each well for 3 minutes to remove the cells. Wells were subsequently washed 3 times in distilled water and left to dry. Images of wells were taken on the EVOS FL Auto Cell Imaging System (Life Technologies; UK) light microscope, using 2x magnification to capture the entire well in 1 image. Subsequent analysis of the proportion of the cell culture well with resorbed mineral was calculated on ImageJ software, where the contrast between resorbed and intact material could be discriminated using greyscale darkness intensity.

2.2.2.4 RNA Extraction from NA-BM Cultures

RNA extracts were also taken from BM osteoclasts at various time points in order to analyse the transcriptional differences between WT and *par2*$^{-/-}$ OCs. In brief, media was removed from OCPs/OCs and all relevant control wells at 0 hours (prior to RANKL addition), 6 hours, 24 hours, 48 hours, and 72 hours post RANKL exposure or at the end point of OC culture (5 days), and RNA lysis buffer (RLT) containing 1% β-mercaptoethanol was added to each well (100μl). This was stored at -20°C until ready for RNA extraction.

2.2.2.5 Calvarial Osteoblast Isolation and Culture

Calvaria were dissected from the skull of WT or *par2*$^{-/-}$ pups aged 3-5 days. These were digested in Collagenase II in order to isolate osteoblast cells. In brief, dissected calvaria were initially washed in PBS, 3 calvaria were pooled per sample and these were submerged in 3ml of 1mg/ml of Collagenase II (dissolved in FBS free α-MEM media) and incubated at 37°C, with shaking, for 10 minutes. This initial collagenase step degrades soft tissue and is discarded. The 3 calvaria were then again incubated in 3ml of 1mg/ml Collagenase II at 37°C, with shaking, this time for 30 minutes. The resulting supernatant was collected as digestion 1, which contains early osteoblast-like cells. The calvaria were then washed in 6ml PBS and this wash supernatant was combined with digestion 1. The calvaria were then incubated in 3ml of 4mM EDTA at 37°C, with shaking, for 10 minutes. The EDTA supernatant was subsequently collected (digestion 2) which contains a more mature population of osteoblasts and again the samples were washed in 6ml PBS and wash supernatant combined with digestion 2. Both of the collected digestions were centrifuged at 350xg for 5 minutes to pellet the

isolated cells immediately, to prevent cell death by prolonged EDTA exposure. Meanwhile, the calvaria were digested for a final time in 3ml of 1mg/ml Collagenase II at 37°C, with shaking, for 30 minutes. The resulting digestion was the final collected supernatant and this was also washed in the same way described above and centrifuged at 350xg for 5 minutes. Each stage of calvarial digestion was resuspended in 5ml of complete α-MEM media and then combined (Digestion 1, 2, and 3 for each donor) and cultured in a 75cm^2 tissue culture flask.

After 4-5 days the isolated stromal cells reached confluency. Dependent on the experimental set up it was at this point that they were harvested for co-culture with monocytes in a 96 well plate or osteoblast PAR2 stimulation experiments, or the cells were split (1:5) and further differentiation was carried out. The stromal cells were either differentiated in 1μM Prostaglandin E_2 (PGE_2; Sigma, UK) and 10nM Vitamin D (VitD; Sigma, UK) to promote osteoclastogenic functions, or they were differentiated in 10nM Dexamethasone (Dex; Sigma, UK), 100μM ascorbic acid (AA; Sigma, UK), and 2mM β glycerol-2-phosphate (βGP; Sigma, UK), which is traditionally used to promote a mineralising phenotype. Both differentiation protocols were maintained for 8 days, with media changed every 3 days and cells split if reaching 70-80% confluency. Post short term maturation OBs were then taken forward for subsequent co-culture or osteoblast phenotype analysis.

2.2.2.6 Osteoblast PAR2 Stimulation

Osteoblasts were harvested from 75cm^2 tissue culture flasks by incubating with 5ml of TrypLE (Thermofisher, UK) for 10 minutes at 37°C. The harvested osteoblasts were counted and resuspended in α-MEM at a concentration of 4x10^4 cells/ml and 1 ml of cells were plated per well into a 12 well plate. The cells were left to rest and adhere overnight in the murine cell culture incubator (37°C, 5% CO_2). The following day media was changed to include either 10nM Dex, 100μM AA, and 2mM βGP, or 1μM PGE, and 10nM VitD, or a vehicle control (ethanol (eth) 0.1%). Across a time course of osteoblast maturation; including day 1, 3, 6, and 9, these cells received a further 4 hour incubation with PAR2 activating peptide FLIGRL (2μM, Tocris;UK), or PAR2 inhibitor AZ3343 (3μM,

AstraZeneca; Sweden), or were left with maturation growth factors only (unstimulated, with vehicle dimethyl sulphoxide (DMSO) 0.005%). After 4 hours of stimulation in a cell culture incubator (37°C, 5% CO_2) media was removed and cells were lysed for RNA extraction using 300μl RNA lysis buffer (RLT buffer). Cell lysates were stored at -20°C

2.2.2.7 Bone Marrow Monocyte and Calvarial Osteoblast Osteoclastogenic Co-culture

WT and *par2*$^{-/-}$ calvarial osteoblasts 4 days after tissue digestion, or 8 days after maturation with growth factors (detailed in section 2.2.2.5) were harvested from 75cm^2 tissue culture flasks, counted, and plated in flat bottom 96 well tissue culture plates, at a cell concentration of 2x10^3 cells per well, or 5x10^3 cells per well respectively in complete α-MEM. Osteoblasts were also seeded onto osteo-assay wells at 3x10^3 or 7.5x10^3 cells per well respectively dependent on maturation. The osteoblasts were left to settle and adhere to the plates overnight. The following morning adult WT and *par2*$^{-/-}$ mice aged 6-10 weeks were culled under a schedule 1 procedure and tibia and femurs dissected. The bone marrow was isolated from these as detailed above (2.2.2.1). A homogeneous solution of bone marrow from 2 mice were pooled for an N=1 sample, this is centrifuged at 400g for 5 minutes and resuspended in 10ml of cell separation buffer (1% FBS, 2mM EDTA in PBS). At this point cells were counted and centrifuged again as before, and resuspended at 1x10^8 cells/ml in cell separation buffer. The cells were transferred to a 6ml sterile FACs tube for monocyte isolation via negative cell selection kit: EasySep Mouse Monocyte Isolation Kit (STEMCELL Technologies; UK). Initially, 50μl of rat serum per ml of cells was added to block available Fc receptors and prevent non-specific binding of antibodies. This was incubated for 5 minutes at room temperature, meanwhile component A and component B of the separation cocktail were mixed at a ratio of 1:1. 100μl of this was added per ml of the cell sample and this was incubated for 5 minutes on ice. Meanwhile, magnetic rapidspheres were vortexed to ensure homogenous solution and post 5 minute incubation with the antibody cocktail, 75μl of rapidspheres was added per ml of sample and incubated for a further 3 minutes on ice. Samples were topped up to 2.5ml with cell separation buffer and placed inside in a purple EasySep Magnet (STEMCELL Technologies; UK) and incubated for 3 minutes at room temperature. Post

incubation, in one continuous motion the magnet and tube were inverted into a 15ml centrifuge tube (Corning; UK), with the monocyte fraction contained in solution while all other cell types were magnetically maintained at the side of the tube. The negatively purified sample was incubated in the magnet 3 further times to ensure optimal purity. Monocytes were counted and resuspended in complete α-MEM at $1x10^6$ cells/ml. Media was then removed from the osteoblast cultures in 96 well plates and 100μl of monocytes were plated on top of these cells. These cultures were either exposed to 10nM of Dex, 100μM of AA, and 2mM of βGP, or they were cultured in 1μM PGE, and 10nM VitD. As a negative control for osteoclast formation these cells were also cultured in α-MEM with vehicle control only (eth, 0.1%). These cultures were also conducted with or without PAR2 activating peptide (FLIGRL, 2μM), or PAR2 inhibitor (AZ3383, 3μM). Media was first changed after 3 days by removing 50% of the media (50μl) and replacing with 2x concentrated 50μl of replacement media. This method of media replacement was repeated every 2 days from then on. OCs were visible after 7-9 days of culture and TRAP stain was performed after 8-10 days. Resorption osteo-assay wells were continued until 12 days of culture and again bleached to remove cells and analysed as detailed above (2.2.2.3).

2.2.2.8 Static Adhesion Assay

Full well ELISA plates were coated with 6μg/ml of ICAM-1 (50μl per well) diluted in PBS, with some wells receiving PBS only as a plastic adhesion control. Plates were covered with parafilm and incubated at 4°C overnight. The following morning plates were washed twice with PBS (200μl per well) and wells were blocked with 1% milk in PBS for 1 hour and 15 minutes at 37°C. During this time monocytes were isolated from fresh murine bone marrow (see section 2.2.2.7 for detailed protocol)with the EasySep Murine Monocyte isolation kit (STEMCELL Technologies; UK). Monocytes were counted and resuspended at 1.5 $x10^6$cells/ml in adhesion medium (RPMI1640 + 0.1% BSA + 20mM HEPES (pH 7.25) + 2mM $MgCl_2$). Monocytes were stimulated with PMA (1μg/ml), PAR2 activating peptide (FLIGRL, 2μM), or PAR2 inhibitor (AZ3383, 3μM) for a 15 minute pre-incubation at 37°C. Blocking buffer was removed from the ELISA plates and 400μl of monocytes (+/- treatment) was added to each well. The plate was incubated on ice for 8 minutes to allow all cells to settle to the bottom and then placed in the

incubator at 37°C for 30 minutes. During this incubation period a plate was prepared which was used to calculate the absorption from the total cells added to the plate. To do this 400μl of each sample was transferred to Eppendorf tubes and spun down at 400g for 5 minutes, supernatant removed. These cells were resuspended in 200μl of PBS and 50μl of each sample added to a new ELISA plate in triplicate, PBS only was also added to 3 wells as a negative control for cells. This plate was placed to the side until the cell lysis stage.

Post incubation of monocytes in the ICAM-1 coated ELISA sample plate, this was removed from the incubator and placed upside down in a bucket of 2.5L PBS + 2mM $MgCl_2$ and left, wells completely submerged, for 50 minutes. After this incubation the plate was carefully removed retaining liquid in the wells (by inverting whilst submerged). 350μl of liquid was removed from all wells at this stage (leaving 50μl remaining) and cells could be examined under the microscope. At this stage cells were lysed by addition of 100μl of 3mg/ml para-nitrophenyl phosphate (PNP) in 1%Tx-100/50nM acetate buffer pH5, which was incubated for 60 minutes at 37°C in the dark. This same procedure was conducted with the "total plate". After the 60 minute incubation 50μl of NaOH was added to each well to stop the reaction and the observable colour change was measured on a colorimetric plate reader at absorption 405nm.

Absorption measurements were transferred to Excel for analysis. In order to calculate the absorption of the total cells added to each well for each sample, the mean was calculated for the measured absorption of the triplicates for each sample. This value was then multiplied by 4 (since 1 quarter of the total cells was added per well), this value equates to the absorption from the total number of cells added per well. The absorption measured from the sample wells can then be compared with the total cell lysate and a percentage of monocytes that have adhered to ICAM-1 calculated. The calculated % adhesion for each genotype +/- treatments, was transferred to Graphpad Prism to generate graphs and calculate statistics.

2.2.3 Polymerase Chain Reaction

2.2.3.1 RNA extraction

RNA extraction was performed using PureLink mini kit as per manufacturer's instructions. Briefly, RNA lysis buffer containing β-mercaptoethanol (RLT) was added to the cells and stored at -20°C until required. Prior to extraction, lysates were defrosted on ice. An equal volume of 70% ethanol was added to each sample and mixed by pipetting. The lysate was added to a spin column, and centrifuged at 12,000g for 15 seconds. The flow-through was discarded and 700μl of wash buffer 1 added. The column was centrifuged as before. Two further washes with 500μl wash buffer 2 were carried out, to remove impurities. The column was transferred to a fresh 2ml collection tube and centrifuged at maximum speed for 2 minutes. Transferring the column reduces the risk of contamination from previous buffers and removes any factors that may inhibit RNA elution. The column was transferred to a 1.5ml collection tube and RNA eluted using nuclease-free water. RNA was quantified and purity checked using a Nanodrop 2000/2000c (Thermo; UK). Absorbance was measured at 230, 260 and 280nm. A 260/280 ratio of 2.0 and a 260/230 ratio between 1.8-2.2 was considered 'pure' RNA. No further quality control steps were carried out. RNA samples were stored at -80°C until required.

2.2.3.2 cDNA synthesis

cDNA was synthesized using High Capacity cDNA synthesis kit (Applied Biosystems). 100ng of RNA was converted per reaction. The reaction was assumed to go to completion, creating 100ng cDNA. Briefly, RNA samples were diluted to 10ng/μl and 10μl added to a reaction mix containing reverse transcriptase, dNTPs and random primers as per manufacturer's instructions. Samples were incubated at 25°C for 10 minutes, followed by 37°C for 2 hours and then 95°C for 5 minutes to inactivate the enzyme. cDNA was diluted to 2ng/μl using nuclease free water. cDNA samples were stored at -20°C until required.

2.2.3.3 Quantitative PCR

All primers for qPCR analysis were obtained from the previously designed stocks within the laboratory, the sequences for these can be found in Table 2.6. Upon first use, all qPCR primers were validated with a melt curve to ensure the presence of a single product without evidence of primer dimerization.

Transcripts were analysed by qPCR in duplicate in either 96- or 384- well plate formats. Regardless of plate format, a 10μl reaction was carried out using 5μl PowerSYBR Green, 0.1 μl of each forward and reverse primer (stock 100μM; see Table 2.5), 3.8μl nuclease free water and 1μl of cDNA at 2ng/μl. A non-template control (NTC) was carried out for each primer set to control for reagent contamination. For this, 1μl of nuclease free water was added instead of cDNA. The plates were sealed and centrifuged for 30 seconds. Plates were run on Applied Biosystems StepOne Plus or QuantStudio 7 Flex Real-Time System. Cycling conditions were as follows: 10 minutes at 95°C, then 40 cycles of 95°C for 15 seconds, and 60°C for 1 minute. Samples were normalized to 18s housekeeping gene using the following equation:

$$2^{-\Delta Ct} = 2^{-(Ct\ (gene\ of\ interest) - Ct(housekeeping\ gene))}$$

Table 2.6 Murine Primer Sequences

Gene	Species	Forward Sequence (5'-3')	Reverse Sequence (5'-3')
Csfr1	Murine	TGAAGGTGGCTGTGAAGATG	AGGCTCCCAAGAGGTTGACT
oscar	Murine	GTTTTGGGGGTTTGTTCGTT	TTACCTGGGAGATGGGATTG
Acp5	Murine	GGTATGTGCTGGCTGGAAAC	GGTAGTAAGGGCTGGGGAAGT
Tnfrsf11a	Murine	TTTGTGGTTTTGGCATCCTT	CTGGCACCTTCATTTTGTCC
Mmp9	Murine	TCTACTGGGCGTTAGGGACA	AGGAGTCTGGGGTCTGGTTT
OCSTAMP	Murine	TGGGCCTCCATATGACCTCGAGTAG	TCAAAGGCTTGTAAATTGGAGGAGT
DCSTAMP	Murine	TCTGCTGTATCGGCTCATCTC	ACTCCTTGGGTTCCTTGCTT
Nfatc1	Murine	TCATCCTGTCCAACACCAAA	ATGTCTGTCTCCCCTTTCCTC
Ctsk	Murine	GGAACGAGAAAGCCCTGAA	CACACCTCTGCTGTAAAACTG
18S	Murine	GACTCAACACGGGAAACCTC	AGACAAATCGCTCCACCAAC
Tnfrsf11	Murine	TCTGTTCCTGTACTTTC	TTCATGGAGTCTCAGGATTC
Col1a1	Murine	GCCAAGAAGACATCCCTGAA	CTTCCGGGCAGAAAGCA

bplag	Murine	ACCATGAGGACCATCTTTC	GGACATGAAGGCTTTGTC
Alpl	Murine	CGCACGCGATGCAACACCAC	TGCCCACGGACTTCCCAGCA
Sp7	Murine	TGCTTGAGGAAGAAGCTC	CTTCTTTGTGCCTCCTTTC
Tnfrsf11b	Murine	CTTGCCCTGACCACTCTTATAC	CTTCCTCACACTCACACACTC
RUNX2	Murine	GAGAGGTACCAGATGGGACT	CACTTGGGGAGGATTTGTGA
Spp1	Murine	GCAGAATCTCCTTGCGCCAC	CGAGTCCACAGAATCCTCGC

2.3 Statistical analysis

All statistical analysis was performed using GraphPad Prism 6 software (GraphPad). Depending on the data being analysed, different statistical tests were carried out. On all applicable data, a test for normal distribution was carried out to determine what type of statistical analysis should be used. When data followed a normal (Gaussian) distribution pattern, as determined using D'Agostino & Pearson test of normality, parametric tests were used. When data was not normally distributed, or where there was insufficient data to test distribution, non-parametric tests were used. See figure legends for details of the specific statistical tests used for each set of data. A *p* value less than 0.05 was considered significant.

3 Assessment of Commercially Available Antibodies Against PAR2

3.1 Introduction

PAR2 has been reported to play a key role in immune function and the inflammatory response. Surface PAR2 expression has been detected and quantified in many immune cells such as monocytes, lymphocyte subsets[286], neutrophils[268], macrophages[271] and mast cells[269]. PAR2 surface expression has previously reported associations with inflammation, and expression correlation with inflammatory diseases. Circulating monocytes in rheumatoid arthritis (RA) patients express higher levels of surface PAR2 than healthy controls, and this has been demonstrated to further correlate with flare status, as determined by circulating markers of inflammation (CRP) and the requirement for in-patient admission [297]. In addition to this, $CD68^{+}$ macrophages in RA synovial biopsies have been shown to be $PAR2^{+}$ and have greater PAR2 expression than those found in OA synovial tissue. These findings are not isolated to articular joint or rheumatic associated inflammation; it has also been reported that peripheral blood monocytes from asthmatic patients have enhanced PAR2 surface expression, which correlates with disease activity[299]. This enhanced expression during chronic inflammation has been found both in peripheral blood monocytes of these patients and monocyte-derived tissue phagocytes at the sites of inflammation, potentially indicative of the systemic nature of these conditions.

Studies were undertaken in the present chapter to expand our understanding of this phenomenon through investigation of which stimuli may trigger upregulation of the receptor. An additional aim was to investigate whether increased expression is limited to particular subtypes of monocytes and if receptor expression is found on terminally differentiated monocytes such as macrophages or OCs.

In order to further investigate the effect of monocyte stimulation and differentiation on PAR2 expression, a reliable and robust methodology to definitively measure this is required. The most common anti-PAR2 antibody used in the literature is the antibody clone SAM-11. This clone, along with other anti-PAR2 antibodies have previously been scrutinised for their selectiveness[300]. The

challenge of generating reliable antibodies against GPCRs has been recognised and discussed in the literature as one of the potentially limiting factors in the advancement of GPCR research and the translation of GPCR research to a clinical application of findings[301,302]. Thus, PAR2 is not the only GPCR to have reported problems with antibody reliability. A study published in 2009 debated the antibody issue for a number of different GPCR families [303]. The study generated 49 different anti-sera raised against 19 different receptors and determined that none of the anti-sera could withstand robust specificity or selectivity testing for their respective targets. It is therefore not surprising that an issue has arisen with regards to PAR2. Attempts have been made in the literature to confirm SAM-11 specificity, including use of pre-incubation with known epitope as an experimental control. Moreover, an in-depth investigation of the range of available anti-PAR2 antibodies was conducted and published in 2012, through comparison of antibody staining pattern with PAR2-GFP transgenic cells. They evaluated a number of techniques including western blot, immunofluorescence, and flow cytometry[300]. SAM-11 performed best overall and based on this work became recognised as the gold standard for use in PAR2 research.

Since the publication of this initial PAR2 antibody assessment, new antibodies have become available. Considering all of the above, and before generating data to analyse the expression of PAR2 in monocytes, validation of the current commercially available antibodies against human PAR2 was performed within the methodologies planned. The most successful clone from the previous antibody study and most commonly published anti-PAR2, SAM-11 clone, was chosen for comparison with newly available PAR2 antibodies.

The research presented in this chapter sought to compare and thereby select the best antibody now available to quantify the protein expression of human PAR2. To achieve this the central aims were:

1. Confirm antibody binding to recombinant human PAR2

2. Use stable transfected hPAR2 human cell line, and a naive control to test selectivity of antibodies under different staining conditions.

    a. Denatured and solubilised protein (Western Blot)

b. Fixed protein (Immunofluorescence microscopy)

c. Live *in-vitro* staining in suspension (Immunofluorescence flow cytometry and ImageStream analysis)

3.2 Results

3.2.1 Assessment of antibody binding to recombinant human PAR2

The antibody clones investigated in this chapter include SAM-11, D61D5 and a polyclonal antibody from Alomone Labs (Table 3.1). The amino acid sequence of human PAR2 is shown in Figure 3.1. This sequence is compared to both murine and rat PAR2 sequences, with all aligning amino acids shown in the second line, between the 2 sequences. Each antibody binds to a discrete epitope on PAR2 (although SAM-11 and D61D5 have an overlapping epitope) and the binding regions are marked on the sequences in Figure 3.1.

Table 3.1 Anti-PAR2 Antibodies

Clone	Supplier	Poly/mono clonal	Species	Species Raised Against	Region of Receptor	Amino Acid Sequence of Binding Site	Isotype/ Control
SAM-11	Santa Cruz Biotech	Monoclonal	Mouse	Human	N-terminus (post cleavage site)	SLIGKVDGTSHVTG (37-50)	Supplied isotype Ab
D61D5	Cell Signalling Tech	Monoclonal	Rabbit	Human	N-terminus (post cleavage site)	Unknown Around Gly 44	Secondary only stain
Alomone	Alomone Labs	Polyclonal	Rabbit	Rat	C terminus	KRMQISLTSNK (368-378)	Secondary only stain

The full region of binding for SAM-11 is 14 amino acids in length and immediately after the conventional cleavage site at amino acids 37-50. It encompasses the activating tethered ligand region and therefore can inhibit activation of the receptor. It is recommended by the manufacturer for the detection of human, mouse, and rat PAR2 protein. However, the sequence alignment at the epitope region of binding between the human protein the antibody was raised against, and the murine protein is less than 50% (42.8% similarity, Figure 3.1A) and contains 50% alignment to the rat epitope sequence (Figure 3.1B).

The exact antigenic binding region of the D61D5 clone is proprietary information and therefore cannot be mapped exactly to the sequence, however, it has been disclosed to be around glycine 44. This indicates that the binding region of this antibody is after the conventional cleavage site, meaning it can recognise both full sequence and cleaved, activated receptor. Due to the proprietary epitope we are unable to map sequence homology to any other species but sequence

homology to the murine protein was disclosed by the producer, as 57% (Figure 3.1A). This homology was viewed as too low to warrant further investigation into binding to murine protein and therefore the distributor (Cell Signalling Technologies) of this antibody only confirms reactivity with the human PAR2 protein.

Finally, the third antibody in our assessment is a polyclonal antibody raised against the rat C terminal amino acids 368-382. The sequence homology between the rat protein and human epitope at that region is 73.3% (11/15 amino acids, Figure 3.1B) and 93.3% homology to murine protein (14/15 amino acids). While amino acid similarity is higher than either of the N terminal region binding antibodies the capability of polyclonal antibodies to recognise multiple epitope regions of 1 protein increases the risk of cross-reactivity with other peptides. Therefore, staining PAR2 with this antibody on cells/tissues of another species may increase the risk of non-specific binding.

All of the above antibodies have been recommended for detection human PAR2 protein by the manufacturers. As an initial assessment of their suitability a dot plot was conducted using recombinant human PAR2 protein to test whether these antibodies were capable of directly binding the recombinant human protein. Human PAR2 protein was dotted onto a membrane at 3 concentrations with a 10-fold increase between them. Full recombinant human PAR2 was dotted on the first row, the SLIGKV tethered ligand region of the receptor on the second, and the C terminus fraction, amino acids 368-382 on a third row. These blots were then incubated overnight with each respective antibody of interest and anti-mouse or anti-rabbit secondary conjugated to HRP (dependent on primary antibody host) was used to conduct chemiluminescent assessment of antibody binding to protein. As can be seen in Figure 3.2, all of the antibodies tested bound to full length recombinant human PAR2 in a concentration dependent manner. The polyclonal antibody from Alomone also interacted with the C terminal peptide whilst neither SAM-11 nor the D61D5 clones displayed any interaction. None of the antibodies were able to bind to the SLIGKV peptide.

Figure 3.1 PAR2 Amino Acid Sequence Comparison Across Species
Utilising uniport and BLAST software the amino acid sequence of human PAR2 was aligned with either (A) murine protein, or (C) rat protein. Where amino acids were positively aligned they are stated in the intermediate line between the 2 sequences. The estimated epitope region for SAM-11 (orange), D61D5 (blue), and the polyclonal antibody purchased from Alomone (red) were overlaid onto these sequences. The overall alignment of the species was then graphically represented in C for murine sequence and D for rat, with red areas demonstrating misalignment and grey regions as positively aligned and regions of antibody binding also highlighted in these graphics.

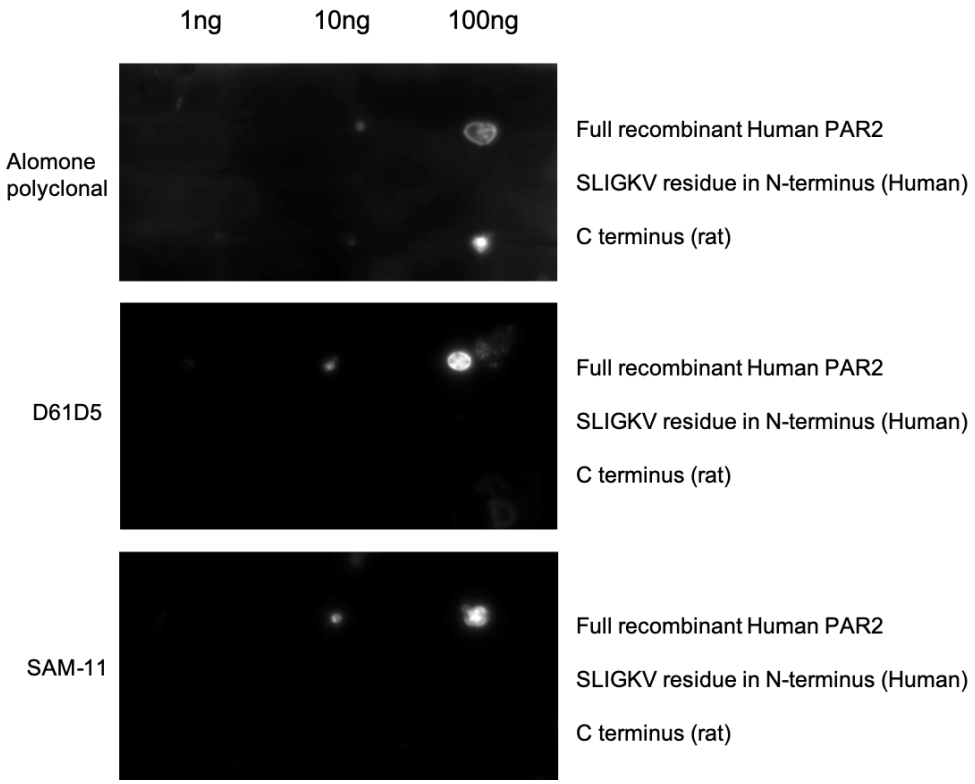

Figure 3.2 Anti-PAR2 Antibodies Bind to Recombinant Human PAR2.
Full recombinant human PAR2 protein, SLIGKV or the C terminal rat peptide (immunising epitope from Alomone Labs) was dotted onto PVDF membrane at 3 successive concentrations (1ng, 10ng, and 100ng). The blots were incubated with either Alomone polyclonal, D61D5 clone, or SAM-11 overnight and secondary HRP was used to visualise antibody binding by chemiluminescence.

3.2.2 Ability of Anti-PAR2 Antibodies to Detect PAR2 via Western Blot of Total Cell Protein Lysates

The dot blots provided evidence that the antibodies can interact with a preparation of purified recombinant PAR2. In order to test the specificity of these interactions, a human astrocyte cell line (1321N1) stably transfected with human PAR2 (1321N1-hPAR2) was acquired from AstraZeneca alongside its wildtype counterpart (1321N1) that does not express PAR2[304]. To initially confirm that the cell lines did or did not express human PAR2, transcript levels were evaluated via quantitative PCR. Both cells lines contained equivalent levels of the housekeeping GAPDH transcript (Table 3.2) but only the 1321N1-hPAR2 cell line had detectable levels of the PAR2 transcript. Thus, from this data it can be concluded that the transfected cell line has the potential to express higher levels of PAR2 protein over its naive counterpart due to substantially higher gene expression levels.

Table 3.2 Quantitative PCR Cycle Threshold of Housekeeping Gene (GAPDH) and F2RL1 in both Naive 1321N1 and Transfected 1321N1-hPAR2
Representative of 2 experimental repeats.

CT Values		
	GAPDH	F2RL1
1321N1	19.65	Undetermined
1321N1-hPAR2	19.58	24.95

Given the detection of PAR2 transcript in 1321N1-hPAR2 cell but not 1321N1, these cells were used to not only evaluate the expression of PAR2 at a protein level but also determine whether the various antibodies are specific for PAR2. Protein lysates from both 1321N1 and 1321N1-hPAR2 were separated by molecular weight using gel electrophoresis and these were transferred onto a PVDF membrane for probing with the PAR2 antibodies (Table 3.1). The staining pattern detected by the polyclonal Alomone anti-PAR2 is shown in Figure 3.3A. Multiple bands were observed in the transfected cell extract, ranging from 135kDa down to around 26kDa. Notably, the predicted molecular weight of PAR2 is 44kDa, and there were 2 bands observed between the 32 and 46kDa molecular weight markers in the ladder. Furthermore, the brightest band in the extract appears just below 58kDa. When compared to the cell lysates from the WT cell

line many of the same bands were observed, such as the highest band at 135, and the band between 32 and 46kDa. The band observed in the transfected cells just below 58kDa is not completely equivalent to that band observed in the naïve cells (slightly lower molecular weight), however, based on the data obtained, the presence of the 58kDa band in the naïve cells cannot be completely ruled out. There is one very faint band at 80kDa in the transfected cell line lysate that does not appear to be present in the naïve cells, but it is unlikely to be PAR2. Overall, the multiple band staining pattern is similar between the transfected and naïve cell lysates when stained with the polyclonal anti-PAR2.

In Figure 3.3B the same protein lysates have been run and stained with the D61D5 antibody. In the PAR2 expressing 1321N1-hPAR2 lysate, 1 strong, clean band can be seen at around 40kDa followed by a faint smear and another band at a very high molecular weight (out with the ladder). The molecular weight of the strongest band on this blot is very close to the predicted molecular weight of the PAR2 protein. When comparing with the staining pattern found in the wildtype cells it can be clearly seen that another band of matching molecular weight is found, albeit at a lower staining intensity. This band does not have the same smear found in the transfected cells.

We finally assessed the western blot staining pattern of SAM-11 clone with the same cell lysates as the other antibodies (Figure 3.3C). This blot also contains multiple bands ranging from high molecular weight (245kDa) right down to the predicted weight of 40-44kDa. The strongest bands are found at 190kDa, 60kDa, and 58kDa, with fainter bands at 40 and 44kDa. No bands were found in the wildtype 1321N1 cells, which appears to confirm that these cells do not express PAR2, as found with transcript analysis (Table 3.2). It also indicates that SAM-11 is able to discriminate between PAR2 expressing cells and cells which do not express the protein of interest using western blot, even if the bands do not reflect the expected molecular weight.

If the antibodies were specific for PAR2 using this technique, we would expect to find a single band at the predicted molecular weight of PAR2 (44kDa) in the transfected cell lysates and not in the naive cell line. None of the tested antibodies conformed to the expected profile.

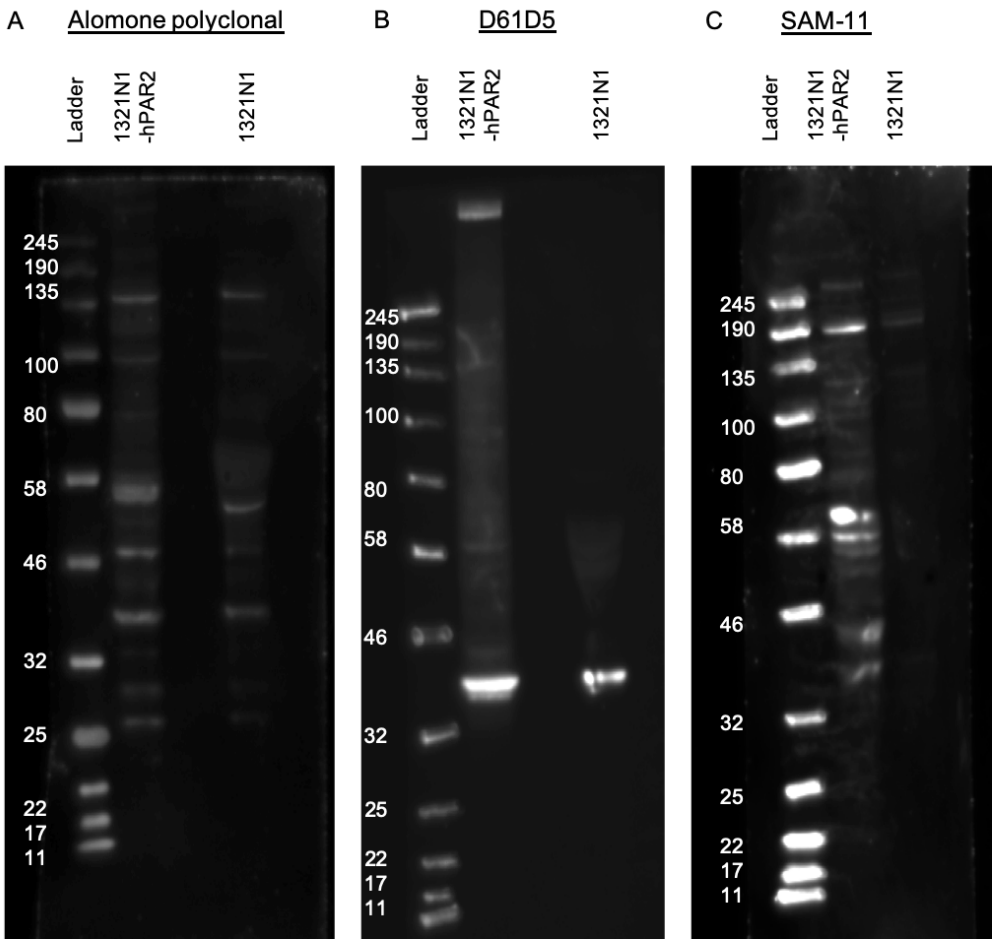

Figure 3.3 Western Blots Conducted with Different Antibody Clones Against PAR2 Resulted in Detection of a Different Pattern of Bands.
Cell protein lysates were taken from naive 1321N1 cells and transfected 1321N1-hPAR2 cells using RIPA buffer and separated by molecular weight through gel electrophoresis alongside a visible protein ladder of known band sizes Proteins were then transferred to a PVDF membrane and incubated with either (A) Alomone polyclonal, (B) D61D5, or (C) SAM-11 overnight. Blots were then washed and incubated with secondary antibodies conjected to HRP. Detection of antibody binding was determined via chemiluminescence. Each blot contained lysates from the same protein isolation that were prepared for electrophoresis in the same manner.

Despite the use of the same cell lysates with identical preparation, the detected staining pattern for each antibody differs greatly (Figure 3.3). This suggests that some antibodies are able to pick up PAR2 in alternative isoforms (such as dimerisation states or post translational modifications) that the others are not capable of detecting. Alternatively, it suggests that all of the antibodies are not able to specifically detect PAR2 protein with western blotting techniques.

In order to assess whether the multiband properties of SAM-11 and Alomone polyclonal western blot staining (Figure 3.3A and B) were caused by dimerization of PAR2, methods were adopted from a previous paper studying another family of G protein coupled receptors - chemokine receptors[305]. This publication

demonstrated that the temperature at which a protein is denatured during sample preparation can influence the ratio of monomer to dimer expression of the chemokine receptor, which can then be detected with gel electrophoresis. The same method of sample preparation used in this publication was applied to new cell lysates from transfected cells, denaturing at 37°C, 60°C, and the original temperature of 90°C. As can be seen from the blots in Figure 3.4 differing denature temperatures made no difference to the size or number of bands found with polyclonal Alomone stains (A), D61D5 (B), or the SAM-11 clone (C). The polyclonal stain remained consistent with the previous experiment (Figure 3.3A) expressing many bands of various molecular weights with no change between preparations (Figure 3.4A). SAM-11 also did not change with sample prep temperature alterations (Figure 3.4C) but the bands on this blot do not resemble the previous cell lysate experiment (Figure 3.4C). On this occasion there is only 1 band featured at 82kDa, whilst in other experimental conditions multiple bands were found (Figure 3.3) despite sample preparation consistency between experiments (90°C sample in Figure 3.4C and Figure 3.3C), so the source of this variation is unknown.

While we cannot definitively say that multiple bands found in this assay were not caused by dimerisation, adoption of this previously established method to detect G-protein coupled receptor dimers did not provide any evidence to support that possibility.

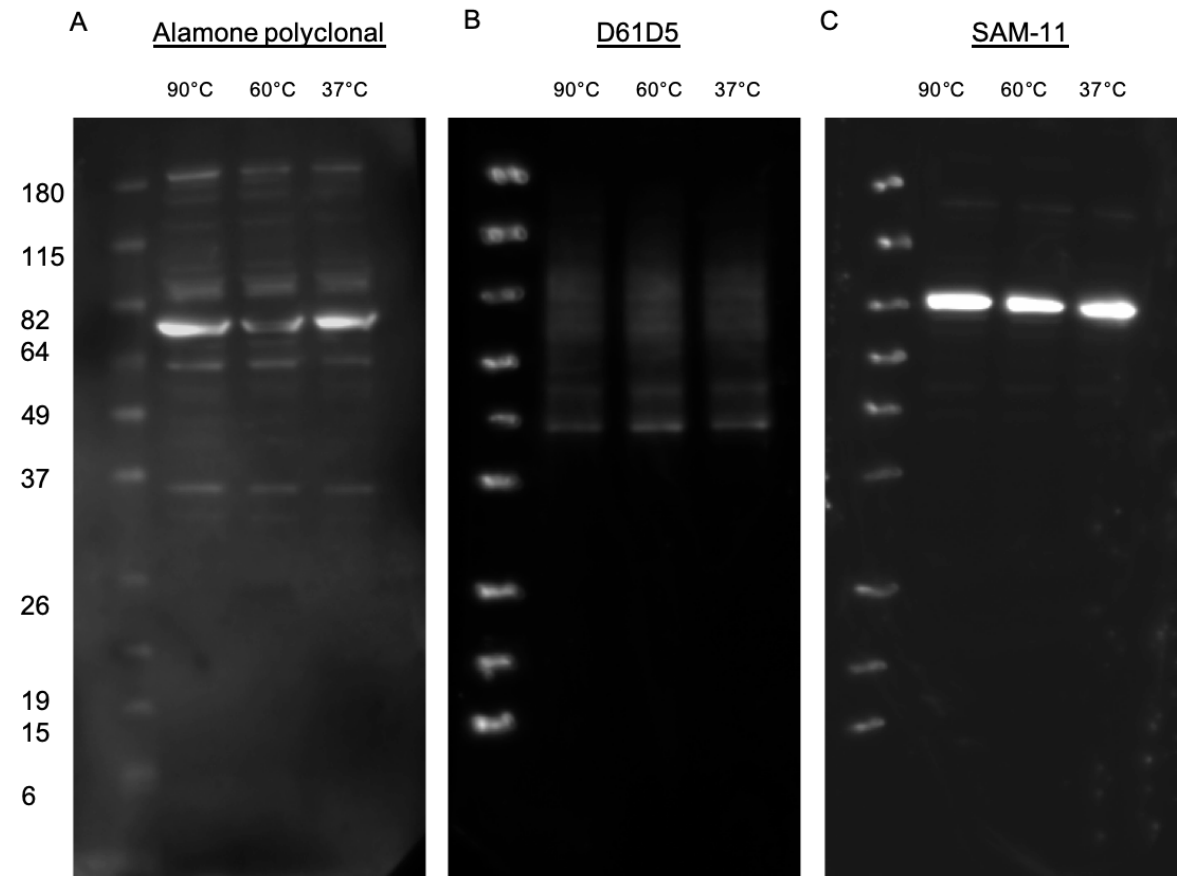

Figure 3.4 There was no Evidence of Temperature Dependent Dimerization of PAR2 in Cell Lysates.
Protein lysates were isolated from transfected 1321N1-hPAR2 and denatured at various temperatures (90°C, 60°C, or 37°C) before proteins were separated by molecular weight via gel electrophoresis alongside a visible ladder of known molecular weight. Proteins were then transferred to PVDF membrane and incubated with either (A) Alomone polyclonal, (B) D61D5 clone, or (C) SAM-11 clone overnight. Secondary antibody conjugated to HRP was used to detect antibody binding by chemiluminescence. The same cell lysates were run for each blot.

3.2.3 Assessment of Antibody detection of PAR2 via Fluorescent Microscopy

Some antibodies optimally perform or are more appropriately used under different staining protocols and conditions. Therefore, in order to test the suitability of these antibodies in a fixed cell scenario we adopted fluorescent microscopy methodology. This enabled testing of each antibody under new constraints and the data acquired from this technique provided insight into the cellular location of the protein. Again, the 1321N1 cell lines were used to compare transfected and wildtype cells as positive and negative controls. Representative images can be seen in Figure 3.5 and semi-quantitative analysis was performed on these images using ImageJ. The integrated density of fluorescence was calculated by subtracting the background fluorescence intensity and DAPI nuclear dye was used to locate cells via the nuclei (blue). PAR2 was stained using the tested antibodies (Table 3.1), with Alomone and D61D5 fluorescence generated using a secondary antibody conjugated to FITC, while the SAM-11 antibody used was a direct conjugate to fluorophore PE.

Immunofluorescence (IF) staining on the 1321N1-hPAR2 cells conducted with the polyclonal Alomone resulted in very bright, high intensity stain, as seen in Figure 3.5A. Due to the nature of a polyclonal, it will contain multiple antibody clones which are able to bind different areas of the known epitope. For this reason, polyclonal antibody stains can result in more antibody bound to the protein of interest, resulting in a higher signal. This high signal was not limited to the transfected cells, naïve cells also had a bright signal (Figure 3.5B). This signal was dimmer than the transfected cell fluorescence intensity as seen in quantification (Figure 3.5G). It was also unexpected to find that the staining appeared to localise strongly to the nucleus.

Staining from the D61D5 was much dimmer than the Alomone antibody (Figure 3.5C). However, this stain could differentiate between transfected and naïve cells, with transfected cells appearing brighter (Figure 3.5C, D, and G). Unlike the polyclonal this single clone is limited to how many primary antibodies can bind to the protein due to the limitation of one specific epitope. This may account for dimmer staining in comparison to the Alomone polyclonal. Dimmer

staining could also be attributed to a lack of availability of the D61D5 epitope in post-fixation conditions that this assay was conducted under.

With IF microscopy, the SAM-11 antibody was unable to detect any visible PAR2 staining on either transfected (Figure 3.5E) or wildtype cells (Figure 3.5F). When the images were analysed using ImageJ this analysis was able to detect very low levels of staining and could distinguish between naïve and transfected cells (Figure 3.5G), but this detection level was so low it may not be considered reliable. However, it is worth considering that this may not be the most efficient method of protein detection using IF microscopy for 2 reasons. Firstly, a direct conjugate was utilised as opposed to using a primary antibody against PAR2 and then amplifying the signal of this with a secondary conjugated to the fluorophore. A limited quantity of monoclonal antibody is capable of binding its protein of interest and this can limit the intensity of the signal. Secondary antibodies are thus commonly used to amplify this signal as multiple secondary antibodies can then bind 1 primary. In addition the fluorophore (PE) applied in this instance is not optimal for IF microscopy applications, as this is a bright dye with limited photostability, it is more suitable for flow cytometry applications. Due to the requirement for longer exposure of fluorescent excitation required for acquiring an image with microscopy this can result in photo-bleaching of this fluorophore before images are acquired. While flow cytometry is a more sensitive detection method with very fast excitation and detection and thus PE is an ideal fluorophore in this context. Overall, the direct conjugate of SAM-11 antibody with PE in this context is not suitable for this application and is unable to detect PAR2 protein.

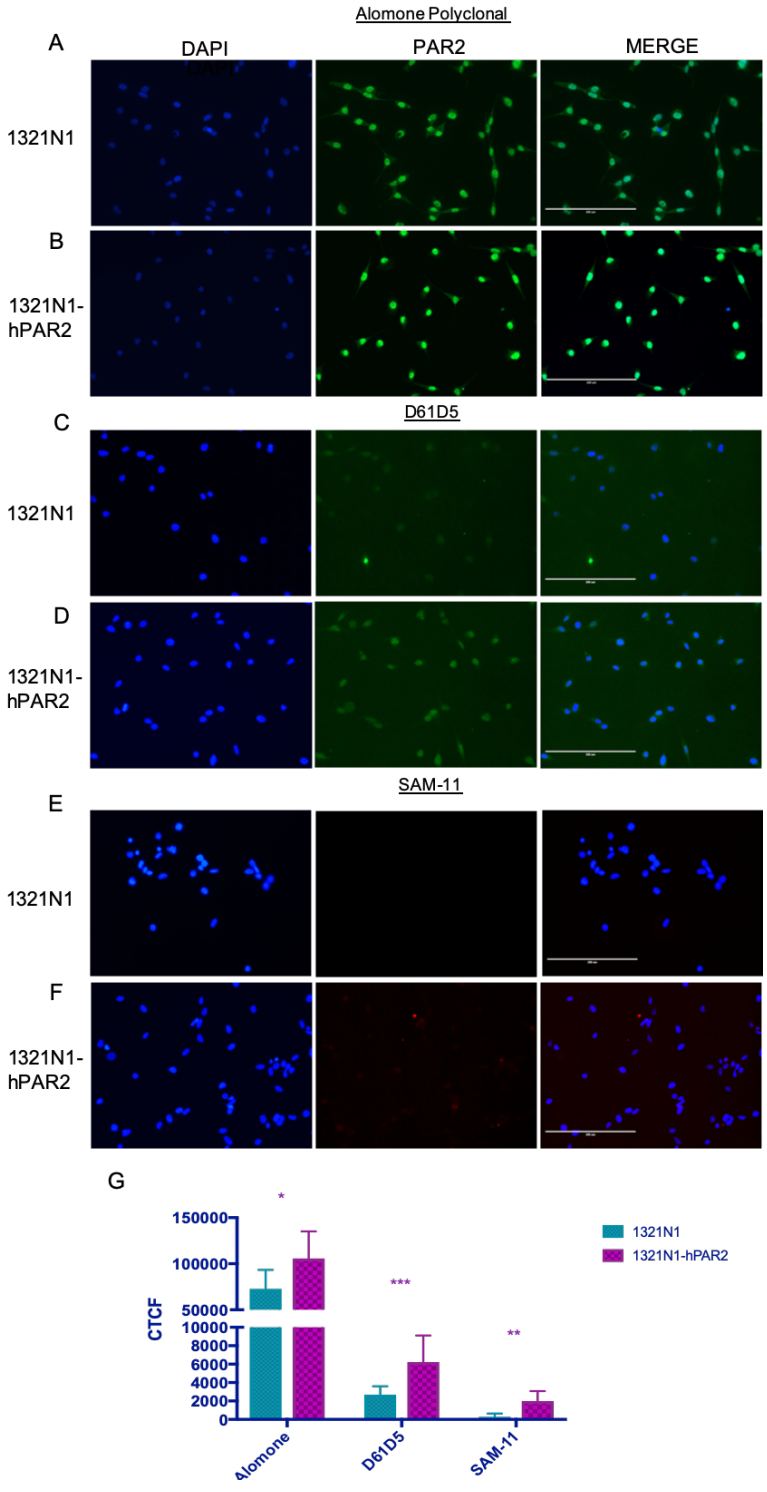

Figure 3.5 Detection of PAR2 via Immunofluorescent Microscopy.
(A, C, E) Naive 1321N1 cells and (B, D, F) transfected 1321N1-hPAR2 cells were cultured overnight on glass chamber slides. Cells were fixed and permeabilised before staining with either (A, B) Alomone polyclonal antibody, (C, D) D61D5 clone, or (E, F) SAM-11. DAPI (Blue) mounting media was used to stain and identify nuclei. Stains were then imaged at 10x magnification on the EVOS FLAuto. (G) Subsequent quantification of fluorescence intensity was conducted on ImageJ. Cells were defined and background (area containing no cells) fluorescence was subtracted from the fluorescent intensity of the stained cells. This was conducted on an average of 15 cells across multiple images for each antibody. Representative images of this experiment have been shown. Quantification and images are representative of 1 experiment which has been repeated twice. The Kolmogorov-Sminov test which does not assume Gaussian distribution of the data was used to determine statistical significance; * $p<0.05$, ** $p<0.01$, *** $p<0.001$

3.2.4 Assessment of antibody detection of surface and intracellular PAR2 expression via Flow Cytometry

Flow cytometry is a central technique used in the immunology field and beyond for the detection and quantification of proteins in various cell types simultaneously. This technique allows for a greater number of fluorescent probes than IF microscopy and thus enables staining of various cell markers to be used in conjunction with the protein of interest, allowing determination of cell subsets within a mixed population. This technique has been applied for the detection of PAR2 in a number of immune cells previously published. Most papers have utilised the SAM-11 clone for this application [267,271,272,297,299]. However many groups have also produced their own polyclonal antibody through immunisation of small animals and purification of the anti-serum [268,285,306]. The application of different antibody clones to detect this protein have resulted in a confusing and contradictory literature with regards to PAR2 expression. Appropriate assessment of the tools available and a standardised method for PAR2 detection via flow cytometry is urgently required to regain clarity in this matter. The anti-PAR2 antibodies listed in Table 3.1 were assessed for their use in flow cytometry, with the exception of the Alomone polyclonal. This antibody detects the internal C terminus and therefore cells would have to be permeabilised for detection. This would include detection of all intracellular stores of the receptor and cell surface membrane only detection would not be possible. Again, the wildtype and stably transfected 1321N1 cells were used to determine if these antibodies could robustly differentiate between high expression and low/no PAR2 expression (Table 3.2).

The cell lines were stained both for surface protein expression only, and also permeabilised to detect intracellular stores of receptor - which have been shown to be present in other transfected cell lines[307-309]. The mean fluorescence intensity (MFI) of an isotype or secondary only control was then used to determine the delta MFI (ΔMFI) for each stain and this was compared between transfected and naïve counterparts. Histograms of the D61D5 stain compared with secondary only are presented in Figure 3.6A. Transfected 1321N1-hPAR2 cells have a clear and bright signal detecting surface PAR2 expression and a brighter signal detected in permeabilised samples. While the naïve cells, had no detectable surface expression and a substantially lower MFI expression (Figure

3.6B) of intracellular PAR2, which indicates the presence of low level PAR2 expression stored within the cell. Overall the staining patterns found using the D61D5 antibody reflect the detected differences in transcript levels identified between the 2 cells. While the naive cells were negative for surface expression, this indicates that these cells contain some intracellular stores of the receptor. This data also supports the western blot results generated using this antibody which suggested higher expression levels of PAR2 in 1321N1-hPAR2 over naïve 1321N1, but still contained some dim staining in naïve cells. This dim western blot band may reflect the intracellular stores detected via flow cytometry.

Similar flow cytometry staining was conducted using a SAM-11 directly conjugated to PE fluorophore, compared with a PE isotype stain (Figure 3.6C). Unlike the staining conducted with the D61D6 clone, SAM-11 failed to detect differential expression between naïve and transfected cells, both cells contained surface and intracellular PAR2 and for both of these sites delta MFI of the naïve 1321N1 was higher than the transfected cells (Figure 3.6D). This does not reflect the data generated using the SAM-11 clone in western blotting, nor does it match the expected differences in expression as indicated by transcript detection (Table 3.2).

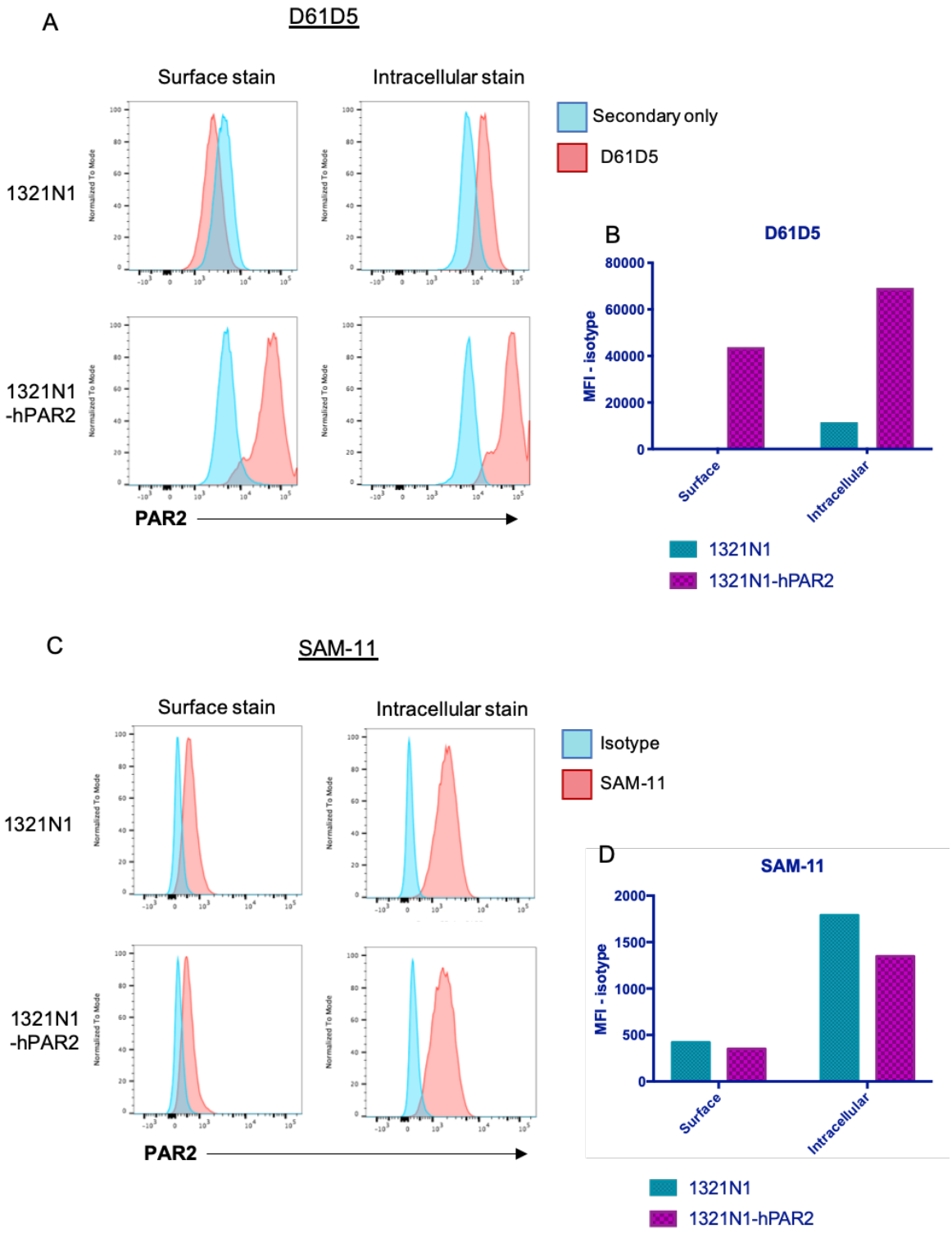

Figure 3.6 Clone D61D5 is Capable of Discriminating Between Naive and Transfected 1321N1 Cells on the Basis of PAR2 Expression.
Naive and transfected 1321N1 were lifted and maintained in suspension where cells were either stained with (A, B) D61D5 clone or (C, D) SAM-11 clone and samples run on the BD LSR II Flow Cytometer. A control for non-specific binding of antibodies was also conducted on both naive and transfected 1321N1 with (A) secondary antibody alone, or (C) a PE isotype. Histograms are displayed for each sample, which have been gated on cells with doublet exclusion for (A) D61D5 stain and (C) SAM-11 stain with control stains in blue and PAR2 stains in red. (B, D) Quantification of MFI was calculated by subtracting control stain MFI from the PAR2 stain MFI and these values were plotted with naive 1321N1 in green and transfected 1321N1-hPAR2 in purple. 1 experiment shown which is representative of 2 experimental repeats.

Since staining intensity detected using D61D5 and secondary fluorophore was much higher using flow cytometry techniques compared with detection using IF microscopy, the ImageStream was utilised to generate microscopic images. ImageStream is a method of flow cytometry which simultaneously acquires microscopic images of brightfield and fluorescence while also generating conventional flow cytometry data. Using this technique samples could be prepared and run in the same way as flow cytometry while also acquiring images of each processed event. By adopting this technique both MFI of the stain via flow cytometry and an image accompaniment for each event could be obtained, providing information on cellular location of the receptor. This was conducted using the D61D5 clone, as above with both naive 1321N1 and transfected 1321N1-hPAR2 to detect surface expression.

Images acquired from the brightfield, AF647 PAR2, and side scatter, for naive cells (Figure 3.7A) show little to no visible detection of the receptor. This is in contrast with the transfected cells (Figure 3.7B) which show clear surface membrane staining of variable intensities. The fluorescence intensity of the PAR2 across the two cells is shown in histograms where the threshold for positive staining was defined using a secondary only antibody stained negative control. This further confirms the flow cytometry data (Figure 3.6) and demonstrates that PAR2 expression is diffuse across the surface membrane of transfected 1321N1-hPAR2 cells.

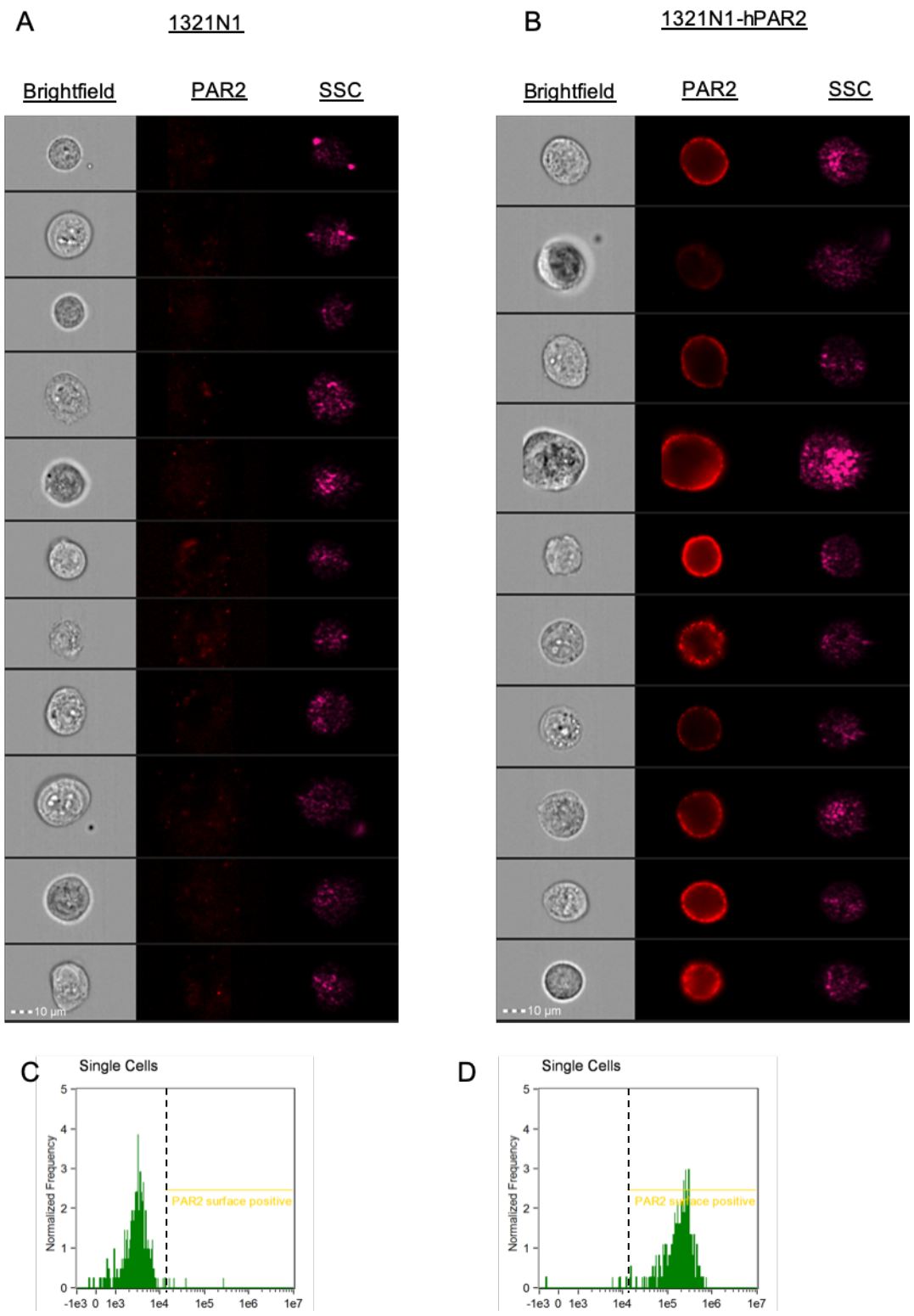

Figure 3.7 D61D5 Clone can Detect Visible Surface Membrane PAR2 via ImageStream. (A, C) 1321N1 and (B, D) 1321N1-hPAR2 cells were surface stained for PAR2 using the D61D5 clone and samples run on the ImageStream. Brightfield, AF647 (PAR2), and SSC images from a representative sample of cell events which had been gated for doublet exclusion are shown for (A) naive and (B) transfected cells. Samples with control stain (only the secondary antibody) on the respective cell type were used to establish positive staining for PAR2 expression. (C, D) The staining intensity of a positive stain is delineated with dotted lines on the histograms. N=1 for each genotype, experiment was repeated twice with the same findings, data only shown from 1 experiment.

In order to validate the observed surface PAR2 flow cytometry stain, we conducted short term stimulation with high concentration of PAR2 activating peptide (FLIGRL), which is known to lead to receptor internalisation. Cell surface membrane stain was then conducted using both SAM-11 and D61D5 clones as above, on unstimulated controls and FLIGRL stimulated samples. This assay was once again conducted in both naive and transfected cell lines.

As expected, the D61D5 clone could not detect any surface PAR2 in the naive cell line and this was unchanged upon stimulation (Figure 3.8A). As shown previously SAM-11 detected very low levels of PAR2 expression in naive cells, and upon stimulation the fluorescence intensity of this stain more than doubled (Figure 3.8C), however the staining intensity of this was so low the relevance of a 2 fold increase in this instance is limited. The D61D5 clone detected high levels of PAR2 on the surface of transfected cells (Figure 3.8B) (as seen previously, Figure 3.7B, and Figure 3.6B). The MFI of this expression was reduced 49% upon stimulation (Figure 3.8E, F). Transfected cells had low levels of detection with SAM-11 and this was slightly increased upon stimulation (Figure 3.8D) although MFI increase was not as high as the SAM-11 reported in the naive cells (Figure 3.8E, F). If the stain was specifically detecting surface PAR2 we would expect to lose some of the cell surface signal after this stimulation as the receptor is activated and internalised. The loss of surface stain in transfected cells stimulated with FLIGRL using D61D5 detection, confirms that this method is identifying PAR2. While SAM-11 stain does not detect a loss of the receptor expression upon stimulation dependent internalisation, indicating non-specific binding of this clone.

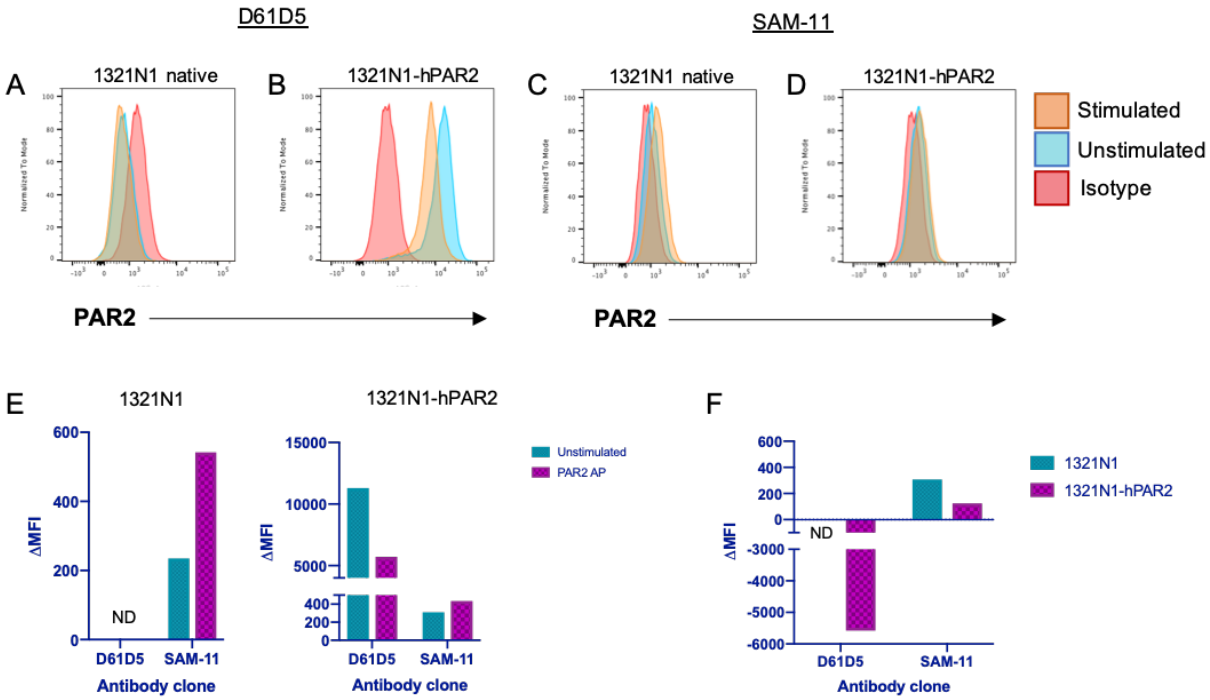

Figure 3.8 Stimulation Dependent Internalisation of Surface PAR2 is Detected Using the D61D5 Clone.

Cells were stimulated with PAR2 activating peptide (FLIGRL, 2μM) for 20 minutes while in suspension and then put on ice. Both stimulated and unstimulated cells were then surface stained for PAR2 using (A, B) D61D5, (C, D) SAM-11 or the (A, B) control secondary only or (C, D) isotype stain. All staining procedures were conducted on ice. (E) MFI was calculated through subtraction of the MFI of control stains from PAR2 stain and this is plotted for each antibody and stimulation in. (F) The difference between stimulated and unstimulated samples for each antibody was calculated. N=1 for each genotype, 1 experiment conducted.

3.3 Discussion

The literature surrounding PAR2 cellular expression is fraught with inconsistencies and contradictory data. For example, a study conducted by Colognato and colleagues employed the use of the SAM-11 and N19 antibody clones to identify PAR2 cell surface expression in human monocytes[272]. Using both western blotting and flow cytometry techniques they found that primary human monocytes from healthy donors did not express any PAR2. Transcript analysis via end point PCR amplified a product which could be seen with a faint band. Differentiation of the monocytes over a period of 7 days with M-CSF resulted in positive expression of PAR2 as detected via flow cytometry and western blot, again using the SAM-11 clone. A subsequent publication that utilized a newer anti-PAR2 antibody clone (34422, R&D), analysed PAR2 expression across peripheral blood immune cell populations and found on average 40% of peripheral blood monocytes were PAR2 expressing[286]. In this study monocytes were shown to have the highest PAR2 surface expression of all of the PBMCs analysed. These differing results could be attributed to variations within diverse human populations and limited sample sizes tested (both studies only repeated this experiment with 5-6 donors). However, it is also potentially the result of unsuitable tools employed for the detection of PAR2. If both antibodies are capable of detecting human PAR2 through western blot and flow cytometry techniques it seems unlikely that they would generate completely contradicting data. In order to facilitate reliable human expression studies, the antibodies available were validated to find a clone fit for the purposes of this study. It is advisable and good laboratory practice to validate antibodies in this manner before proceeding with data collection.

Initial confirmation that all of the antibodies used in this study bound to their target came from the use of recombinant human PAR2 which was simply dotted onto a membrane, results of which are found in Figure 3.2. The Alomone polyclonal can definitively bind to the epitope it was raised against, as demonstrated with detectable signal from the C terminal protein. There was no detected binding of the SAM-11 or D61D5 clones to the SLIGKV peptide. While this peptide sequence is a known area of the SAM-11 binding epitope it is only 6 out of the total of 14 amino acids of the complete epitope. It is unsurprising that the incomplete epitope was not sufficient for detection by SAM-11 or D61D5

clones, as antibodies often require the entirety of their cognate antigen for sufficient binding affinity. The SLIGKV peptide was used because this peptide is readily available.

Confirming positive binding to the receptor of interest does not confirm that this interaction is specific. In order to test the specificity of these interactions, an astrocyte cell line stably transfected with human PAR2 (1321N1-hPAR2) was acquired from Astra Zeneca, alongside its naïve counterpart (1321N1) that does not contain PAR2 to be used as a negative control for all staining protocols. The lack of PAR2 expression in the naive form of this cell line was originally demonstrated by Grishina and colleagues, showing undetectable RNA transcript levels and a lack of calcium flux signal in response to PAR2 activating peptides[304]. A lack of detectable levels of PAR2 transcript was also demonstrated within this chapter (Table 3.2) in the naive 1321N1 while simultaneously confirming transcript expression in the transfected cells.

The staining pattern detected by the polyclonal Alomone antibody via western blot is similar between the transfected and wildtype cell lysates, with dimmer stain intensity in the naïve (Figure 3.3 A). The blot also contains multiple bands, none of which appear to be at the expected molecular weight. This does not provide compelling evidence that the polyclonal Alomone antibody is selective for PAR2. For both the western blot and immunofluorescence there was detectable staining intensity differences between the 2 cell lines (Figure 3.3A, Figure 3.5A, and G), however both wildtype and transfected cells have very high intensity staining. Due to the nature of a polyclonal, it will contain multiple antibody clones which are often able to bind different areas of the known epitope. For this reason, polyclonal antibody stains can result in a higher concentration of antibody bound to the protein of interest, resulting in a higher detectable signal than that from a monoclonal antibody. However, overall the data generated from the Alomone polyclonal did not provide compelling evidence of specific staining, since both naive and transfected h-PAR2 cell lines have high staining intensities of multiple molecular weights.

Staining soluble lysates of 1321N1-hPAR2 cells via western blot with the D61D5 clone produced one clean band around the expected molecular weight of 44kDa followed by a faint smear (Figure 3.3B). This pattern is often found in blots of

proteins which carry post translational modifications such as glycosylation, with molecular weight correlating with the quantity of bound glycan, which can vary. PAR2 is known to post-translationally modified in many ways, including palmitoylation [307], glycosylation [20,21] and phosphorylation[309]. The protein is often dependent on these modifications for its function. For example, it has been demonstrated that the cellular location of the receptor is directed by palmitoylation. Addition of this post translational modification directs the receptor to the cell surface membrane [307]. Therefore, it is possible that the concentrated band at the 44kDa weight is PAR2 protein and the smear is caused by various post translational modifications. To investigate this hypothesis, we could employ techniques used to remove palmitoylation and glycosylation from cell lysates and reblot. However, investigating the modification status of the receptor was not essential for confirming the validity of the antibody binding and thus out with the scope of this project, so not performed.

A similar band of dimmer intensity but the same molecular weight is observed in the naive cell lysates when stained with D61D5 (Figure 3.3B). This indicates that the D61D5 is either picking up non-specific protein of a similar molecular weight or an alternative possibility is that the naive 1321N1 cells do contain some PAR2 protein. While negative transcript of 1321N1 indicates lack of expression it is possible that transcript levels are too low to detect or quickly degraded, not necessarily that it is not transcribed at all. It has also been previously shown with other thrombin receptors that an internal storage of receptor is found in endosomes[310] which enables rapid upregulation of surface expression. This could also be possible in naive cells, meaning they do contain some internal stores but are unable to respond to activation. It is also of note that naive cell staining detects no smear of post translational modification. Studying the data collected as a whole this detail may be indicative of how the receptor could be expressed in naive cells. The flow cytometry data generated using the D61D5 antibody demonstrated PAR2 surface expression in 1321N1-hPAR2 cells while the naive cells were negative at the cell surface (Figure 3.6). The lack of surface expression of endogenous receptor in the wildtype cells could be reflective of their lack of post translational marks denoted on the western blot smear, as we know from work discussed above that post translational modification is required for receptor mobilisation to the surface[307]. This hypothesis is based on research

from the surrounding literature and to provide evidence to support this, the presence of modification in transfected h-PAR2 1321N1 cells would need to be confirmed. Further to this, in order to confirm post translational modifications detected in the transfected cell line are driving the mobilisation of this receptor to the cells surface, inhibition of these modifications could be performed and further staining of their surface PAR2. However, this question is out with the scope of this thesis and therefore was not carried out.

Immuno-Fluorescent staining of fixed/permeabilised adherent cells for microscopy using the D61D5 antibody was somewhat successful. A faint but visible stain was located in transfected cells (Figure 3.5C) and reduced staining detected in the naive cells (Figure 3.5D). However, the staining intensity was very faint in what is probably an overexpressing PAR2 transfected cell line, which may not be useful for detection of lower levels of expression in primary cells. As well as this, it was of note that while there was some staining of the cell body there was also a high concentration of nuclear staining(Figure 3.5D), a pattern mirrored in the Alomone polyclonal stains (Figure 3.5A and B). Nuclear localisation of PAR2 has not previously been observed in studies analysing the trafficking of this protein using labelled PAR2, such as GFP-PAR2[300], mCherry-PAR2[307] and flag tagged-PAR2[244,248]. These papers primarily reported surface expression and an intracellular localisation within the cytoplasm, which is increased upon post-stimulation internalisation. However, there have been previous reports of GPCR localisation to the nucleus[311], which includes PAR2, where this observation was made in neuronal cell types. The study conducted by Chemtob and colleagues identified that nuclear translocation post cell surface activation was an essential function of PAR2 in driving neo-angiogenesis in neurons [312]. In doing so this group identified a novel method of PAR2s function to directly drive gene transcription (in this case vegfa) via interaction with the genome [313]. While the 1321N1 cell line is not neuronal, it is an astrocyte and these cells are also located in the central nervous system (CNS). It may be possible that this nuclear localisation function is present in other CNS cell types – such as astrocytes. However, localisation of PAR2 to the nucleus was driven by cell surface PAR2 activation [313]. The 1321N1 cells in these experiments had received no treatment of PAR2 activating ligands, and therefore we would not expect to visualize nuclear localization. One possibility is that the cell culture

media used to maintain these cells contained some serine proteases, which could be a possible source of PAR2 activators. The source of proteins in the cell culture media is Foetal Bovine Serum (FBS) and the exact composition of this is not defined and varies from batch to batch. Supernatant was not stored from these experiments, so it was not possible to investigate this hypothesis.

Final investigation of the suitability of D61D5 antibody stain was confirmed with flow cytometric analysis. As flow cytometry would be the most utilised method for investigating PAR2 expression in human monocytes, this test would confirm the suitability of this antibody clone to take forward for further use. Expression of PAR2 on the cell surface membrane was detected in 1321N1-hPAR2 cell line via D61D5 staining, while surface stain in naive 1321N1 cells was absent (Figure 3.6A and B).

From here the specificity of the surface stain was confirmed using activation induced internalisation of the receptor. As conventional activation of PAR2 involves cleavage of the receptor, this leads to internalisation and subsequent degradation of PAR2; a necessary step to halt receptor activation. This has been confirmed in multiple publications [244,246,308,314,315]. Internalisation of PAR2 has also been reported after stimulation with activating peptides which mimic the cleaved N terminus[244,308,314]. If surface binding of the D61D5 antibody was specific for the PAR2 protein a loss of the detectable surface stain would be expected after 20 minutes of stimulation. The time-point of 20 mins was specifically chosen because previous publications have demonstrated that between 5 min and 30 min receptor internalisation is ongoing[248] and complete replenishment of receptor at the cell surface occurs after 120 min[308]. In the interim it has been shown that cells are unresponsive to PAR2 stimulation further confirming the period of internalisation without replenishment of receptor. As can be seen in Figure 3.8B, E, and F, surface levels of PAR2 dropped to 50% of the unstimulated fluorescence intensity. While not all receptor expression was lost, this is not a major concern. It would be unlikely to achieve 100% loss of surface PAR2 for many reasons, such as not achieving a significant enough dose to saturate the high level of surface expression in transfected cell lines, or faster than anticipated recruitment of new PAR2 receptors to the cell surface. Therefore a 50% reduction is significant enough to have confidence that this

antibody is detecting PAR2 on the surface of cells, and will be able to detect changes to surface expression in human cells.

Since this antibody clone appears to be useful in the detection of PAR2 using flow cytometric techniques but failed to robustly detect PAR2 with IF microscopy, Imagestream analysis was conducted. This application enables the generation of both microscopy images and flow cytometric data, with the same cell preparation required for flow cytometry. Staining for IF microscopy involved fixation and permeabilization prior to the staining process, while flow cytometry staining did not require any fixation, and if the cells do need to be fixed this can be conducted post staining. It is therefore possible that the failure to generate a bright signal with the D61D5 antibody clone for IF microscopy was due to a lack of epitope availability post fixation. The ability to generate microscopy images with flow cytometric cell preparations with the Image stream provide detailed information on the surface expression pattern of this receptor in the transfected cell line, showing a largely uniform distribution across the surface membrane. This may be a more useful technique to employ in order to identify the localisation of the receptor when using the D61D5 clone than IF microscopy. Especially in non-adherent cell types which will not be influenced by maintenance in suspension for this technique.

Overall, evaluation of the SAM-11 antibody had variable outcomes from the tests conducted. The western blot staining pattern of SAM-11 stain contained multiple bands, none of which were at the expected weight and the patterns do not match those found with the polyclonal or D61D5 stain (Figure 3.3C). The SAM-11 antibody, however, did not stain the negative control lysates (naive 1321N1) (Figure 3.3C). Therefore, it is possible that the multiple bands found are indeed PAR2 protein in different forms. It has been demonstrated that PAR2 is able to homo-dimerise [316], and hetero-dimerise with other PAR family members [317,318]. These multiple bands could reflect this dimerization, or co-localisation with other proteins, as well as potential post-translational modifications discussed earlier. The variations between the staining patterns found with each antibody when using the same cellular lysates indicates that either some antibodies are binding non-specific proteins or it is also possible that one clone of anti-PAR2 may be more inclined to detect specific dimers, or post-translational

modifications than another, potentially due to loss of some visible epitopes post-dimerization/modification.

Inconsistencies were identified in the application of the SAM-11 antibody for western blot. Different patterns of bands were detected between one experiment and another when all conditions were kept consistent. For example, the staining patterns found between Figure 3.3C and Figure 3.4C. In these figures new cell lysates from the 1321N1-hPAR2 cells were made but these cells had been cultured in the exact same manner, and proteins extracted in the same way. There were no major differences between the staining patterns with the Alomone (Figure 3.3A and Figure 3.4A) or D61D5 antibodies (Figure 3.3B and Figure 3.4B) between these experiments. It may be of note to refer to the previous PAR2 antibody evaluation paper[300] and note the variation in types (weight and number) of bands found when looking at endogenous protein over transfected cell proteins. Variation in SAM-11 staining patterns within the same cell lines across different experiments was also identified in this antibody evaluation paper, similar to what was found between Figure 3.3C and Figure 3.4C. It is possible that the receptor dimerises or post-translational modifications are different between different cell lysates taken at different times but this adds further complication to analysing these blots.

When investigated for use in IF microscopy (Figure 3.5E and F), the SAM-11 clone failed to detect any PAR2 in either transfected or naive cell lines. Due to the direct conjugate method used with this clone, this may have limited the potential staining intensity. Instead, using a method with SAM-11 as a primary antibody and a secondary anti-mouse antibody with a conjugated fluorescent probe could amplify the signal and may give detectable PAR2 staining. However, given the time implications, this additional experiment was not considered to be of priority.

Flow cytometry staining methodology was then tested with the SAM-11 antibody (also a direct conjugate). This stain failed to detect higher receptor presence in transfected cell lines (Figure 3.6C and D), which would be expected based on the transcript data from Table 3.2 and the D61D5 flow cytometry data shown in Figure 3.6A and B. This antibody also failed to detect any internalisation of the receptor post short term stimulation (Figure 3.8C, D, E, and F) unlike the D61D5

clone (Figure 3.8A, B, E, and F). Therefore, using this protocol we were unable to get robust PAR2 staining. The reason behind the discrepancy between our data and previously published data, which demonstrated that SAM-11 could detect surface PAR2 in transfected cells lines and could also detect internalisation post stimulation[300], is unknown. It is possible that there are some manufacturing discrepancies between batches of this antibody. This would be likely in the case of a polyclonal antibody which is expected to have lot to lot variation due to uncontrolled or defined clones present. However, this would not be expected from a known monoclonal antibody.

3.4 Conclusion

Taken together the data presented in this chapter provides evidence to support the D61D5 antibody clone as a reliable means of detecting cell surface human PAR2 via flow cytometry. Since the primary technique to be used in this thesis to detect changes in surface receptor expression was planned to be cytometry, this antibody clone was taken forward for PAR2 detection in human cells for the remaining experimental studies reported in this thesis. In order to confirm suitability of this clone for western blot applications, further validation is required. Using knock down techniques in the naive cell line to ensure negative staining would be valuable to confirm suitability in this technique. However, the staining intensity found with IF is less than optimal for discriminating expression changes. Nuclear focused staining identified in IF indicates that this antibody could potentially be bound to something non-specific in this application and therefore the IF staining protocol would not be recommended with this clone. By utilising flow cytometry to only stain the cell surface membrane should eliminate any concern with regards to potential non-specific nuclear staining. Any intracellular staining experiments should be performed in the knowledge that the specificity of this stain has not been confirmed. Confirmation of specificity for cell surface flow cytometry detection should also be conducted in all new cell types, through detection of receptor internalisation.

Conversely, the other antibodies failed to robustly detect PAR2 expression differences between wildtype and transfected cells across all applications tested. The Alomone polyclonal antibody failed to determine differential expression of human PAR2 in transfected vs naive cells using western blotting techniques and stained proteins of varying molecular weight. While the SAM-11 antibody did detect the presence of protein in transfected cells and none in naive cells, there was still large variation of bands present and different band patterns when using different lysates. This antibody also failed to detect differential expression of PAR2 between the 2 cell lines using flow cytometry techniques and failed to detect internalisation of protein post stimulation. Therefore, for these reasons the SAM-11 clone and Alomone polyclonal were not taken any further for human studies in this thesis.

4 Expression and Function of PAR2 in Human Monocytes

4.1 Introduction

Monocytes are an integral cell type in the inflammatory response. In chronic disease settings such as RA they are continually recruited to the inflamed joint. Due to heightened demand during chronic inflammation, these cells undergo premature egress from the bone marrow, which is thought to contribute to their altered phenotype[186]. Furthermore in RA, monocytes have an altered transcriptome when compared to healthy individuals [319]. In addition to altered state, RA patients have higher numbers of monocytes present in peripheral blood, and increased numbers of monocytes in patients correlates with non-responsiveness to both methotrexate[320] and anti-TNF therapy[321]. When these cells are recruited into the joint they are capable of playing a dual role in the inflamed arthritic joint. They have capacity to differentiate into macrophage, producing inflammatory cytokines and chemokines, further perpetuating the chronicity of the disease; or alternatively, they can develop tissue specific functions and fuse into multinucleated, bone resorptive, osteoclasts contributing to end stage joint damage through bone erosion.

The RA joint is a site of high inflammatory activity, with active immune cells and stroma producing a plethora of cytokines and chemokines, as well as catabolic proteases. These enzymatically active components not only function to break down the surrounding tissue but they also act in a hormone like manner, through activation of the G protein coupled receptors responsive to proteases (PARs, reviewed in the introduction, see section 1.4). PAR2 is responsive to proteases highly associated with active immune cells, such as neutrophil elastase and mast cell tryptase. Thus it is hypothesised that upon entering the inflamed RA joint, cells expressing PAR2 will be responsive to the inflammatory proteases present.

The expression of PAR2 in human monocytes and their subsequent macrophage or osteoclast differentiation potentials and whether they can respond to proteases via PAR2 is debated in the literature. Some papers have previously reported that human monocytes do not express PAR2[272]. While other reports have shown consistent expression of both transcript and cell surface protein in

around 50% of the human monocyte population [286]. It has been established through adoption of murine models of disease that PAR2 plays a functional role in multiple inflammatory diseases[264,276,283,322,323]. In addition, multiple studies have also found an increase in the expression of PAR2 in human monocytes in the context of inflammatory diseases, including severe asthmatic patients [299], and RA patients [297,324].

Previously, research conducted in our group demonstrated increased PAR2 expression in peripheral blood monocytes from RA patients compared with matched healthy controls[297]. This increase in expression correlated with disease activity, with patients in severe flare showing significant enhancement in PAR2 expression. However, this data was generated using the SAM-11 clone of anti-PAR2 antibody, and data from chapter 3 of this thesis established that this antibody could not reliably detect PAR2 expression in transfected cells known to express this receptor.

Overall the aims of this chapter were to:

1. Adopt the optimised protocol for PAR2 cell surface detection using clone D61D5 from chapter 3 of this thesis, in order to:

    a. Determine expression of PAR2 in monocytic cell line THP-1

    b. Clarify PAR2 expression levels in primary healthy human monocyte subsets

    c. Measure PAR2 expression in response to differentiation signals and inflammatory signals

    d. Confirm enhanced expression of PAR2 in RA patients with new antibody clone

4.2 Results

4.2.1 PAR2 Expression in Human Monocyte Cell line THP-1

THP-1 cells are a spontaneously immortalised human monocyte cell line which were originally isolated from a patient with acute monocytic leukaemia in 1980 [325]. As an immortalised cell line these "monocyte-like" cells could be a valuable tool for dissecting the functions of PAR2 in monocyte biology. However, in order to assess if this cell line is suitable for investigation of PAR2 function the expression of this receptor in this cell line had to be confirmed. Therefore, PAR2 cellular staining techniques validated in the previous chapter were applied for the detection of PAR2 in THP-1 cells. This method utilises a primary antibody detection of PAR2 (clone D61D5) and secondary antibody conjugated to a fluorophore (in this case AF647) binding to the primary and enhancing the detectable signal. Optimisation of the secondary antibody concentration for both surface and intracellular stains was initially conducted . Notably, the secondary antibody was associated with increased fluorescence due to non-specific binding Figure 4.1A. Based on this data, 1μl per sample was chosen the in order to minimise non-specific staining. This was then applied to PAR2 stains of THP 1 cells for surface expression (Figure 4.1B) and intracellular stores (Figure 4.1C). PAR2 surface expression was consistently negative in naïve THP-1 cells which is consistent across increasing concentrations of antibody (Figure 4.1B). However, these cells do appear to express some intracellular stores of receptor (Figure 4.1C).

A lack of PAR2 expression in naïve THP-1 cells suggests that they may not be a valuable tool to assess PAR2 function in naïve monocytes. However, the presence of intracellular storage of this receptor (Figure 4.1C) suggests that it could be recruited to the surface under certain circumstances. To determine whether maturation of THP-1 cells alters receptor expression (i.e., increased surface expression), which would make a THP-1 knock out of this receptor a valuable for assessing PAR2s function in differentiated monocytes, the cells were differentiated into macrophage-like cells.

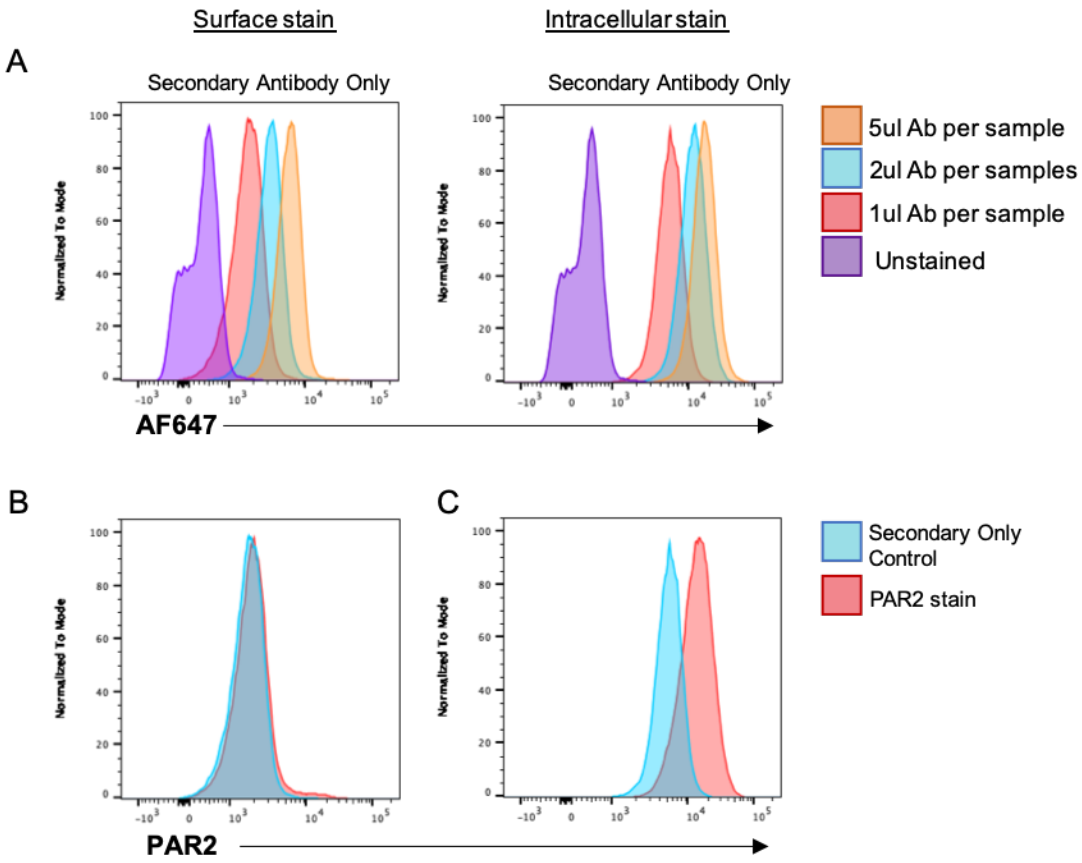

Figure 4.1 Naive Human Monocyte Cell Line - THP1- do not Express Cell Surface PAR2 but do Contain Intracellular Stores of Receptor
Titration of the anti-rabbit-AF647 secondary antibody was conducted on THP1 cells for both cell surface and intracellular staining. (A) Cells were incubated with an Fc block and either 1, 2, or 5ul of anti-rabbit AF647 and histograms were plotted to demonstrate the different AF647 baselines compared with unstained cells. (B) THP1 cells were then incubated with Fc Block and either 1μl of D61D5, followed by 1μl of secondary AF647 cell surface staining or (C) permeabilised for intracellular staining with secondary only staining controls. Histograms presenting with logarithmic X axis. N=1, 1 experiment shown representative of 2 experimental repeats.

In order to generate THP-1 derived macrophage like cells, naïve THP-1s were stimulated with 10ng/ml of phorbol 12-myristate 13-acetate (PMA). This promoted naïve THP-1 cells to adhere to tissue culture plastic and adopt a more elongated, macrophage-like morphology. The expression of PAR2 was assessed in response to both initial PMA stimulation events of 1 and 4 hours (Figure 4.2 A, B, C) and then across a differentiation time course including 24 hours (D), 48 hours (E), until full differentiation at 72 hours (F). At no point in the differentiation process assessed did THP-1 cells express surface PAR2. Thus, differentiation into macrophage-like cells does not transport intracellular stores of PAR2 to the surface of THP-1 cells.

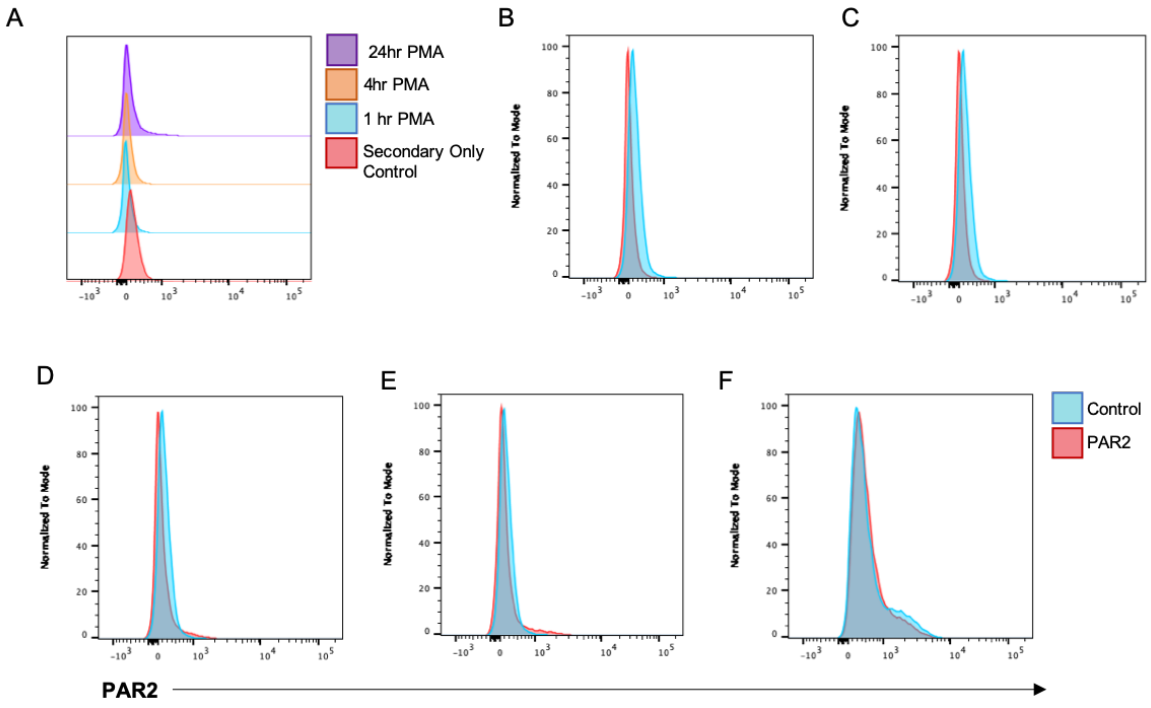

Figure 4.2 Adherence of THP-1 Cells via PMA Differentiation Does Not Induce Cell Surface PAR2 Expression
THP1 cells are stimulated with PMA (10ng/ml) and cells were analysed for PAR2 expression multiple times across a time course of (A) early response and (E, F) later responses when cells begin to adhere. Early time points included (B) 1 hour, (C) 4 hours, or (D) 24 hours. Extended time points included (E) 48, or (F) 72 hours. All staining was conducted on ice. N=1, 1 experiment shown representative of 2 experimental repeats

Although PAR2 was not detected in naïve or macrophage-like THP-1 cells, it is possible that it would be expressed on alternative differentiation states. Prior studies [326] have suggested that it is possible to differentiate THP-1 cells into osteoclast-like cells. Thus, using this published protocol THP-1s were stimulated with an initial high dose of PMA (100ng/ml) for 3 days, and then exposed to 50ng/ml of both M-CSF and RANKL for a further 6 days (Figure 4.3A). At the end point of this culture the cells were TRAP stained, in order to identify an osteoclast associated enzyme - Tartrate-Resistant Acid Phosphatase. Osteoclasts were defined as TRAP+ cells which contain at least 3 nuclei. In this setting, TRAP+ multinucleated osteoclasts were formed and these are highlighted with red arrows (Figure 4.3B). Interestingly, while many of the cells fused into multinucleated cells several of these cells did not stain positively for TRAP enzyme (black arrowhead, Figure 4.3B). To evaluate PAR2 expression in this setting, the cells were lifted from plastic using trypsin replacement cell dissociation buffer TrypLE (in order to limit potential PAR2 activation) and these

cells were stained for PAR2 surface expression. Expression was evaluated on both day 5 (prior to osteoclast maturation)(Figure 4.3C) and also at terminal differentiation (Figure 4.3D). At both time points assessed the osteoclast-like cells did not express any surface PAR2.

Taken together, it was clear that THP-1s are not a valuable cell line for the investigation of PAR2 biology in monocytes/macrophage or osteoclasts. Thus, although plans were in place to generate PAR-2 knockout THP-1 cells, due to a lack of detectable receptor in these differentiated cells there would not be any value in taking them forward to generate a human monocyte *par2*$^{-/-}$ line.

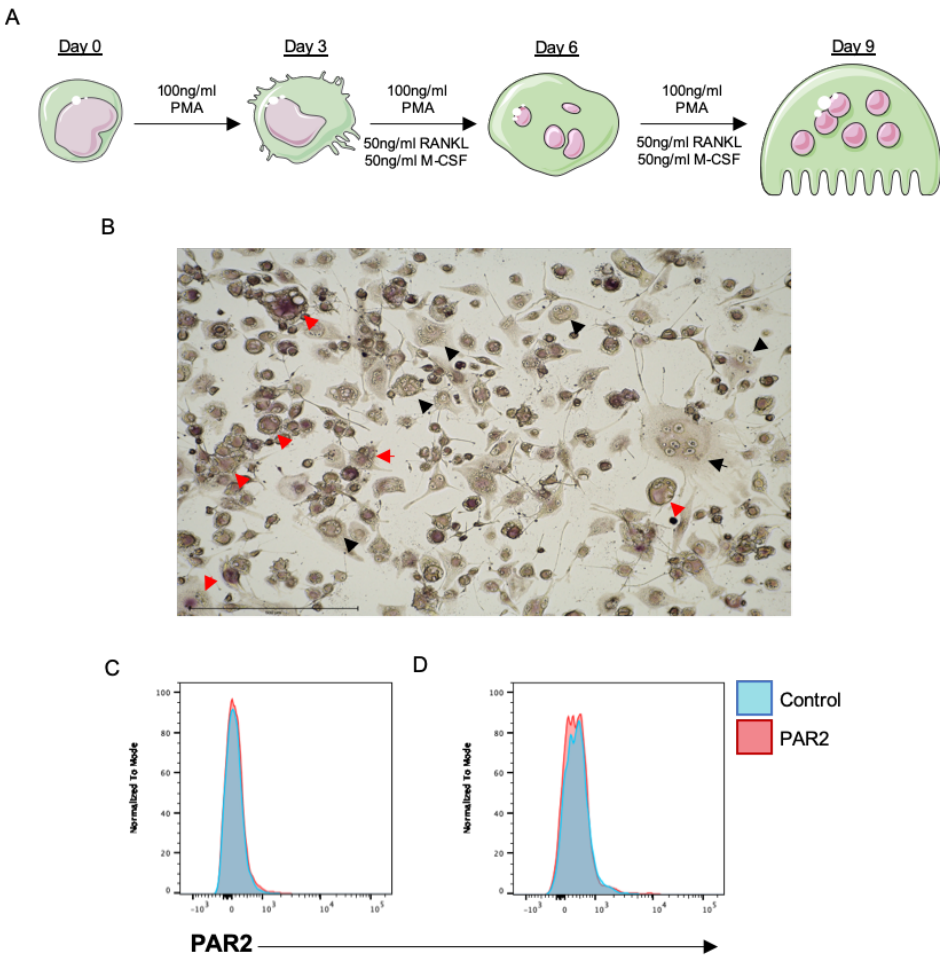

Figure 4.3 Differentiation of THP-1s into Osteoclast-like Cells does not Promote Surface PAR2 Expression
(A) THPs were first matured with 3 days of PMA (100ng/ml) promoting cellular adherence to plastic, addition of M-CSF and RANKL (50ng/ml) was then added to the culture for another 6 days, with a media change every 3 days. (B) TRAP stain was conducted at day 9, with TRAP positive multinucleated cells shown with a red arrowheads and multinucleated cell TRAP negative are displayed with a black arrowheads. Cells were detached from the plates and stained for PAR2 (or control stain) on (C) Day 5 or (D) Day 9 of the culture. N=1, 1 experiment shown representative of 2 experimental repeats

4.2.2 PAR2 is Expressed on the Cell Surface of Healthy Human Monocytes

As previously discussed, the literature contains conflicting data surrounding the presence of PAR2 on the plasma membrane of human monocytes[300]. This may largely be due to the application of different antibody clones across laboratories for the detection PAR2; including polyclonal antibodies generated "in-house". In order to clarify this issue the staining technique optimised in chapter 3 using the validated anti-PAR2 antibody clone D61D5 for PAR2 detection was applied to primary healthy human monocytes.

Peripheral blood mononuclear cells (PBMCs) were isolated from healthy human buffy coat. These cells were then stained to exclude (a) dead cells (DAPI: V450), and (b) lineage markers (FITC) for T cells (CD3), B cells (CD19), NK cells (CD56), and granulocytes (CD15). To identify monocytes, cells were stained with HLADR-PECy7 (MHC II expression), CD14 (BV605), and CD16 (PE). Samples were also stained with the anti-PAR2 D61D5 clone for both surface expression and intracellular stores. A secondary anti-rabbit conjugated AF647 was used to detect the PAR2 stain via fluorescence. Monocytes were identified by positive gating of the PBMC population, excluding doublets, excluding lineage positive cells and positively gating for HLADR, CD14, and CD16 (Figure 4.4A). Monocyte populations were further sub-divided based on CD14 and CD16 expression with classical monocytes expressing $CD14^{hi}CD16^{-}$, intermediate $CD14^{+}CD16^{+}$, and non-classical $CD14^{lo}CD16^{hi}$ (Figure 4.4A).

PAR2 expression on each of these subsets was analysed for both surface PAR2 expression (Figure 4.4B) and intracellular stores (Figure 4.4C). To ensure that negative fluorescence baseline (secondary only staining) remained unchanged across the different subsets of monocytes, the secondary only control MFI of each subset was compared (Figure 4.4D). This was conducted to ensure there was no differential influence of non-specific antibody binding on PAR2 expression analysis between different subsets. The secondary only antibody surface stain ranged from 300 to 800 MFI, which represents variation across the human population (Figure 4.4D). Importantly, it was consistent across the subsets. Thus the PAR2 expression was comparable across these groups.

All samples consistently expressed intracellular PAR2 stores at consistent levels across all the monocyte populations (Figure 4.4C). All healthy donors expressed surface PAR2 in intermediate and classical monocyte populations, with PAR2 absent in some donor non-classical monocytes (Figure 4.4B). Across the 14 buffy coats sampled each individual had the highest PAR2 expression levels in their classical monocyte population, with slightly decreased expression in intermediate monocytes and significantly reduced surface PAR2 expression in non-classical monocytes (Figure 4.4F). Therefore, with the validated anti-PAR2 clone, D61D5, this data confirmed that healthy human monocytes do express surface PAR2 and the population with the highest expression of this receptor are the classical monocytes.

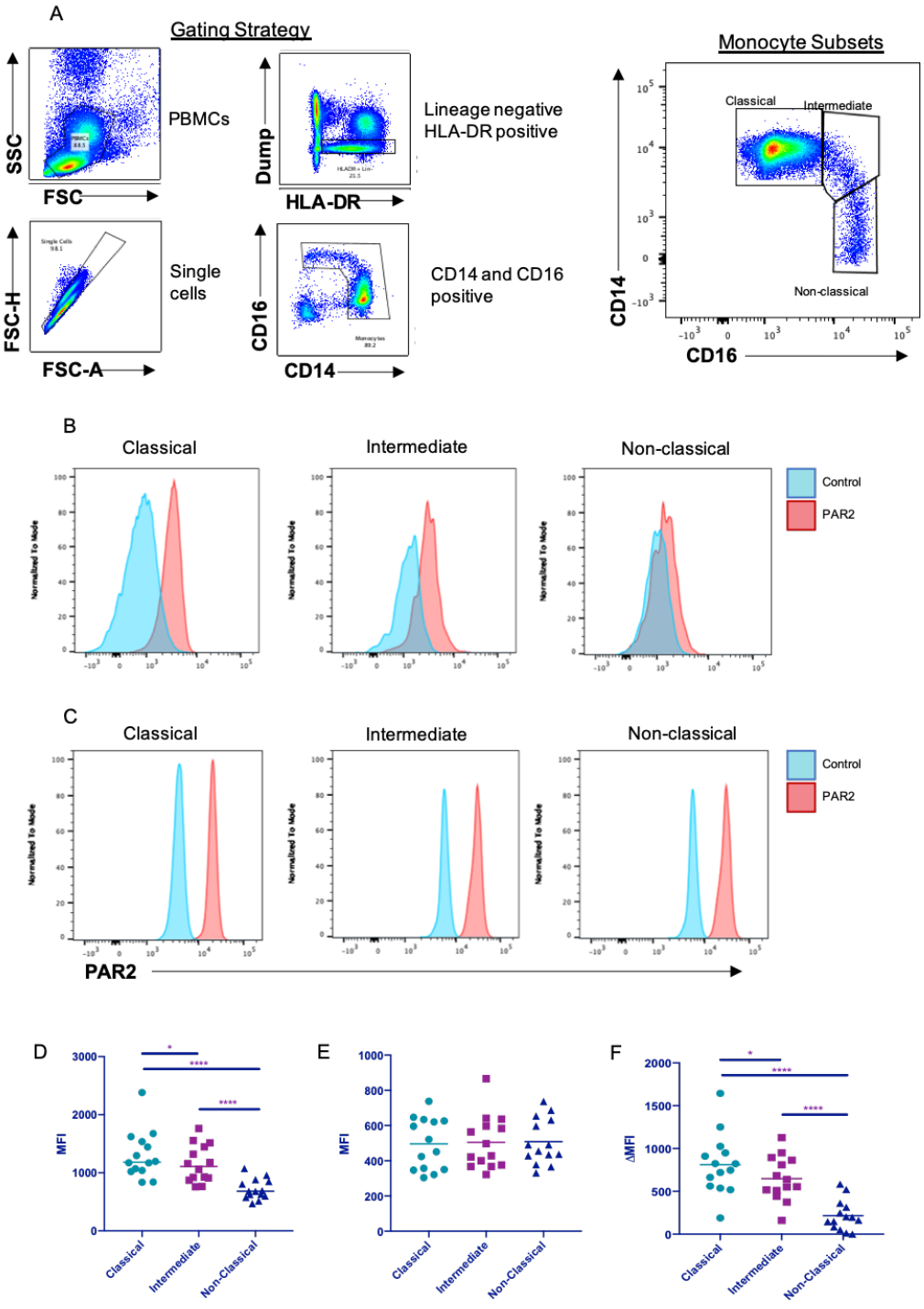

Figure 4.4 Healthy Human Peripheral Blood Monocytes Express Plasma Membrane PAR2
Peripheral blood mononuclear cells were isolated from healthy donors and stained for monocyte discrimination – HLADR positive, Lineage (CD3, CD19, CD56, CD15) negative, CD14 and/or CD16 positive – and PAR2. Gating strategy for analysis is shown in A. Monocyte subpopulations were discriminated based on expression levels of CD14 and CD16, Classical monocytes $CD14^{hi}$ $CD16^{lo}$, Intermediate monocytes $CD14^{+}$ $CD16^{+}$, Non-classical $CD14^{lo}$ $CD16^{hi}$. (B) Surface expression of PAR2 was measured in subpopulations of monocytes and (C) intracellular expression of PAR2 found through permeabilization prior to PAR2 stain for each subpopulation, histograms show representative graphs from 1 donor. The unadjusted PAR2 stain MFI for each sample is represented in figure D the MFI values for the control stains shown in E and the delta MFI for surface PAR2 stain (subtraction of the control MFI from the PAR2 stain MFI) is represented in figure F. One way ANOVA with paired analysis using the Geisser-Greenhouse correction which does not assume sphericity was conducted with Turkey's multiple comparisons test. * $p < 0.05$, **** $p < 0.0001$ N=14.

Since this was the first time using human monocytes for PAR2 stain with this antibody, much like the 1321N1 cell line it was important to confirm this staining was specific and reliable in the context of these cells. In order to demonstrate antibody specificity in human monocytes, activation-dependent internalisation was performed to determine if a loss of surface stain upon internalisation could be detected. On this occasion 3 healthy donor PBMCs were isolated in the same fashion as above and were left either unstimulated (Figure 4.5A) or stimulated with 2μM of PAR2 activating peptide FLIGRL for 20 minutes (Figure 4.5B). Once again these stains were compared with a control secondary only stain (Figure 4.5 A and B). Unstimulated surface PAR2 stains of all 3 donors were low but detectable (range from 118-191 ΔMFI). After 20 minutes of FLIGRL stimulation, PAR2 expression in all donors dropped to undetectable levels as can be seen in the histogram comparisons with secondary only antibody (Figure 4.5B). The difference in PAR2 expression MFI between unstimulated and FLIGRL internalisation is shown in Figure 4.5C and the ΔMFI (subtraction of control stain) differences are represented in graphical form in Figure 4.5D. From this it can be determined that the PAR2 surface stain appears to be reliably detecting PAR2 on the plasma membrane, which is completely lost upon stimulation-dependent internalisation of the receptor.

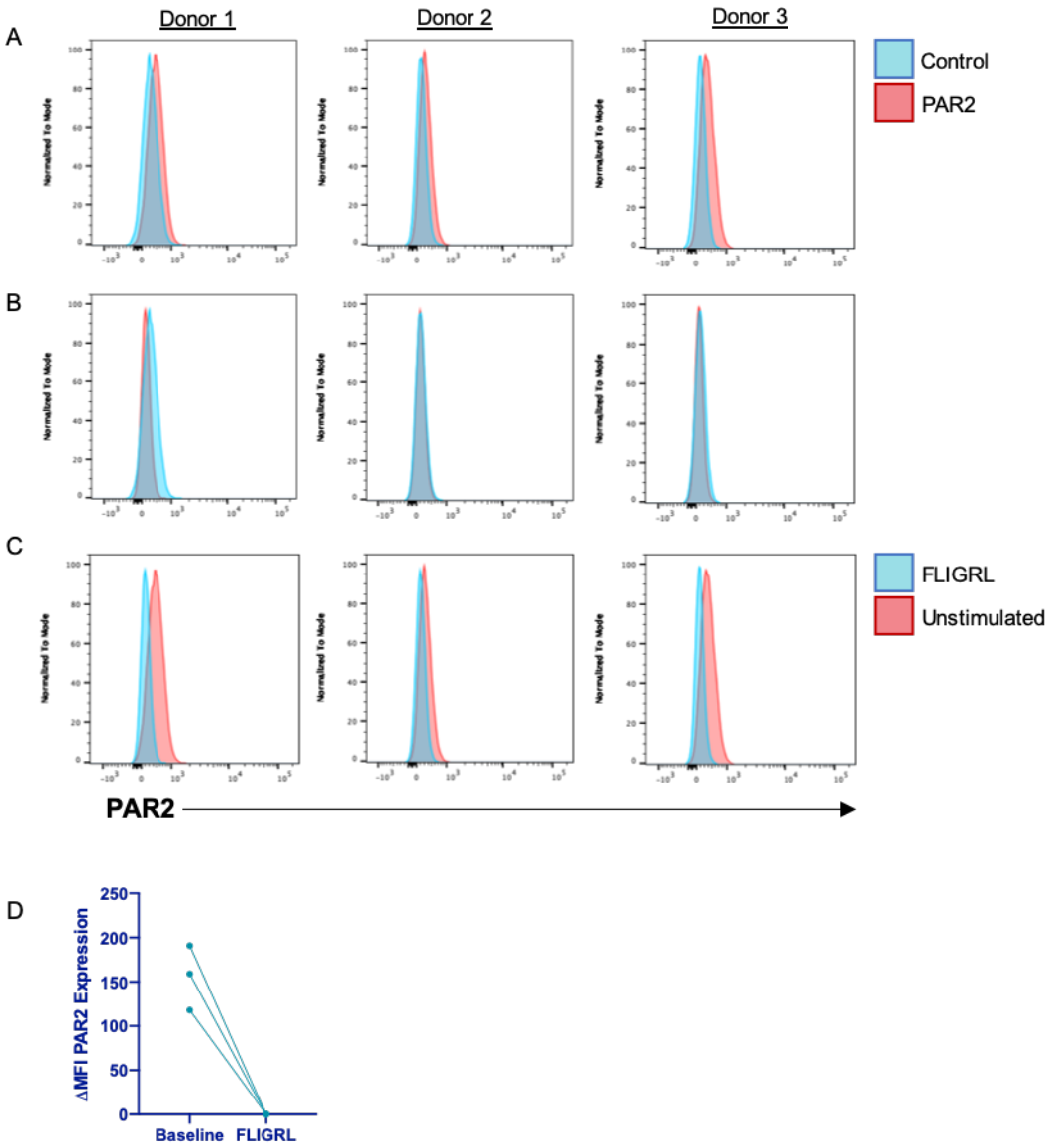

Figure 4.5 D61D5 Antibody Clone Can Detect FLIGRL Internalisation of PAR2 in Human Monocytes.
Peripheral blood mononuclear cells were isolated from healthy human blood and either left (A) unstimulated or (B) stimulated with 2μM PAR2 activating peptide FLIGRL for 20 minutes. Cells were then immediately put on ice and stained for surface markers (CD3, 20, 56, 15, HLADR, CD14, CD16) and PAR2. Using surface marker expression monocytes were gated as in Figure 4 and PAR2 expression assessed for (A) unstimulated and (B) FLIGRL and (C) PAR2 expression was compared between these 2 groups. (D) The delta MFI was calculated by subtraction of the control 2nd only antibody stain from PAR2 D61D5 stain and these were plotted for each donor for both unstimulated baseline levels of PAR2 and FLIGRL stimulated; lines connect paired data. N=3, data form 1 experiment shown representative of 2 experimental repeats.

4.2.3 PAR2 Expression in Monocyte Derived Differentiation States

The experiments conducted in 4.2.2 established reliability of our PAR2 surface measurement in human monocytes and confirmed that primary human monocytes express PAR2 with some population variation. Therefore, differences in PAR2 expression in response to stimulation and monocyte differentiation could subsequently be conducted, which will hopefully provide indication of the function of this receptor in monocyte biology. As previously discussed, monocytes can differentiate (given the appropriate signals) into either macrophage or osteoclasts. The next step was therefore to evaluate the effect of monocyte differentiation on PAR2 expression levels. To achieve this, optimised *in vitro* methods were used to recapitulate these differentiation states.

Prior to initiating *in vitro* monocyte differentiation verification of a pure CD14+ monocyte isolation was conducted, as contamination with other immune cells could influence experimental outcomes. A CD14 positive EasySep Cell isolation kit was used to selectively isolate CD14 expressing cells from PBMCs. The positive selection method was chosen because the CD14 high monocyte population expresses the highest levels of PAR2 (Figure 4.4), and thus they represented a monocyte population that may be most influenced by PAR2-mediated signalling. Cells were isolated from peripheral blood using this kit; and the original PBMC sample, the negative discarded sample, and the positively isolated monocyte sample, were all stained for flow cytometric analysis to determine the purity of the resulting monocyte isolation. The original PBMC sample proportionally contained 65.5% T cells, 10.7% B cells, 3.88% NK cells, and 8.52% monocytes (Figure 4.6A). These frequencies are within the standard range expected for healthy human PBMCs [327]. The negative fraction proportionally increased levels of T cells, B cells, and NK cells in response to monocyte depletion (Figure 4.6B), and while monocytes were depleted in this sample some remained (proportionally 2.87% of the sample acquired). Which meant a small number of monocytes was lost to this method. The purity of the monocyte isolation was very high at 91.3% (Figure 4.6C). This is a reliable purity level to be certain that the measurable biological effects observed in upcoming assays will be from the monocyte compartment, with negligible influence from other PBMC components.

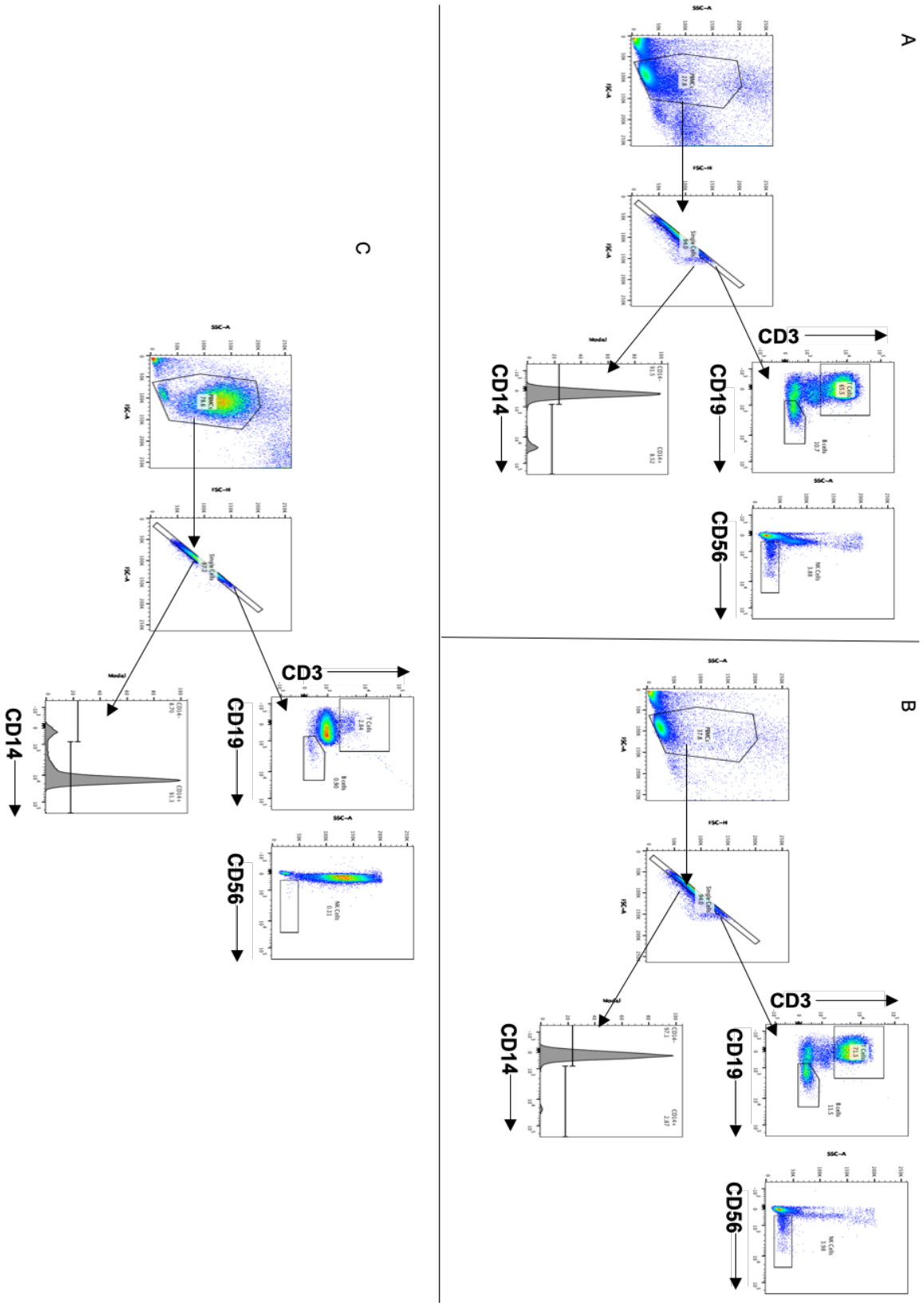

Figure 4.6 Assessment of Monocyte Purity using CD14 Positive Isolation
Peripheral blood mononuclear cells are separated from blood via density based centrifugation and CD14+ Monocytes isolated using Stem Cell Easy Sep Isolation Kit II. The purity of this isolation was assessed using flow cytometry. (A) The total PBMC population, (B) negative fraction which is discarded, (C) and isolated CD14 monocyte fraction were all stained for T cells (CD3), B cells (CD20), NK cells (CD56), and Monocytes (CD14 and CD16). N=1, 1 experiment shown representative of 2 experimental repeats

Macrophage colony stimulating factor (M-CSF) is a haemopoietic cytokine/growth factor found endogenously in the body, required for the survival, proliferation and the differentiation of monocytes, their precursors and their differentiation potentials[328,329]. It is therefore a central growth factor in the maintenance of monocytes in cell culture. When monocytes encounter this growth factor *in vitro* they begin to adhere to plastic and over time develop an elongated morphology resembling monocyte derived macrophages (Figure 4.7A).

As well as monocyte derived macrophage differentiation, it was also of interest to investigate PAR2 expression upon monocytic differentiation into OCs. PAR2 has previously been implicated in bone biology [330] and now with known expression in OC precursor monocytes (Figure 4.4) it is of interest to further clarify the role of this receptor in monocyte derived osteoclast differentiation. The protocol followed to differentiate human monocytes into osteoclasts is shown in Figure 4.7 B. OCs will positively stain for the TRAP enzyme (appears purple), while macrophage-like differentiated cells will not express this enzyme and will not stain (Figure 4.7 C and D). These protocols were sufficient to generate adherent monocyte derived cells which morphologically resemble macrophages (Figure 4.7 A and C) and TRAP positive, multinucleated OCs (Figure 4.7 B and C). Using these in vitro differentiation states the plasma membrane expression of PAR2 in monocyte differentiation potentials could be explored.

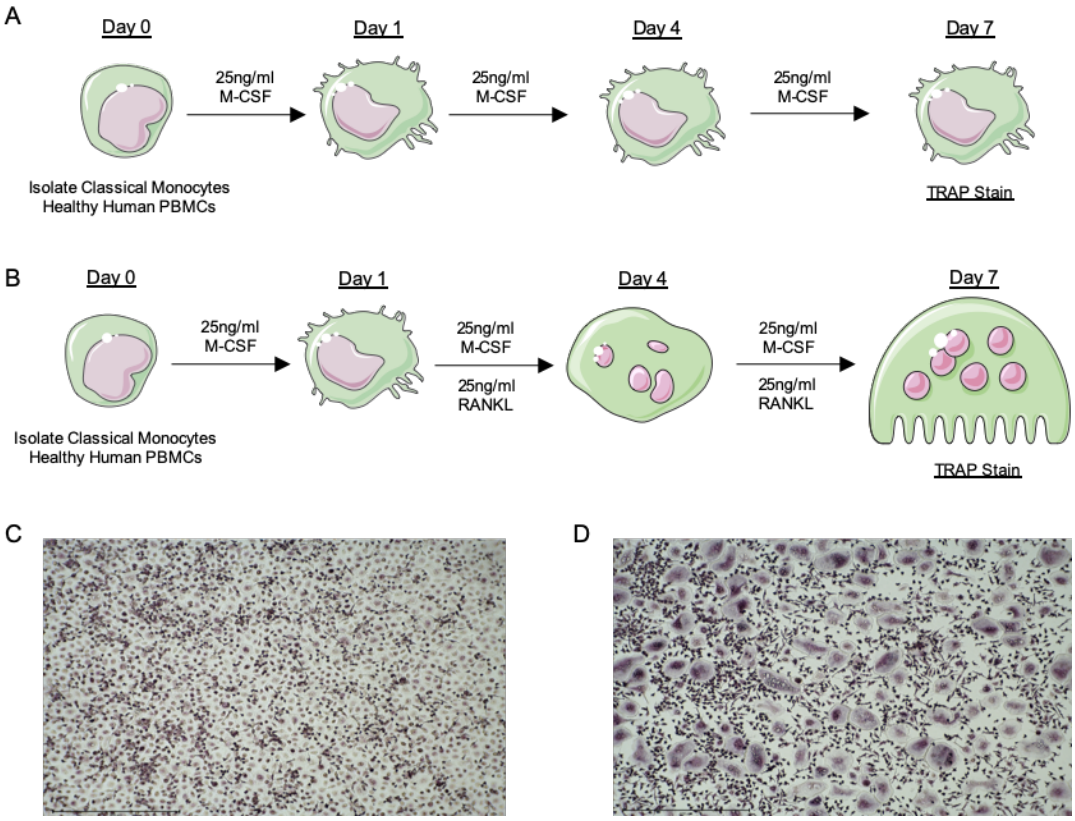

Figure 4.7 Protocols for Monocyte Differentiation Successfully Generate Monocyte derived Macrophages and Osteoclasts.
The monocyte fraction isolated from PBMCs was then cultured in (A) M-CSF alone as a macrophage control, or (B) cultured in the presence of M-CSF and RANKL to differentiate into multinucleated osteoclasts. At the end point of these cultures both (C) macrophage controls and (D) osteoclasts were TRAP stained in order to observe and quantify osteoclastogenesis, representative images of 1 donor are shown.

To assess whether monocyte differentiation via M-CSF changed the plasma membrane expression of PAR2, a time-course of PAR2 detection was conducted throughout monocyte differentiation (Figure 4.7A). In the first instance, monocytes were isolated from buffy coats and immediately stained for surface PAR2 (Figure 4.8A), this *ex vivo* plasma membrane stain was positive in both donors. To evaluate whether this expression changed over time monocytes/monocyte-derived macrophages were harvested and stained for PAR2 (Figure 4.8A). After 24 hours of culture in M-CSF, monocytes lost PAR2 expression (Figure 4.8A and C). Further differentiation was then completed and fully adherent and matured macrophages were harvested on days 5 and 6 post M-CSF culture and stained for PAR2. The expression of PAR2 on the plasma membrane of macrophages re-surfaces on day 5 of this culture, and then is reduced to undetectable levels again on day 6 (Figure 4.8 A and C).

One confounding factor with regard to this longitudinal data was that the non-specific staining increased over time as the monocytes differentiated down the macrophage lineage (Figure 4.8B). The secondary only control is a control stain which sets the baseline of non-specific antibody binding. The increase in non-specific antibody binding may be attributed to an increase in the expression of IgG receptors. Further optimisation of this assay could be conducted for its use in macrophages. Modification of the protocol to include higher levels of FcR blocking agent or additional washes could be employed to limit the non-specific binding of antibodies with these highly adherent cells. The enhanced baseline fluorescence levels detected could also be ascribed to influences out-with additional antibody binding. For example, macrophages have an increase in autofluorescence levels. Overall the change in baseline fluorescence between monocytes and matured macrophages may limit their direct comparison to other time points and the enhanced baseline fluorescence may influence the reliability and interpretation of the data. This data as a whole indicates that freshly isolated monocytes express high levels of plasma membrane PAR2 which is less consistently expressed during macrophage differentiation and culture (Figure 4.8).

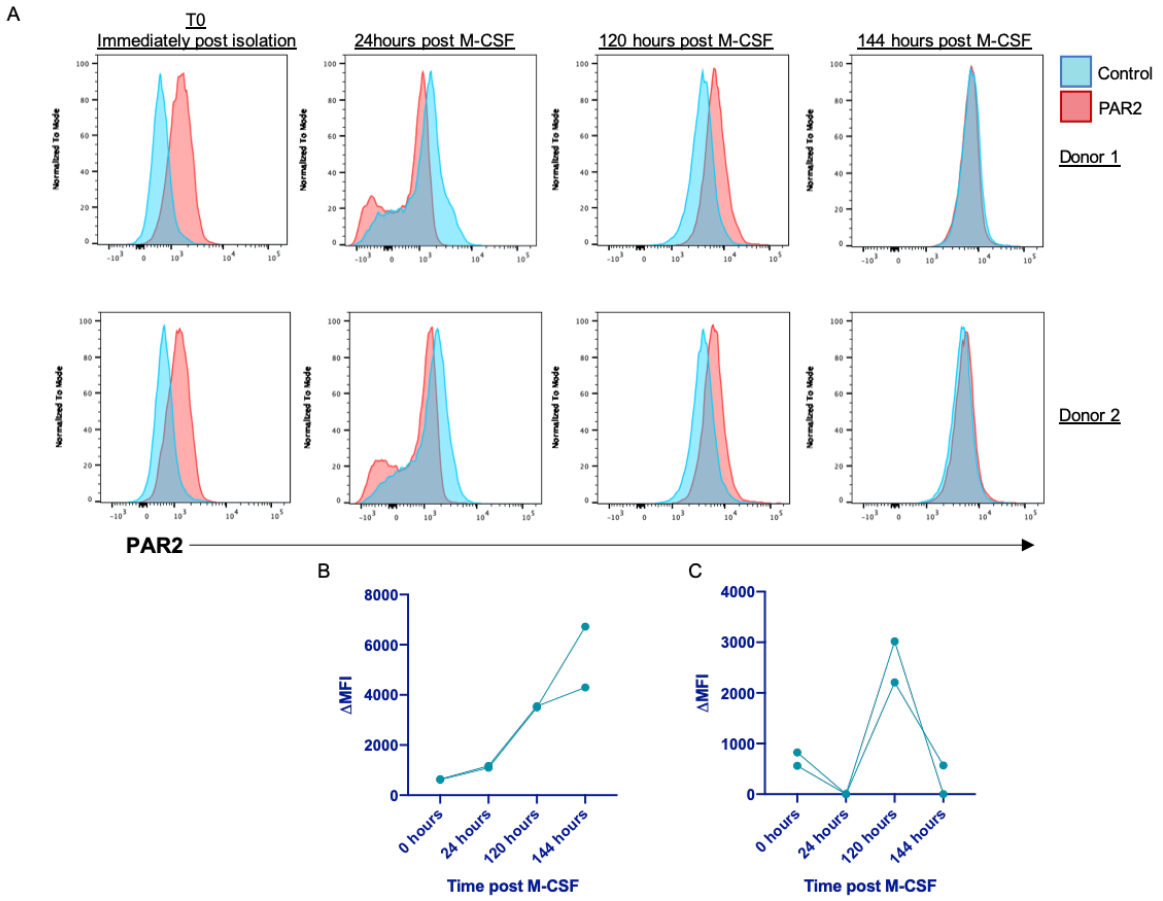

Figure 4.8 PAR2 Expression Across M-CSF Macrophage Differentiation.
A time course of M-CSF dependent macrophage differentiation was conducted to analyse PAR2 surface expression in response to differentiation. (A) Initially PBMCs were stained for PAR2 and monocyte PAR2 expression shown. (A) Cells were then cultured as per protocol outlined previously and lifted on days 1, 5, and 6 for flow cytometry PAR2 detection in 2 donors. (B) The Mean fluorescence intensity was plotted across time for the secondary only stain and (C) delta MFI calculated from this for the PAR2 stain (D61D5 stain – 2nd only stain) and also plotted against time. N=2,no additional experimental repeats.

The same donors that were assessed in the above macrophage differentiation staining (Figure 4.8) were also used to detect PAR2 during OC differentiation. On each day of differentiation cells were harvested and stained for PAR2 (Figure 4.9A). The expression of plasma membrane PAR2 is reduced in response to differentiation and culture comparative to freshly isolated monocytes (Figure 4.9 A and C). Once again the baseline fluorescence, as represented with the secondary only control stain, is significantly increased as the monocytes develop down the route of osteoclast differentiation (Figure 4.9B), with comparable levels of non-specific binding found in the M-CSF differentiated cells (Figure 4.8B). Therefore, while there appears to be moderate fluctuation in low levels of PAR2 expression in matured OCs, the reliability of this low expression level is limited by the enhanced baseline fluorescence.

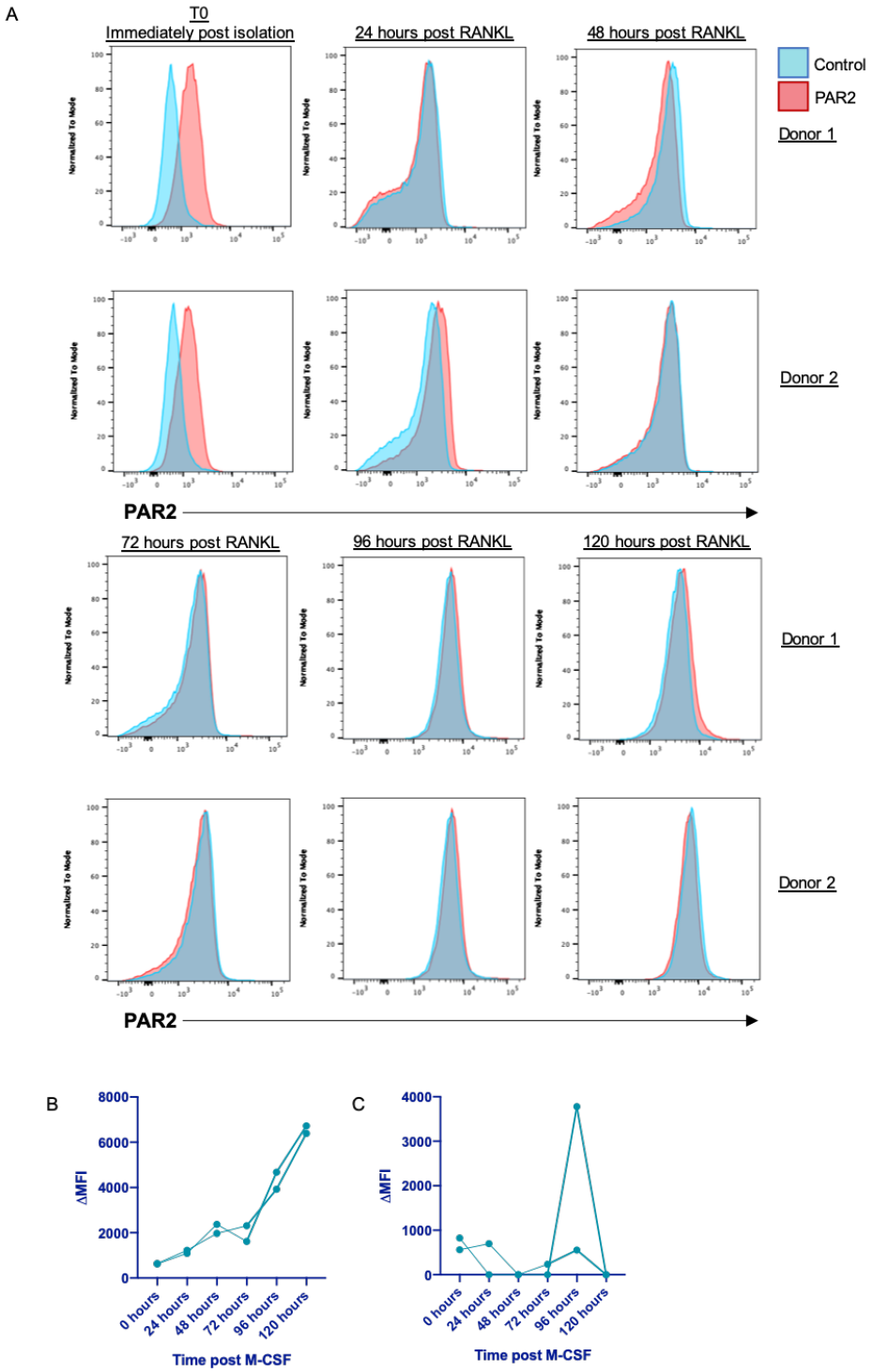

Figure 4.9 PAR2 Expression Across Human Osteoclast Differentiation.
A time course of M-CSF and RANKL dependent osteoclast differentiation was conducted to analyse PAR2 surface expression in response to differentiation. (A) Initially PBMCs were stained for PAR2 and monocyte PAR2 expression shown. Cells were then cultured as per protocol outlined previously (Figure 4.7) and lifted every day for 6 days for flow cytometry PAR2 detection in 2 donors. The Mean fluorescence intensity was plotted across time for (B) the secondary only stain and (C) delta MFI calculated from this for the PAR2 stain (D61D5 stain – 2nd only stain) and also plotted against time. N=2, no additional experimental repeats.

4.2.4 PAR2 Expression Changes in Response to Monocyte Maturation or Inflammatory Signals

While the limitations of the current stain are appreciated, when comparing with the control stain differentiated cells appear to down-regulate their PAR2 expression once in culture, with either M-CSF or M-CSF and RANKL. There are multiple potential interpretations that could be made from this data. 1) The growth factor M-CSF downregulates the PAR2 surface expression; 2) *In vitro* culturing conditions downregulate PAR2 expression; 3) *In vitro* differentiating monocytes begin to produce serine proteases which stimulate PAR2 and result in continual internalisation of the receptor making detection difficult. Short term incubations of human monocytes with monocytic growth factors; M-CSF, and GM-CSF, were then conducted to limit the issues experienced with long term maturation. This would determine whether monocytes downregulate PAR2 in response to these maturation signals. Analysing the response to 2 distinct growth factor signals allows interpretation of whether a change in PAR2 levels was M-CSF pathway specific.

PBMCs were isolated from 6 new buffy coat donors and 90 minute stimulations with 50ng/ml of M-CSF (Figure 4.10A) or GM-CSF (Figure 4.10B) were performed and samples then stained for PAR2. Each monocyte population was plotted separately to identify potential differences between classical, intermediate, and non-classical PAR2 responses. Due to the high proportion of classical monocytes in the blood, the total monocyte population is heavily biased by the response of these cells, and the possible influence on other monocyte populations is often lost in this analysis. Further analysis of each monocyte subpopulation was conducted in order to observe potential changes in the intermediate (Figure 4.10E and I) and non-classical populations (Figure 4.10F and J). Overall no change in PAR2 expression was found in response to M-CSF in any monocyte population (Figure 4.10 C-F). There was also no change in plasma membrane PAR2 expression in response to short term GM-CSF responses (Figure 4.10B, G-J). This data indicates that short term exposure to monocyte associated growth factors which initiate cell differentiation do not robustly change PAR2 plasma membrane expression in primary human monocytes.

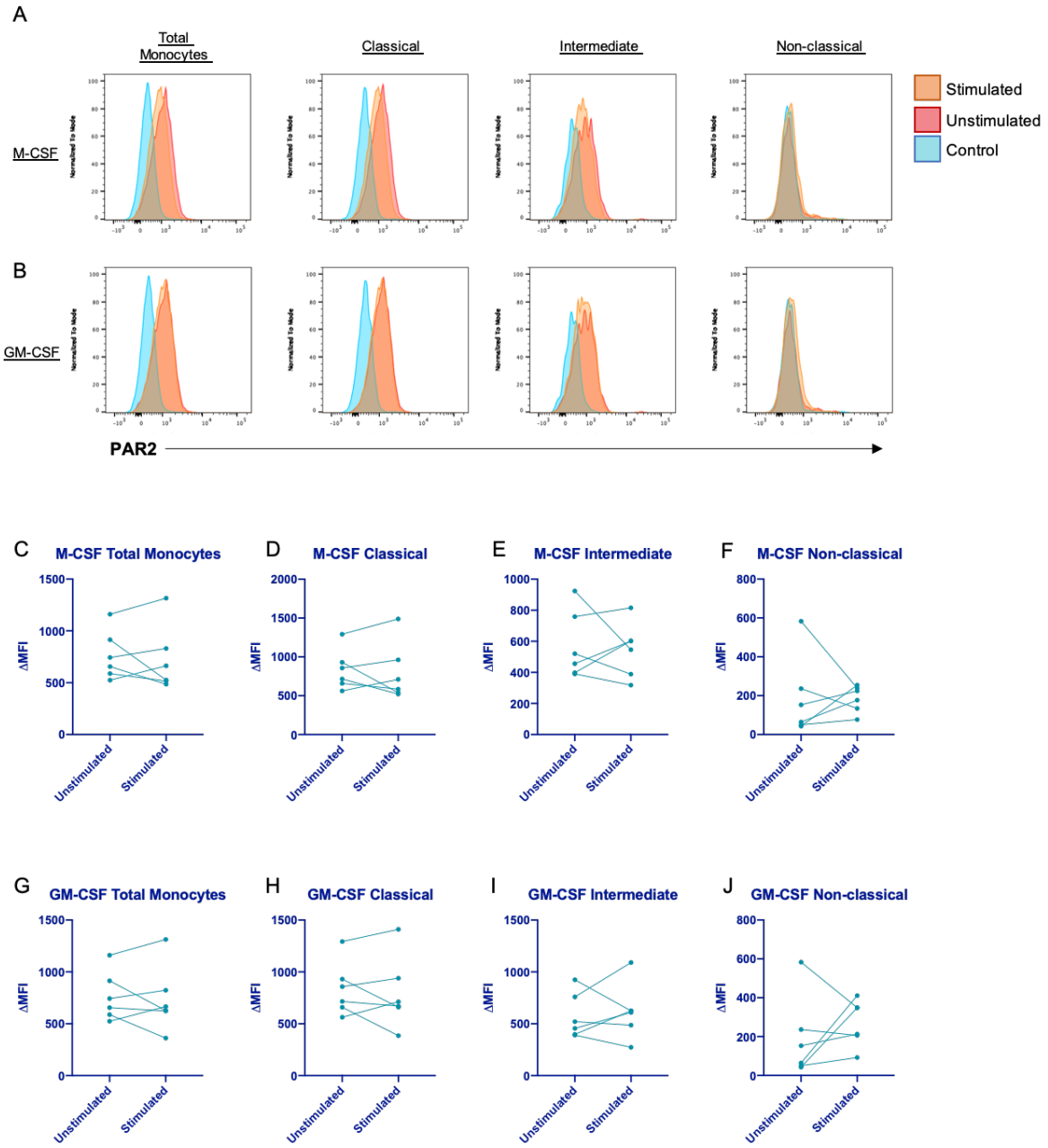

Figure 4.10 Monocyte PAR2 Surface Expression Does Not Change in Response to short term M-CSF and GM-CSF.
PBMCs were isolated from healthy human blood and left unstimulated in media (red histogram) or stimulated (orange histogram) for 90 mins with (A) 50ng/ml M-CSF or (B) 50ng/ml GM-CSF. The ΔMFI was then calculated by subtracting the control 2nd only antibody (blue histogram) from the D61D5 stain and plotted with paired analysis to unstimulated conditions for both (B) M-CSF stimulation and (C) GM-CSF stimulation. N=6, no additional experimental repeats performed.

To expand on this, investigation of the impact of inflammatory signals on PAR2 surface expression of human monocytes was conducted. Ligands which drive alternate inflammatory signals were chosen; TLR4 stimulation via LPS, and NFκB stimulator and RA associated cytokine, TNF. Again short term stimulation of

these inflammatory signals (90 minutes) was analysed. The same 6 PBMC donors from the previous experiment (Figure 4.10) were stimulated for 90 minutes with TNF (Figure 4.11A) or LPS (Figure 4.11B). All staining was subsequently conducted on ice in order to prevent modulation of surface antigens out-with this time frame. Deeper analysis of the MFI for each donor was then conducted to interrogate the influence of stimulation on each subpopulation of monocytes for TNF (Figure 4.11C-F) and LPS (Figure 4.11G-J) responses. There was no consistent modulation of PAR2 expression in any population of human monocytes in response to short term TNF stimulation (Figure 4.11 C-F).

Analysis of subpopulations of monocytes in response to short term LPS stimulation identified that $CD14^{hi}$ classical monocytes consistently, across donors, reduce PAR2 expression (Figure 4.11 H). This shift in PAR2 surface expression is not replicated in either the intermediate or classical monocytes (Figure 4.11 I and J respectively). From this data it is clear that PAR2 expression is consistently reduced across multiple donors in response to TLR4 stimulation, but only in the classical subpopulation of healthy human monocytes. While PAR2 expression does not appear to be robustly altered in any monocyte population in response to a short term alternative inflammatory signal TNF.

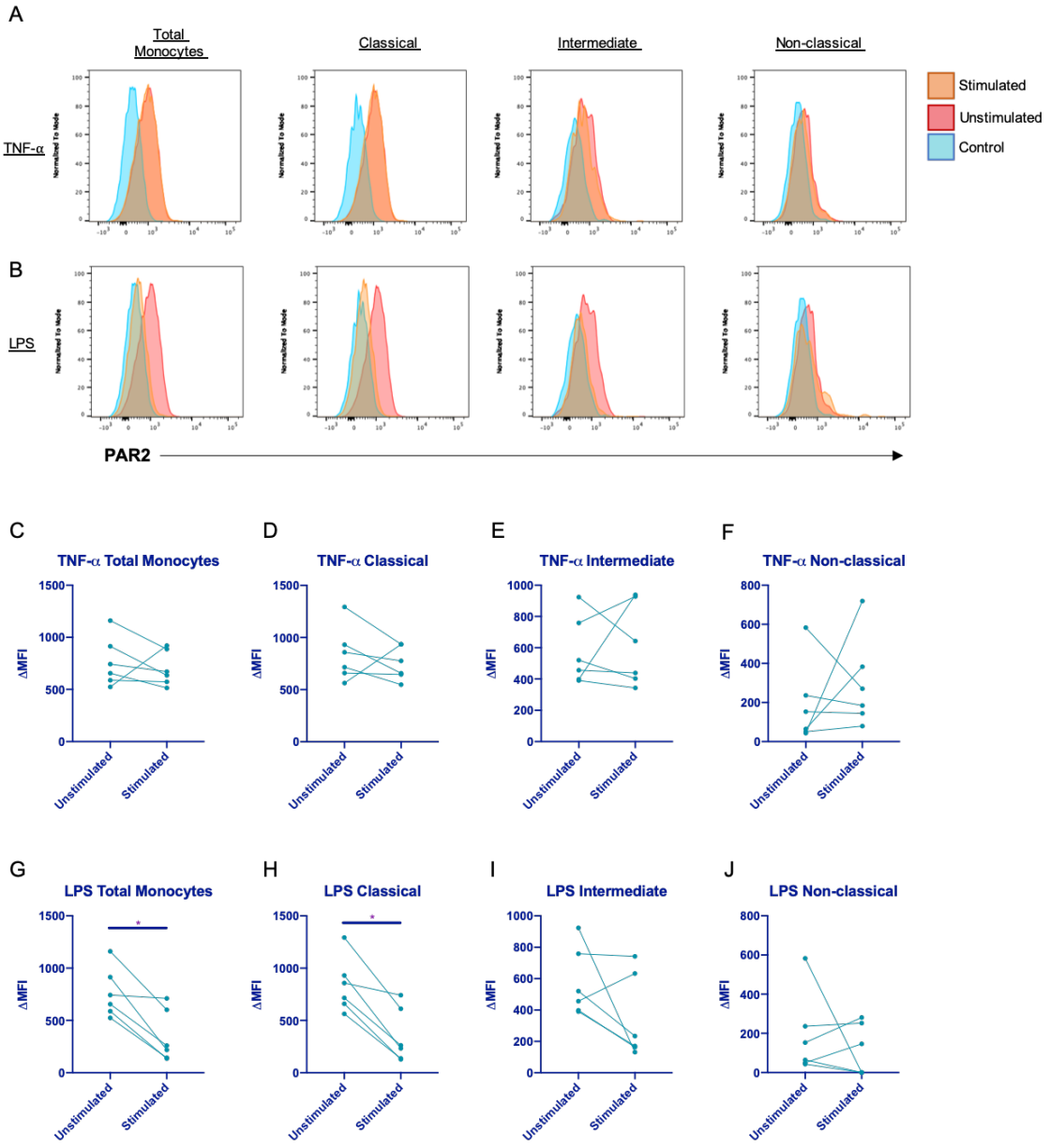

Figure 4.11 . Monocyte PAR2 Surface Expression is Reduced in Response to short term LPS Stimulation.
PBMCs were isolated from healthy human blood and left unstimulated in media (red histogram) or stimulated for 90 mins with (A) 100ng/ml TNF or (B) 100ng/ml LPS (orange histogram). The delta MFI was then calculated by subtracting the control 2nd only antibody (blue histogram) from the D61D5 stain and plotted with paired analysis to unstimulated conditions for both (C-F) TNF stimulation and (G-J) LPS stimulation. Wilcoxon paired analysis test was used for statistical testing, this does not assume gaussian distribution of data as not enough samples were collected to confirm normal distribution. N=6, no additional experimental repeats performed.

4.2.5 PAR2 Expression in Monocytes Isolated from Rheumatoid Arthritis Patients

Prior work and publications from our group analysed PBMCs from individuals with RA for PAR2 plasma membrane expression. This study concluded that within the PBMC populations monocytes had the strongest differential PAR2 expression, with increased surface PAR2 in RA patients compared with age and gender matched individuals with no joint disease[297]. It was also concluded that PAR2 expression was further enhanced on monocyte plasma membrane when individuals were admitted into hospital with flare, compared with those experiencing lower disease activity in outpatient clinics. Moreover, PAR2 expression in $CD14^+$ monocytes correlated with blood markers of systemic inflammation in these patients such as CRP and ESR. This study was conducted using the SAM-11 clone for detecting surface expression of PAR2. The data presented in Chapter 3 of this thesis demonstrated that this particular clone of antibody could not reliably detect differential expression of PAR2 in transfected cells versus naïve control cells. The assessment concluded that this clone was not suitable for PAR2 expression assessment using flow cytometry. In light of this, reassessment of the PAR2 expression on monocytes from individuals with RA, utilising the antibody clone (D61D5) and the optimized staining assays, would be valuable to ensure the robust nature of this finding.

To conduct this study outpatients were recruited from rheumatology clinics across hospitals in the Greater Glasgow and Clyde area. In total, peripheral blood was collected from 25 patients and the demographic and clinical information of these patients is shown in Table 4.1. The samples collected had a female to male ratio of 19:6, which reflects the generally female dominant epidemiology of this condition. The mean age of patients was 64, ranging from 37 to 88 years. These demographics were matched as closely as possible with healthy human samples collected as comparison. The details of this population are shown in Table 4.2. Again, a more female predominant population of healthy controls was collected (62.5% female), with a median age of 60.5 (ranging 56-64).

Table 4.1 Clinical Parameters of RA Patients

	Range	Median
Age	37-81 (years)	64 (years)
Gender	6 male, 19 female	76% female
Symptom Duration	3-23 (years)	10 (years)
Active Disease Status	15 remission, 10 active	40% active
ESR	2-61	16
CRP	1-48	3.5
DAS28-ESR	0.49-6.37	2.64
DAS28-CRP	1.21-6.03	2.89

Table 4.2 Demographics of Healthy Control Samples

	Range	Median
Age	56-64(years)	60.5 (years)
Gender	3 male, 5 female	62.5% female

Utilising the same panel used for all the healthy human monocyte analysis from PBMC populations shown in Figure 4.4 and used throughout 4.2.2, PAR2 plasma membrane expression was analysed. A secondary only control for D61D5 staining was performed for all samples so the ΔMFI of the PAR2 stain was calculated against internal controls. The ΔMFI (subtracted from control stain) was calculated for all RA patients and healthy controls in each subpopulation of monocytes and this data is shown in Figure 4.12A. Each monocyte population is also represented individually for ease of viewing, with classical monocytes in Figure 4.12B, intermediate monocytes in Figure 4.12C, and non-classical monocytes in Figure 4.12D. Firstly, there were no robust detectable differences in monocyte PAR2 expression between individuals with RA and healthy controls in any subpopulation of monocytes (Figure 4.12A-D). There is an observable difference in the mean MFI of PAR2 in the classical subset, with RA samples averaging at 1127.65 and healthy samples at 731.75 (Figure 4.12B). This is mirrored in intermediate monocyte populations, with RA samples mean at 651.3 while healthy samples 447.125 (Figure 4.12C). This is driven by a very small population of RA patients which appear to express high levels of PAR2 (Figure

4.12E), compared with RA patients with low to moderate PAR2 expression (Figure 4.12F) and the healthy controls (Figure 4.12G). However, this could be purely based on general variability in PAR2 expression within the population. From this data we cannot be certain that if the sample size of healthy controls was increased (a group which is currently under powered) that these samples would not also contain high PAR2 expressors. One valuable observation that remains consistent from previously analysed buffy coat monocytes is that classical monocytes have the highest PAR2 expression in RA patient samples as well, with receptor expression decreasing as monocytes mature to the non-classical phenotype (Figure 4.12 B-D).

This study did not confirm the previously established statistical differences between health samples and samples from people with RA, in terms of their monocyte PAR2 expression. Despite this further investigation of PAR2 expression in relation to clinical parameters was still conducted. It was previously established that PAR2 expression in monocytes correlated with clinical measurements of disease activity and systemic inflammation[297]. The relationship between clinical measurements and PAR2 expression was therefore investigated in this data set and the clinical parameters examined were extended beyond what was analysed in the original study by Crilly et al [297].

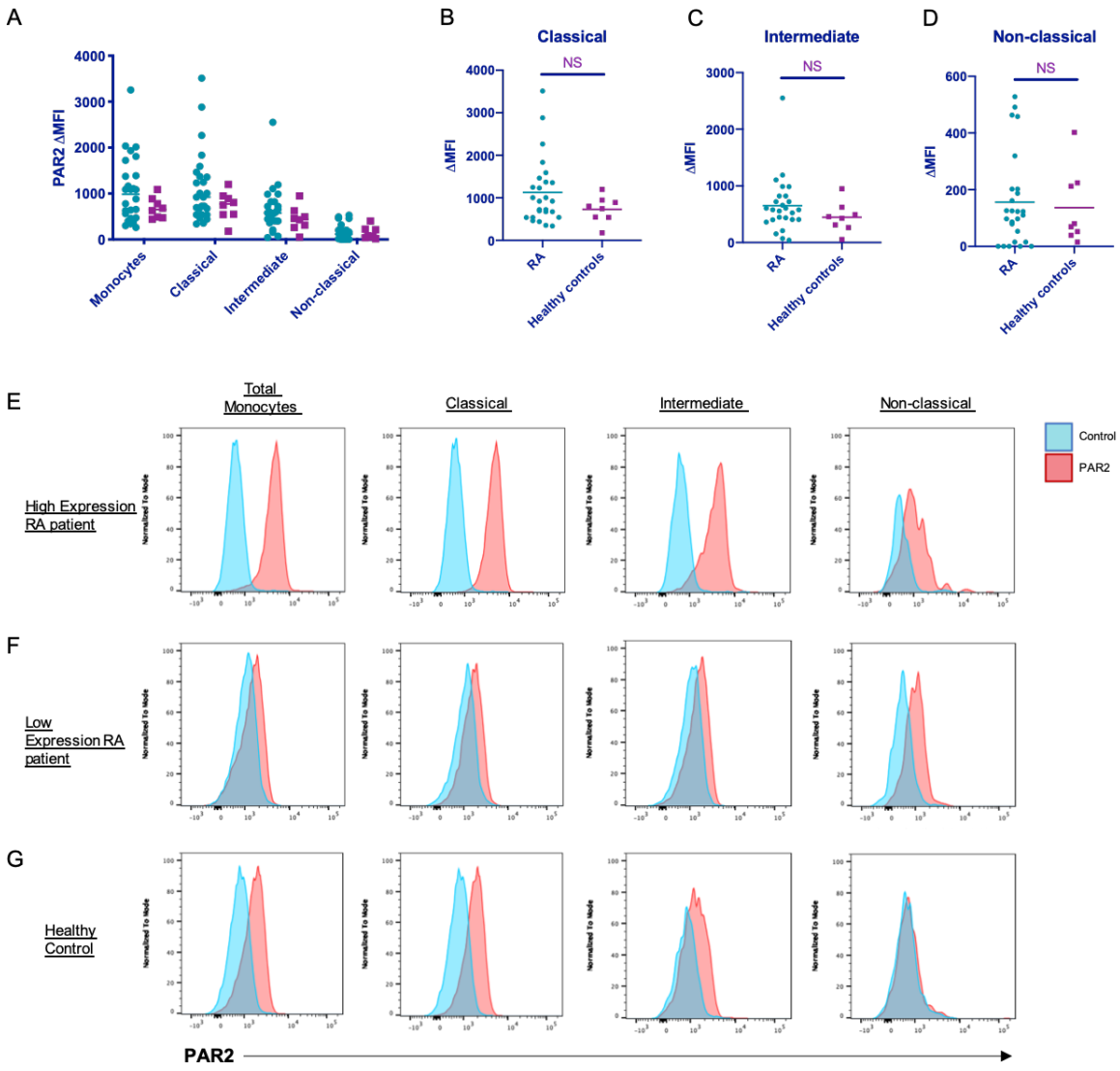

Figure 4.12 Monocyte Surface Expression of PAR2 is not Altered in RA Patients Compared with Healthy Controls.
Blood samples were collected from RA patients attending out-patient clinics in the Great Glasgow area (N=25) and healthy individuals with no joint pathology or anti-inflammatory treatments (N=8). PBMCs were isolated from blood samples via gradient dependent centrifugation and whole PBMC population was stained on ice with a panel of antibodies to identify monocytes and PAR2 expression via flow cytometry. Monocytes were gated for as shown in Figure 4.4, with classical, intermediate, and non-classical populations located based on CD14 and CD16 expression. Each sample was stained with the anti-PAR2 D61D5 antibody and subsequent secondary conjugated with AF647 fluorophore, or alternatively stained with the secondary only as a control negative stain. The AF647 MFI of the negative control stained sample was subtracted from the PAR2 stained sample to generate a *Δ*MFI of PAR2 expression. (A) This is plotted individually for each sample with RA samples in green and healthy samples in purple. The PAR2 expression in the total monocyte population, and in each subpopulation of monocytes is plotted in A. Each monocyte population; (B) classical, (C) intermediate, and (D) non-classical is also plotted separately for ease of viewing. Expression pattern of PAR2 followed normal Gaussian distribution in the healthy control samples but not in RA patients as tested with the D'Agostino & Pearson test, and therefore non parametric Mann-Whitney statistical tests were applied to the data. Representative histograms of (E) high PAR2 expressing RA patients, (F) low PAR2 expressing RA patients, and (G) healthy controls, for total monocytes and each sub population of monocytes. PAR2 stain in red, and control stain in blue.

The primary clinical measurements to gauge and measure disease activity in RA patients involves calculation of the Disease Activity Score 28 (DAS28). This American College of Rheumatology (ACR) approved assessment of disease activity involves calculation of the number of swollen joints, the number of tender joints (out of a possible 28 joints included in this measurement), a blood marker of inflammation (either ESR or CRP) and finally incorporation of the patients global assessment of health. Therefore, the correlative relationship between the ΔMFI of PAR2 expression on monocyte populations and the ESR value (Figure 4.13A), and then the DAS28-ESR (Figure 4.13B) was assessed. The ΔMFI of PAR2 expression in monocyte subsets was then compared to CRP (Figure 4.13C) and DAS28-CRP (Figure 4.13D) for all of the individuals with RA recruited. PAR2 expression in all monocyte populations failed to correlate with any of these recognised measurements of disease activity (Figure 4.13). This new data set fails to replicate the previous observations from the former cohort of patients stained with SAM-11 antibody clone which identified correlation between both CRP and ESR and PAR2 expression in $CD14^{+}$ monocytes [297].

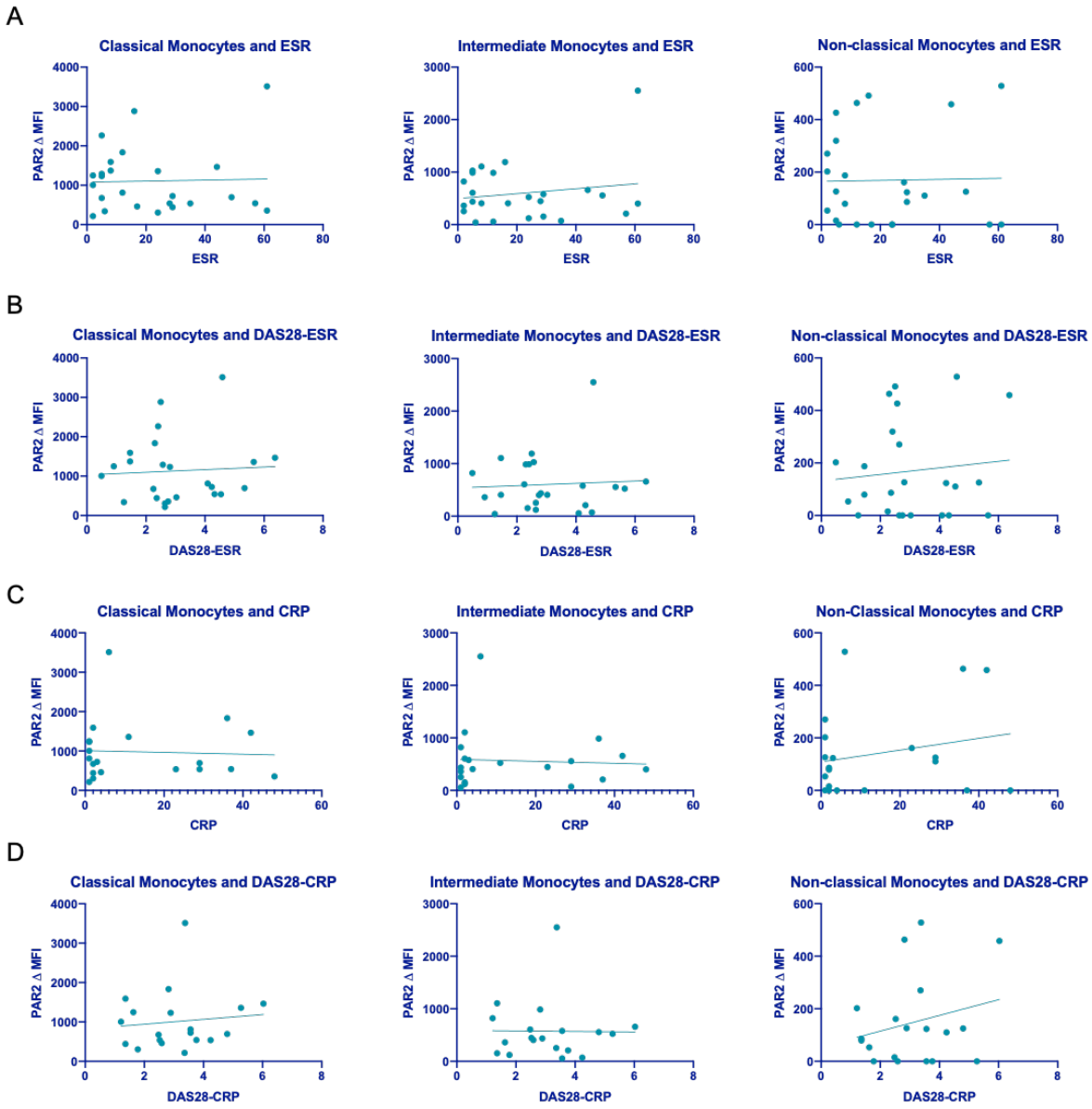

Figure 4.13 PAR2 Surface Expression in RA Monocytes Does Not Correlate with Clinical Disease Measurements.
The ΔMFI for PAR2 expression in each monocyte sub population (classical, intermediate, and non-classical) was plotted against clinical measurements of disease activity, (A) ESR, (B) DAS28-ESR, (C) CRP, and (D) DAS28-CRP. The linear regression of the data was plotted. N=25

Subsequently, correlation analysis was extended to include more clinical and general demographic data for comparison with levels of PAR2 plasma membrane expression. Based on clinical measurements patients can be grouped into active disease or remission status, a binary representation of disease activity. This cohort contained a significant group of patients in remission (15/25), therefore this binary status descriptor may be a better method of analysis for this particular cohort. The PAR2 expression ΔMFI of each monocyte population was

split dependent on whether the patient had active disease or was in remission (Figure 4.14A). This type of analysis was not performed in the Crilly study because they did not recruit any patients in remission. Again there were no distinctions in PAR2 expression between monocytes from active disease or remission in any subpopulation of monocytes (Figure 4.14A). PAR2 expression in relation to years since diagnosis was then investigated, which may suggest whether this receptor has more prevalence in early development/ establishment of disease, or if its more prominent in chronic long term stages of disease. There was no correlation between PAR2 expression and duration of symptoms in any of the monocyte populations measured (Figure 4.14C), indicating that it is not prominently expressed at any particular stage of disease progression.

Generic demographics unrelated to disease activity were then analysed to ensure PAR2 expression wasn't related to these factors which may be overshadowing disease associated differences. There were no significant differences in PAR2 expression dependent on gender (Figure 4.14B) and there was also no correlation between PAR2 and the age of the patients, consistent across all monocyte populations (Figure 4.14D). Therefore, overall there were no measured general demographics which associate with PAR2 expression.

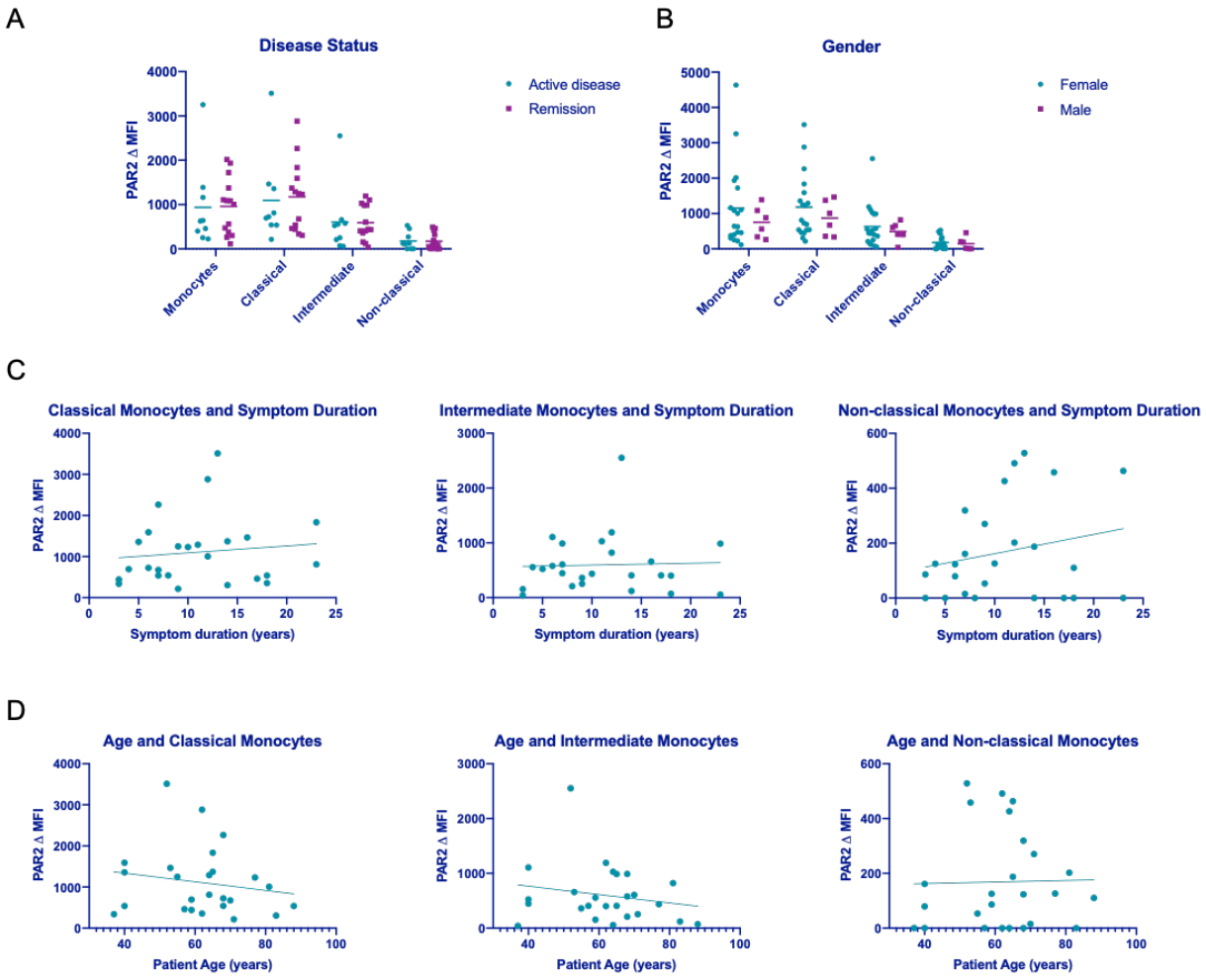

Figure 4.14 PAR2 Surface Expression in RA Monocytes Does Not Correlate with Disease status, Gender, Age, or Symptom Duration.
Patient samples collected at out-patient clinics were separated clinically as those with active disease (blue, N=10) or those in remission (purple, N=15), and (A) the ΔMFI of PAR2 expression in total monocytes and classical, intermediate, and non-classical monocyte subsets of these patients plotted individually. (B) The samples were then separated by gender; female (blue; N=19), or male (purple, N=6). (C) The ΔMFI of PAR2 expression in each monocyte population was plotted against symptom duration in years for each patient and linear regression calculated (N=25). (D) The ΔMFI of PAR2 expression in each monocyte population was plotted against the age of each patient and linear regression calculated (N=25).

Immuno-suppressing treatments were taken by all patients recruited to this study in order to control their disease. These systemic therapies will influence immune cell behaviour and in-turn could impact PAR2 plasma membrane expression in circulating immune cells. There was a large breadth of variation in treatment options employed in this cohort, thus the samples could not be divided by their exact treatment regime. Patients were sub-categorised based on whether they were receiving methotrexate or not (Figure 4.15A), or whether they were currently on any biologics (Figure 4.15B). In short, none of the

treatment conditions analysed were associated with a significant difference in PAR2 expression (Figure 4.15).

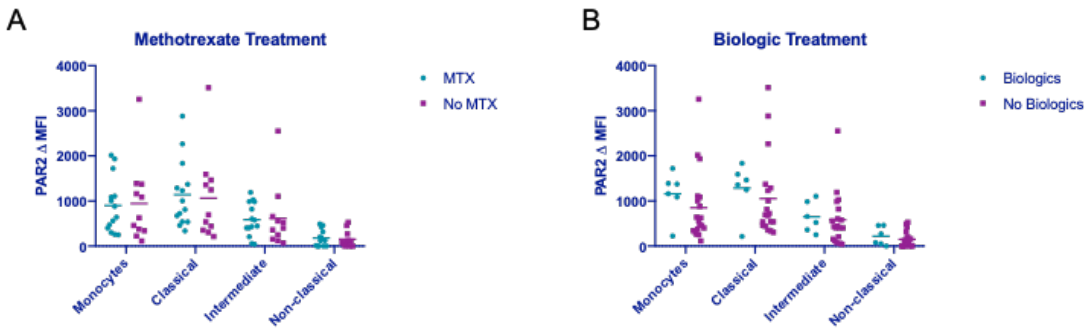

Figure 4.15 Analysis of Monocyte PAR2 Surface Expression in Rheumatoid Arthritis Patients and Treatment Status
Patients were sub divided based on treatment status and again plotted for ΔMFI of PAR2 expression in each monocyte population. Patients were separated by (A) methotrexate treatment, with those receiving methotrexate in green (N=14) and individuals not in purple (N=11), and (B) separated by biologic status, with those receiving biologics in green (N=6) and biologic naïve in purple (N=19). Each population was statistically tested using Mann Whitney to identify any significant differences in PAR2 expression with treatment status, no populations had significantly differential PAR2 expression based on drug treatment.

Table 4.3 Sero-status of RA Patient Cohort

Sero-status	Donor Number
Seropositive	18 donors (85.7%)
Double RF+ CCP+	13 donors (61.9%)
Single RF+	3 donors (14.28%)
Single CCP+	2 donors (9.5%)

The final analysis of the patient data investigated the relationship between PAR2 expression and auto-antibody status. The sero-status of recruited patients was known and thus individuals were sub-divided based on the presence or absence of both rheumatoid factor (RF) and antibodies against cyclic citrullinated peptides (CCP). Most of the samples collected were from sero-positive patients, with only 3 completely sero-negative patients included in the study (Table 4.3).

It is therefore challenging to draw any comparisons between seropositive and seronegative patients with one group having such low sample numbers (Figure 4.16A). This was further divided to separate RF positive patients and RF negative patients. No relationship between PAR2 expression and the presence of RF was identified (Figure 4.16B). The same analysis was also applied for CCP positive and negative samples (Figure 4.16C). Again this analysis is challenging to interoperate due to very few CCP negative patients (N=4). The data was then further divided to display double positive, RF alone positive, CCP alone positive and sero-negative samples separately (Figure 4.16D, E). However, the double positive autoantibody group was so prominent in this cohort it is challenging to make any comparisons. Overall, it may be of value to expand this study to include a larger variety of autoantibody positive combinations which would open up this data for further analysis on this clinical parameter.

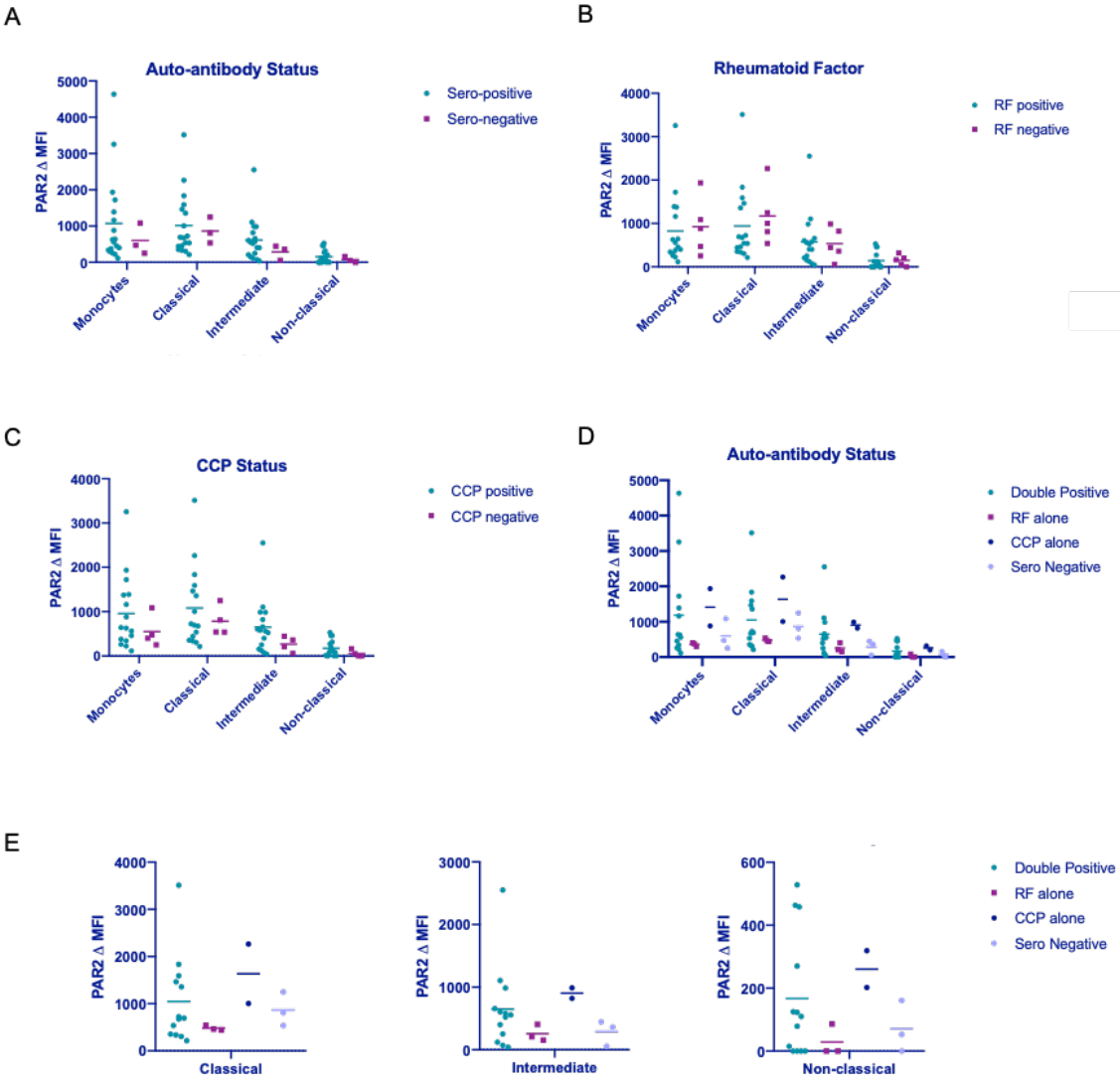

Figure 4.16 Analysis of Monocyte PAR2 Surface Expression in Rheumatoid Arthritis Patients and Autoantibody Status.
Patient samples were sub divided based on Rheumatoid Factor and anti-CCP autoantibody status. The ΔMFI of PAR2 expression was plotted for total monocytes and each monocyte population for (A) sero-positive (N=18) vs sero-negative (N=3), (B) separated by Rheumatoid factor positive (N=16) and negative (N=5), and (C) by anti-CCP positive (N=15) and negative (N=6). (D) Patients were then separated as double RF and CCP positive (N=13), single positive for either CCP (N=2) or RF (N=G), or sero-negative (N=3) and (E) then plotted each monocyte population separately.

4.3 Discussion

Despite the abundant data in the current literature surrounding the role of PAR2 in the immune system and the inflammatory response[284,295,331-337], there is limited confidence in our current knowledge of PAR2 expression in immune cells. This uncertainty is reinforced by conflicting published data and a lack of confidence in the reliability of the antibodies currently available to detect PAR2 protein[300]. The literature remains conflicted on whether monocytes express PAR2 on their surface. Some papers have confirmed expression of PAR2 on healthy human monocytes[286], while others report no detectable expression[272]. Further to this, within studies that find positive staining, some display extremely low expression levels [270] while others report much higher levels of detection[286]. While the majority of these papers use the SAM-11 clone of anti-PAR2 there is also the use of other commercially available antibodies and generation of polyclonal antibodies in house to further complicate this issue. Differences between clones in detection level of PAR2 was also noted by Lopez et al, who found different levels of expression in cell line HT-29 with SAM-11 and clone 344222 from R&D[286]. However, an evaluation of studies which only used the SAM-11 clone for monocytic PAR2 detection also did not provide consistent findings, with some analyses reporting very low or no expression with this antibody[270-272], while others reported strongly positive staining[338]. It is therefore not only an issue resulting from the application of different antibody clones. Overall, the literature is not lacking in publications attempting to clarify PAR2 expression on monocytes, but thus far has failed to resolve the issue.

Our ability to detect this receptor, or conversely confirm its lack of expression in human monocytes, would be extremely valuable. This would inform us as to whether it is worth pursuit of determining the functional influence of PAR2 on this cell type. Also with the reported increased expression of this receptor in many disease settings[297,299,324] this may present a potential distinguishing feature of different phenotypes of disease or be indicative of disease activity.

The data presented in chapter 3 determined that SAM-11 was not reliable for detection of this receptor via flow cytometry in our hands. One anti-PAR2 antibody clone that generated reliable flow cytometric detection of PAR2 in transfected cells line was D61D5. This clone has featured in a limited number of

cancer publications, where it has only been used for western blot analysis [339], or immunohistochemistry (IHC) [340]. Using the optimised methodology from chapter 3 PAR2 expression was consistently detected in healthy human monocytes, with substantial donor to donor variation in detected levels (Figure 4.4). Positive PAR2 expression was detected in all of the 14 healthy samples acquired from SNBTS. The expression level of PAR2 was also analysed in each subset of monocytes; classical, intermediate, and non-classical, which has never been published before. From this it was determined that classical $CD14^{hi}$ monocytes express significantly higher levels of PAR2 compared with other monocyte populations. A significant reduction in PAR2 expression was detected in intermediate monocytes and a further, highly significant reduction in non-classical monocytes, with some donors expressing no detectable PAR2 on their non-classical cells.

The down regulation of this receptor upon monocyte conversion towards a luminal patrolling state may be indicative of its functional role in monocyte biology. Classical monocytes are the inflammatory responders with rapid recruitment into inflamed tissue sites, while intermediate and non-classical monocytes do not as readily migrate to these sites to enhance the inflammatory response. This could suggest that PAR2 may play a role in the recruitment, the transmigration, or the inflammatory activity of classical monocytes when in an inflamed tissue. Its lack of expression in the "less inflammatory" monocyte subsets may be suggestive of its role in inflammation.

The expression pattern found on healthy primary monocytes was very different from that in THP-1s, which had no detectable PAR2 expression (Figure 4.1). It is well recognised that there are many differences between primary monocytes and the immortalised monocytic cancer cell line THP-1[341] and it is therefore not surprising to identify differences in PAR2 expression levels between these cell types. However, previous data published by Kang and colleagues determined using the SAM-11 clone of antibody that THP-1 cells expressed PAR2 protein on their cell surface, as well as transcript levels of FRL2R as detected via endpoint PCR. They also demonstrated that PAR2 activation in naive THP-1s via both classical trypsin cleavage and activating peptide resulted in activation of MAP-kinase signalling pathway, increased THP-1 proliferation, and the production of

TNF[342]. It is well recognised that cancer cell lines evolve very quickly due to positive clonal selection driven by cell culture conditions. This genetic drift results in the same cell line from different labs expressing a very different genetic profile, leading to irreproducible results from one lab to another[343]. Further functional testing such as ERK phosphorylation could have been performed to determine if there was a functional receptor in our THP-1 cells. However, this was beyond the scope of the current project and fundamentally if work could be conducted in primary monocytes this would be a more preferable method of determining PAR2 function in human monocytes.

A lot of work has been conducted looking at the role of PAR2 in monocyte derived macrophages. Detection of this receptor has been reported in macrophages located in synovial biopsies from RA patients[344]. Previous studies have shown that human *in vitro* monocyte derived macrophages respond to PAR2 activation, through production of inflammatory mediators[271,345]. Low levels of surface PAR2 have been detected in human monocyte derived macrophages, differing slightly between M-CSF and GM-CSF matured macrophages[271]. Additionally, a study conducted by Colognato and colleagues proposed that CD14+ human monocytes do not express PAR2 but begin to upregulate this expression upon differentiation with M-CSF in culture[272]. Surface expression of PAR2 in cultured monocyte derived macrophages was not reliably detected in our hands (Figure 4.8). This may be due to the staining protocol used being unsuitable for the cells type they were applied to, as demonstrated with the differentiation time dependent increase in non-specific staining (Figure 4.8B). However the lack of detectable PAR2 in human monocytes and positive expression in macrophages found by Colognato completely contradicts our findings with the D61D5 antibody in human monocytes and macrophages. The data generated in the Colognato and the Steven study were both acquired with the SAM-11 clone of anti-PAR2. The difference in antibody clone used may be the significant factor resulting in disparate results from these 2 studies.

It is also possible that the reason a down regulation of PAR2 was detected for both the macrophage and osteoclast differentiation cultures is in fact not dependent on the differentiation response. Instead, this could be the result of a response to the static, 2 dimensional nature of this cell culture which does not

deliver the additional stimuli provided *in vivo* through bio mechanical activation, or fluid flow. It has been previously reported at the bone research society meeting in 2015 that chondrocyte cell line SW1353s did not express PAR2 in static cell culture conditions, but when this cell was exposed to fluid flow sheer stress for only 1 hour there was a marked increase in the expression of this receptor [346]. This mechanism may not be limited to this cell type and may be a requirement for expression in other cell types. It may also explain differences in PAR2 detection found between THP-1 cell line which has been maintained in static cell culture, versus *ex vivo* primary human monocytes recently isolated from peripheral blood under constant flow stress.

Alternatively, loss of detectable PAR2 in cell culture maintained monocyte derived cells could also be the result of endogenous protease production in culture, causing continuous internalization of the receptor, making it challenging to detect. Macrophages are also known protease producers, especially cysteine proteases such as cathepsin S[347,348]. In addition, the primary function of osteoclasts is the production of acids and proteases in order to break down the mineral content of bone, making them more catabolically active than macrophages[287]. While the protease which is most highly produced by osteoclasts is cathepsin K, a cysteine protease, which does not have reported interaction with PAR2, this protease does have known activity with PAR3 and PAR4. Cathepsin K results in platelet aggregation in a PAR3 and PAR4 dependent mechanism, inducing the MAPKinase signalling pathway through these receptors[349]. Other cysteine proteases such as cathepsin S have been reported to cleave PAR2 and result in alternative signalling pathways, in a non-canonical activation of the receptor[350]. Therefore, while it has not been widely reported that osteoclasts produce PAR2 activating proteases, it would be possible that they do, given their known proteolytic activity. Both macrophage and osteoclast *in vitro* cultures may therefore contain endogenously produced proteases which cause internalisation of PAR2, limiting our capacity to detect it on the cell surface.

Further to this it is also possible that the method of removal of these adherent, differentiated cells using TrypLE still activated PAR2. Cells had to be put into suspension in order to run through the flow cytometer. This method of

dissociation was chosen because TrypLE buffer does not contain trypsin, however it does still have enzymatic activity. The proteases used in this solution are proprietary information and could not be checked for known PAR2 activators. Attempts were also made to dissociate cells from the tissue culture plastic using non-enzymatic methods of high concentrations of EDTA and ice, however these methods were ineffective and cells remained adherent.

In order to limit the effect of long term culture and removal on potential alteration of the surface expression of PAR2 short term stimulations of freshly isolated monocytes were conducted. There was no consistent impact on PAR2 expression by monocyte growth factors M-CSF and GM-CSF in the short term (Figure 4.10). It is most likely that these stimuli do not have a direct impact upon PAR2 expression. Of all the growth factors and stimulations tested for short term impact on PAR2 expression a consistent change in receptor expression was only found with LPS stimulation (Figure 4.11). Every donor (N=6) had reduced PAR2 expression in the classical monocyte compartment. This was somewhat surprising as previous reports have shown LPS stimulation elevated PAR2 expression and responsiveness in endothelial cells[351].

The LPS receptor, TLR4, has been associated with PAR2 in multiple publications, which is interesting as these receptors both function as an innate sensor of damage and infection. It has been proposed that these signals work co-operatively, with one receptors activity enhancing the other. Synergistic enhancement of PAR2 signals through TLR4 activity have been observed by Chi and colleagues in 2001, when they observed PAR2 dependent IL-6 release in HUVECs was enhanced with LPS co-stimulation[352]. Evidence of co-operation of these receptors and their signals was further demonstrated when PAR2 activating peptides were shown to enhance tlr4 mRNA expression and LPS stimulated F2RL1 mRNA expression[353]. When these signals were stimulated in combination this further enhanced the migratory potential of PAR2 and TLR4 expressing carcinoma cell line SW620, over single stimulation with either of these signals[353]. In airway epithelial cells PAR2 activating peptide alone and LPS alone induce production of chemokine IL-8. However, when these stimulations are used in combination the production of IL-8 by epithelial cells is significantly enhanced, confirming the role for this synergistic signal enhancement in

directing increased cellular migration[354]. Further to this an increase in PAR2 induced NFκB signal was found to be dependent on the presence of TLR4. Indicating that inflammatory NFκB signalling through PAR2 protease detection was somewhat dependent on co-operation with TLR4[355].

Current working models for how these receptors interact includes both interaction via crosstalk of signalling intermediates and adaptor proteins but also through direct interaction at the plasma membrane and within endosomes. Direct interaction of these receptors was proposed after detection of these receptors by co-immunoprecipitation [355]. In the system adopted by Rallabhandi and colleagues, the physical interaction of these 2 receptors was dependent upon the presence of PAR2 activating peptide. It is known that in CD14 expressing cells such as monocytes and macrophages TLR4 stimulation results in endosomal dependent internalization of the TLR4 receptor and initiation of MyD88 independent signalling [356]. Internalisation of TLR4 can be initiated by LPS activation, in a LPS Binding Protein (LBP) dependent fashion, and this has been observed within 1 hour of LPS stimulation [357]. It is therefore possible that our observed reduction in PAR2 expression after short term LPS stimulation (30 mins to 2 hours) is the product of internalization of PAR2-TLR4 heterodimers upon TLR4 stimulation and not necessarily an LPS dependent regulation of PAR2 expression. To test this hypothesis FRET technology could be applied to identify whether these receptors closely interact during LPS stimulation and internalise together. Protein FRET probes were not available for these receptors to explore this question further, but it may be valuable to do so in the future.

The report which previously demonstrated an increased PAR2 expression in endothelial cells found that this was only detected after 12 hours of LPS treatment and increased responsiveness to PAR2 activators observed only after 12 hours of LPS pre-treatment [351]. The method of detection used in these assays was western blot which would reflect total PAR2 protein as opposed to only surface expression. Therefore, it is entirely possible that initial responses to LPS involve PAR2 internalisation and subsequent, later timepoints could show an enhanced expression. However, timepoints beyond 2 hours were not examined and this cannot be confirmed.

With confirmation that healthy monocytes expressed cell surface membrane PAR2, this investigation could be taken further to analyse PAR2 monocyte expression under inflammatory conditions. Previous research from our group determined that RA peripheral blood monocytes had significantly enhanced expression of PAR2 over healthy comparisons. This study was conducted with the SAM-11 clone of antibody so it was important to ensure that the same enhanced expression was found using the optimised D61D5 clone protocol. The data generated with this anti-PAR2 clone did not show any significant difference in PAR2 expression between healthy individuals and RA patients (Figure 4.12) and no correlation of PAR2 MFI with any of the clinical parameters known (Figure 4.13, Figure 4.14, and Figure 4.15). While there was no significant difference between healthy and RA in our study, there is an observable small subset of patients (N=6 out of 25 total patients) which had higher PAR2 expression than the highest expressing healthy control. The distribution of RA patient PAR2 stain data was not normally distributed as found by D'Agostino & Pearson test (data not shown), while the healthy control data spread did follow Gaussian distribution. This is likely a reflection of the small subset of patients with enhanced PAR2 expression. This trend is also observed in the Crilly et al paper[297]. Out of the total 75 patients recruited in this previous study, only 15-20 appear to have an enhanced % of PAR2 expressing monocytes over the general expression found in healthy individuals. It is possible that the statistical significance achieved in this study was aided by a higher powered study (N=94 RA, N=15 healthy controls). The patients in our study which had enhanced PAR2 expression over healthy controls were not further defined by any clinical parameter that was assessed. So whether the observation of a small subset of high PAR2 expressors in this study has any clinical relevance is unlikely. According to the Crilly et al paper their enhanced PAR2 expression did correlate with systemic inflammation clinical measures ESR and CRP, however the plots for this are not shown[297].

There were also significant differences in the demographics and clinical severity of the patient samples collected in this cohort in comparison with the previous. The study conducted by Crilly et al, only included patients with active disease. It also included patients during a flare which resulted in hospital admission, the most severe phase of disease. This study included more patients that were

currently in remission, and people with active disease with lower DAS scores; the maximum DAS28-ESR was 6.37, with only 8 recruited patients having a DAS28-ESR of over 3.5. Therefore, patient cohort presented here had significantly lower disease severity overall. From this it cannot be identified whether the differences observed between the 2 studies was the result of a different patient demographic with regards to disease severity, lower powered trial in terms of number of recruited patients and healthy controls, or whether this can be attributed to the antibody used.

In order to directly compare to the previous study, the same demographic and clinical severity of patients could have been recruited. However, given the frequency of samples from in-patient flare, and the number of patients required for appropriately powered experiment, this recruitment could not be conducted within the time-frame available. Another method of directly comparing SAM-11 and the D61D5 antibodies, would be to stain the current cohort with both of these and compare the staining intensity. For the first few patients this was performed, and while the D61D5 protocol staining procedure resulted in positive PAR2 expression in patient samples, SAM-11 stain was consistently negative, both for healthy controls and patient samples (data not shown). The use of SAM-11 was then discontinued in this study. Overall, the use of SAM-11 during this study did not mimic the staining patterns reported previously. The cause of this is still unknown, and could possibly be the result of inconsistencies between the batch production of this clone. Overall, the D61D5 clone provided a more reliable PAR2 stain, and in the current demographic and number of patients collected the PAR2 expression measured with this method did not correlate with disease activity.

In addition, the type of analysis conducted between this study and the Crilly cohort also differed[297]. In the previous study the percentage of PAR2 positive monocytes were compared, while the data presented here was the ΔMFI of the PAR2 stain. This method of data representation was chosen as it was observed that the population adjusted as a whole and never presented as distinct populations of PAR2 expression. The spread of data found by Crilly et al was never shown in the publication and the reported MFI was significantly lower than what our stain and panel set up detected. The MFI detected by Crilly et al was

on average 0 for healthy controls and 0.7 for RA patients. The staining protocol used in this study detected an average of 683.1 ΔMFI for healthy controls and 1070.1 ΔMFI in the RA patient cohort. This indicates that the detection levels of PAR2 with SAM-11 in the previous study are extremely low in comparison with the detected PAR2 expression presented here, which brings into question the reliability of the previous observations. When looking at other published studies of PAR2 expression in inflammatory disease a similar problem is encountered. A study investigating PAR2 expression in peripheral blood monocytes of asthmatic patients using the SAM-11 antibody clone also detected very low MFI of PAR2 expression (average MFI of 3) [299]. While this expression is very low they did find that it correlated with clinical parameters of disease severity (airway function and total inhaled corticosteroid dose).

In terms of comparing clinical data with PAR2 expression it would also be more valuable to increase the number of active disease samples so that there isn't a skew towards lower disease activity in our cohort. As mentioned in the results section it may also be of interest to increase the diversity of auto-antibody expression in our samples in order to further explore the impact of auto-antibody types on PAR2 expression. This cohort is highly dominated by double positive (RF and anti-CCP) sero-status with a lack of single positive and sero-negative patients.

Replicating the previously published study of RA patient samples was not the central priority of this thesis. Because of this, the time that could be dedicated to recruitment of patient and aged matched healthy controls was limited and this is the most complete study that could have been conducted in the time frame available.

4.4 Conclusion

Overall the data presented in this chapter confirmed that healthy human monocytes do express cell surface PAR2. This expression level is highest in the classical monocyte population, with reduced expression in intermediate and non-classical populations. PAR2 expression on classical monocytes is reduced upon short term TLR4 activation via LPS, further supporting previous research which closely linked these 2 immune associated receptors.

Previous findings which correlated PAR2 expression rates in RA patient monocytes with clinical disease severity measurements were not reproduced in this study with the new anti-PAR2 clone D61D5. There were additional modifications to the study cohort this time around. The clinical severity of patients recruited in this study was significantly lower than the previous cohort, reducing the comparability of the 2 independent studies. However, the data presented in this chapter did not detect significant changes in RA patient PAR2 expression from healthy donors. Nor did it correlate PAR2 expression with any clinical parameters in this cohort of patients. Overall, the experiments presented in this chapter refute the hypothesis that PAR2 plasma membrane expression on RA circulating monocytes correlates with measurements of the clinical severity of disease.

5 Investigating the Function of PAR2 in Murine Osteoclastogenesis

5.1 Introduction

Monocytes are found in the peripheral blood (PB) and arise from a common myeloid progenitor (CMP) in the bone marrow (BM). Both BM and the PB monocytes exist as a heterogeneous population, which reflects their differentiation state and function. As discussed in the previous chapter, human monocytes in PB exist in 3 populations, classical ($CD14^{hi}CD16^{lo}$), intermediate ($CD14^{+}CD16^{+}$), and non-classical ($CD14^{lo}$ $CD16^{hi}$) [358]. Murine monocytes have similar distinct populations based on function, however these differ from the human cells in the markers distinguishing these populations and also the proportions of these populations. Similar to $CD14^{hi}$ classical human monocytes, $Ly6C^{hi}$ $CD11b^{+}$ monocytes reflect this population in the murine system[16]. These cells are rapidly recruited to inflamed sites, developing into inflammatory monocyte derived phagocytes, while $Ly6C^{lo}$ $CD11b^{+}$ monocytes reflect the non-classical population of human monocytes, which patrol the luminal vessel walls[24]. The differentiation potentials of human monocytes are also mirrored in the murine system. Upon entering the tissue they can develop monocyte-derived phagocytic functions, or acquire tissue specific functions, for example at the bone surface where they can fuse to become osteoclasts.

Osteoclasts (OCs) are large multinucleated, catabolically active cells, responsible for the resorption of bone during skeletal development and remodelling. Not all monocytes have the same potential to develop into OCs and the optimal precursors of these cells are termed osteoclast progenitor cells (OCPs). OCPs have been more specifically defined in the murine system than in human cells, with some myeloid precursors identified as more capable than other monocyte populations at differentiating into osteoclastogenic cells *in vitro*. Through adoption of a murine KO of the OC master transcription factor NFATc1 these OCPs were also shown to be capable of repopulating the osteoclast repertoire in these OC deficient *nfatc1*$^{-/-}$ animals. Julia Charles and colleagues defined this sub-population of myeloid cells as $Ly6C^{hi}$, $CD11b^{lo}$, CX_3CR1^{+}, $CD11c^{-}$ [63]. Current understanding of defined OCPs has been fully explored in the introduction chapter (see section 1.2.1). To summarise, it is now recognised that

an embryonic source of OC is essential for skeletal development, while hematopoietic monocyte contributions to the osteoclast pool are most relevant post development, during bone remodelling and maintenance throughout life[64].

The fusion and differentiation of monocytic OCP into multinucleated osteoclasts is dependent upon the direct action of M-CSF and RANKL on OCPs as discussed in detail in the introduction of this thesis (see section 1.2.2). *In vivo,* the regulation of OC generation is largely conducted by stromal osteoblasts (OBs); the partnering cell type during bone remodelling (see section 1.2.5). The crosstalk between OCs and OBs is crucial for the regulation of the activity of both of these cell types. OBs produce a number of both soluble and cell surface factors which activate or inhibit the action/formation of OCs and thus prevent excessive or inadequate bone resorption. The primary example of this is the production of RANKL on both the membrane of osteoblasts and released as a soluble factor stimulating osteoclastogenesis via direct cell-cell interactions and within the environment. This cell type then also releases osteoprotegerin (OPG), which acts as decoy receptor for RANKL, reducing the availability of this protein. Thus OBs regulate the activity of OCs through a ratio of RANKL to OPG production and thus regulation of the availability of osteoclast stimulatory factors.

There are many other mechanisms which regulate osteoclast differentiation and activity, either directly or indirectly via osteoblasts and known mechanisms are detailed in the introductory chapter of this thesis (see section 1.2.5). Serine protease sensing via PAR2 is one pathway that has been briefly explored for its role in the bone remodelling process. Thus far, experimental work has indicated that the loss of this receptor in mice resulted in modest changes to the gross architecture of the skeleton, and slower initial recovery in response to bone injury[76]. The receptor has known expression on OBs[285], monocyte precursors of OCs in humans (see section 4.2.2), and increasing transcript expression in murine cell line RAW 264.7 in response to OC differentiation signals[75]. During *in vitro* bone marrow cultures, activation of PAR2 has been shown to inhibit osteoclastogenesis[75], while other studies in contradiction have shown a reduction in osteoclast formation in bone marrow lacking PAR2 [76]. Overall, the current literature indicates that PAR2 plays a role in bone remodelling and maintenance,

however the nature of that function is still conflicting and largely unknown. In addition, PAR2 has been shown to drive pathological bone changes in bone associated diseases. For example, in murine models of osteoarthritis osteophyte formation and volume were limited in *par2*$^{-/-}$ animals[288].

In the previous chapter of this thesis we established that human monocytes, a pre-cursor of OCs, express PAR2. However, we also established that the expression levels of this receptor were highly variable between human donors. Thus, inhibition or activation of PAR2 in human monocyte assays may have a high degree of variability in the potential response of the cells, as a result of their differential receptor expression rates. We chose to utilise *par2*$^{-/-}$ animals to investigate the function of PAR2 in the process of osteoclast differentiation in order to establish a clear biological influence of this receptor. Phenotypes identified in mice could then be applied and tested using PAR2 inhibitors and activators in a human system.

Overall the aims of this chapter are:

1. To clarify the role of PAR2 in the differentiation of murine BM cells into osteoclasts

2. Determine the stromal and myeloid roles of PAR2 in driving or regulating osteoclastogenesis

3. Determine the role of PAR2 in inflammatory-driven osteoclastogenesis

5.2 Results

5.2.1 Analysis of *par2*$^{-/-}$ Bone Marrow Monocyte Compartment

Prior to conducting *in vitro* assays with bone marrow from C57BL/6 WT and *par2*$^{-/-}$ mice, gross changes to the composition of the monocyte compartment were assessed to check the BM myeloid composition was not impacted by PAR2 deletion. Previous reports had highlighted a significantly greater number of bone marrow cells in the *par2*$^{-/-}$ mice. It was also proposed that despite this there were lower numbers of stromal cells and osteoblast precursors[76]. With this in mind, the frequency of monocytes in the *par2*$^{-/-}$ bone marrow was assessed to identify potential alteration from WT composition. Moreover, it was also important to evaluate monocyte subpopulations to ensure no significant change to the frequency of OCP, inflammatory, or patrolling monocytes were caused by the loss of PAR2. An alteration in the composition of the monocyte compartment in *par2*$^{-/-}$ would not only skew *in vitro* assay results, it would also be of significant biological interest for the role of PAR2 in haematopoiesis.

In order to do this bone marrow from long bones of 6-8 week old WT and *par2*$^{-/-}$ mice was extracted. BM cells were stained with a panel of markers to discriminate granulocytes (Ly6G), T cells (CD3), B cells (B220), and monocytes (Ly6C and CD11b). Monocytes were identified as lineage negative (Ly6G-, CD3-, B220-) and divided by CD11b and Ly6C expression levels (Figure 5.1). Representative FACS plots of WT and *par2*$^{-/-}$ monocytes from the bone marrow are shown in Figure 5.2A and B respectively. Further analysis of the percentage of gated populations from total bone marrow cells (from single cells) or the percentage of gated monocyte populations from the Ly6C^{+} total monocyte population was conducted. There were no changes in the frequency of total monocytes in the BM compartment (Figure 5.2B), and no alteration in the frequency of inflammatory monocytes (Figure 5.2C), patrolling monocytes (Figure 5.2D), or OCPs (Figure 5.2E) in the monocyte compartment in *par2*$^{-/-}$ BM. Therefore, from these data, we concluded that there were no changes in the monocyte frequencies in KO bone marrow and thus any differences observed in future assays was not the result of different monocyte frequencies at the beginning of the culture.

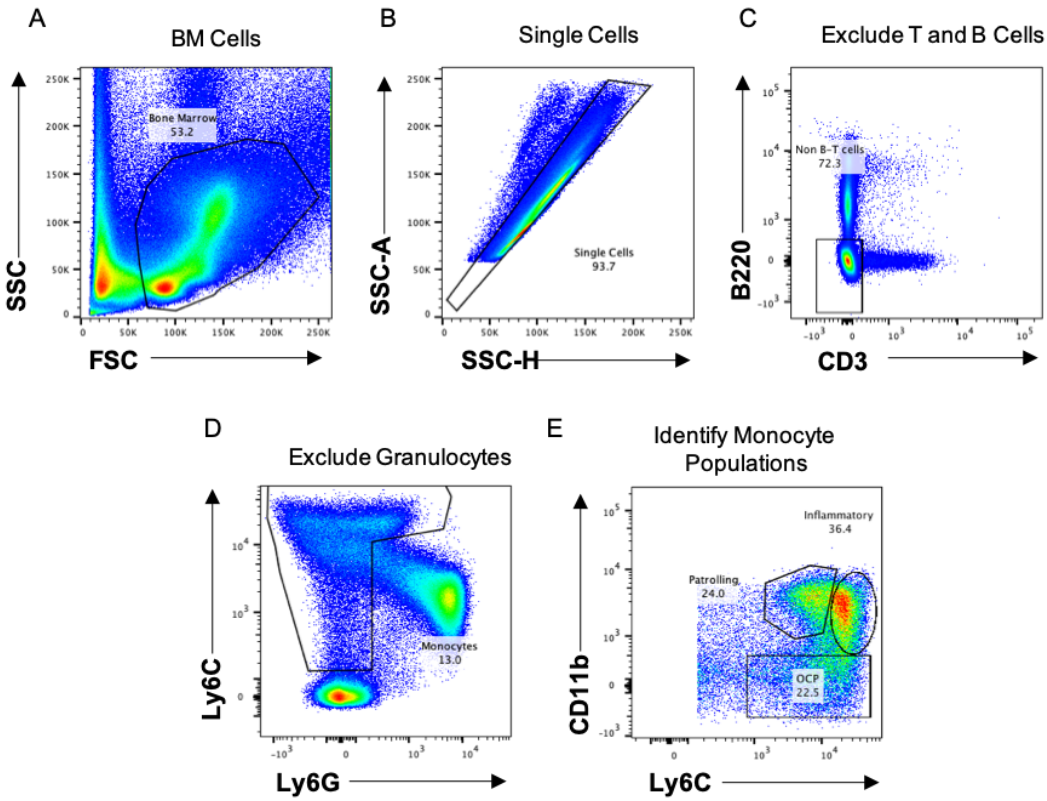

Figure 5.1 Gating Strategy for Monocyte Analysis in Murine Bone Marrow
Bone marrow was isolated from the long bones of adult WT and *par2*$^{-/-}$ mice and resuspended in a homogenous solution in FACS buffer for subsequent staining. Non-specific binding of antibodies to Fc receptors was prevented by pre incubation (10mins) of anti-CD16/32 to block these FcRs. BM was then stained with a cocktail of antibodies to identify T cells (CD3-PE), B cells (B220-PECy7), granulocytes (Ly6G AF700), and monocytes (Ly6C-PerCP Cy5.5, and CD11b-APC Cy7). Cells were then washed in FACS buffer before running on the BD LSRII flow cytometer. The gating strategy employed to identify monocytes in this mixed population is shown above. (A)Initially erythrocytes and other waste was excluded and (B) single cells were positively gated for. (C) Gating to exclude both T and B cells was performed, (D) and then on this non-T and B cell gate granulocytes were excluded from further analysis. (E) The granulocyte, T cell, and B cell negative gate was further sub divided based on Ly6C and CD11b expression to identify BM monocytes. Monocytes were further subset based on expression levels of these surface markers, with inflammatory monocytes expressing a Ly6C^{hi}CD11b^{hi} profile, patrolling monocytes Ly6C^{lo} and CD11b^{hi}, while OCPs were Ly6C^{+} CD11b^{-}. Representative FACS plots shown of N=1.

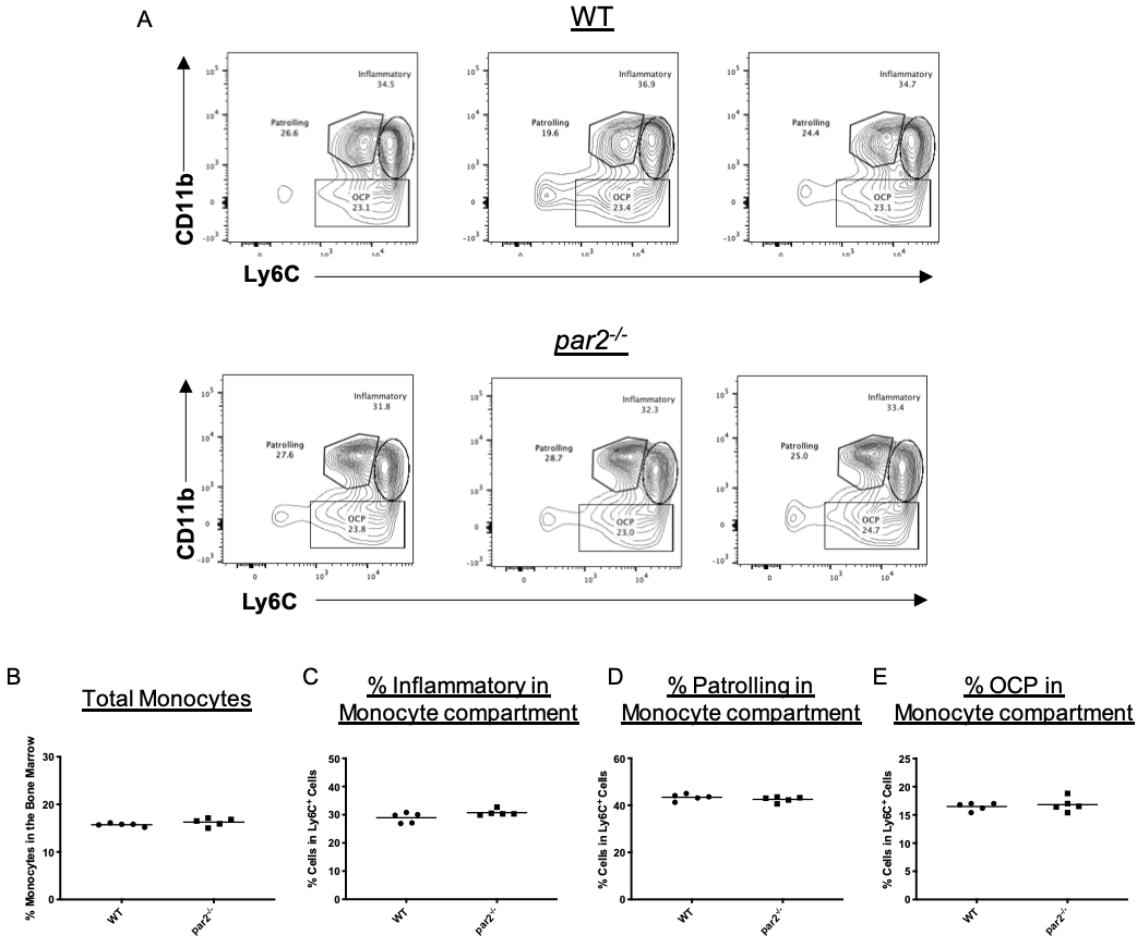

Figure 5.2 No Difference in Monocyte Cell Composition in *par2*$^{-/-}$ Bone Marrow.
FACS plots detailing the BM monocyte compartment composition of inflammatory, patrolling, and OCP populations are shown for both WT and *par2*$^{-/-}$. (A) Representative plots from a biological sample size of 5 for each genotype are shown. (B) The frequency of monocytes in the total bone marrow compartment was calculated from single cells. Further analysis of the frequency of (C) inflammatory, (D) patrolling, and (E) OCPs in the monocyte compartment is shown for all samples. WT N=5, *par2*$^{-/-}$ N=5. 1 representative experiment shown of 3 experimental repeats.

5.2.2 Enhanced CD11b Expression on Patrolling Monocytes from *par2*$^{-/-}$ Bone Marrow

While conducting flow cytometric analysis of the bone marrow to analyse the frequencies of monocytic cells in WT and *par2*$^{-/-}$ an observation was made regarding the expression level of CD11b, one of the markers used to distinguish monocyte populations. Notably, the monocyte FACS plots between WT and *par2*$^{-/-}$ looked consistently different with regards to fluorescence levels of CD11b. Upon further investigation of the MFI of CD11b staining, it was confirmed that patrolling monocytes from *par2*$^{-/-}$ bone marrow had significantly elevated levels of CD11b expression. This same phenomenon was not identified on any other subset of bone marrow monocytes. This finding was consistent across multiple experiments (Figure 5.3 A and B).

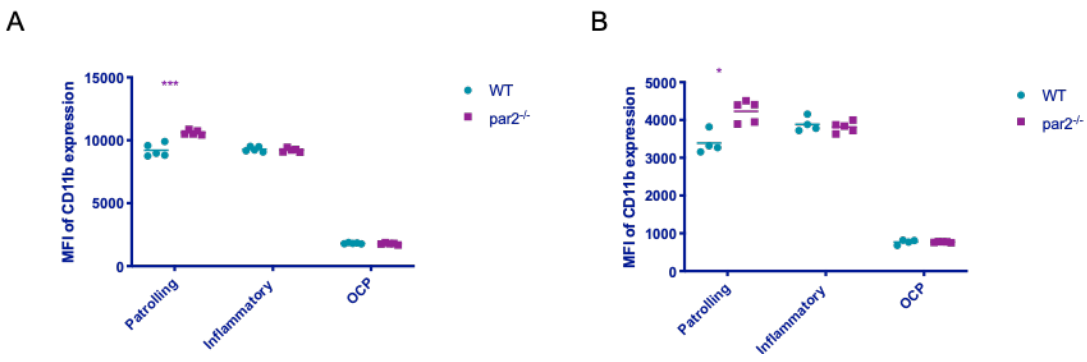

Figure 5.3 Increased Expression of CD11b in Patrolling Monocytes from *par2*$^{-/-}$ Compared with WT Patrolling Monocytes.
(A) The mean fluorescent intensity (MFI) of CD11b staining for each monocyte subset (inflammatory, patrolling, OCP) was compared between WT and *par2*$^{-/-}$ BM monocyte; N=5 for each genotype. (B) An independent repeat experiment; N=4 WT and N=5 *par2*$^{-/-}$. Multiple T tests were conducted, with Holm-Sidak correction for multiple comparison, adjusted p values as follows *** = $p<0.005$, * = $p<0.05$.

In order to conduct osteoclast assays, total bone marrow from long bone was extracted, cultured overnight, and non-adherent cells (NA-BM) taken forward for further culture. A change in integrin expression could potentially alter the capacity for these cells to adhere to tissue culture plastic[359]. Monocyte proportions and CD11b expression were subsequently analysed in WT and *par2*$^{-/-}$ post overnight culture to identify if this enhanced integrin expression is maintained in cell culture and thus potentially altering the cellular adherence of BM cells. Flow cytometric analysis was conducted on both the non-adherent BM

and the adherent fraction of BM post overnight culture. For this, the same panel used above (Figure 5.1A) was applied. After overnight culture monocytes did not maintain the phenotypic markers that allow the identification of patrolling, inflammatory, and OCP populations. Instead these cells became a more homogenous population of monocytes in terms of CD11b and Ly6C expression (data not shown). Thus, the total cultured monocyte population was evaluated. Interestingly, a higher frequency of monocytes was found in the adherent fraction of both WT and KO BM cells, when compared to the non-adherent fraction (Figure 5.4A). Considering the non-adherent fraction is most commonly used for murine bone marrow macrophage and osteoclast assays this was somewhat surprising. No changes in the frequency of monocytes in the non-adherent fraction of bone marrow was identified between genotypes. However, when PAR2 was absent (*par2*$^{-/-}$) an enhanced proportion of monocytes was identified in the adherent fraction of bone marrow (Figure 5.4A). This may reflect the increased adhesion capacity of monocytes in knock out cells, as reflected by the observed enhancement in integrin subunit CD11b expression in the previous figure (Figure 5.3). However, it is also worth considering that frequency based analysis was used and therefore this enhanced monocyte proportion could in fact reflect a reduction in the proportion of another type of adherent cells. As mentioned above, a reduction in the stromal compartment has been observed in *par2*$^{-/-}$ bone marrow[76], so this may skew proportional analysis of populations within the adherent bone marrow.

In order to investigate whether the observed increase in *par2*$^{-/-}$ CD11b expression was sustained, subsequent analysis was conducted of CD11b expression on monocytes post overnight culture. Interestingly, after overnight culture we observed a significant reduction of CD11b expression level in *par2*$^{-/-}$ monocytes comparative to WT monocytes, reflected by the reduction of MFI (Figure 5.4B). This was observed in both monocytes present in the non-adherent fraction and those that had adhered during overnight culture.

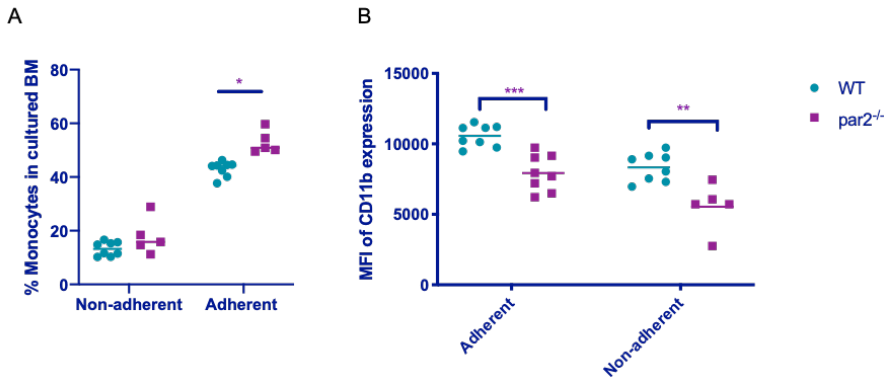

Figure 5.4 After Overnight Cell Culture Expression Levels of CD11b are Reduced in *par2*$^{-/-}$ Monocytes.
Total BM was cultured overnight and the following morning non-adherent cells lifted and counted, cell counts of NA-BM from WT and *par2*$^{-/-}$ cultures are shown in A. Using D'Agostino & Pearson test for normality we determined this data conformed to Gaussian distribution and thus unpaired T test with Welches correction was conducted; * = $p<0.05$. (B) The frequency of Ly6C^{+} monocytes in the total cell population of both NA-BM and NA-BM cells after overnight culture is shown for both WT and *par2*$^{-/-}$.The MFI of CD11b in Ly6C^{+} monocytes after overnight culture was then analysed for both adherent and non-adherent cells. Multiple T test were conducted with Holm-Sidak correction for multiple comparisons, adjusted p values as follows: * = $p<0.05$, ** = $p<0.005$, *** = $p<0.0005$. WT adherent and non-adherent N=8, *par2*$^{-/-}$ adherent N=8 and non-adherent N=5. 1 experiment shown representative of 2 experimental repeats.

While differences in total expression of integrin subunits indicates there could be potential changes in adhesion capacity, total expression does not directly translate to functional activity. Integrins are present on the cell membrane in an inactive state until, in response to chemokine signals, they change their conformation to an active state. In order to test potential differences in the functional capacity of *par2*$^{-/-}$ to adhere to CD11b ligands we conducted a static adhesion assay with ICAM-1, a binding partner of the CD11b/CD18 integrin heterodimer. A heterogeneous population of cells would not be appropriate for this analysis. Therefore in order to conduct this assay monocytes were isolated from murine BM using a negative selection magnetic bead method. The binding capacity of purified monocytes (Figure 5.5) from both WT and *par2* KO, to the integrin ligand ICAM-1 was then assessed under different stimuli. Monocytes were ultimately defined by their expression of CD115 (M-CSF receptor). The total BM compartment contained 13.3% of CD115^{+} monocytes, while post magnetic bead isolation the cell samples contained around 75% of CD115^{+} monocytes.

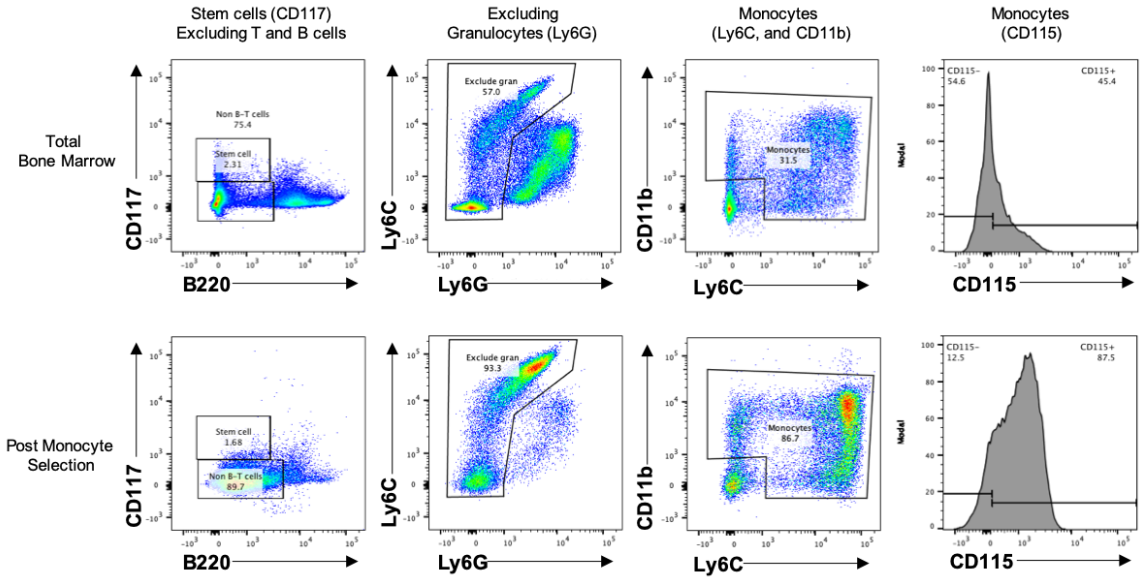

Figure 5.5 Murine Monocytes were Successfully Enriched by Magnetic Separation. Using negative magnetic selection murine monocytes were enriched from the total BM compartment. Flow cytometry techniques were used to ensure adequate enrichment of monocytes from the total population. Total BM and monocyte isolates were stained for stem cells (CD117-V450), B and T cells (B220, CD3-PE), granulocytes (Ly6G-AF700), and monocytes (Ly6C-PerCP Cy5.5, CD11b-APC Cy7, and CD115-APC). The total BM compartment contained T and B cells (23%), stem cells (2.3%), and granulocytes (32.4%), with around 19% of BM cells $CD115^+$ monocytes. Post enrichment, on average over 75% of cells were $CD115^+$ and a significant reduction of T and B cells (9%), stem cells (1%) and granulocytes (6%) observed. Representative FACS plots N=1.

Optimisation of this assay for monocyte cell number and appropriate positive stimulations was conducted. Different concentrations of murine monocyte numbers were assessed with PMA stimulation (positive control), known to stimulate activation of integrins. A cell concentration that had clear distinction between negative control unstimulated cells and PMA activation was required. As a negative control for binding to plastic, some wells were not coated with ligand. Importantly, these wells were blocked to eliminate non-specific binding in the same way as the ICAM-1 coated wells. A cellular concentration of $1x10^6$ monocytes was not sufficient to robustly detect monocyte activation and ICAM-1 binding upon stimulation (Figure 5.6A). In comparison, cells at a concentration of $1.5x10^6$ and $2x10^6$ showed a clear induction of ICAM-1 binding upon PMA stimulation (Figure 5.6B and C). In order to limit the number of cells required for this assay but still detect clear induction of cell adhesion to ICAM-1 a concentration of $1.5x10^6$ monocytes/ml was taken forward. This assay was then conducted with WT and *par2*$^{-/-}$ monocytes. The adhesion of unstimulated and PMA activated WT and *par2*$^{-/-}$ cells to ICAM-1 was assessed. In addition, PAR2

stimulation was also evaluated for its capacity to impact ICAM-1 binding using PAR2 activation peptide 2-Furoyl-LIGRLO-amide (FLIGRL, 2μM). No differences were detected between WT and *par2*$^{-/-}$ monocytes under any condition tested (Figure 5.6D). This assay was conducted with just 2 samples per condition, however, because no obvious changes were observed it was not pursued any further.

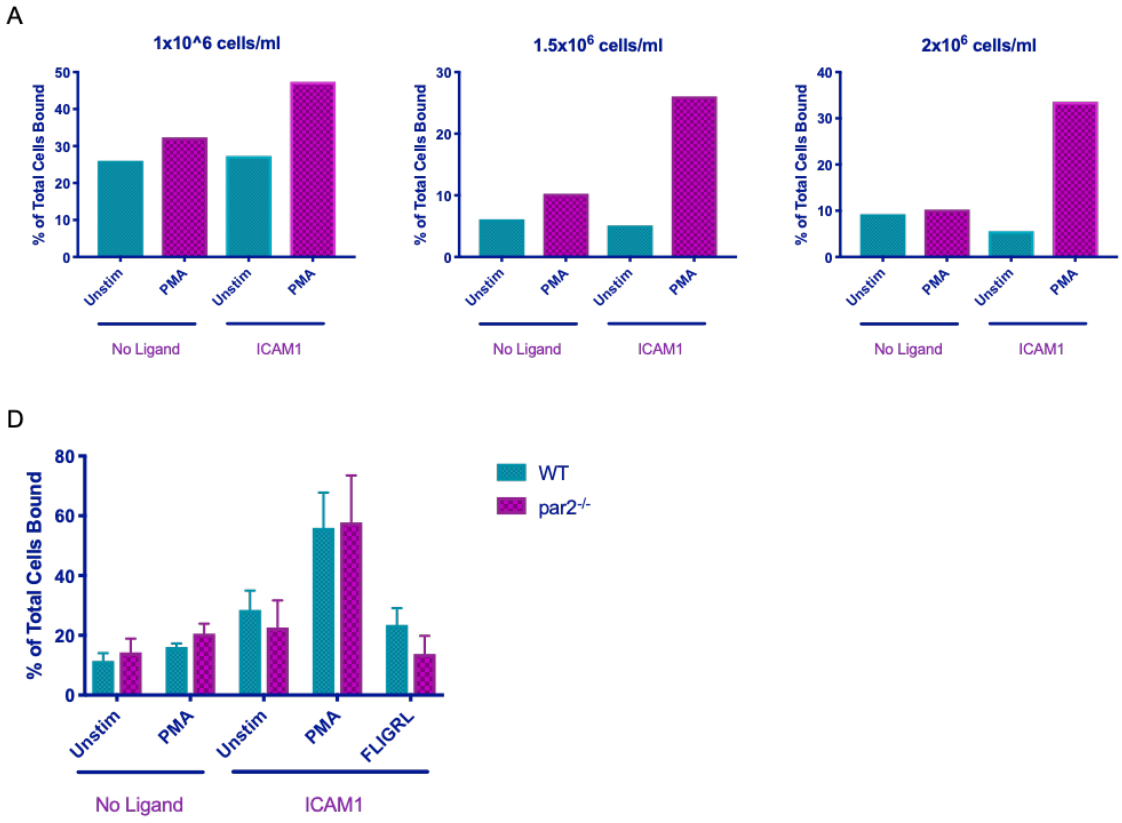

Figure 5.6 PAR2 Activation Does Not Impact Monocyte Static Adhesion to ICAM-1. Monocytes isolated from murine BM were prepared at 3 different cell concentrations and left unstimulated in adhesion assay media or stimulated with PMA (1μg/ml) for 10 minutes. Cells were then incubated on plates coated with ICAM1 ligand or uncoated. (A, B, C) The percentage of cells which adhered to the plate for each cell concentration N=1. (D)The concentration of 1.5x10^6 monocytes was taken forward and monocytes from WT and *par2*$^{-/-}$ BM were either left unstimulated, stimulated with PMA (100nM), or FLIGRL (2μM) for 10 minutes and then subsequently incubated at 37ºC in an ICAM1 coated plate (or left uncoated as a negative control) for 30 minutes. The frequency of adherent monocytes from the total monocyte addition to the wells was calculated. WT and *par2*$^{-/-}$ N=2, no additional experimental repeats performed.

5.2.3 Increased Osteoclastogenic Potential of *par2*$^{-/-}$ Bone Marrow

In order to investigate the role of PAR2 in osteoclastogenesis an *in vitro* OC assay system had to be initially tested. There are high levels of variability in published protocols however, in all published assays, osteoclastogenesis was dependent upon the presence of M-CSF and RANKL. The concentrations and time at which these growth factors are employed in these assays are highly variably between publications. The method adopted is outlined in Figure 5.7. This involves overnight culture of the total BM and then removal of the non-adherent (NA) or adherent cells for further culture in M-CSF, followed by addition of RANKL the next day. While most published OC differentiation protocols utilise the NA-BM fraction some papers generate OCs using the entire BM; not separating any cell types. Therefore, the capability of both non-adherent and adherent BM cells to differentiate into OCs was assessed initially. The benefit of utilising this assay is that if the NA fraction from the BM is used, the stromal cells of the adherent fraction can be utilised for other experiments without having M-CSF contamination. These stromal cells were required by other members of the lab and thus BM from 1 animal could be utilised for multiple experimental procedures, as complying with the 3Rs (Replacement, Reduction, Refinement).

TRAP stain images presented in Figure 5.7 demonstrate that both NA and adherent BM cells generated multinucleated, TRAP positive osteoclasts. Adherent BM cells actually generated more and larger TRAP OCs (Figure 5.7). The observation of a higher frequency of Ly6C^{+} monocytes in adherent BM over NA-BM cells (Figure 5.4A) indicates that the abundance of these cells contributes to the enhanced OC number and is therefore somewhat unsurprising. Despite the higher rate of OCs generated with adherent BM, this fraction will contain the highest level of stromal contamination. The presence of stroma from the bone marrow can significantly influence OC generation as these cells can express RANKL. Therefore, as is most commonly done in the literature, the non-adherent fraction of BM was used for all future OC generation assays. Since this initial experiment confirmed that OCPs are still viable post overnight culture without additional factors, and OCs were successfully generated with this protocol it was determined that OC generation assays would be conducted with the NA-BM from the protocol in Figure 5.7.

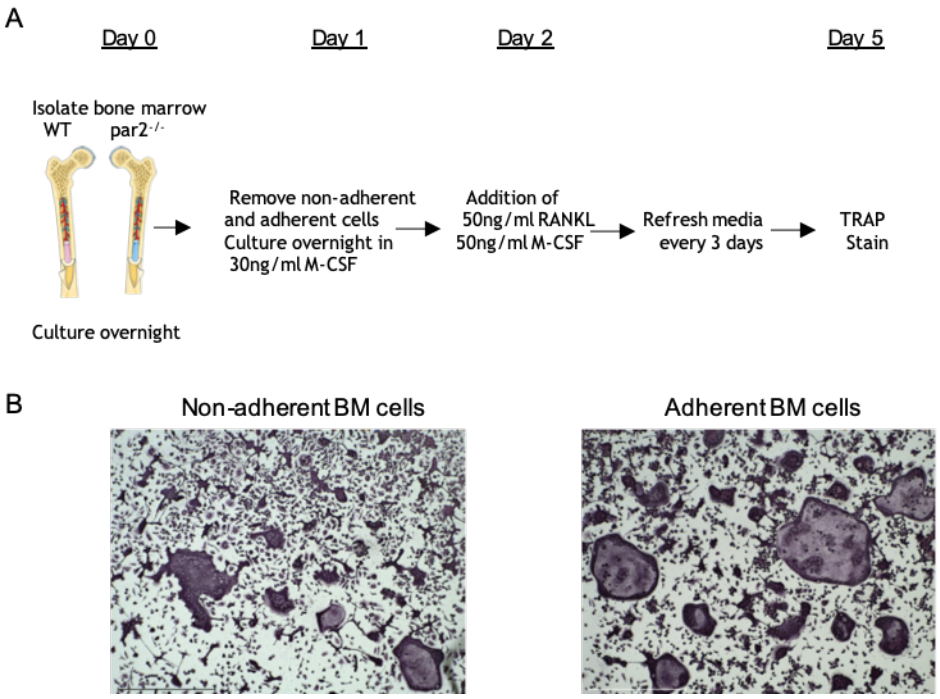

Figure 5.7 Murine BM Osteoclastogenesis Cultures.
Total BM was cultured overnight without the addition of any cytokine and then addition of M-CSF the following day and addition of RANKL on day 2. Both non-adherent and adherent BM cells were taken after overnight culture and exposed to the OC generation protocol. (B) Representative TRAP stain images at 10x magnification are shown.

The protocol from Figure 5.7A with NA-BM was applied to cell cultures from the BM of both WT and *par2*$^{-/-}$ animals. BM was isolated, cultured overnight, the NA-BM fraction taken the following day and counted to plate out 1x10^5 cells per well of a 96 well plate. These cells were given 30ng/ml of M-CSF overnight and then the following day the media was half changed to include both 50ng/ml of M-CSF and RANKL. After 5 days osteoclasts were visible, TRAP stained (Figure 5.8A), and counted. To get a complete insight into the level of osteoclastogenesis, rather than counting random areas of the well, the entire well area was counted. This is important, as OC generation tends to be uneven across the well (possibly caused by media changes pushing cells more to one side), and therefore a random selection of areas could cause a counting bias. The quantification of OC numbers in WT and *par2*$^{-/-}$ cultures revealed that there was an enhanced number of OCs generated from *par2*$^{-/-}$ BM (Figure 5.8B). Moreover, the OCs generated in the *par2*$^{-/-}$ cultures were visibly larger. In order to quantify this, osteoclasts were counted based on the number of nuclei that they contained. For example, osteoclasts were group in to those with 3-5, 6-10 nuclei

and so on. By applying this form of analysis, it was apparent that there was a significant enhancement in all groups in the *par2*$^{-/-}$ cell cultures (Figure 5.8C). The data also revealed that *par2*$^{-/-}$ cultures also contained very large OC cells (11+ nuclei) that were not present in WT cultures.

In addition to conventional TRAP staining protocols, which enabled quantification of cell number and an insight to cellular morphology, osteoclastogenesis assays were also conducted on osteo-assay plates, which enable quantification of the functional activity of OCs. The same osteoclastogenesis assays were conducted on these plates and cells were removed with bleaching on day 12. The contrast between resorbed and minerally intact areas could easily be discriminated when images were transferred to 8 bit. The percentage of the total well which had been resorbed was quantified. Evaluation of resorbed areas (black) vs non-resorbed (white) did not result in a significant difference between WT or *par2*$^{-/-}$ cultures (Figure 5.8 D and E). This suggests that while there are more OCs in *par2*$^{-/-}$cultures, the activity of these individual cells may not be enhanced. It is also possible that the time point of 12 days was too long to identify potential differences in cellular activity between WT and *par2*$^{-/-}$ cultures. By this point in the culture WT cells may have caught up with the enhanced *par2*$^{-/-}$ cultures, therefore a time course of cellular activity might perhaps have been a better method of assessing true differences in resorption between the 2 genotypes.

In order to assess whether OC activity was altered per cell with a change in genotype the % resorption was normalised to OC count (Figure 5.8 F). This analysis indicates that while OC size appears larger in *par2*$^{-/-}$ cultures, resorption activity is in fact significantly decreased. Further supporting the possibility that PAR2 action in these cultures acts to limit excessive fusion, distinct from OC activity.

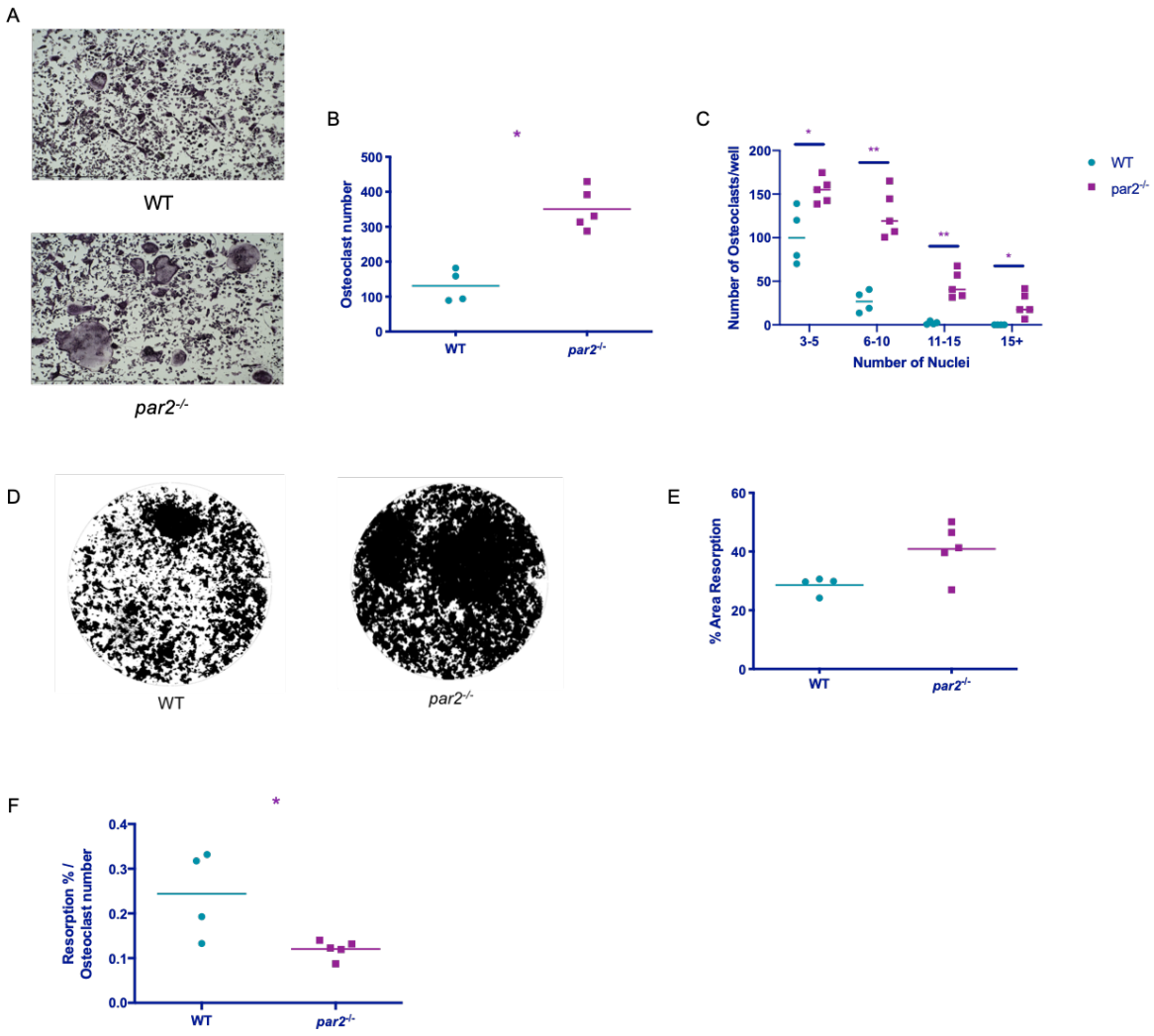

Figure 5.8 Increased Osteoclastogenesis from NA-BM of *par2*$^{-/-}$ Mice.
NA-BM from both WT and *par2*$^{-/-}$ mice was subjected to *in vitro* osteoclastogenesis assay (Figure 5.7A) and cultures were TRAP stained on day 5, and osteo-resorption plates bleached to remove cells after 12 days. (A) Representative images of WT and *par2*$^{-/-}$ TRAP stained osteoclasts at 10x magnification. (B, C) Quantification was performed of the number of TRAP+, multinucleated osteoclasts per well in a 96 well plate for each WT and *par2*$^{-/-}$ sample, N=4 and N=5 respectively. Images of osteo-assay plates were taken at 2x magnification and images were analysed on ImageJ software. The colour contrast between areas of resorbed mineral and intact mineral mean that these can be easily discriminated. (D) Representative images show resorbed areas in black and intact mineral in white. (E) Whole well images were converted to 8 bit grey scale and the threshold set between the two contrasting areas and the resorbed area was measured as a percentage of the entire well. (F) The area of resorption was then normalised to the number of OC per well. WT N=4, KO N=5. There were too few data points to determine normal distribution and therefore a Mann-Whitney tests were used to determine significance, * = $p<0.05$, ** = $p<0.005$. Representative of 3 experimental repeats performed.

To confirm the enhancement of osteoclastogenesis in *par2*$^{-/-}$ cultures and identify specific OC associated pathways which may be specifically enhanced in *par2*$^{-/-}$, transcript analysis was conducted. RNA was isolated on day 5 (peak OC formation) and qPCR was conducted to quantify osteoclast associated genes. Monocyte-derived macrophage controls that do not initiate the osteoclastogenic

transcriptional cascade, were used for comparison to identify RANKL dependent gene expression enhancement. The $2^{-\Delta Ct}$ was calculated using housekeeping gene 18s for each transcript (Cathepsin K, NFATc1, TRAP, DC STAMP, OC STAMP, MMP9, OSCAR) and statistical testing conducted on the $2^{-\Delta ct}$. All gene transcripts, with the exception of RANK and CD115, were significantly upregulated in response to M-CSF and RANKL (MR) for both WT and *par2*$^{-/-}$. The fold change enhancement with RANKL over M-CSF alone controls of OC associated transcripts ranged from 4 to 300 fold depending on the gene (Figure 5.9A). WT and *par2*$^{-/-}$ MR transcripts were then compared to each other directly (Figure 5.9B, C, and D). A significant enhancement in expression levels of Cathepsin K, NFATc1, TRAP, DC STAMP, MMP9, and OSCAR expression was found in *par2*$^{-/-}$ cultures. This confirmed enhancement of osteoclast generation in these cultures but does not provide indication of any specific pathways enhanced in these cultures. However, the enhancement in gene expression of these transcripts between WT and *par2*$^{-/-}$ is less than 2 fold. Therefore, despite the robust statistical differences due to the consistency of these observations in replication, the enhance gene expression measured may have limited biological relevance. In addition, transcripts of RANK and CD115 are not enhanced over M-CSF alone samples at this time point (data not shown). This is most likely the result of downregulation of these receptors at this end stage of osteoclast generation.

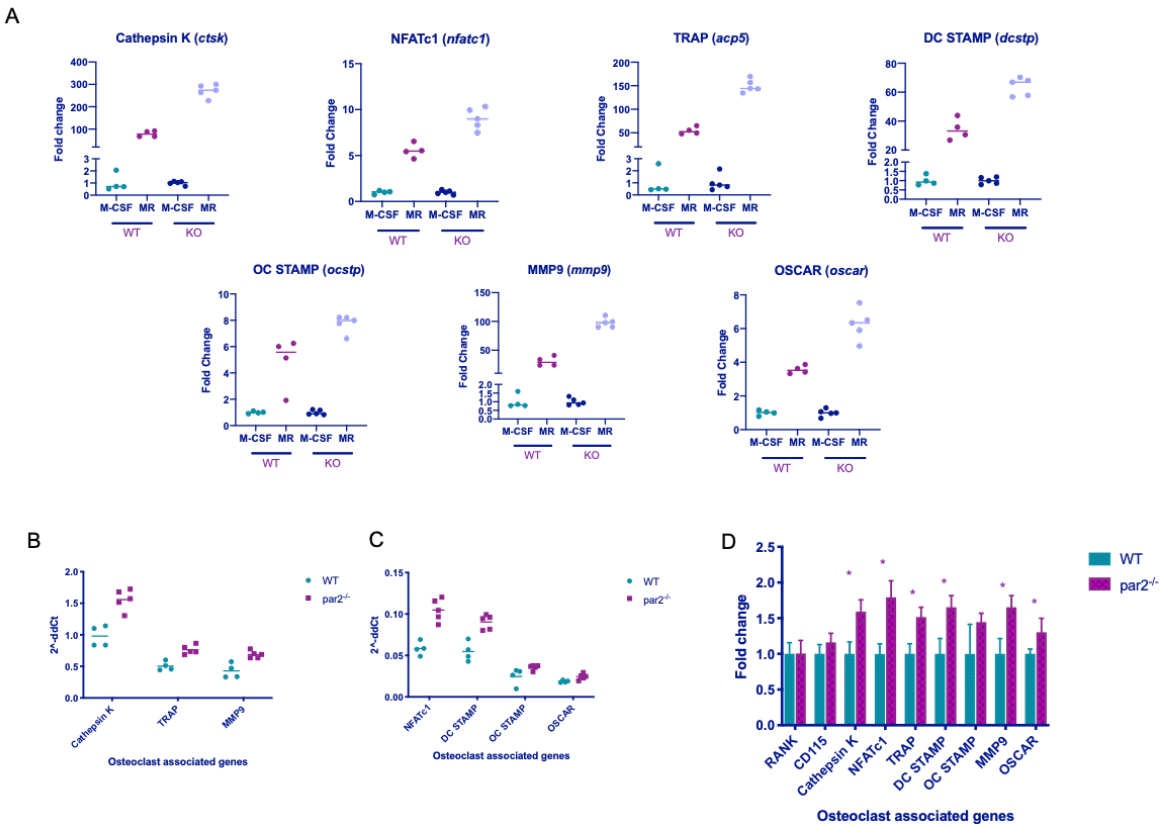

Figure 5.9 Terminally Differentiated OC Cultures from *par2*$^{-/-}$ BM have an Enhanced Profile of OC Associated Gene Transcripts.
Transcript analysis was performed on both WT and *par2*$^{-/-}$ cell cultures differentiated in M-CSF alone, or M-CSF and RANKL for 5 days. (A) The fold change of WT MR over WT M alone, and *par2*$^{-/-}$ MR over *par2*$^{-/-}$ M alone of osteoclast associated genes in MR samples compared with M-CSF alone cells for Cathepsin K (*ctsk*), NFATc1 (*nfatc1*), TRAP (*acp5*), DC STAMP (*dcstp*), OC STAMP (*ocstp*), MMP9 (*mmp9*), and OSCAR (*oscar*). (B) The $2^{-\Delta Ct}$ of MR cultures from WT (green) and *par2*$^{-/-}$ cells (red) of highly expressed genes and (C) independently plotted genes with lower expression graphed separately for ease of viewing. (D) The fold change of MR cultures normalised to average WT $2^{-\Delta Ct}$ for *par2*$^{-/-}$ osteoclasts, with all stats performed on $2^{-\Delta Ct}$ data. Mann-Whitney was applied to determine statistical significance * = $p<0.05$. WT N=4, *par2*$^{-/-}$ N=5. No additional experimental repeats performed

In order to assess changes in osteoclast transcripts upon MR stimulation and potential differences in genotypes at early time points, RNA extraction was conducted at 6, 24, 48 and 72 hours after initial RANKL stimulation (Figure 5.10A). This data was plotted as a fold change over time 0. Time 0 samples were NA-BM, which had been exposed to M-CSF overnight but not yet exposed to RANKL. Both WT and KO samples were plotted along this time course, with WT shown in green and KO in purple. RANK and CD115 were not changed over time. These transcript levels will increase in response to M-CSF, and therefore it is unsurprising that RANK and CD115 gene expression is not enhanced in response to RANKL treatment. In this experiment transcriptional profiles were not

compared to naïve NA-BM, so it is not possible to detect these initial changes with the current experimental set up. Transcripts such as Cathepsin K, TRAP, MMP9 and DC STAMP have a low level of expression at the earliest time points and then by 48 hours these genes have high levels of expression, which continues to increase at 72 hours. These are late induced transcripts that enable cell fusion (DC-STAMP), and initiation of OC resorption functions (Cathepsin K, TRAP, MMP9). Central OC transcription factor NFATc1 expression increases at 24 hours, continues to increase at 48 hours and then expression levels begin to fall by 72 hours. This is also to be expected. NFATc1 plays an essential role in the induction of OC functional genes and by 72 hours these genes are now being highly transcribed.

Fold change of each gene normalised to the WT samples was then conducted, in order to identify any possible changes to the transcript levels in the KO cells at each time point. Largely there is no obvious change in expression level of the OC associated genes in the KO cells at these earlier timepoints. The only statistically significant differences detected are an early increase in cathepsin K expression in the KO cells at 6 hours and a higher expression of DC STAMP in *par2*$^{-/-}$ cultures before these cells are exposed to RANKL (Figure 5.10B). However, these short term, minimal fold change differences are unlikely to reflect biologically relevant observations. Overall, the transcript changes at the early time points are very modest and no obvious pathways stand out at the initial differentiation stages.

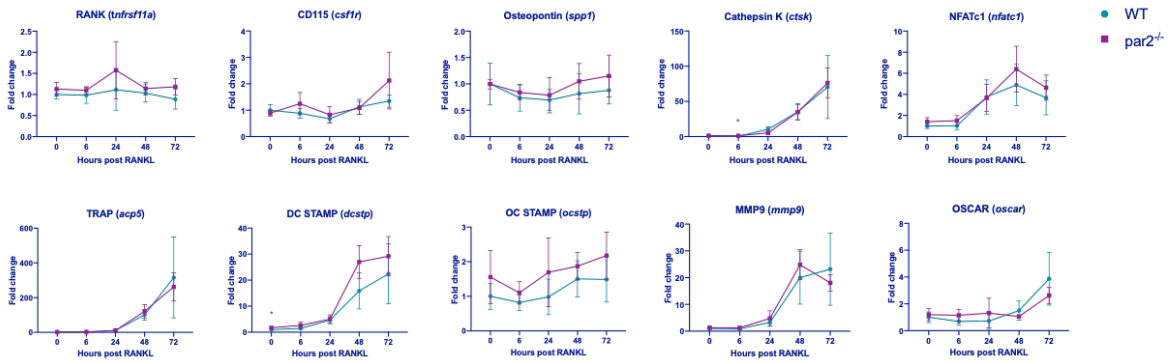

Figure 5.10 Early Time Points of M-CSF and RANKL Differentiation do not show Significant Alteration in OC Associated Transcripts in *par2*$^{-/-}$ cultures.
Transcript analysis was performed on cell cultures from both WT and *par2*$^{-/-}$ cell cultures differentiated in M-CSF and RANKL, at time 0 (M-CSF overnight, not yet exposed to RANKL), 6 hrs, 24hrs, 48hrs, and 72 hrs post RANKL exposure. The $2^{-\Delta\Delta Ct}$ (fold change) of OC associated genes in WT and *par2*$^{-/-}$ MR cultures across time are shown for RANK (*tnfrsf11a*), CD115 (*csf1r*), Osteopontin (*spp1*), Cathepsin K (*ctsk*), NFATc1 (*nfatc1*), TRAP (*acp5*), DC STAMP (*dcstp*), OC STAMP (*ocstp*), MMP9 (*mmp9*), and OSCAR (*oscar*). All statistical tests performed on $2^{-\Delta Ct}$ data. Mann-Whitney was applied to determine statistical significance * = $p<0.05$, WT N=5, *par2*$^{-/-}$ N=4. No additional experimental repeats performed.

The above experiments indicate that PAR2 is a regulator of OC differentiation, especially important at later time points of OC fusion. However, these experiments provide no insight as to whether active signalling of PAR2 is required during the OC differentiation assays to drive this phenotypic difference observed between the genotypes. No PAR2 activating proteases or peptides have been included in the assays above, thus the impact on OC differentiation must either be the result of endogenous protease production and PAR2 activation, or this phenotype is present without the requirement of PAR2 signalling within the culture. PAR2 activating protease have been previously identified in the murine BM compartment including trypsin I/IV, matriptase, and hepsin [76]. OCPs may have been previously primed via PAR2 within the BM, impacting their activity in these cell cultures. Therefore, in order to test whether active PAR2 signalling is required during the differentiation process to regulate the formation of OCs, the OC assay (as described in Figure 5.7) was repeated with inclusion of PAR2 activating peptide (FLIGRL, 2μM) or PAR2 inhibitor (AZ8838, 3μM). The repeat of the OC assay again resulted in enhanced OC differentiation from *par2*$^{-/-}$ BM cells over WT counterparts(Figure 5.11A). Evaluation of the KO cultures revealed that neither FLIGRL nor AZ8838 altered the number of OCs (Figure 5.11D); an expected non-response due lack of receptor. Moreover, comparison of WT and KO cultures showed that there was a significant difference in OC number when

cells were unstimulated and FLIGRL stimulated (Figure 5.11D). Addition of PAR2 activating peptide to the WT culture did not consistently change the number of osteoclasts generated (Figure 5.11B). However, addition of AZ8838 to WT BM cells consistently increased the number of OCs generated by each sample (Figure 5.11C). This observation did not reach statistical significance. Importantly, treatment of WT cells with AZ8838 resulted in equivalent osteoclast number to those observed in *par2*$^{-/-}$ cultures (Figure 5.11D). In order to analyse whether PAR2 inhibition influences OC size, OC counts were then subdivided based on nuclei number and analysed independently (Figure 5.11E). This analysis identified that PAR2 inhibition in WT cells did not alter the number of small OC (3-10 nuclei) but significantly reduced the number of large cells (10 nuclei +). Overall, this data suggests that in this setting active PAR2 signalling, potentially through endogenous proteases, is suppressing the formation of giant OC cells. This may further indicate the role of this receptor in preventing excessive cell fusion.

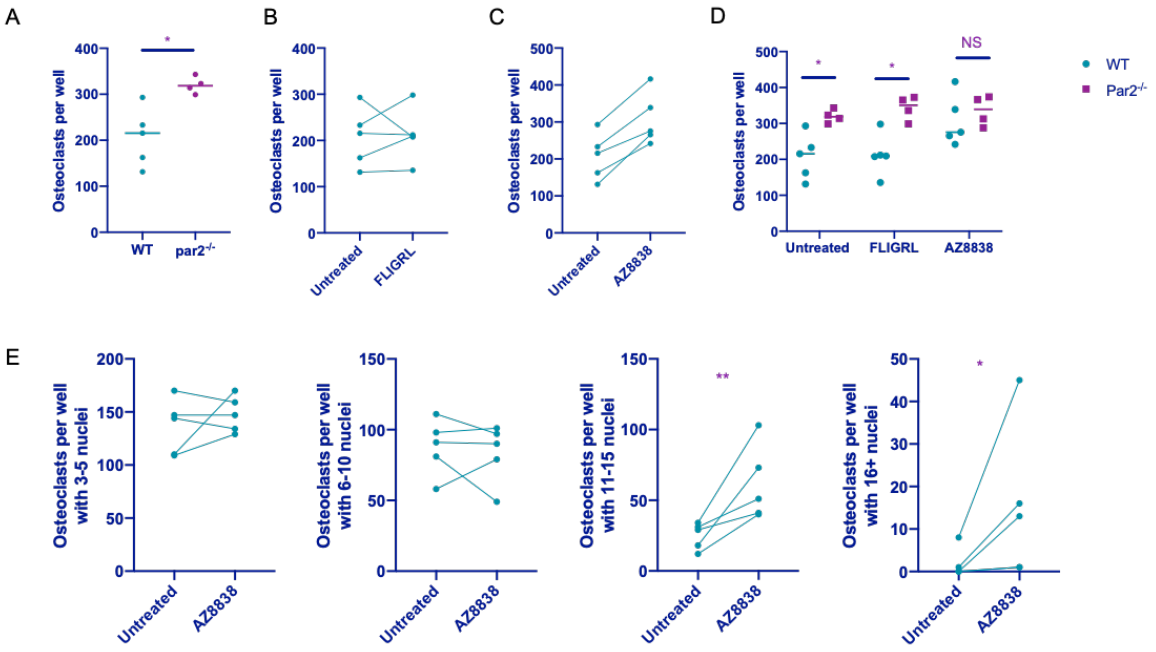

Figure 5.11 Canonical PAR2 Activation Does Not Inhibit *in vitro* OC Differentiation. OC differentiation was repeated with the protocol described in Figure 5.7 (A) with both WT and *par2*$^{-/-}$ BM and OC were counted. (B) PAR2 activating peptide (FLIGRL 2μM) and (C) PAR2 inhibitor (AZ8838 3μM) were included in this assay with both WT and *par2*$^{-/-}$ cultures. Multiple T tests were conducted with Holm-Sidak correction for multiple comparisons (N=5 WT, N=4 *par2*$^{-/-}$), adjusted p values as follows: * = $p<0.05$. The number of OC generated from NA-BM with (B, D) FLIGRL (2μM) PAR2 activation and (C, D) AZ8838 (3μM) PAR2 inhibition in WT BM cultures was compared with untreated OC culture. (E) Subsequent analysis separated OCs by number of nuclei and analysed these OC counts independently. Paired statistical analysis with Wilcoxon T test was conducted for WT treatments. WT N=5, *par2*$^{-/-}$ N=4, no additional experimental repeats performed.

5.2.4 PAR2 Regulates Osteoclast Formation via Stromal Osteoblasts

PAR2 regulates the formation of OCs in a hematopoietic OC enriched *in vitro* culture dependent upon M-CSF and RANKL driven conditions. OB stromal cells are a central regulator of OC generation *in vivo*. During homeostatic conditions these cells are the primary source of OC stimulatory factors such as RANKL, while also regulating this process through the production of RANKL decoy receptor - OPG. In addition, it has been previously reported that OB express PAR2. The impact of the PAR2 pathway on the ability of OB-like stromal cells to generate OCs was therefore investigated. *In vitro* co-culture of stromal OB-like cells and BM monocytes was set up in order to study this, where alternate genotypes for stromal cells and immune cell components could be cultured together. Stromal OB like cells were generated through digestion of the calvaria of murine pups day 3-5 post-natal. These were isolated from both WT and *par2*$^{-/-}$ pups and expanded in culture for 5 days. Once these cells had reached 80% confluency they were harvested and plated in 96 well plates and left to settle overnight in preparation for monocyte co-culture. Bone marrow was extracted from long bones of 6-10 week WT and *par2*$^{-/-}$ mice (as per section 5.2.3). However, instead of using the mixed NA-BM fraction, monocytes were specifically isolated using magnetic negative selection kit. This enabled the elimination of contamination by other cell types in this culture. These monocytes were then cultured with the OB-like stroma in the presence of prostaglandin E (PGE_2) and vitamin D (VitD), which promotes the production of mediators to support the generation of OCs. As a negative control, the vehicle of these growth factors (ethanol) was used instead of PGE_2 and VitD, resulting in no OC formation (data not shown). The co-cultures were arranged in a mix and match fashion, meaning WT stroma was cultured alongside both WT monocytes and *par2*$^{-/-}$ monocytes and vice versa (Figure 5.12A).

These cultures were continued for 8-10 days, with OC fusion detectable around day 7. Cultures were fixed and TRAP stained when OCs were visibly present in the culture (Figure 5.12B) and TRAP stains were quantified as previously outlined (Figure 5.12C). Interestingly, the number of osteoclasts generated was significantly increased in cultures with *par2*$^{-/-}$ OB genotype (Figure 5.12C). Further analysis of these cultures was conducted to assess the proportional area

of the well that contained large TRAP+ cells. This measurement was used as a surrogate to provide an indication of the size of osteoclasts generated. This type of analysis was employed because in the co-culture stains exact nuclei numbers for OCs could not be identified. A significant enhancement in the proportion of the well stained TRAP+ was identified when both monocyte and stromal genotypes were *par2*$^{-/-}$(Figure 5.12D). This data indicates an enhancement in OC size in total KO cultures, with TRAP+ area over double that measured in WT cultures (Figure 5.12D). There was also a significant enhancement in OC size from WT OB/KO OC culture to KO OB/KO OC culture (Figure 5.12D). Again, this indicates that the genotype of OB-like cells was essential to the enhancement of osteoclast generation.

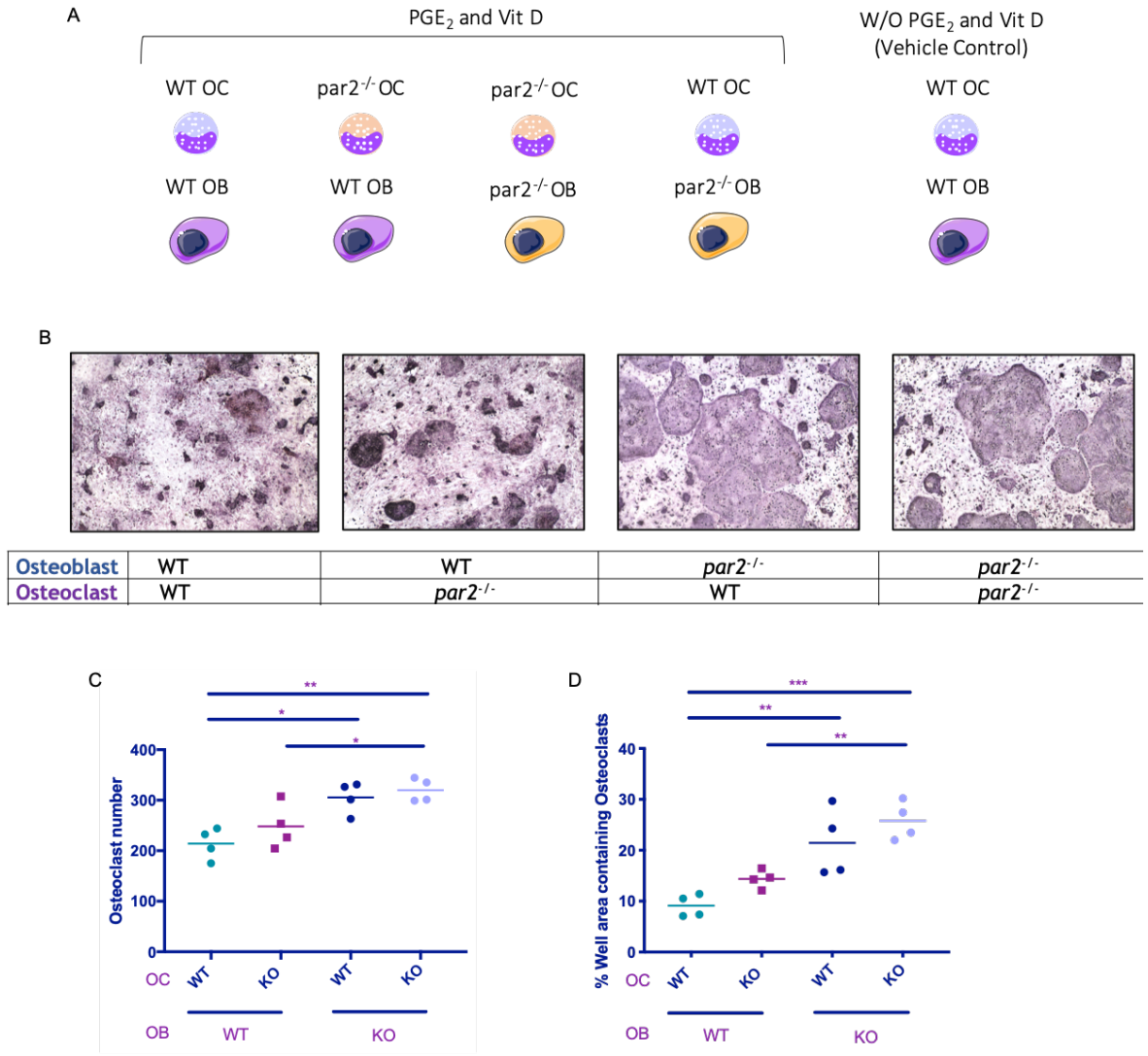

Figure 5.12 PAR2 Regulates OC Differentiation via OBs
Osteoblast like cells were digested from the calvaria of 3-5 day old pups of either WT or *par2*$^{-/-}$ genotype and expanded in culture. These were then plated in 96 well plates ($2.5x10^3$ cells/well) and co-cultured alongside monocytes isolated from adult BM from WT or *par2*$^{-/-}$ animals. (A) These culture combinations were arranged so the genotype of each cell type was cultured with each genotype of the other cell type. These cultures were stimulated with 1μM PGE_2 and 10nM VitD, or left unstimulated with vehicle control (ethanol 0.1%). Media was changed initially after 3 day and then subsequently every 2 days until osteoclasts were visible (8-10 days) and then fixed and TRAP stained. (B) Representative TRAP stain images for each genotype combination of the co-culture were taken at 10x magnification. (C) Quantification of osteoclast number for each condition was performed on images taken of the entire well. (D) Using ImageJ software, the area of each well which was covered by osteoclasts was calculated as a percentage of the total well area. (C and D) WT OB - WT OC (green), WT OB – KO OC (pink), KO OB – WT OC (blue), KO OB – KO OC (lilac). One-way ANOVA with Tukey's multiple comparisons test was used, p values represented as follows; * = p<0.05, ** = p<0.005, *** = p=0.0005. WT OB N=2, *par2*$^{-/-}$ OB N=2, WT OC N=2, *par2*$^{-/-}$ N=2. Representative of 2 experimental repeats.

The primary factors known to regulate OC generation by OBs are RANKL and OPG, as mentioned above. Since the *par2*$^{-/-}$ stroma appeared to have an enhanced capability of generating OC cells, transcript analysis of these 2 factors was conducted to identify any potential change in their expression with

genotype. This was conducted in RNA isolated from OB-like cells just before they would have been used for co culture; day 0 of the co-culture protocol. Using qPCR analysis of these transcripts, no change in either RANKL or OPG gene expression was identified between WT and *par2*$^{-/-}$ stromal cells (Figure 5.13). When the ratio of RANKL and OPG transcripts were analysed there was no significant change based on genotype, possibly due to large levels of variation.

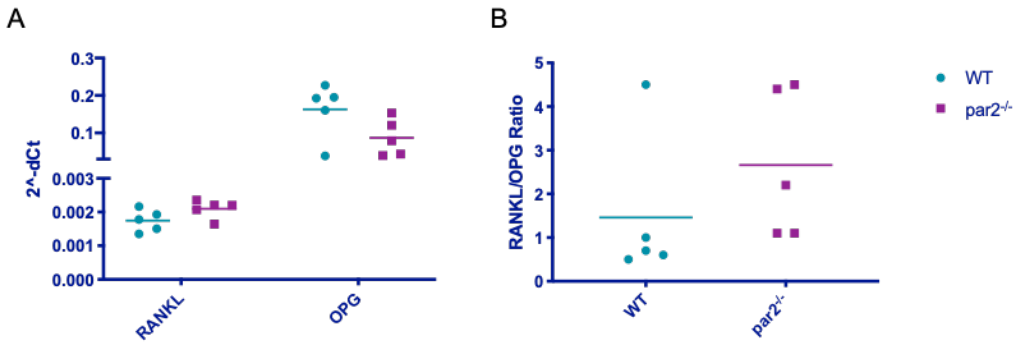

Figure 5.13 Freshly Isolated Calvarial OB-like cells from WT and *par2*$^{-/-}$ Do Not Have Significantly Differing Expression of OC Regulatory Factors RANKL and OPG.
Calvaria from 3-5 day old pups was digested for OB extraction and expanded in culture for 4 days prior to RNA isolation. (A) Transcript levels of RANKL and OPG were measured by qPCR and normalised to house-keeping gene *18s*. (B) The transcript level of RANKL was divided by OPG to measure the ratio of these genes. WT N=5, *par2*$^{-/-}$ N=5, no additional experimental repeats performed.

Osteoclastogenic factors are not highly expressed in naïve calvarial stromal OB-like cells. The expression of RANKL is driven over time with culture in stromal growth factors such as PGE_2 and VitD. Enhanced OC generation by *par2*$^{-/-}$ may be due to faster maturation of OB-like cells from *par2*$^{-/-}$ genotype, resulting in enhanced RANKL expression quicker than WT counterparts. To determine if maturation of OB-like stroma will impact enhanced OC generation of *par2*$^{-/-}$ OB, a pre-maturation stage was conducted prior to co-culture. OB maturation is commonly conducted with a combination of ascorbic acid (AA), dexamethasone (Dex), and glycerol-2-phosphate (βGP), in order to generate mineralising OBs. Two methods of pre maturation and osteoblast stimulation were compared, AA, Dex, and βGP (ABD), or the growth factor combination used previously, PGE_2 and VitD (PV) (Figure 5.12A). Calvarial stroma was expanded in 75cm tissue culture flasks for 5 days in growth factor free medium (as above) and then flasks were split and for each OB sample one flask was exposed to AA, Dex, and βGP, and the second flask was cultured in PGE_2 and VitD. Maturation was conducted for 8

days with media replaced every 3 days and cells split as and when required (Figure 5.14).

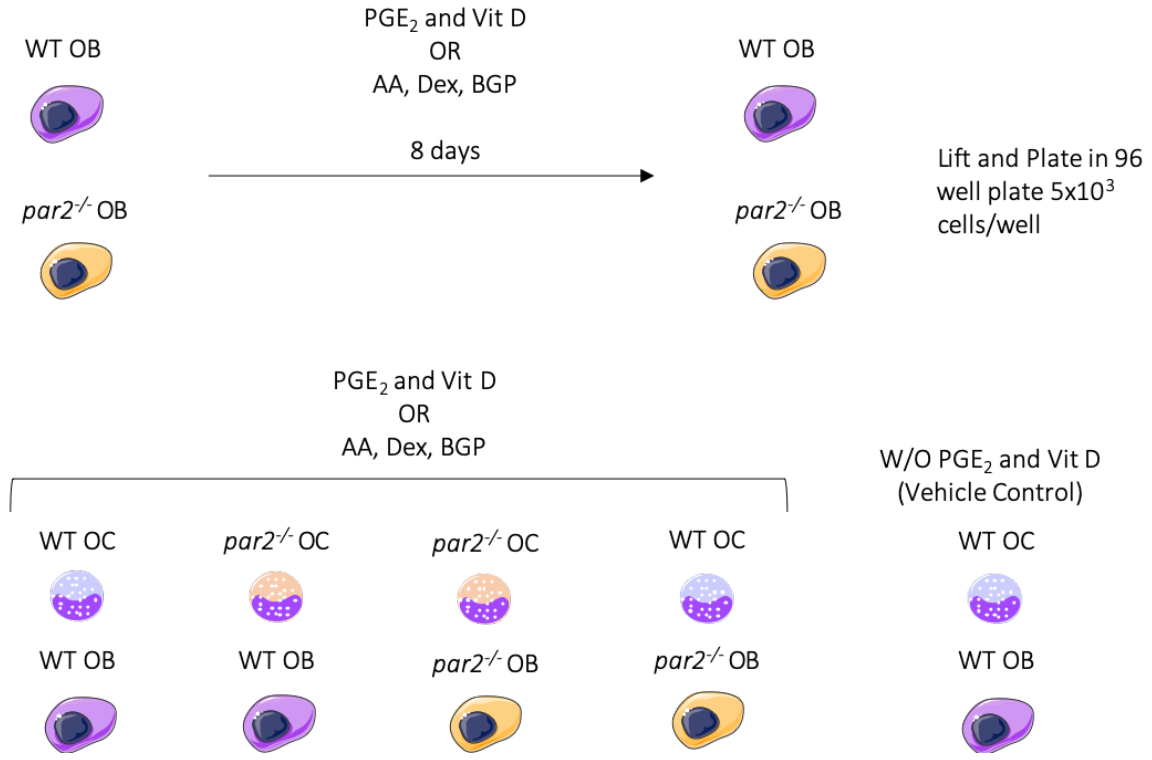

Figure 5.14 Additional Maturation of OB-like Cells was Conducted Before Co-culture. After calvarial OB digestion and expansion, OBs were then matured in a growth factor cocktail of 1μM PGE_2 and 10nM Vit D, or 100μM AA, 10nM Dex, and 2mM βGP, for 8 days. The co-culture was then conducted again with isolated BM monocytes from WT and *par2*$^{-/-}$. Growth factor cocktails that were used for maturation were maintained during co-culture.

In order to asses if the maturation enhanced RANKL transcript and assess whether either maturation protocol was more effective than the other, we again analysed transcript expression of these factors 3 days into maturation and after the 8 day maturation period. Transcripts were normalised to ABD WT cultures and fold change between genotypes and maturation protocols compared (Figure 5.15). Interestingly, maturation of stromal OB-like cells differed between the differentiation protocols. Transcript levels of OC stimulatory (RANKL gene, *tnfsf11)* and regulatory (OPG gene *tnfsf11b)* factors were analysed as a starting point to gauge OC stimulatory potential. Cells matured in PGE_2 and Vit D had higher expression levels of *tnfsf11* (RANKL) over cells cultured in AA, Dex, and βGP (Figure 5.15), on both day 3 (A) and day 5 (B) of the maturation protocol.

Transcript levels of *tnfsf11b* (OPG), on the other hand, remained fairly consistent across different protocols (Figure 5.15 A and B). This indicates PV cultures will have more available RANKL and thus a higher capacity to stimulate the generation of OC cells. The genotype of these cells did not influence their production of *tnfsf11* or *tnfsf11b* transcripts (Figure 5.15). However, only 2 biological replicates were matured with these protocols, so it is difficult to identify any potential differences, especially considering the level of variation between the samples.

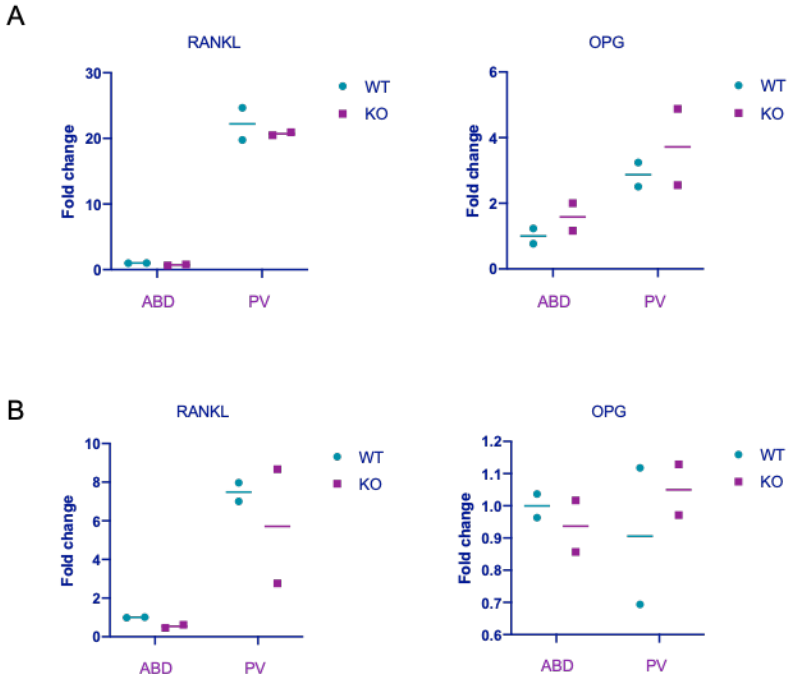

Figure 5.15 Maturation of OB-like cells in PGE_2 and Vit D Primes Cells for More Efficient OC Differentiation than AA, Dex, and βGP Maturation.
Calvarial OB-like stromal cells were matured in a growth factor cocktail of 1μM PGE_2 and 10nM VitD, or 100μM AA, 10nM Dex, and 2mM βGP for a total of 8 days prior to co-culture. RNA was isolated on (A) day 3 and (B) day 8 of maturation from both protocols and transcript analysis for RANKL (*tnfsf11*) and OPG (*tnfsf11b*) expression levels performed. Gene transcript was normalised to housekeeping gene 18s and fold change in transcript expression calculated over WT samples matured in AA, Dex, and βGP. N=2 for both WT and *par2*$^{-/-}$ samples, no additional experimental repeats performed.

After maturation, these cells were then co-cultured with monocytes in the same way as above. OBs which were matured in AA, Dex, and βGP were maintained in this growth factor combination throughout the co-culture (Figure 5.16C and D). When OCs were visible in this culture all plates were TRAP stained and quantification conducted as above. OBs which had been matured in PGE_2 and

VitD were more capable of generating OCs than AA, Dex, βGP matured, which can be seen in cell culture images and in cell number quantification (Figure 5.16A and C respectively). This is reflected in the quantification of OC activity/resorption, which was also higher in PV cultures (Figure 5.16 C and D). This was to be expected after detection of higher level of RANKL transcript levels in the OB-like cells from PGE_2 and VitD matured cultures (Figure 5.16).

As with the previous unmatured culture, in the PGE_2 and VitD matured OB cell culture, the double KO (both OC and OB) contained significantly more osteoclasts than double WT co-cultures. However, differences were not as pronounced as the non-matured OB cultures and there were no differences between any other cell combinations. OC activity measured in these cultures found no change in cellular activity in these assays between genotype combinations (Figure 5.16B and D), and when resorption levels were normalised to OC number no change in OC activity per cell was found (Figure 5.16E). This may be partially due to significant variation in osteoblast samples after maturation. No significant differences in OC number were found between genotype combinations in AA, Dex, and βGP cultures. This may be reflective of the limited osteoclastogenic potential of this protocol. While resorption activity appeared slightly increased when OC genotype was *par2*$^{-/-}$, this did not reach significance, and when resorption levels were normalised to OC number no change in OC activity per cell was found (Figure 5.16F). Again, the variability between samples and low osteoclastogenesis limited the interpretation of this assay.

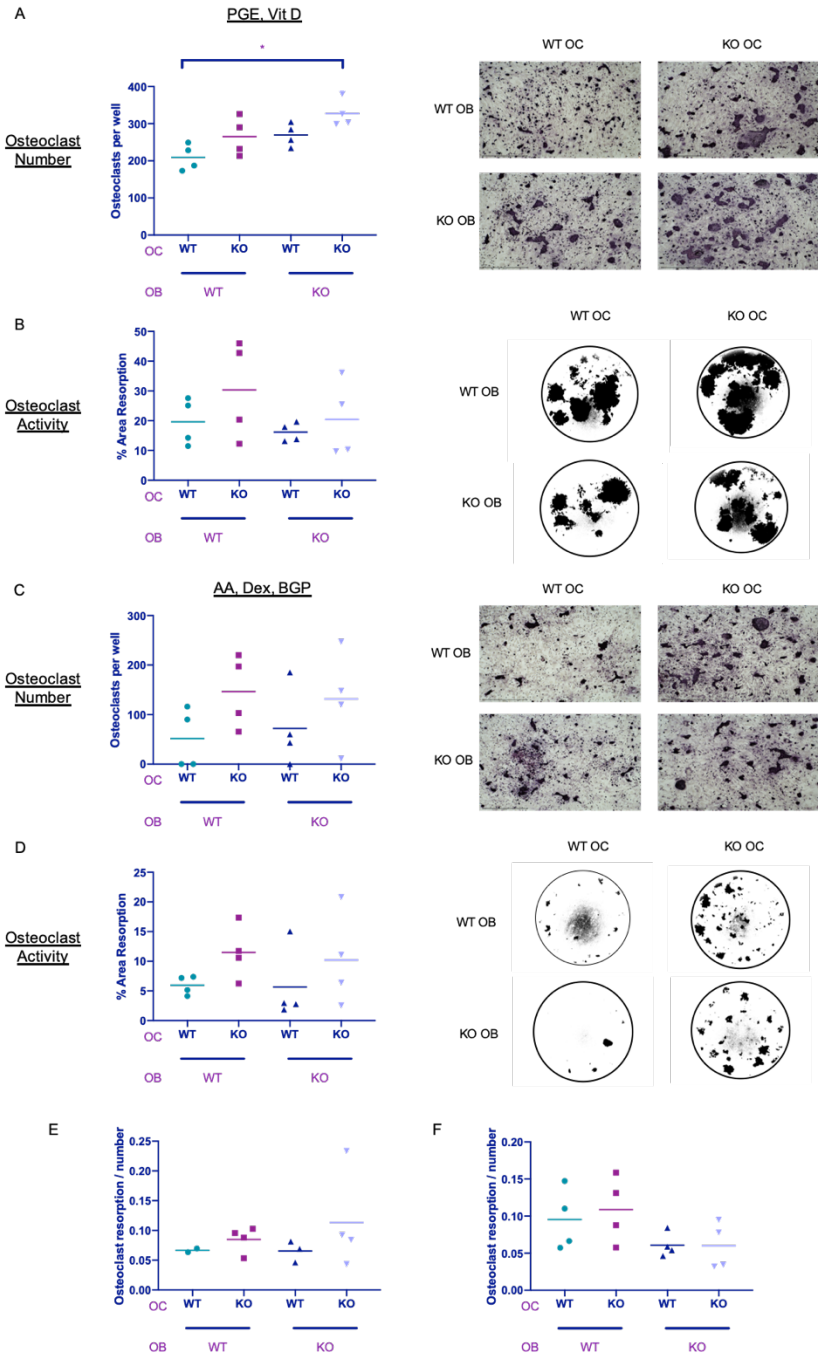

Figure 5.16 Osteoblast Maturation Limits the Potential for par2$^{-/-}$ Stroma to Enhance Osteoclast Differentiation.
OB-like cells were differentiated in (A, B) 1μM PGE_2 and 10nM VitD, or (C, D) 100μM AA, 10nM Dex, and 2mM β-GP, for 8 days and then co-cultured with BM monocytes from WT or *par2*$^{-/-}$ maintained in the same growth factor. (A, C) Cultures were fixed and TRAP stained after 10 days. Representative images of TRAP stained cultures (10x magnification) and quantification of OC numbers from all genotype combinations are shown for both (A) PGE, VitD and (C) AA, Dex, βGP cultures. (B, D) Representative images of cultures conducted on osteo-assay wells were bleached after 14 days to analyse resorptive activity of the culture. Images of osteo-assay plates were taken at 2x magnification and images were analysed on ImageJ software. The colour contrast between areas of resorbed mineral (black) and intact mineral (white) enable discrimination of these areas. The proportion of the total mineral area resorbed was calculated for both (B) PGE, VitD and (D) AA, Dex, βGP cultures. The levels of resorption were normalised by OC number for both (E) PGE, VitD and (D) AA, Dex, βGP cultures. One-way ANOVA with Tukey's multiple comparisons test was used, p values represented as follows; * = $p<0.05$. WT OB N=2, WT OC N=2, *par2*$^{-/-}$ OB N=2, *par2*$^{-/-}$ OC N=2. No additional experimental repeats performed.

To observe any potential changes in osteoblast maturation with the loss of PAR2, a time course of RNA transcript analysis was conducted across OB-like maturation in response to PGE_2 and VitD signals (Figure 5.17), or AA, Dex, and βGP (Figure 5.18). RNA was isolated from OB-like cell cultures on days 1, 3, 6, and 9 post culture in maturation media. A panel of osteoblast associated transcripts was analysed which included RANKL (*tnfsf11*), OPG (*tnfsf11b*), alkaline phosphate (ALP, *alpl*), osterix (*sp7*), osteocalcin (*bglap*), RunX2 (*runx2*), and osteopontin (OSP, *spp1*) (Figure 5.17 and Figure 5.18). Data represented as fold change over WT samples on day 1. There were no significant changes to the panel of OB-associated transcripts measured between WT or *par2*$^{-/-}$ for either method of maturation. However, there was an observational enhancement of OSP transcript with a loss of PAR2, in both PGE_2 and VitD maturation (Figure 5.17G), and AA, Dex, and βGP (Figure 5.18G) especially after 9 days of maturation. This change was not significant for PV maturation, and due to low sample number in AA, Dex, and βGP cultures (N=3 WT, N=2 *par2*$^{-/-}$), the statistical significance could not be assessed in this culture. With this observation analysis was then conducted with OB-like cells in these conditions with the addition of AZ8388 PAR2 inhibitor (Figure 5.17 H Figure 5.18 H). Once again this could indicate whether endogenous signals within the culture were driving the change in OSP. WT OB like cells in PV maturation media did not respond to PAR2 inhibition with any change in OSP transcription (Figure 5.17 H). This may indicate that in this environment OSP transcript is not directly regulated by PAR2 signals. However the inhibition duration was not throughout the culture period, only in the 4 hours prior to cell lysis. Therefore the OSP transcript may be regulated by PAR2 signals received prior to this 4 hour window. In contrast, WT OB-like cells matured in ABD maturation media did respond to short term PAR2 inhibition with AZ8388, increasing transcript levels over untreated WT counterparts (Figure 5.18 H). Again, statistical significance could not be assessed in these experiments due to low N numbers. Overall, this observation may be worth follow up as it could suggest a role for the PAR2 pathway in regulating the production of bone mineral components essential for OC adherence which includes OSP.

Thus far the data presented in this chapter demonstrates that during a homeostatic state, a loss of PAR2 in both the OC/myeloid cultures and in OB

stromal driven cultures results in excessive OC formation. The loss of this receptor increased both the size and number of OCs formed in these cultures. This data indicates that endogenous proteases are functioning in an autocrine or paracrine manner within the culture to act upon OCs or OBs to regulate pro-osteoclastogenic signals or responses.

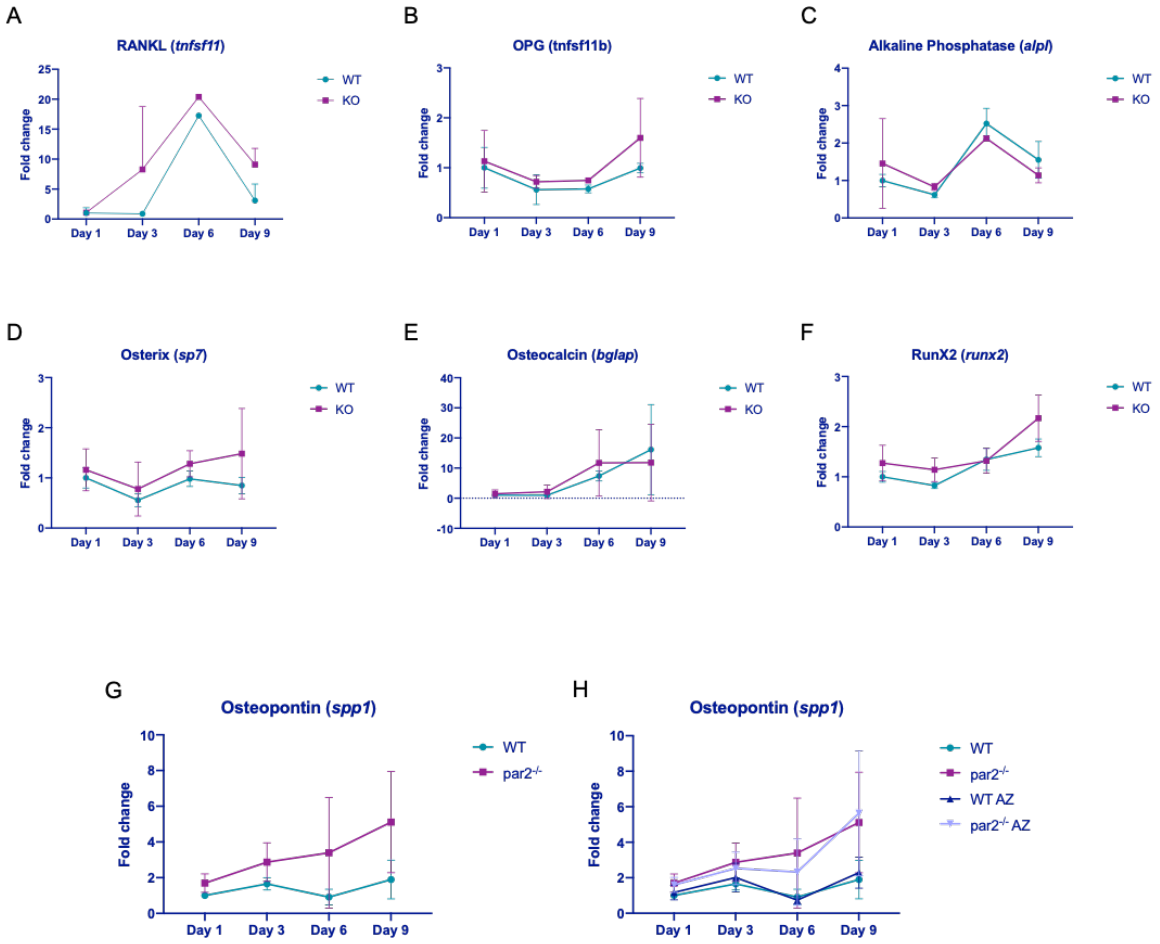

Figure 5.17 Loss of PAR2 does not Result in Significant Difference in OB Associated Gene Transcripts During Maturation of OB-like cells with PGE2 and VitD.
OB-like stromal cells isolated from the calvaria of WT and *par2*$^{-/-}$ animals were matured in 1μM PGE_2 and 10nM VitD for up to 9 days. RNA was extracted from cells on day 1, day 3, day 6, and day 9 post growth factor maturation initiation. Transcript analysis was conducted for OB associated genes, (A) *tnfs11*, (B) *tnfsf11b*, (C) *alpl*, (D) *sp7*, (E) *bglap*, (F) *runx2*, and (G) *spp1*, using qPCR methods. Gene expression was normalised to housekeeping gene 18s, and fold change calculated over WT samples on day 1. (H) Cells were also treated with or without AZ8838 4 hours prior to RNA isolation and these samples were further analysed for *spp1* transcript levels. N=4 WT and *par2*$^{-/-}$, no additional experimental repeats performed.

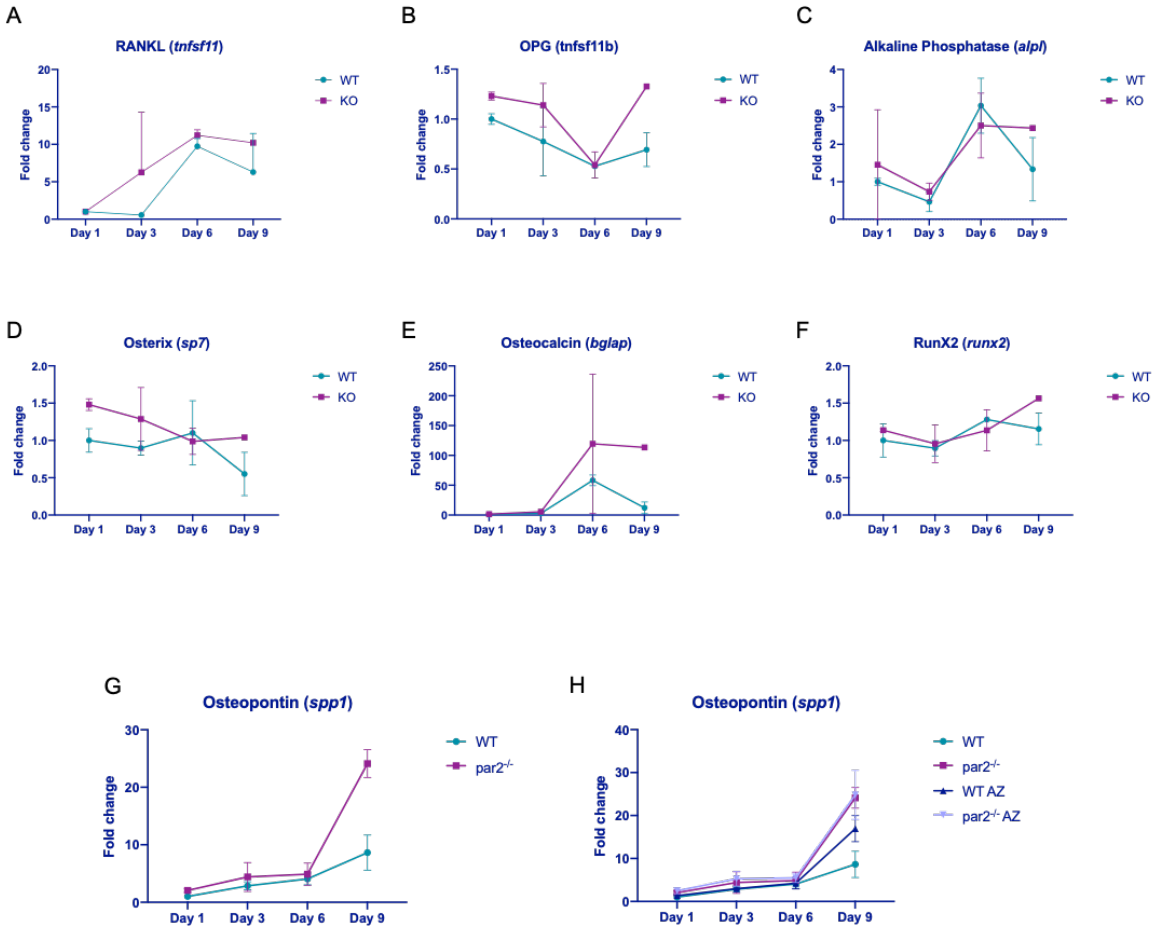

Figure 5.18 Loss of PAR2 does not Result in Significant Difference in OB Associated Gene Transcripts During Maturation of OB-like cells with AA, Dex, and βGP.
OB-like stromal cells isolated from the calvaria of WT and *par2*$^{-/-}$ animals were matured in 100μM AA, 10nM Dex, and 2mM β-GP for up to 9 days. RNA was extracted from cells on day 1, day 3, day 6, and day 9 post growth factor maturation initiation. Transcript analysis was conducted for OB associated genes, (A) *tnfs11*, (B) *tnfsf11b*, (C) *alpl*, (D) *sp7*, (E) *bglap*, (F) *runx2*, and (G) *spp1*, using qPCR methods. Gene expression was normalised to housekeeping gene 18s, and fold change calculated over WT samples on day 1. (H) Cells were also treated with or without AZ8838 for 4 hours prior to RNA isolation and these samples were further analysed for *spp1* transcript levels. N=3 WT, N=2 *par2*$^{-/-}$, no additional experimental repeats performed.

5.2.5 PAR2 Contributes to TNF Enhanced Osteoclastogenesis

The data shown in the previous sections indicate that PAR2 plays a regulatory role in preventing excessive osteoclastogenesis and the formation of giant OC cells under certain homeostatic conditions. PAR2 is known to have a role in inflammation, with reports of the receptor both enhancing inflammation but also contributing to resolution of inflammation. TNF is the central cytokine known to enhance RANKL induced osteoclastogenesis, especially in rheumatic conditions, but also in other bone disorders [360]. TNF has been shown to enhance RANKL induced OC differentiation from murine BM-derived precursors [46]. In addition, therapeutic blockade of TNF in RA patients shows marked reduction in bone erosion[361]. In order to assess the impact of PAR2 on the process of inflammatory enhanced osteoclastogenesis, NA-BM from WT and *par2*$^{-/-}$ animals were subjected to a TNF enhanced osteoclast differentiation protocol. There have been multiple publications involving this type of OC assay, but these all vary slightly. Therefore, optimisation of the TNF enhanced OC assay was performed to find the protocol that was most effective at enhancing OC differentiation.

In order to assess TNF enhanced osteoclastogenesis, a suboptimal concentration of RANKL should be used that does not result in overt osteoclastogenesis and allows enhancement to be easily observed. Reduced concentrations of RANKL including 1ng/ml and 10ng/ml were assessed in conjunction with M-CSF with NA BM cells. However, 1ng/ml of RANKL failed to generate any OCs (data not shown). Therefore 10ng/ml was taken forward for this culture in order to differentiate a reduced number of OCs for the detection of TNF enhancement without losing OC generation entirely. Optimisation of the concentration of TNF used and time point for addition to the culture was conducted on NA-BM from WT mice. Two concentrations of TNF were tested: 20ng/ml and 40ng/ml, as this was within the range of various concentrations reported for this purpose in the literature. While TNF is known to enhance osteoclastogenesis, if this cytokine is added into monocyte cultures too early it will instead inhibit osteoclastogenesis. This was first demonstrated by Lam and colleagues, who found that when TNF was added on the same day or the following day post RANKL exposure, osteoclastogenesis was completely inhibited. In comparison, if TNF is added on days 2 to 5 post RANKL addition there is enhanced osteoclast differentiation[46]. In light of this, addition of TNF to the cell cultures was assessed at 2 or 3 days post

RANKL exposure, which equates to day 4 or 5 of the culture (Figure 5.19A). Low numbers of osteoclasts were generated in reduced RANKL (10ng/ml) cultures as can be seen in the representative light microscopy images (Figure 5.19B), and quantification of OC numbers (Figure 5.19C). The protocol which generated the most consistent and highest increase in osteoclast number in response to TNF was 40ng/ml of TNF added on day 4 of the culture (Figure 5.19C). Therefore, this protocol was taken forward for comparison of WT and *par2*$^{-/-}$ BM.

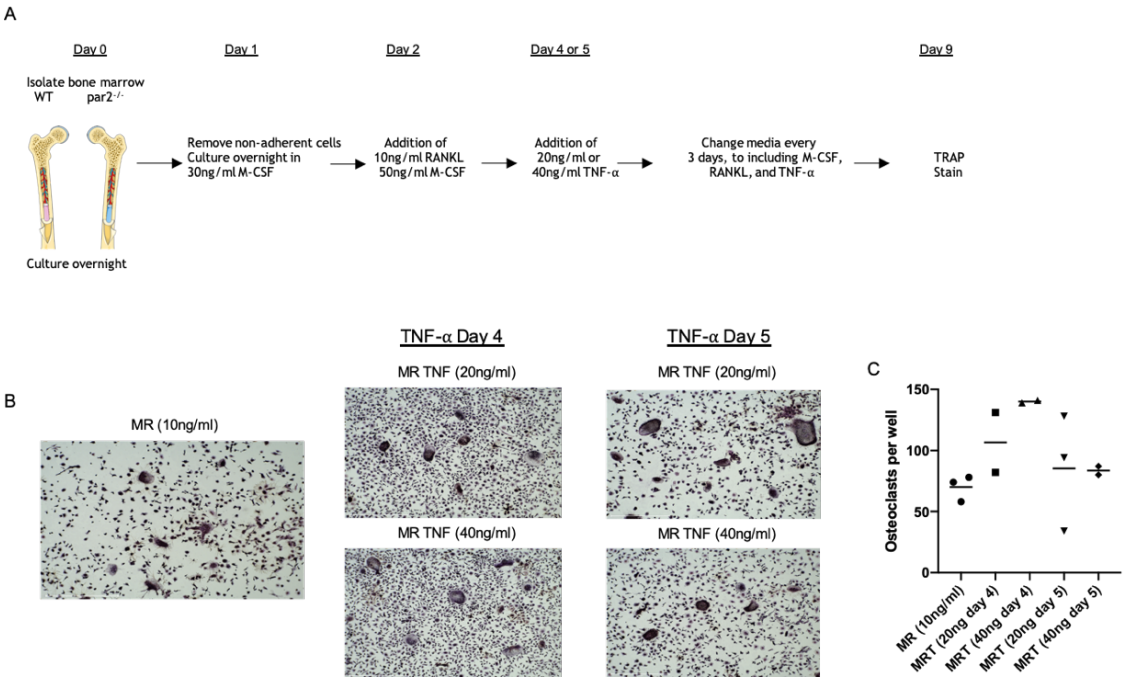

Figure 5.19 Optimisation of TNF Enhanced Osteoclastogenesis.
(A) BM was flushed from the long bones of adult WT and *par2*$^{-/-}$ mice and cultured overnight. The following day (Day 1) NA-BM was removed and cultured overnight in 30ng/ml M-CSF. On day 2 media was half changed to include 10ng/ml RANKL and 50ng/ml M-CSF. On days 4 or 5 of the protocol 20 or 40ng/ml of TNF was added to the cell culture. Media was half changed every 3 days maintaining the M-CSF, RANKL, and TNF cytokine concentrations until well were TRAP stained on day 9. (B) Representative TRAP images of negative control MR, and all possible TNF addition concentrations and time points. (C) Osteoclast numbers were quantified in all conditions; individual points reflect technical replicates of the same murine BM donor (N=1), no additional experimental repeats performed.

In WT and *par2*$^{-/-}$ cultures TRAP stain quantification of osteoclast number was conducted for both M-CSF and RANKL (MR) and M-CSF, RANKL, and TNF (MRT) conditions. Significant enhancement of osteoclast numbers upon TNF addition were found in both WT and *par2*$^{-/-}$ cultures (Figure 5.20A). However, the WT NA-BM had a higher induction of osteoclast formation upon TNF addition with 4-8 times more osteoclasts generated under inflammatory conditions. While *par2*$^{-/-}$

NA-BM only had an average of 2 fold increase in total osteoclast number in response to TNF addition (Figure 5.20B). Visually the TRAP stain images of WT cultures looked as though they contained more large OC cells, representative images shown in Figure 5.20C. In order to quantify this, osteoclasts were subdivided based on the number of nuclei they contain. The number of osteoclasts containing 11-15 nuclei (large OC cells) were significantly reduced in *par2*$^{-/-}$ cultures (Figure 5.20C). This data demonstrates that *par2*$^{-/-}$ BM-NA cells have a limited enhancement of OC formation in response to TNF, especially the formation of large OCs. This suggests that PAR2 partially drives enhanced OC formation during TNF osteoclastogenesis. The impact of PAR2 during inflammatory OC formation completely opposes the impact of this receptor during homeostasis (5.2.3). During homeostatic M-CSF and RANKL alone driven OC formation *par2*$^{-/-}$ cells generate increased numbers of OCs with more nuclei. Overall, this suggests that the mechanism of PAR2 in OC formation changes depending on the signals it is partnered with. How this receptor impacts these cultures differently, dependent on the inflammatory TNF signal is still elusive and merits further investigation.

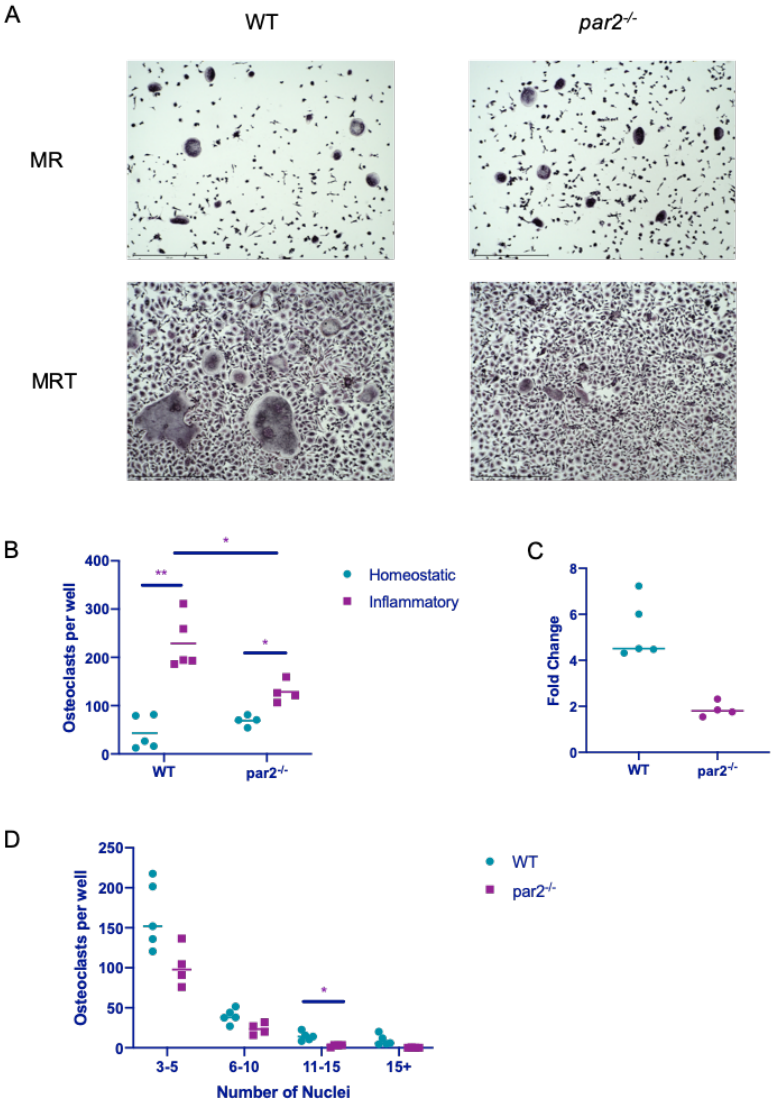

Figure 5.20 NA-BM from *par2*$^{-/-}$ has Limited TNF Enhanced Osteoclastogenic Potential. NA-BM from WT and *par2*$^{-/-}$ were exposed to TNF enhanced osteoclast differentiation protocol. (A) Representative images of TRAP stained cultures from both sub-optimal MR, and MRT TNF enhanced OC differentiation, taken at 10x magnification. (B) Quantification of OC numbers compare the reduced MR assay with the enhanced MRT for both WT and *par2*$^{-/-}$, with MR quantification points shown in blue and MRT shown in pink. (C) Fold change increase in osteoclast numbers with the addition of TNF to cultures over control MR was calculated, (D) OC quantification was further subdivided to separate larger and smaller OCs, grouping into 4 categories based on the number of nuclei present. The smallest osteoclasts counted had 3-5 nuclei, then a further group of 6-10, 11-15, and finally the largest cells were defined as more than 15 nuclei per cell. (C and D) WT data points in green and *par2*$^{-/-}$ in pink. Multiple T test were conducted with Holm-Sidak correction for multiple comparisons, adjusted p values as follows: * = $p<0.05$, ** = $p<0.005$. WT N=5, *par2*$^{-/-}$ N=4, no additional experimental repeats performed.

5.3 Discussion

Despite a known role for protease sensing via PAR2 in inflammation, the impact of a loss of this receptor on the bone marrow cellular compartments has not been reported. It has been suggested that the total number of BM cells is increased in PAR2 KO animals[76]. However, this finding has not been followed up and no subsequent analysis of the bone marrow components were performed. The central focus of this thesis is the role of the PAR2 pathway in cells from the monocytic lineage. Therefore, prior to investigation of the function of PAR2, potential changes to the BM monocyte compartment as a result of the knock out was investigated. Flow cytometry techniques were employed to analyse the frequency of monocytes and monocyte subsets in the BM compartment of WT and *par2*$^{-/-}$ animals (Figure 5.1). The frequency of monocytes and their subsequent populations (inflammatory, patrolling, and OCPs) were unchanged between genotypes (Figure 5.2). This suggests that PAR2 does not impact monocytic haematopoiesis, or retention of monocytes in the bone marrow under homeostatic conditions.

Interestingly, while analysing the cellular composition of the BM, the expression levels of CD11b – a cell surface protein used to identify monocyte populations - was enhanced in the patrolling subset of monocytes from *par2*$^{-/-}$ animals. CD11b is an integrin subunit also known as integrin αM that pairs with the β2 subunit also known as CD18, to form a complete integrin heterodimer. This integrin binds ligand ICAM-1 and this interaction is essential for monocyte cell adhesion and migration. ICAM-1 binds to all β2 associated integrins; CD11a/CD18, CD11b/CD18, CD11c/CD18, CD11d/CD18. Members of the β2 integrin family are crucial regulators of myeloid cell function, by directing cellular migration, the ability for cells to partake in cell-cell adhesion, as well as mediating-signalling cascades. While all of these subunits are expressed in myeloid cells including monocytes, macrophages and DCs, expression patterns change with each myeloid cell type. The CD11b subunit is the most highly expressed in monocytes, hence its use as a discriminatory marker for identifying monocytes via flow cytometry. CD11b is thought to be essential in mediating the migration of monocytes from the blood into tissue, through adhesion to endothelial cells. While it may be initially thought that this drives migration of monocytes to inflamed sites, it

appears that CD11a and b are dispensable in the recruitment of myeloid cells during inflammation. The role of these subunits is more important in homeostatic migration to tissues[1]. The enhanced expression of the CD11b subunit on patrolling monocytes in *par2*$^{-/-}$ is then of further interest. The primary function of these cells is adhesion and rolling on the endothelial surface monitoring endothelial function, as opposed to migrating into tissues upon inflammatory assault [24].

Total expression levels of integrins are not necessarily important in terms of their function. The activation status of integrins is essential for mediating their functions appropriately. Integrins in an inactive state have very low affinity to their ligands. However, upon activation integrin heterodimers change their conformation and their affinity to ligands increases significantly[362]. Despite increased expression levels of CD11b in *par2*$^{-/-}$ monocytes, there was no enhancement in *par2*$^{-/-}$ monocyte ICAM-1 binding capacity (Figure 5.6B). Essentially, isolated BM monocytes from *par2*$^{-/-}$ did not have enhanced ICAM-1 binding with PMA stimulation, nor did WT cells have any change in ICAM-1 binding over unstimulated conditions with FLIGRL PAR2 stimulation. Alternative forms of PAR2 activation with proteases were not tested, as the generated data suggests that while there is enhanced CD11b expression in *par2*$^{-/-}$ monocytes, this does not seem to translate to a functional outcome in this experimental setting. However, it is also of note that the observed enhancement of this protein was only found in patrolling monocytes, and the cell population used in these experiments were total BM monocytes. Patrolling monocytes make up around 20-30% of the total monocyte population and so it is possible that potentially enhanced binding of *par2*$^{-/-}$ patrolling monocytes was not observable using this assay. FACS sorting of these specific cells could have been conducted, however, the cell numbers were very low, and this would have required significantly more animals. Whether the observed enhancement in total surface levels of CD11b has any functional implications *in vitro* or *in vivo* is yet to be determined.

The PAR2 pathway has previously been associated with integrin expression, cellular adhesion, and migration in other cell types. *In vivo* work by Nathalie Vergnolle demonstrated that intra-peritoneal (IP) injection of PAR2 activating

peptides drove the recruitment of leukocytes to the peritoneal cavity[282]. Shaoheng He and colleagues found that trypsin stimulated mast cell accumulation via PAR2 and ICAM-1 driven mechanisms[363], while McDougall and colleagues showed PAR2 activation in the rat knee joint resulted in leukocyte rolling and adherence at the site[364]. In addition, *in vitro* activation of PAR2 in neutrophils drove enhanced migration within a 3D lattice, as well as the modulation in the expression of selectins and integrins, and stimulated chemokine production in these cells[365]. Furthermore, trypsin was shown to stimulate $\alpha5\beta1$ dependent adhesion of gastric carcinoma cells to fibronectin via PAR2[366]. Therefore, the data presented in this chapter is not the first recorded association between PAR2 and mechanisms of cellular adhesion, migration and integrin expression. This function of PAR2 signalling may contribute to some of the many observed phenotypes with the loss of PAR2; such as reduced inflammation in arthritis models[276], and reduced cancer cell migration and metastasis[367,368]. This mechanism could also play a role in processes which depend upon cell-cell interaction such as OCP fusion.

Previous work has suggested a role for the PAR2 pathway in bone remodelling[285], injury response[76], and bone related diseases[288]. As well as the conformation of PAR2 expression in human monocytes in chapter 4 (see section 4.2.2), an interesting link between monocyte integrin expression and the PAR2 pathway was presented in this chapter. The role of PAR2 in the differentiation of OCs was subsequently investigated. Under the standard M-CSF and RANKL driven *in vitro* OC differentiation assay, *par2*$^{-/-}$ NA-BM produced a significantly enhanced number of TRAP+, multinucleated OCs (Figure 5.8 A and B). Enhancement of the number of larger osteoclasts (more than 5 nuclei) was more significant than smaller osteoclasts of 3-5 nuclei (Figure 5.8C), indicating that OCPs from *par2*$^{-/-}$ BM are more likely to fuse to form giant OC cells as opposed to their WT counterparts. There was no significant enhancement in the overall activity of *par2*$^{-/-}$ OCs despite the significant enhancement in size and number of OC cells. This indicates that while there are more OCs formed, these large cells are in fact less active than their WT counterparts (Figure 5.8D and E). The *par2*$^{-/-}$ OC cultures have a more prominent enhanced fusion phenotype rather than an enhancement of all OC associated functions, suggesting that protease signalling via PAR2 prevents excessive fusion and the formation of giant OCs. Alternatively,

the duration of the culture was too long to identify differences in resorption between genotypes, WT cultures potentially caught up with the KOs. In order to confirm there were no differences in OC activity between genotypes it would be valuable to conduct a time-course of resorption osteoassay plates, which included earlier points in the culture.

The differences observed between these 2 genotypes without addition of proteases or peptides which activate PAR2, is somewhat surprising. This suggests that proteases are produced within the culture and act in an autocrine, or paracrine manner via PAR2 to regulate the formation of OCs in WT cultures. This form of regulation is thus lost in *par2*$^{-/-}$ cells. In order to test whether PAR2 activation within the culture drives this difference between genotypes, another NA-BM OC differentiation assay was set up, which included either PAR2 stimulation via FLIGRL (2μM) or PAR2 inhibition using AZ compound AZ8838 (Figure 5.11).

FLIGRL is a modified version of the original activating peptide SLIGRL, which mimics the tethered ligand sequence and binds to the 2nd extracellular loop of the receptor, inducing non-enzymatic activation. The furoylated derivative of the SLIGRL peptide developed by Hollenberg and colleagues[369] is a more metabolically stable activating peptide with significantly enhanced potency[370]. However, the specificity of these activating peptides has come into question when Eleanor Mackie and colleagues reported Ca^{2+} flux in *par2*$^{-/-}$ cells, in response to both SLIGRL and FLIGRL peptides, albeit attenuated in comparison to WT responses [371]. They established that the reduction in apoptotic osteoblasts (OBs), and the reduction in OB mineralisation observed with PAR2 activating peptide treatment was via a PAR2 independent mechanism, as the same effect was detected in *par2*$^{-/-}$ OBs. No scrambled peptide controls were applied in this study, so it is possible that the activating peptide contained contaminants (eg. lipopolysaccharides), which drove the non-PAR2 related responses. Despite this controversy, SLIGRL and FLIGRL remain the primary PAR2 agonists used in the literature and are the most cost effective agonists available. Keeping this in mind, since *par2*$^{-/-}$ cells were used in these assays, both WT and *par2*$^{-/-}$ cells could be treated with FLIGRL and the specificity of the observed effects for PAR2 determined by examination of *par2*$^{-/-}$ responses (Figure 5.11).

Previous PAR2 antagonists have often failed to fully antagonise the receptor. For example GB88 was traditionally used as a PAR2 antagonist, however it is now recognised as a biased agonist of PAR2 activity, inhibiting PAR2 induced calcium mobilisation but stimulating RhoA activation and ERK phosphorylation via PAR2[372]. New small molecules were developed by AstraZeneca to selectively inhibit the activity of PAR2 without causing any partial agonistic effects. The crystal structure of the receptor with both of these antagonists, including the AZ8838 used in this study, was published in 2017[373]. This antagonist has slow binding kinetics, with 1 hour incubation required for full inhibition. In this study we chose to use the inhibitor throughout the culture, with each media change containing AZ8838, to thus maintain continuous inhibition of the activity of PAR2 in this culture.

Addition of the PAR2 agonist FLIGRL (2μM) in the NA-BM OC differentiation cultures had no impact on the number of generated OCs in either WT or PAR2 KO cell cultures (Figure 5.11 B and D). If this mode of PAR2 activation within the OC assay culture resulted in the regulation of OC formation, we would expect a reduction in WT OC numbers with PAR2 activation. However, this was not the case. This suggests that either PAR2 activation in this culture system is at a maximum, which seems unlikely from endogenous protease production, or that "canonical" PAR2 activation is not driving the PAR2 mediated regulation of OC formation. Rather there could be alternative PAR2 activation which drives bias signalling (PAR2 bias signalling is fully reviewed in Chapter 1, section 1.4.2.1). Finally, it could indicate that PAR2 activation within the culture system is not what drives the differences, that pre-priming of cells *in vivo* is altered instead.

To determine the impact of PAR2 blockade on osteoclastogenesis, the PAR2 antagonist was used throughout the cell culture. This inhibition of PAR2 in WT cells did impact the number of osteoclasts formed (Figure 5.11C, and D). When WT cell cultures were treated with AZ8838 each murine donor had enhanced osteoclast numbers (Figure 5.11C), however, this enhancement did not reach statistical significance. Unlike untreated and FLIGRL treated WT cultures that contain significantly lower numbers of OC than *par2*$^{-/-}$ cells, WT cultures treated with AZ8838 no longer had significantly lower OC counts than *par2*$^{-/-}$ cell cultures. While the WT AZ8838 OC count was not significantly enhanced over

untreated WT cultures, PAR2 inhibition increased the OC number enough to no longer be significantly different from the KO culture. Therefore, this indicates that PAR2 activation is required within the cell culture to drive the regulation of OC formation. Thus, either maximal activation of PAR2 is occurring endogenously within these cell cultures, or a non-canonical PAR2 signal drives the regulation of OC formation observed.

The observation that addition of a PAR2 inhibitor in this assay drives increased OC formation also indicates that there is an endogenous activator of PAR2 present within BM OC cultures. A recent publication isolated the proteases released from murine BM-derived OCs and via mass spectrometry identified 42 proteases preferentially released by osteoclasts over macrophage cultures [287]. Of these isolated proteases, 2 were of the trypsin family (Try10, and 2210010C04Rik). While these proteases have not been tested for their ability to activate PAR2, it is possible that these trypsin family members could activate the receptor. The most highly detected protease was pro-thrombin, the inactive form of thrombin. While it was previously thought that PAR2 cannot be activated by thrombin, it is now recognised that at higher concentrations than required for PAR1, thrombin does activate PAR2[374]. In addition, this study also identified multiple cathepsins (a, b, and j), and MMPs (2, 8, 9, 12, 19) preferentially secreted by murine BM osteoclast cultures. While none of the reported proteases have been reported as PAR2 activators, new activating proteases are still being discovered and the potential for PAR2 activating protease production within murine BM OC cultures is entirely plausible. It is also of note that this paper only discloses proteases released by BM OC cultures not found in BM macrophage cultures; it is eminently possible that PAR2 activating proteases are released by both cell types but this was not discussed in the publication.

The experimental work utilising PAR2 inhibitors therefore indicates that PAR2 signalling does regulate OC formation and during *in vitro* OC cultures a source of PAR2 activating proteases is produced endogenously, stimulating that regulation. Overall, this suggests a regulatory role for non-canonical PAR2 driven G-protein coupled receptor signalling in the regulation of OC formation. This is not the first occasion where G protein coupled receptor signalling has been attributed to the regulation of osteoclastogenesis, and limiting OC formation. A regulatory

function of G protein signalling via Gα13 was recently identified, which controlled and prevented excessive OC generation[375]. Using conditional Gα13 knock out animals, it was identified that the loss of this signal *in vitro* resulted in a significant enhancement in osteoclast size, an observation mirrored in *par2*$^{-/-}$ OC cultures (Figure 5.8). An enhanced number and size of osteoclasts *in vivo* was also observed in the Gα13 conditional KOs. Further investigation of this phenotype showed osteoclast associated gene expression differences between WT and Gα13 KO cultures were only found in late stage OC development genes such as cathepsin K, TRAP, and DC-STAMP, and the enhancement of these genes were only found after 3-5 days of RANKL exposure. Interestingly Gα13 KO cells also had enhanced expression of integrin β3, and faster adhesion and f-actin ring formation than WT comparators, suggesting a role for this signal in regulating the adhesion of OCs. All of these phenotypes were observed without the addition of any activators of G protein coupled receptors to the culture indicating a potential endogenous activator, also similar to the observations made in *par2*$^{-/-}$ assays. No specific G protein coupled receptor was proposed as the driver of this regulatory signal by the authors, and none of the G protein coupled receptors associated with OC function that they tested contributed to this phenotype, including GPR103, EBI2, GPR68, GPR55.

Interestingly the phenotype observed in the Gα13 conditional KO discussed above has some striking similarities with those observed in *par2*$^{-/-}$ cultures. Enhancement of OC associated transcripts were only observed at later time points of differentiation (Figure 5.9 and Figure 5.10), and the most significant feature of our enhanced OC phenotype is the observed larger size of these cells (Figure 5.8C). In addition, observed differences in *par2*$^{-/-}$ BM monocyte integrin expression in CD11b also indicates potential roles for this receptor in driving or limiting cellular adhesion (Figure 5.3 and Figure 5.4). PAR2 is known to signal via multiple Gα subunits including Gαq, Gαs, and Gα12/13, and it is now recognised that the method of activation of this receptor can influence the signalling route taken (PAR2 signalling and bias signalling reviewed in detail in Chapter 1, see sections 1.4.2 and 1.4.2.1). For example, neutrophil elastase cleavage of the N terminus, at an alternative site from canonical trypsin cleavage, is known to induce Gα13 activation and ERK phosphorylation but does not induce Ca^{2+} flux, unlike canonical activation. Drivers of alternate, or selective signalling of PAR2

may be a source of the Gα13 signal in this culture, that control OC formation and prevention of giant OC formation. For the above reasons PAR2 should be considered as one of the potential G protein coupled receptors responsible for this regulatory Gα13 signal.

In the last 20 years, our understanding of the complexity of G-protein coupled receptors has been extended to include new modes of activity such as internal G protein coupled receptor signalling[376]. G-protein coupled receptors activated at the plasma membrane can signal via β-arrestin during endosomal internalisation. In addition to this form of intracellular signalling, it is now appreciated that G-protein coupled receptors can also reside on intercellular organelles such as the mitochondria[377], the endoplasmic reticulum[378], and lysosomes[379], and are able to be activated from these intracellular compartments to initiate signalling. There have been no reports of intracellular activation of PAR receptors in the literature, however, there have been many reports of intracellular stores of PAR2, including the intracellular staining in healthy human monocytes reported in Chapter 4 of this thesis (Figure 4.4C). It may be possible that the intracellular stores observed could be functionally responding to intracellular protease activity. This could be a further alternative reason as to why small molecule inhibitor AZ8838 impacted cell cultures and activating peptide FLIGRL did not. Small molecules such as this inhibitor would be capable of diffusing into the cell while peptides such as FLIGRL would only be expected to have cell surface activity unless endocytosed.

In addition to protease signalling via PAR2, sensing of proteases via the PAR1 receptor has recently been shown to have a regulatory role in controlling osteoclast differentiation[380]. Osteoclasts generated *in vitro* from *par1*$^{-/-}$ murine BM have a similar phenotype to that found in *par2*$^{-/-}$ cultures, with enhanced number and crucially enhanced size of OCs. Paired with the increase in OC differentiation found with the loss of PAR2, this indicates a potential role for protease signalling and the PAR family of receptors in the regulation of OC formation. The authors of this study found that during TNF driven inflammatory osteoclastogenesis, a loss of PAR1 resulted in further enhancement of OC differentiation. This was demonstrated *in vivo* with a TNF induced calvarial bone erosion model. In addition, TNF driven OC differentiation was shown to have a

direct impact on *par1*$^{-/-}$ BM OC cultures *in vitro*, with addition of this osteoclastogenic cytokine giving rise to even further enhancement of *par1*$^{-/-}$ OC formation *in vitro*.

To identify whether the mechanisms driving PAR2 regulation of OC formation were similar to those in PAR1, the effect of a loss of PAR2 in inflammatory TNF enhanced OC differentiation was investigated. A TNF enhanced murine OC differentiation assay was optimised (Figure 5.19), similar to that applied to PAR1 KO cultures. However, unlike the further enhancement of OC size and number found with the loss of PAR1 in this inflammatory system, a loss of PAR2 resulted in significantly limited TNF enhancement of osteoclast numbers (Figure 5.20 A and B). While WT cell cultures had 4 to 6 fold enhancement of osteoclast formation with the addition of TNF, *par2*$^{-/-}$ BM was limited to 2 fold (Figure 5.20 C). Interestingly, when osteoclasts were counted based on number of nuclei in order to determine changes to OC size, *par2*$^{-/-}$ cultures contained significantly reduced numbers of larger OCs (11-15 nuclei), compared to WT counterparts (Figure 5.20 D).

This data suggests that PAR2 signalling contributes to TNF enhancement of OC differentiation, with opposing functions to PAR1 during *in vitro* inflammatory OC formation. While protease signalling appears to be an important regulator of OC formation via multiple receptors, different PARs are most likely driving different mechanisms of OC regulation. The study conducted with *par1*$^{-/-}$ animals determined that in this knock out the enhanced OC phenotype was driven by enhanced notch 2 activity. Thus, PAR1 serves to limit exacerbated OC differentiation by preventing excessive notch 2 activity. We do not show a mechanistic connection between PAR2 signalling and OC differentiation. However, since there are such opposing effects during TNF enhanced OC generation, it is likely that the driving mechanism between PAR2 and OC regulation will be different during inflammation. Multiple factors could be at play during TNF stimulated OC enhancement which could influence and alter PAR2 signalling, driving an alternate response.

It should be noted that PAR2 having opposing roles to PAR1 during inflammation is not surprising. PAR2 has an established role in inflammation and is reported to impact multiple inflammatory disease models and human diseases. PAR2 may

have a more significant role during inflammation as its activity is driven by proteases which are commonly released from active immune cells, whereas the primary activators of PAR1 are more highly associated with blood clotting. PAR1 may therefore play a more significant role in tissue injury response and repair, while PAR2 responds more heavily to inflammatory and infectious agents.

The NA-BM assays are valuable as a basic method for assessing M-CSF and RANKL driven OC formation. Overnight adherence of total BM cells before taking the NA fraction is conducted in order to limit the stromal contamination of this culture. However, OCPs have not been specifically selected or sorted and thus this is still a mixed culture system which could potentially contain other non-osteoclastogenic NA cells or even some adherent cells which have not fully bound to the plastic yet. Therefore in this setting, the contribution of other cell types (stromal, or other immune cells) is not fully known and cannot be dissected. In order to specifically test the role of PAR2 in OC formation in both the monocyte compartment and the potential stromal impact, a co-culture system of calvaria osteoblasts and BM isolated monocytes was used (Figure 5.12A). The role of PAR2 in stromal regulation of OC generation has been more extensively explored than the role of PAR2 in the monocyte/OCP compartment in the bone remodelling literature. Previous work identified PAR2 activation via activating peptides inhibited OB driven osteoclastogenesis in a co-culture assay [75]. In our co-culture system we found that *par2*$^{-/-}$ OBs had a higher potential for stimulating OC differentiation, in both non-differentiated calvarial OB-like cells (Figure 5.12), and to a lesser extent 8 day differentiated calvarial OB-like cells (Figure 5.16). This data appears to support the previous work of Smith and colleagues suggesting a regulatory role for PAR2 in preventing excessive osteoclastogenesis.

Smith and colleagues proposed that PAR2 activation limited the production of RANKL by OBs, as shown by a reduction in transcript levels of *tnfsf11*. This was the proposed mechanism of PAR2 mediated regulation of OC differentiation. The data presented in this chapter also supports a regulatory role for PAR2 in homeostatic OC formation. However, an enhanced *tnfsf11* expression was not found in *par2*$^{-/-}$ OBs, and therefore the data does not support the hypothesis that this regulation is through PAR2 driven RANKL reduction. Freshly isolated OB-like

calvarial cells from WT and *par2*$^{-/-}$ did not have any alteration in *tnfsf11* or *tnfsf11b* expression with a loss of PAR2. There was also no difference in cells which had undergone 8 days of growth factor maturation prior to co-cultures, where investigation of the transcript levels of *tnfsf11* and *tnfsf11b* were conducted on day 8 just prior to co-culture (Figure 5.16). In addition to analysis of OB transcripts just prior to addition to co-culture, a time course of OB-like cell maturation in the presence of growth factors and PAR2 inhibitor (AZ8838) was also conducted for further transcript analysis of OB associated transcripts (Figure 5.17 and Figure 5.18). No change in the expression of OB associated transcripts for RANKL (*tnfsf11)*, OPG (*tnfsf11b)*, RunX2 (*runx2*), osteocalcin (*bglap*), osterix (*sp7*), or ALP (*alpl*) expression between WT and *par2*$^{-/-}$ was found with either maturation protocol (Figure 5.17 and Figure 5.18). However, *par2*$^{-/-}$ OB-like cells had an observable increase in osteopontin (*spp1*) transcript levels over WT comparators. The observed differences did not reach significance in PGE_2, Vit D matured cells, and due to limited sample number of *par2*$^{-/-}$ cells matured with AA, Dex, and βGP (N=2) statistical testing could not be performed on this group. Addition of AZ8838 PAR2 inhibitor for 4 hours prior to RNA lysis also increased the expression levels of spp1 in AA, Dex, and βGP matured WT OB-like cells to almost the observed levels of the *par2*$^{-/-}$, indicating PAR2 activity during the culture was responsible for the reduced *spp1* levels in WT cells. However, there was no change in *spp1* levels in WT cells matured in PGE_2 and Vit D with AZ8838, so that is most likely not the case during PGE_2 and Vit D differentiation.

Osteopontin (OSP) is a key non-collagenous component of the bone matrix that is highly expressed by osteoblasts and an essential mediator of OC adhesion to the bone matrix[381] via interactions with integrin αVβ3. Its role in bone remodelling and OC function is fully explored in section 1.2.3 and 1.2.4 of this thesis. In brief, OSP mediated adhesion of OCs is essential in the formation of a ruffled border, which mediates the enables active resorption. In addition to adhesion and OC activity, OSP also drives the migration of OCPs and OCs[382]. The enhanced expression of this bone matrix component in *par2*$^{-/-}$ OB-like cells may be one method by which these cells drive the enhanced OC formation observed in co-cultures (Figure 5.12 and Figure 5.16). Elevated expression of OSP in *par2*$^{-/-}$ OB is likely to enhance the osteoclastogenic potential of the environment. One

observed phenotype of OC cultured with *par2*$^{-/-}$ OB-like cells again was their enhanced size (Figure 5.12D). Migration of OCPs is crucial for fusion of cells and formation of OCs. An enhanced expression of this glycoprotein mediating the migration of OCPs could encourage enhanced fusion of cells in OB-like *par2*$^{-/-}$ cultures. This could be mediated by potentially bringing them closer together and providing osteoclastogenic signals via OC associated integrins such as $\alpha V\beta 3$. In addition, as mentioned above binding of $\alpha V\beta 3$ to ligands such as OSP is an essential step in mediating the formation of the OC ruffle border, which is required to enable directional secretion of acids to perform erosion of the bone mineral below. In *par2*$^{-/-}$ OB cultures an enhanced resorption capacity was also detected (Figure 5.16). The increased OSP produced may also encourage increased activity of OC, an observation not made when OCs were cultured alone (Figure 5.8). Thus, not only is this matrix protein responsible for the migration and cellular adhesion of OCs but is required for them to fulfil their resorption functions adequately. Therefore an enhanced expression of OSP in these cultures may have been mediating the increased OC formation and activity.

An interesting connection between OSP and PAR2 is that they can both be cleaved by serine proteases for functional purposes. Both non-cleaved and cleaved forms of this protein are functional. Cleavage of OSP somewhat alters the functional responses of OSP as it disrupts the RGD domain, which drives interaction with conventional RGD binding integrins for example OC associated $\alpha V\beta 3$. In doing so, OSP gains the ability to bind many non-RGD dependent integrins such as $\alpha 4$ containing integrin heterodimers [383]. Serine protease cleavage of full length OSP results in 2 functional proteins – OSP N-terminus, and OSP C-terminus. Previous studies have shown that full length OSP is capable of binding multinucleated TRAP positive OCs to mediate their function. However, the cleaved portions of this glycoprotein mediate their function via mononuclear pre-OCs binding via non-RGD-dependent integrin $\alpha 4$[384].

Analysis of OB-like cells was conducted on pure stromal cultures, where RNA was isolated from these cells and transcript analysis for OC stimulating factors conducted. This was done to prevent contamination of other cell transcripts in our analysis, such as monocytes that may be present in a co-culture. However, this means that OB activity and behaviour which will be influenced by their

interaction with OCs would not be detected. It is possible that some OB PAR2 activity may have been dependent upon monocyte or osteoclast protease production, and without the interaction of these cells the impact of a loss of PAR2 may not be evident. As discussed above, osteoclast cultures are a source of active proteases and these can function not only in an autocrine manner but also in a paracrine manner to activate PAR receptors in OB-like cells. Smith and colleagues conducted transcript analysis on mixed whole bone marrow cultures fed with OB stimulatory factors such as IL-11, parathyroid hormone (PTH), and Vit D, so the analysis conducted would factor in all cellular interactions and their influence. By maintaining purity in our transcript analysis, we may have missed the potential influence of OB/OC interactions which occur in the co-culture and possible PAR2 influences dependent upon the presence and interaction with OCs.

5.4 Conclusions

From the data presented in this chapter it has been determined that protease signalling via PAR2 plays differential roles in monocyte maturation into OCs, which is dependent upon their environment. Under homeostatic OC cell culture conditions PAR2 prevents excessive OC formation. This effect is the result of active PAR2 signalling within the culture, as shown through a loss of significant differences between WT and *par2*$^{-/-}$ cells when WT cultures are maintained with PAR2 inhibitors (AZ8838). However, external activation of PAR2 via activating peptide (FLIGRL) does not drive these differences further. This suggests either endogenous proteases maximally activate available PAR2 receptors, a potential role for internal signalling, or bias signalling driving the phenotype in this culture system.

An observed increase in OC size, paired with increased expression of integrin subunits and enhanced production of OSP by stromal compartments all in *par2*$^{-/-}$ cells appears to indicate a role for PAR2 in cellular migration, adhesion, and thus fusion, as the driving mechanisms resulting in enhanced OC formation. In addition, a failure to observe significantly enhanced resorptive activity in the *par2*$^{-/-}$ OC cultures also indicates this phenotype is more predominantly cellular fusion.

In addition to PAR2 signalling directly regulating OC formation, it was also determined from mix-match genotype co-culture of OC and OB-like stromal cells, that PAR2 signalling plays a regulatory role in the formation of OCs via the stromal compartment. The role of PAR2 signalling in OB and how this regulates OC formation has been briefly explored in the literature. The mechanism proposed by Smith and colleagues was that PAR2 regulated OC formation via OBs by through limiting transcription of *tnfsf11* (RANKL). However, no alteration in *tnfsf11* transcript was observed between WT and *par2*$^{-/-}$ OB-like cells in the experiments presented in this chapter. In turn, the data presented here suggests an alternative mechanism, perhaps PAR2 signals in OBs limiting OSP production, which in turn would limit OC adhesion and migratory capacity. However, this proposed hypothesis requires further testing to be confirmed.

Finally, while under TNF stimulated osteoclastogenesis the impact of a loss of PAR2 results in an opposing phenotype, indicating that protease signalling via PAR2 contributes to TNF enhanced OC formation. The mechanisms by which PAR2 drives an alternate response during an inflammatory setting is not understood. The surrounding environment could have many potential impacts on PAR2 function and could include alterations to endogenous proteases produced or available, or changes to receptor heterodimers. Due to time limitations this was not explored within this system, but it would be of interest to further investigate the changing role of PAR2 in OC formation in health vs disease.

6 Functional Role of PAR2 in Primary Human Monocytes

6.1 Introduction

Thus far the literature concerning PAR2s role in osteoclastogenesis and bone has been focused entirely on murine systems and no work has been conducted in human OCs. The murine studies have been contradictory in their conclusions, with one study implying PAR2 plays an enhancing role in osteoclast formation[76] and another demonstrating and inhibitory role[75]. In the previous chapter the role of PAR2 in osteoclast formation was explored utilising *par2*$^{-/-}$ animals. By applying a total knock out murine system the crude biology could be interrogated to clarify the role of this receptor in OC biology. In addition, substantial variation in the levels of PAR2 surface membrane expression within the human population were observed (Figure 4.4E) and thus immediately testing the function of this receptor in a population of primary human monocytes may have been limited by a variable response in the general population. The experiments presented in chapter 5 suggested that protease signalling via PAR2 in routine M-CSF and RANKL-driven OC culture assays limited OC formation and prevent excessive fusion and formation of giant OC cells. However, during inflammatory enhanced OC differentiation driven by M-CSF, RANKL, and TNF, PAR2 appeared to contribute to the TNF-driven enhanced OC formation, with the KO cells displaying limited OC enhancement under TNF-driven conditions. Overall this data demonstrated divergent roles for this receptor, which are dependent upon the surrounding environment and partnering signals received.

While murine systems such as this can provide us with valuable insights to the basic underlying biology of PAR2 in OC formation, it is not a perfect system. Often observations discovered in murine systems do not directly translate to human biology. In order to confirm the relevance of protease signalling via PAR2 in human biology this chapter explores the role of PAR2 in human peripheral blood monocyte differentiation into OCs. To do so, PAR2 activating peptides and inhibitors were used in human OC differentiation cultures.

In addition to observations made regarding OC formation, *par2*$^{-/-}$ BM cells also had altered expression levels of monocyte associated integrin CD11b. This data

indicated a potential function of PAR2 in mediating cellular adhesion in monocytes. These 2 observations may be connected, suggesting that PAR2 could drive or inhibit monocyte adhesion in order to mediate migration or cell fusion.

Overall this chapter is aimed at translating findings from previous chapters (conducted in *par2*$^{-/-}$ animals), to *in vitro* primary human monocytes. In doing so, these experiments confirm or refute the relevance of the PAR2 functions observed in mice, in a human system. The aims of this chapter are:

To investigate the role of PAR2 in human monocyte function and osteoclastogenesis.

1. Using flow cytometric approaches to investigate PAR2 activation/inhibition and monocyte integrin expression and adhesion potential

2. Utilising PAR2 activating peptides and PAR2 antagonists in human osteoclast generation protocols.

6.2 Results

6.2.1 PAR2 Signals via MAPKinase in Human Monocytes

To demonstrate that PAR2 detected on human monocytes (by the D61D5 antibody) was functionally active, PBMCs were stimulated with PAR2 activating peptide. Notably, in other cell types stimulation of PAR2 with either activating peptide or receptor cleavage via trypsin, resulted in activation of the MAPKinase pathway and thus ERK phosphorylation [231,385-387]. Phosphorylation of ERK was therefore used as a surrogate for the detection of PAR2 activation. PAR2 stimulation experiments were conducted using activating peptide (FLIGRL, 2μM) in total PBMC populations, stimulating for a time course of 2, 5, 15, 30, 60, or 90 minutes, using a 15 minute stimulation with 100nM of PMA as a positive control for ERK phosphorylation. The total PBMC population was lysed for protein extraction with RIPA buffer and proteins were separated by molecular weight by means of gel electrophoresis and transferred to a membrane for western blotting. Membrane was blotted for p-ERK and total ERK to check sample loading (Figure 6.1A). Visual analysis of the western blot confirmed that PMA stimulation resulted in high levels of ERK phosphorylation; thick dark bands on the membrane at 40-45kDa weight with anti-pERK staining (Figure 6.1A). In addition, a signal for pERK was detected at 2, 5, 15 and 30 minutes post FLIGRL stimulation, which returns to baseline levels by 60 minutes (Figure 6.1A). Quantification of the intensity of the detected bands was calculated on ImageJ and p-ERK was normalised to the total ERK loading control (Figure 6.1A). Relative p-ERK levels demonstrated that peak phosphorylation was observed 5 minutes post-stimulation (Figure 6.1B). This data confirmed that within a total PBMC population a proportion of cells were responding to PAR2 activation via activation of the MAPKinase signalling pathway.

In order to specifically show this phosphorylation event in monocytes, the same PAR2 stimulation experiment was repeated in a total PBMC population. Instead of generating total protein lysates, these cells were processed for phospho-flow cytometric analysis of p-ERK. This technique enabled staining for cell surface markers in conjunction with the protein of interest and thus enabled identification of cell populations whilst simultaneously detecting intracellular p-ERK. Cells were gated to exclude doublets and then gated on $CD14^{+}$ monocytes

and expression of p-ERK analysed, compared to a secondary only stained control, for each timepoint (Figure 6.1C). The ΔMFI was calculated by subtracting the control stain from the p-ERK stain (Figure 6.1D). From this experiment it was clear that the monocyte population responded to PAR2 stimulation, resulting in phosphorylation of ERK and activation of the MAPKinase signalling pathway. This confirmed that the PAR2 expression detected in human monocytes via flow cytometry (Figure 4.4) was functional and can be activated via conventional activating peptide (FLIGRL) to initiate MAPkinase signalling events.

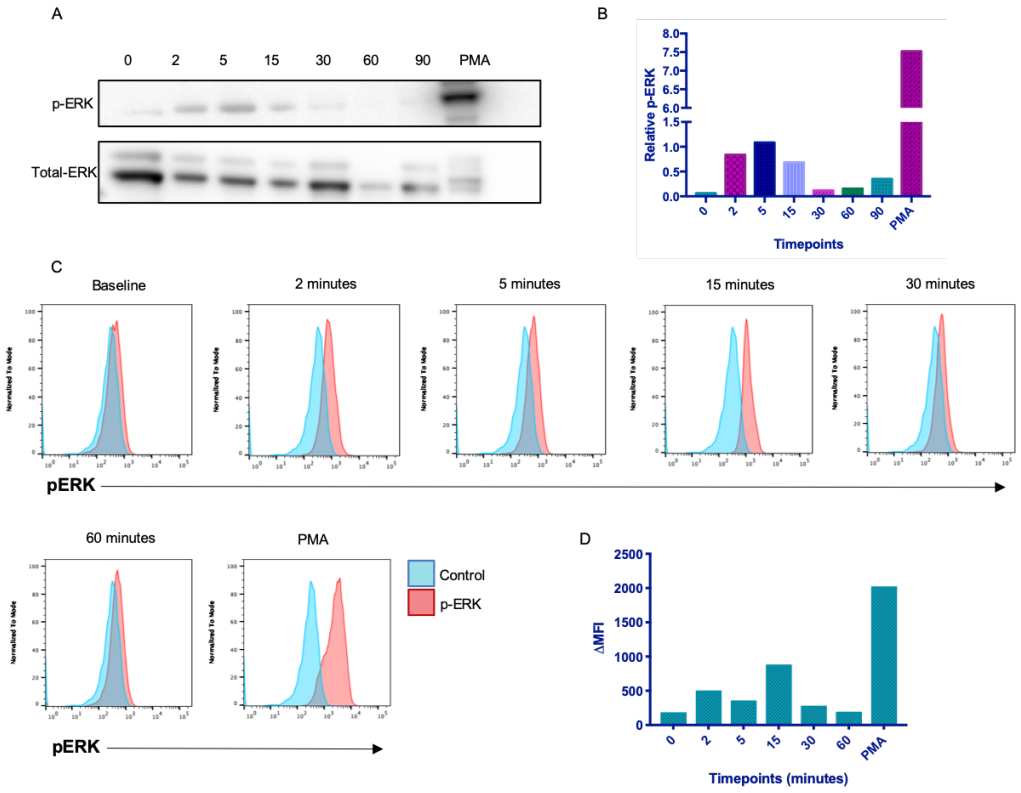

Figure 6.1 Human Monocytes Respond to PAR2 Stimulation Through MAPkinase Signalling Activation.
PBMCs were isolated from peripheral blood via gradient centrifugation and resuspended in complete RPMI. Cells were left unstimulated, stimulated with PAR2 activating peptide (FLIGRL, 2μM) for 2, 5, 15, 30, 60, or 90 minutes, or stimulated with PMA (100nM) for 15 minutes. Cells were fixed in 4% paraformaldehyde to stop cellular activity and cells were spun down and resuspended in 200μl RIPA buffer for protein lysate extraction. Cell lysates were separated by molecular weight by gel electrophoresis and transferred to a PVDF membrane for western blotting. (A) This membrane was blotted for phospho-ERK and loading control total-ERK. (B) Band intensity was quantified using ImageJ and p-ERK bands were normalised to the loading control total ERK. This experiment was repeated with new healthy donor PBMCs instead of protein extraction cells were fixed and permeabilised for intracellular staining of phospho-ERK. Secondary anti-rabbit AF647 was then used to bind to the anti-p-ERK antibody to amplify the fluorescent signal and these samples were run on the LSRII flow cytometry. (C) Histograms are plotted with p-ERK stain (red), and secondary antibody only stain (blue) for each time point and PMA positive control. (D) The mean fluorescent intensity (MFI) of p-ERK in these samples was plotted. N=1, no additional experimental repeats performed.

6.2.2 Role of PAR2 in Integrin Expression in Human Monocytes

The primary function of peripheral blood monocytes is to detect sites of inflammation and damage and migrate from the blood into the tissue. Monocytes must be able to adhere to the luminal surface and transmigrate through the lumen into the tissue. In order to complete these functions, integrin activation and adherence to endothelial cells is essential. There are no previous publications that reveal a role for PAR2 in monocyte adherence or migration, however, there are multiple studies demonstrating a clear role for PAR2 in the migration, adherence, and integrin expression of many other cell types[363,388-390]. Therefore, it is possible that adhesion and migration may be an unexplored function of PAR2 signalling in monocytes.

Evaluation of integrin subunit CD11b levels on murine monocyte populations revealed that there was increased expression on *par2*$^{-/-}$ BM patrolling monocytes (Figure 5.3), indicating a potential regulatory function of PAR2 in integrin expression. Importantly, healthy human monocytes expressed surface PAR2 (Figure 4.4)and are able to respond to PAR2 activating peptides (Figure 6.1). Thus, it is conceivable that integrin expression levels on human monocytes maybe altered via PAR2 activation and inhibition. To test this hypothesis a flow cytometry panel was set up to investigate integrin expression on human monocytes.

Initially changes in total integrin expression were tested in response to stimulation with a positive control. The TLR4 ligand LPS was chosen to drive monocyte activation, as a positive control for activated monocyte phenotype. Three time points of LPS stimulation were tested, 30, 60, and 120 minutes, and post-incubation cells were immediately put on ice to prevent further modulation of surface antigens. At this point cells were stained to identify monocyte populations (the same panel as used in sections 4.2.2 and 4.2.5) with the addition of antibodies against integrin β2 associated antigens, including CD11a, b, c, and CD18. Staining for integrin heterodimer $\alpha v\beta 3$ was also included, as this integrin is required for cellular adhesion to bone and osteoclast differentiation. Visualisation of the of the difference in fluorescence levels of each integrin stain between unstimulated monocytes (blue) and LPS stimulated samples (red) revealed an LPS-associated increase in integrin subunit expression (Figure 6.2A).

In interpreting this data it important to note that the dotted line gates on each histogram represent the point at which staining becomes positive for the protein detected. Positive stain was defined as higher fluorescence detection than the fluorescence minus one control stain (FMO). The FMO stain is a sample of the same cell population stained with all of the other markers used in the flow panel without the marker of interest. This accounts for the impact of the presence of other fluorescent probes, which may contribute to detection of another fluorophore, and is thus a more robust negative control than an unstained sample. Primary human monocytes have clear positive expression of CD11b and CD18, with both of these surface markers increased upon LPS stimulation. While CD11a and CD11c were expressed at low levels in unstimulated monocytes. CD11c is highly upregulated upon LPS and CD11a slightly enhanced upon LPS stimulation. $\alpha v\beta 3$ was not expressed by monocytes and expression was not promoted by LPS stimulation. The fold change over the unstimulated sample for each integrin component stained (except $\alpha v\beta 3$ which stained negative both with and without stimulation) was calculated at each LPS time point and supported the interpretation that CD11a, b, c and CD18 were increased (Figure 6.2B).

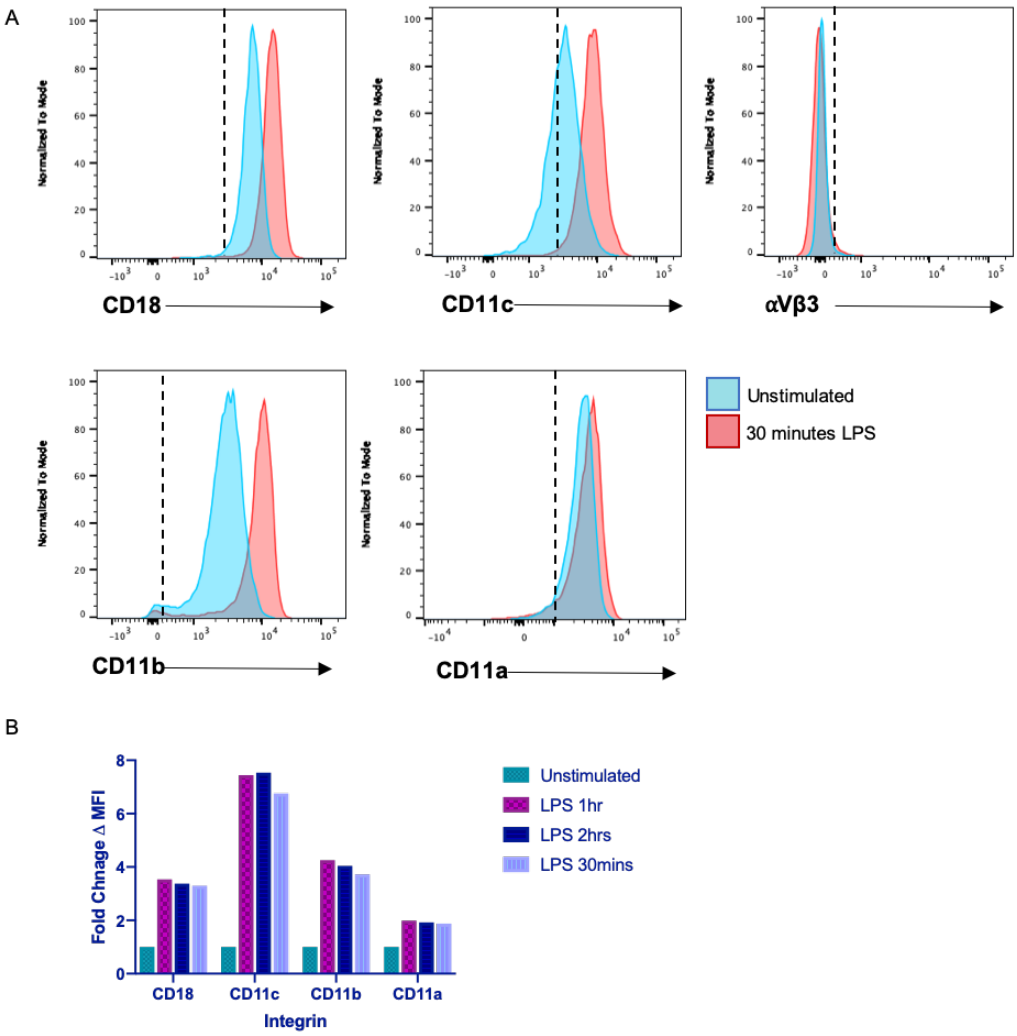

Figure 6.2 Short Term LPS Treatment Stimulates Increased Surface Integrin Expression in Human Monocytes.
Total PBMCs were isolated from healthy buffy coats by gradient centrifugation. PBMCs were then resuspended in RPMI and incubated at 37ºC unstimulated, or stimulated with LPS (100ng/ml) for 30, 60 or 120 minutes. Cells were then immediately put on ice to stop the modulation of surface membrane proteins. Samples were stained in FACS buffer for HLADR, CD14, and CD16 to identify monocytes, lineage negative markers (CD3, CD19, CD15, CD56) to exclude other cell populations, and integrins (CD11a, b, c, CD18, and aVb3). These samples were run on the LSR II and analysis conducted on Flowjo software. (A) Histograms of monocyte events were plotted for each integrin with unstimulated samples in blue and 30 minutes of LPS stimulation in red. Dotted line gates delineate positive and negative staining – all events right of the dotted line are positive over baseline and all events left of the line are negative - as determined by the fluorescence level of fluorescence minus one (FMO). (B) MFI for each integrin was normalised to the MFI of the unstimulated sample and the fold increase in expression plotted for each time point of LPS stimulation. N=1, no additional experimental repeats performed.

After demonstrating that integrin upregulation of β2 integrin (CD18) and its associated heterodimer subunits (CD11a, b, and c) could be achieved in monocytes, the impact of PAR2 activation and inhibition on expression levels of β2 associated integrins could be investigated. PBMCs were isolated from 2 healthy donors, and these cells were stimulated with or without PAR2 activating

peptide (FLIGRL, 2μM), PAR2 inhibitor (AZ3383, 3μM), or LPS (100ng/ml) for 90 minutes. Again cells were stained on ice for all the surface antigens. Of the 2 donors analysed, 1 of the donors (shown in the top row of FACS plots) responded as expected to LPS, increasing expression of CD11b, CD18, and CD11c (Figure 6.3 A and B). Interestingly this donor lost expression of CD11b and CD18 (a promiscuous integrin heterodimer which binds to ICAM-1, complement protein iC3b, alarmin LL-37^{391}) after incubation in PAR2 inhibitor AZ8838. In comparison, the PAR2 activating peptide did not have the opposite impact of the PAR2 inhibitor; increasing expression of these receptors. Surprisingly CD11b was also slightly decreased with PAR2 activation via FLIGRL peptide stimulation compared with unstimulated controls, but to a much lesser extent than the PAR2 inhibited sample. The other donor tested however, had no change in total integrin expression in response to LPS (Figure 6.3 A and B, second row). Both PAR2 activators and inhibitors also had no impact on integrin expression in this donor. Without a reliable positive control for a change in integrin expression in this donor it is not possible to conclude anything about the PAR2 pathway.

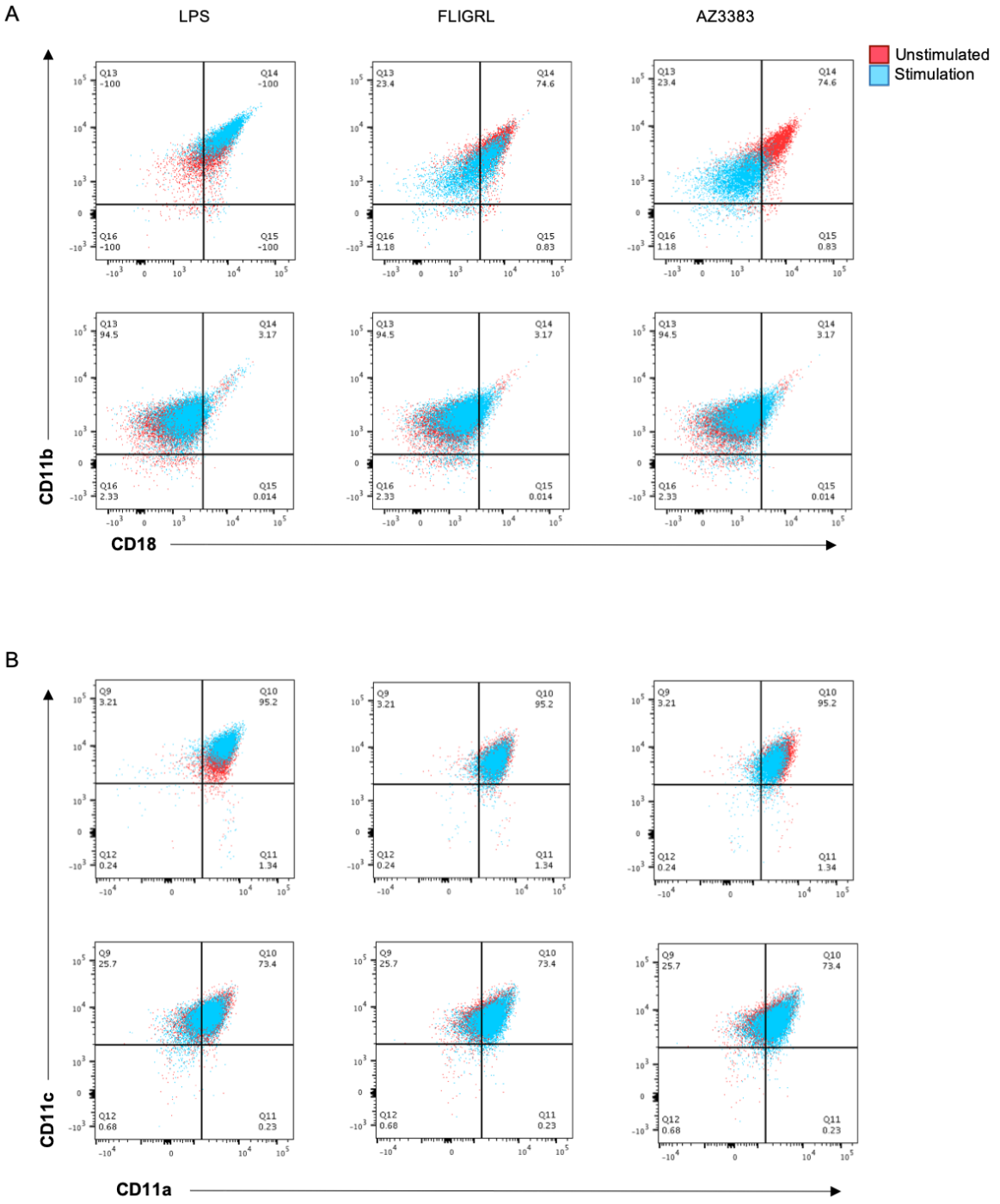

Figure 6.3 Integrin Expression on Healthy Human Monocytes was Not Reliably Altered in Response to PAR2 Stimulation or Inhibition.
PBMCs were isolated from 2 healthy buffy coat samples via density gradient centrifugation. PBMCs were maintained at 37ºC in RPMI unstimulated, or stimulated with LPS (100ng/ml), FLIGRL (2µM), or PAR2 inhibitor AZ8838 (3µM) for 90 minutes. These cells were then immediately placed on ice to prevent modulation of surface antigens and stained in FACS buffer for HLADR, CD14, and CD16 to identify monocytes, lineage negative markers (CD3, CD19, CD15, CD56) to exclude other cell populations, and integrins (CD11a, b, c, CD18, and aVb3). These samples were run on the LSR II and analysis conducted on Flowjo software. FACS plots were created looking at (A) CD11b on the Y axis, vs CD18 on the X axis, and (B) CD11a on the Y axis vs CD11a on the X axis. Stimulated samples (blue) were overlaid on unstimulated samples (red). N=2, no additional experimental repeats performed.

This experiment failed to show consistent response of monocyte integrin expression in response to either the positive control of LPS or PAR2 pathway interventions. The data from the 1 responding donor indicated that blocking PAR2 impacted monocyte associated integrin heterodimer CD11b/CD18 expression. In order to find a more robust, consistent positive control for increased total integrin expression the experiment was repeated instead using PMA stimulation as a positive control for increased total integrin expression. This experiment was repeated with 3 healthy donors, stimulating with PMA, PAR2 activating peptide (FLIGRL, 2μM), or PAR2 inhibitor (AZ3383, 3μM). No change in total integrin expression for CD11b, c or CD18 was detected in response to PMA positive control stimulation (Figure 6.4), while an increase in CD11a expression was found in response to PMA (Figure 6.4).This outcome was the same for all 3 donors, only 1 representative donor for this is shown in Figure 6.4. Interestingly integrin αVβ3, which had undetectable expression and is not induced by LPS stimulation, was brought to the cell surface by PMA stimulation resulting in high expression of this integrin (Figure 6.4C). This suggests that different mitogenic signals in human monocytes influence the total expression levels of different integrins. Some signals proving to be suitable positive controls for the induction of some monocyte associated integrins while others more suitable for different integrin families. A combination of mitogenic factors or the use of multiple different positive controls may be more useful for future investigation into total integrin expression modulation. It is of note that none of the buffy coat donors (N=3) had any detectable change in integrin expression levels in response to PAR2 activation or inhibition in this experiment (Figure 6.4).

The present data remains inconclusive and further studies are required to categorically rule out the potential for PAR2-mediated signalling to influence integrin expression. Further investigation of integrin expression requires substantial optimisation and possibly alternative approaches to enable exploration of the role of PAR2 in this biological response in human monocytes.

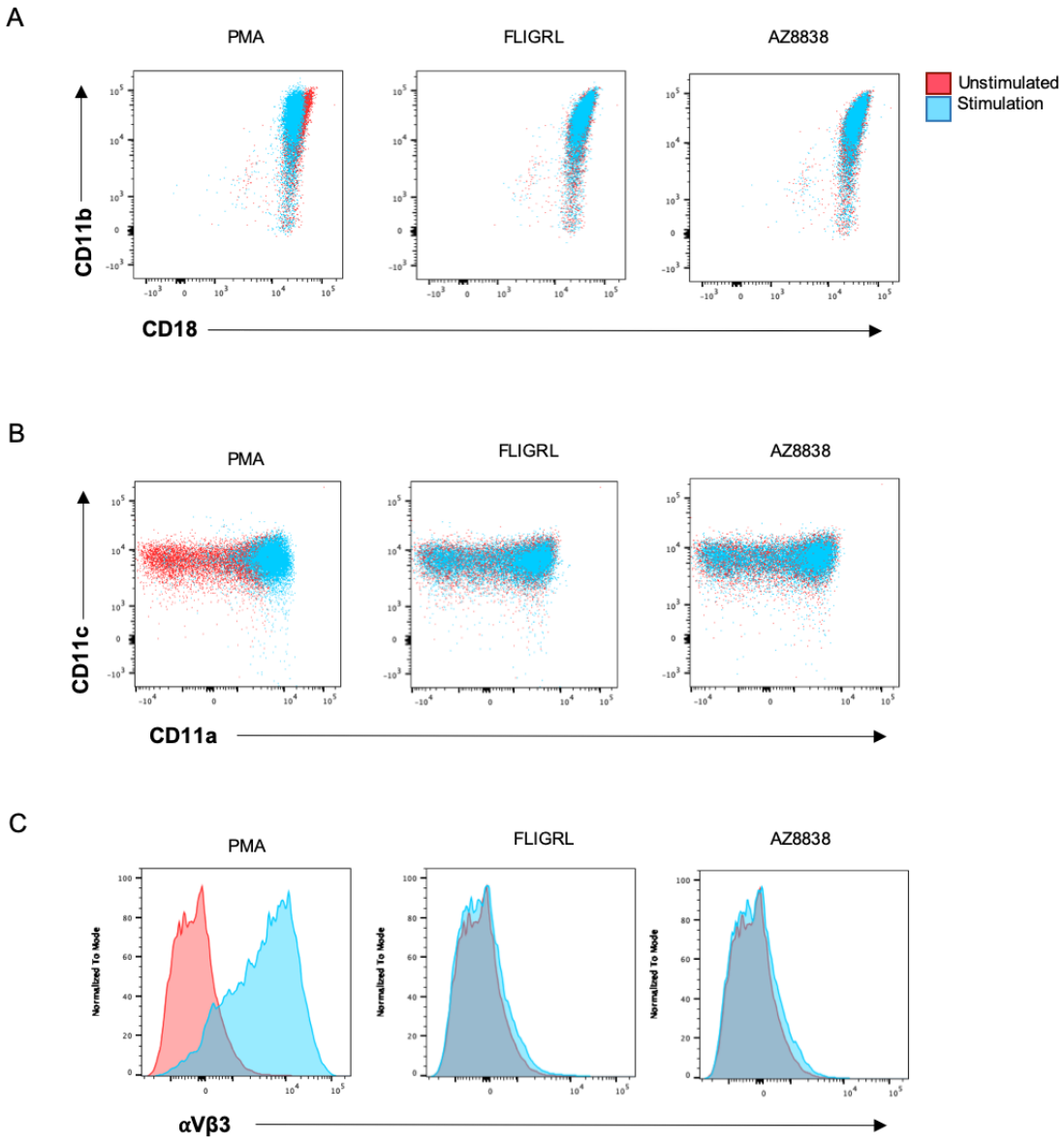

Figure 6.4 PAR2 activation or Inhibition Does not Alter Total Integrin Expression in Healthy Human Monocytes
PBMCs were isolated from 3 healthy buffy coat samples via density gradient centrifugation, one representative donor is shown. PBMCs were maintained at 37ºC in RPMI unstimulated, or stimulated with PMA (100ng/ml), FLIGRL (2μM), or PAR2 inhibitor AZ8838 (3μM) for 90 minutes. These cells were then immediately placed on ice to prevent modulation of surface antigens and stained in FACS buffer for HLA-DR, CD14, and CD16 to identify monocytes, lineage negative markers (CD3, CD19, CD15, CD56) to exclude other cell populations, and integrins (CD11a, b, c, CD18, and aVb3). These samples were run on the LSR II and analysis conducted on Flowjo software. FACS plots were created looking at (A) CD11b on the Y axis, vs CD18 on the X axis, and (B) CD11a on the Y axis vs CD11a on the X axis, and (C) histograms looking at the fluorescence intensity of αVβ3. Stimulated samples (blue) were overlaid on unstimulated samples (red). N=3, representative data shown for N=1, no additional experimental repeats performed.

6.2.3 PAR2 Regulates Human Osteoclast Differentiation Suboptimal RANKL Conditions

As mentioned above (see section 6.1), work conducted in *par2*$^{-/-}$ murine cells identified a regulatory role for PAR2 signalling in the prevention of excessive OC formation during M-CSF and RANKL differentiation (Figure 5.8). Previous studies have implicated PAR2 in bone related human pathologies such as osteoarthritis. However, the current literature exploring the functional mechanisms of PAR2 in bone remodelling and specifically osteoclastogenesis have only been conducted in murine systems. Thus far no peer reviewed studies have been published studying the role of protease signalling via PAR2 in the differentiation of human OCs.

In order to translate the findings from murine *in vitro* assays and clarify the regulatory role of PAR2 extends to human OCs, human osteoclastogenesis assays were conducted with peripheral blood monocyte progenitors. This involved culture of positively selected CD14^{+} monocytes overnight in complete α-MEM media supplemented with M-CSF. This promotes the upregulation of RANK, making these monocytes more receptive to RANKL[60]. Classic in vitro human osteoclastogenesis protocol was followed (Figure 6.5A). Due to the observations of reduced PAR2 expression in human monocytes after overnight M-CSF reported in the chapter 4 (Figure 4.8) PAR2 intervention with either activating peptide (FLIGRL, 2μM) or inhibitor (AZ3383, 3μM) was introduced at the beginning of the culture, concurrent with M-CSF exposure (Figure 6.5A). After 7 days cultures were fixed and TRAP stained (Figure 6.5 D and E), and the number of OCs per well quantified (Figure 6.5 B and C). For both PAR2 stimulation (FLIGRL, Figure 6.5 B and D) and inhibition (AZ8838, Figure 6.5 C and E) paired analysis was performed to take into account variation within human samples. No consistent change in osteoclast number was observed with either PAR2 activation or inhibition (Figure 6.5B and C).

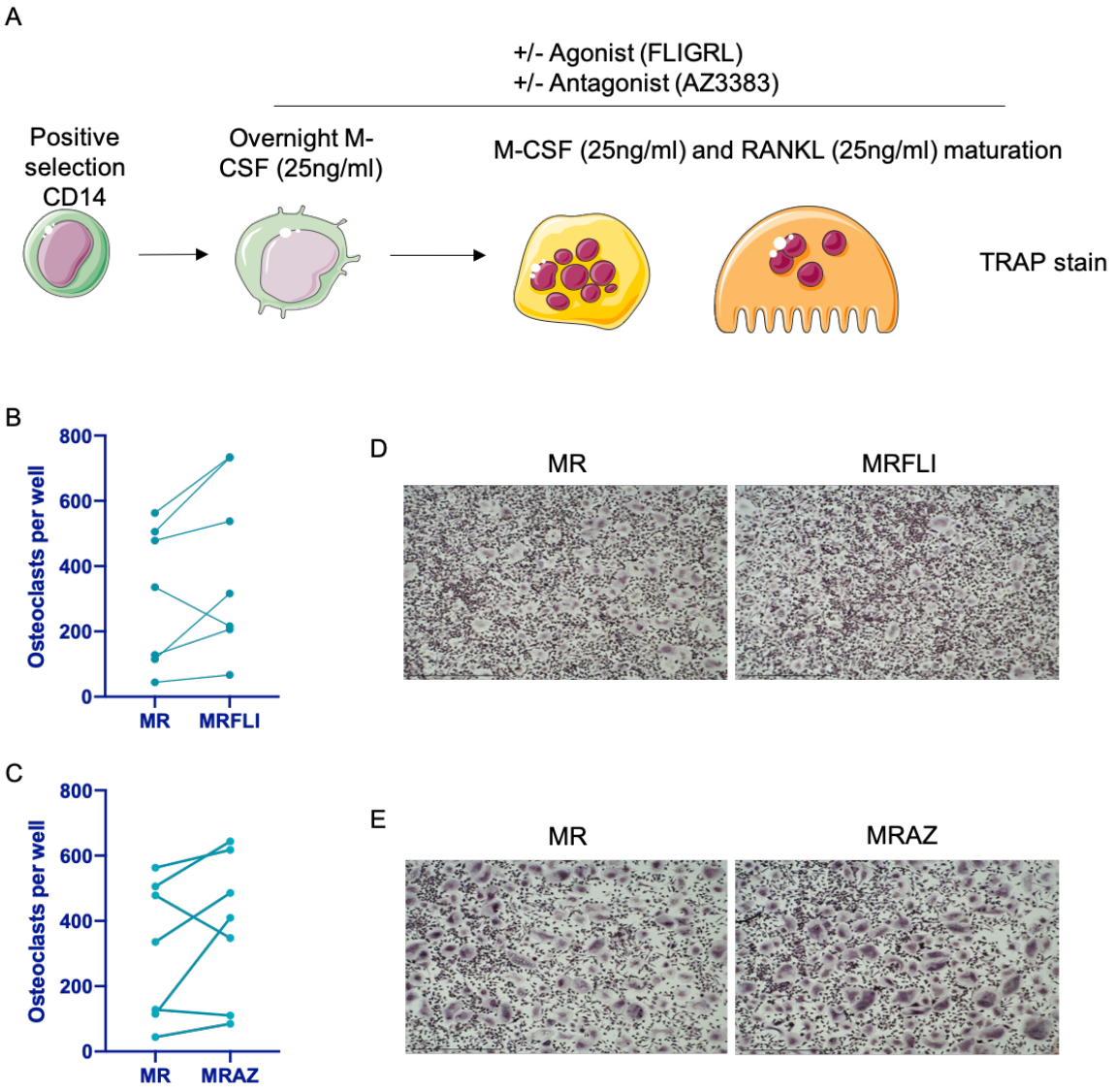

Figure 6.5 No Significant Difference in Human Monocyte Osteoclast Differentiation With PAR2 Stimulation or Inhibition.
(A) PBMCs were separated from healthy buffy coat via density gradient centrifugation and CD14+ monocytes were positively isolated via magnetic separation (N=7). Monocytes were cultured in complete αMEM media in the presence of 25ng/ml of M-CS, +/- FLIGRL (2μM), +/- AZ3383 (3μM) overnight. Media was then half changed the following day to include 25ng/ml M-CSF and RANKL, +/- FLIGRL (2μM), +/- AZ8838 (3μM) and cultured for a further 5 days, changing media every 3 days. Cultures were then fixed in acetone buffered formaldehyde and TRAP stained and osteoclasts quantified for (B) MR and MRFLIGRL, and (C) MR and MRAZ. Representative images of each condition (10x) are shown in D and E. Wilcoxon test statistical analysis conducted on paired samples, which does not assume gaussian distribution. N=7, no additional experimental repeats performed.

Based on the observation that murine WT cultures increased numbers of OCs generated in the presence of PAR2 inhibitors (Figure 5.11), it was surprising that this did not translate to the human cell assay. However, it is conceivable that the ability to detect a consistent increase in osteoclastogenesis with this assay may be limited, as osteoclastogenic differentiation is potentially maximised due

to the concentration of RANKL used. In light of this, the assay was repeated with a reduced concentration of RANKL (Figure 6.6A) in order to observe any potential increase in osteoclastogenesis. As can be seen from representative images chosen at random in Figure 6.6 E, and the quantification of osteoclast numbers from 7 donors, inhibition of PAR2 resulted in a consistent increase in osteoclast number (Figure 6.6 C). Activation of PAR2 under these culture conditions resulted in a more variable response and inconsistent (Figure 6.6 B and D). Indicating overall no change in OC formation with activating peptide-mediated PAR2 activation. These outcomes positively correspond with what was found in the murine system, which found increased OC generation and cell size in *par2*$^{-/-}$ cultures, an increase in OC number in WT cells cultured in AZ8838, and no change in OC numbers in response to PAR2 activating peptide FLIGRL.

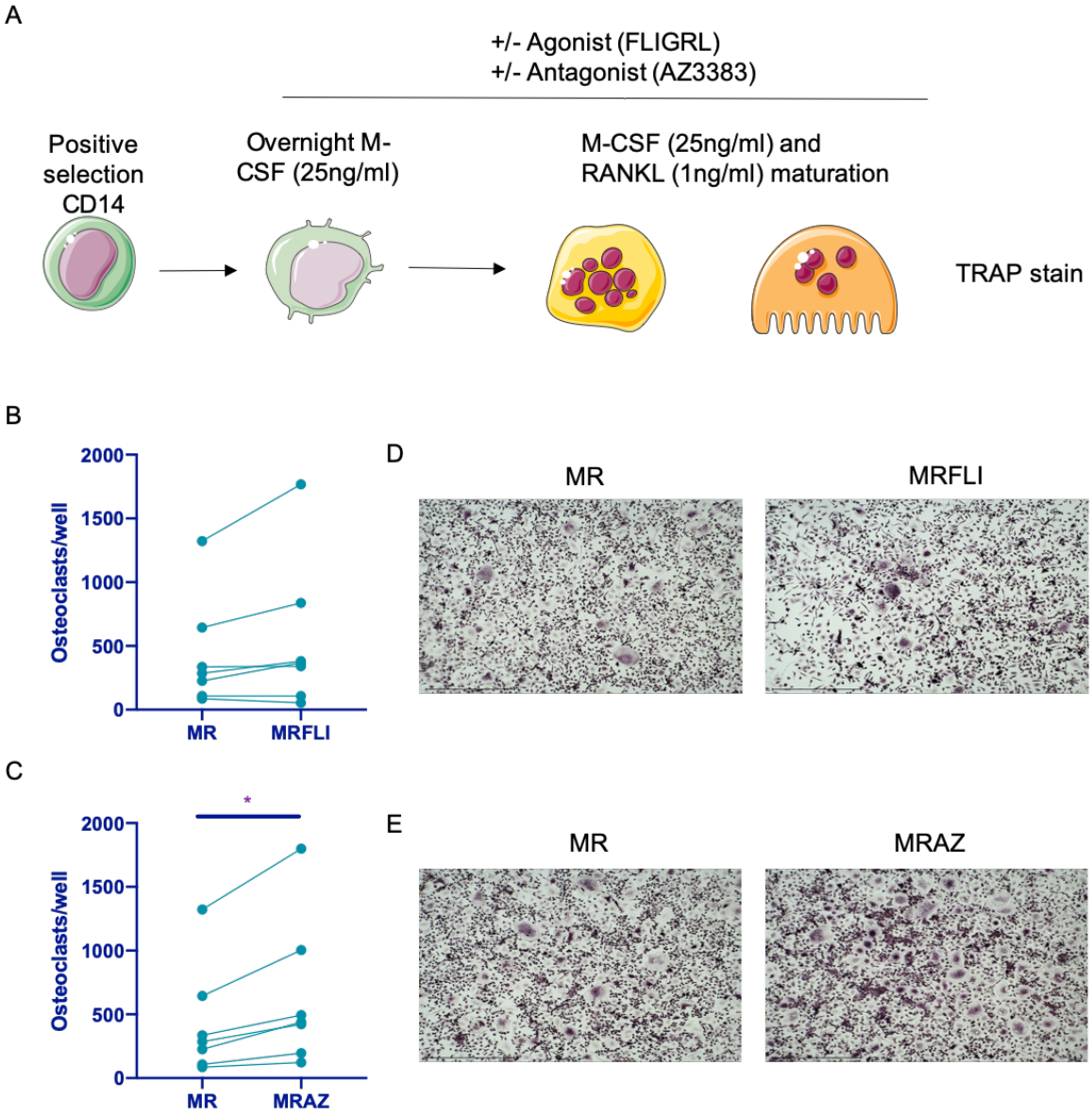

Figure 6.6 PAR2 Inhibition Increased Osteoclastogenesis in Suboptimal RANKL Cultures. (A) PBMCs were separated from healthy buffy coat via density gradient centrifugation and CD14+ monocytes were positively isolated via magnetic separation (N=7). Monocytes were cultured in complete αMEM media in the presence of 25ng/ml of M-CS, +/- FLIGRL (2μM), +/- AZ8838 (3μM) overnight. Media was then half changed the following day to include 25ng/ml M-CSF and 1ng/ml RANKL, +/- FLIGRL (2μM), +/- AZ3383 (3μM) and cultured for a further 5 days, changing media every 3 days. Cultures were then fixed in acetone buffered formaldehyde and (D, E) TRAP stained and osteoclasts quantified for (B) MR and MRFLIGRL, and (C) MR and MRAZ. Representative images of each condition (10x) are shown in D and E. Wilcoxon test statistical analysis conducted on paired samples, which does not assume gaussian distribution. * = $p<0.05$. N=7, no additional experimental repeats performed.

It is known that TNF contributes to inflammatory enhanced OC formation[392]. Levels of detected TNF in RA patients positively correlates with the level of bone erosions[360] and direct inhibition of TNF using biologics as therapy in RA patients is known to reduce the risk of radiographic signs of bone erosions[361]. Human monocytes appear to respond in the same manner as murine BM cultures to PAR2 activating and inhibiting reagents in regulating OC differentiation in regular OC cultures. The cells from *par2*$^{-/-}$ NA-BM had opposing OC differentiation responses during inflammatory enhanced osteoclastogenesis (Figure 5.20). Under TNF enhanced OC cultures instead of further enhancement of OC differentiation found in homeostatic conditions, these cells had limited enhancement in differentiation in response to TNF. To determine whether PAR2 signalling also contributes to TNF enhanced OC formation in human monocytes similar assays as above were applied, to inhibit and activate PAR2 during OC differentiation. Previous work in our laboratory had optimized an inflammatory, TNF enhanced osteoclast assay (Figure 6.7A), which involves addition of TNF on day 4, after precursor cells had committed to an osteoclast differentiation route. With this protocol a consistent enhancement of osteoclast number was observed across 7 donors (Figure 6.7B and C).

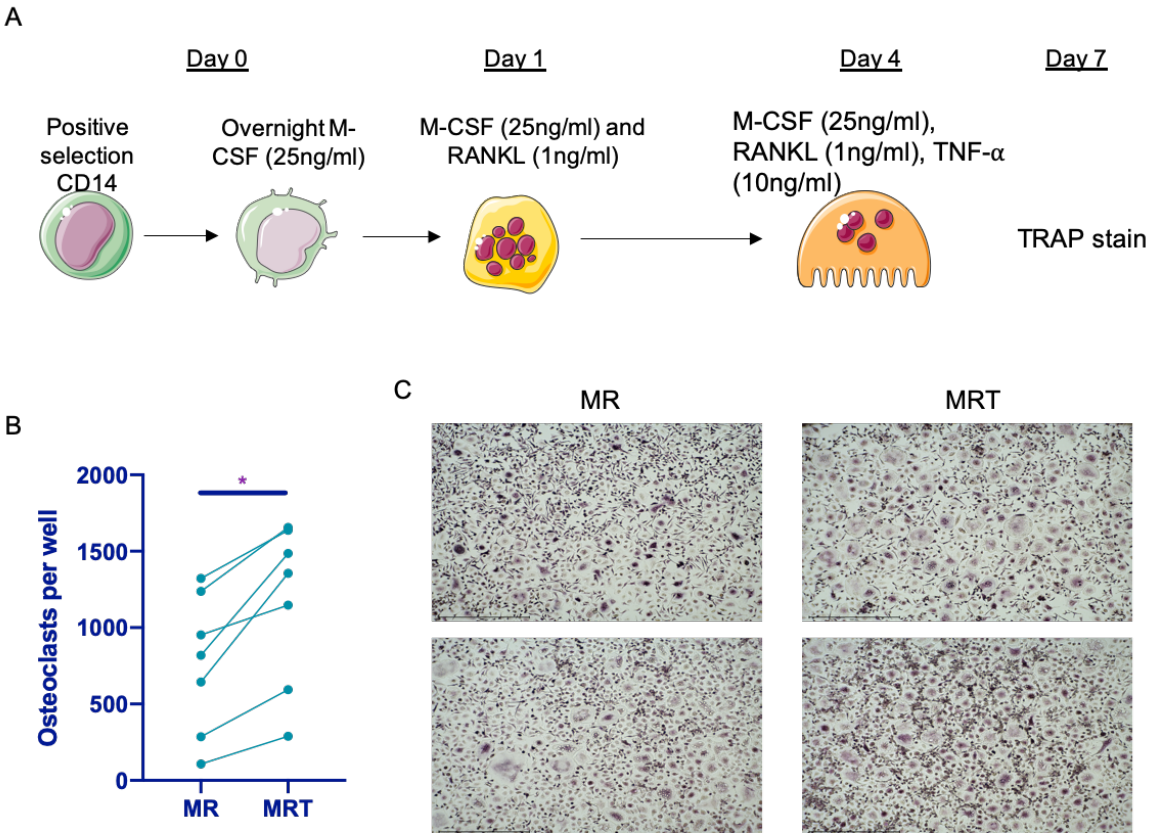

Figure 6.7 Addition of TNF on day 4 of Human Osteoclast Cultures Enhances Osteoclastogenesis.
(A) PBMCs were separated from healthy buffy coat via density gradient centrifugation and CD14+ monocytes were positively isolated via magnetic separation (N=7). Monocytes were cultured in complete αMEM media in the presence of 25ng/ml of M-CSF overnight. Media was then half changed the following day to include 25ng/ml M-CSF and 1ng/ml RANKL and cultured for a further 3 days. Media was again half changed this time to include 25ng/ml M-CSF, 1ng/ml RANKL, and 10ng/ml TNF and cultured for a further 3 days. Cultures were then fixed in acetone buffered formaldehyde and (C) TRAP stained and osteoclasts quantified for (B) MR and MRT. Representative images of each condition (10x) are shown in C, for 2 of the donors. Wilcoxon test statistical analysis conducted on paired samples, which does not assume gaussian distribution. * = $p<0.05$. N=7, no additional experimental repeats performed.

In order to test the impact of PAR2 activity during TNF enhanced osteoclastogenesis PAR2 activating and inhibiting agents were applied to this culture (Figure 6.8A) and the OC number was quantified (Figure 6.8B and C). No significant change was found with either PAR2 activation (Figure 6.8B) or inhibition (Figure 6.8C). There was no observable difference in OC number with PAR2 activation, however, there was a non-significant decrease in OC numbers across all donors tested when PAR2 was inhibited, with an average decrease of 23% in OC number and a standard deviation of 3.799 across the donors (N= 4, Figure 6.8C). Suggesting that further studies are required to conclusively demonstrate whether PAR2 signalling impacts inflammatory driven human OC formation.

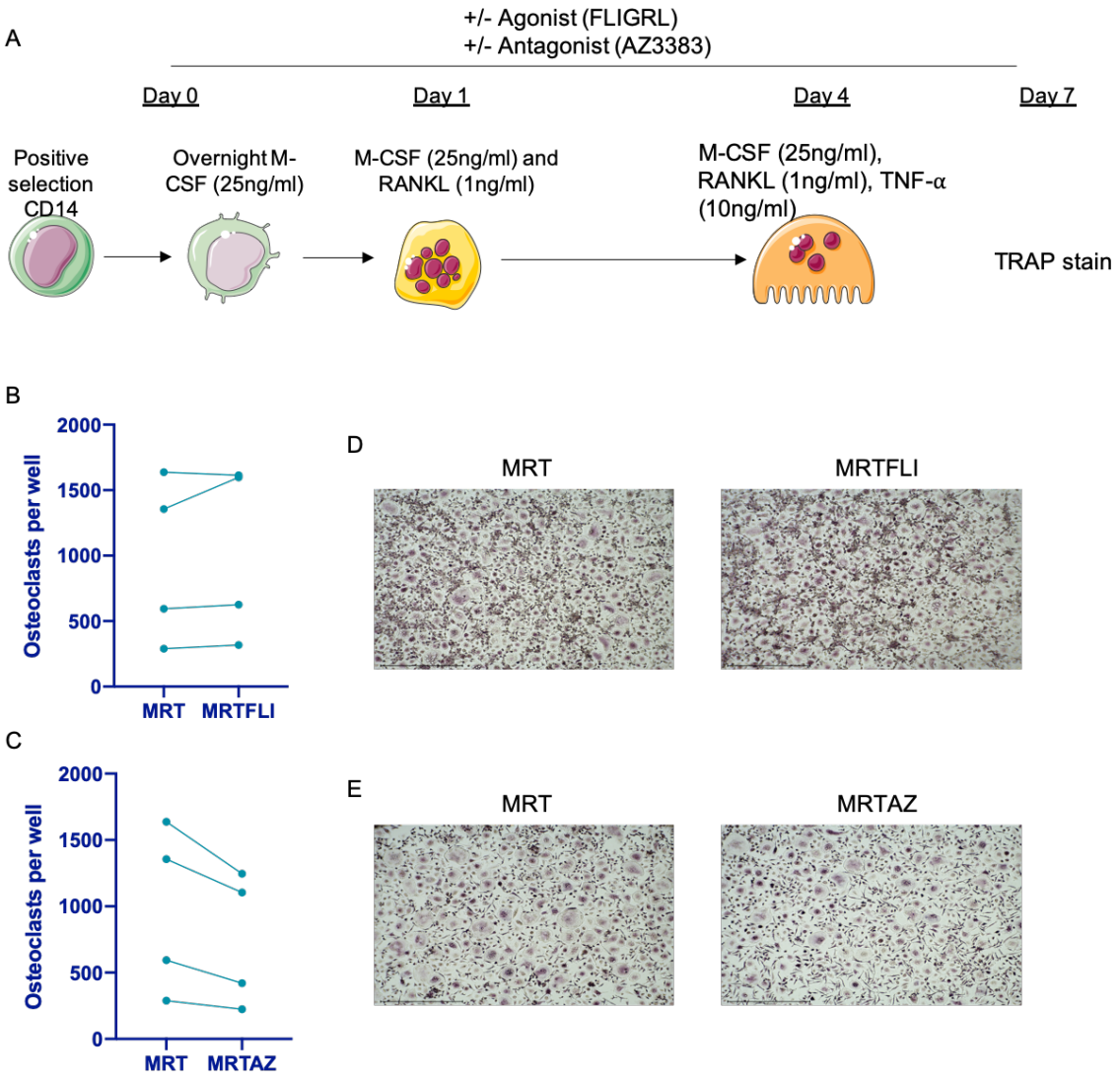

Figure 6.8 PAR2 Activation or Inhibition does not Significantly Influence TNF Enhanced Osteoclastogenesis.
(A) PBMCs were separated from healthy buffy coat via density gradient centrifugation and CD14+ monocytes were positively isolated via magnetic separation (N=4). Monocytes were cultured in complete αMEM media in the presence of 25ng/ml of M-CSF, +/- FLIGRL (2μM), +/- AZ8838 (3μM) overnight. Media was then half changed the following day to include 25ng/ml M-CSF, 1ng/ml RANKL, +/- FLIGRL (2μM), +/- AZ8838 (3μM) and cultured for a further 3 days. Media was again half changed this time to include 25ng/ml M-CSF, 1ng/ml RANKL, and 10ng/ml TNF, +/- FLIGRL (2μM), +/- AZ8838 (3μM) and cultured for a further 3 days. (D, E) Cultures were then fixed in acetone buffered formaldehyde and TRAP stained and osteoclasts quantified for (B) MRT and MRTFLI and (C) MRT and MRTAZ. Representative images of each condition (10x) are shown in D and E. Wilcoxon test statistical analysis conducted on paired samples, which does not assume gaussian distribution. N=4, no additional experimental repeats performed.

6.3 Discussion

Data presented in chapter 3 of this thesis established that PAR2 was expressed on the cell surface of primary human monocytes. The expression levels varied between donors, indicating variability in the potential for different donors to respond to PAR2 activation. Therefore, functional responses of PAR2 in the myeloid compartment were initially investigated through the use *of par2*$^{-/-}$ mice. In conducting cellular assays with WT and *par2*$^{-/-}$ BM cells, 2 key biological pathways had observable changes with a loss of this receptor. One of these biological pathways was cellular migration and adhesion which has previously been associated with PAR2 in other cell types but not yet observed in monocytes. PAR2 stimulation in non-immune cells [366,393] and leukocytes[282,364,394] has been associated with the integrin dependent adhesion and migration. This receptor has also been strongly associated with the production of chemokine mediators that drive cellular migration and integrin activation, especially IL-8 [270,365,395-397]. ICAM-1 was one of the integrin binding partners that was highly associated with PAR2 stimulation [322,363,365,394]. In addition, PAR2 is known to signal through Gα13[398], a signal utilized by chemokine receptors to regulate integrin activation[399].

The role of PAR2 in integrin expression and activity is yet to be explored in monocytes, a cell type where cell adhesion and migration is fundamental to their function. After identifying an enhanced expression of CD11b in the patrolling subset of monocytes from *par2*$^{-/-}$ BM in chapter 5 (see section 5.2.2), it was considered justified to further investigate this in human monocytes. ICAM-1, one of the known binding partners of CD11b and CD18 heterodimers, had been shown to be upregulated in endothelial cells in response to PAR2 activation. Monocytes can adhere to endothelial cells via ICAM-1 and other integrin interactions in order to transmigrate from the vasculature into the tissue. In order to establish whether the observations of enhanced CD11b expression with the loss of PAR2 made in the murine system had biological relevance in human monocytes, experimental focus was put on the expression of β2 associated integrins such as CD11b. β2, also known as CD18, requires partnership with α integrin subunits, which include CD11a, b, c, and d to form a functional integrin heterodimer. Another integrin of interest in monocytes and their differentiation

potential into OCs is αvβ3. This is required for osteoclast function, migration and adhesion to bone[400]. Therefore the expression of CD18, CD11a,b, and c, and αvβ3 on healthy monocytes was explored using flow cytometric assays. Expression of integrin proteins does not necessarily infer activity of these proteins. Integrins are expressed on the surface, often in an inactive conformation. These proteins can then rapidly respond to activating signals such as chemokine detection, and adjust to an active conformation which allows binding to ligand and cellular adhesion. In order to detect functionally relevant integrin expression active conformations can also be detected using antibodies specific for the active conformation of the receptor, in addition to antibodies which detect both active and inactive integrins. Differences in the total protein (no discrimination between active or inactive integrin) expression of CD11b was previously identified in *par2*$^{-/-}$ monocytes. Therefore as a starting point, total integrin expression was measured in human monocytes using antibodies which recognise integrins in both their active and inactive forms to determine whether PAR2 activation or inhibition influences total integrin expression in human monocytes as well.

Exploration of integrin expression was unable to categorically demonstrate that PAR2 influences the expression of these proteins. A positive control for the change in the total expression of these integrins was not consistent across donors (Figure 6.3A and B) and thus comparison of PAR2 activating peptides and inhibitors could not be reliably made. To definitively show that PAR2 alters integrin biology future studies should focus on detection of the active form of integrins rather than just total protein expression. Importantly, the activation status of integrins is a much better indicator of their function, as opposed to total expression. Due to time constraints we were unable to optimize and perform this assay on human monocytes.

Previous investigation into the role of PAR2 in bone remodelling[76], pathogenic bone erosion[401] and formation[288], and osteoclastogenesis[75] has been conducted in the murine setting. The findings and interpretation from the current literature is contradictory, and thus a clear role for PAR2 in this process still unclear. Chapter 5 of this thesis explored the role of PAR2 in osteoclastogenesis during both homeostatic and inflammatory TNF enhanced OC culture conditions with BM

from *par2*$^{-/-}$ mice. This data determined that PAR2 plays divergent roles under non-inflammatory and inflammatory conditions. During RANKL and M-CSF driven OC generation, PAR2 prevented excessive osteoclastogenesis and formation of giant cells. While during TNF-driven inflammatory osteoclastogenesis, PAR2 contributed to the enhancement of OC formation. Utilising the confirmed PAR2 antagonist from AstraZeneca, with no known agonistic properties, meant PAR2 inhibition in primary human cultures could be achieved and this could be used to explore the role of this receptor during human monocyte *in vitro* differentiation into OCs, similar to culture of *par2*$^{-/-}$ cells.

Using conventional osteoclastogenic assays no differences in OC number were detected when PAR2 was either stimulated or inhibited (Figure 6.5). This was unsurprising in the case of PAR2 activating peptide (FLIGRL) stimulation, which also failed to influence WT murine OC cultures (Figure 5.11B). However, inhibition of WT murine PAR2 resulted in an increase in OC numbers, comparable to quantification of the *par2*$^{-/-}$ cultures. If PAR2 activity also influenced human OCs similarly to murine OCs, an increase in OC number would be expected with PAR2 inhibition in these cultures. It was possible that the potential for enhancement of osteoclastogenesis may be limited in this assay (Figure 6.5A), and potentially OC formation had reached a maximum with this concentration of RANKL. For this reason the concentration of RANKL was reduced to 1ng/ml in order to create a suboptimal OC differentiation assay, and provide a method to interrogate potential OC enhancement. By adopting this protocol with a further 7 healthy human donors, again no change in OC number was found with PAR2 activation (Figure 6.6B). However, a modest enhancement in OC number in each donor was detected when PAR2 was inhibited with AZ8838 (Figure 6.6C). This data suggests that in sub-optimal conditions PAR2 activity regulates the formation of human OC. Again due to a lack of response from activating peptides this could potentially be the result of non-canonical PAR2 signal, or internal PAR2 signalling. Human monocyte surface membrane expression levels of PAR2 are highly variable (Figure 4.4) which may account for the variability of the effect size detected by inhibition of this pathway on osteoclast formation between donors.

During TNF driven enhanced OC formation PAR2 inhibition with AZ3383 did not further enhance the rate of OC formation, like it had in M-CSF and RANKL alone cultures. In fact each donor had a modest reduction in osteoclast number during PAR2 inhibition (Figure 6.8C). This reduction did not reach significance but was observed consistently. The differences observed in this culture with PAR2 inhibition were very modest. This indicates that in human OC formation, PAR2 may have a limited biological influence in comparison to the more obvious impact observed in murine cultures.

Overall, the impact of PAR2 intervention in human cultures was not as consistent and clear as the murine cultures, which numerically *par2*$^{-/-}$ had a much bigger difference in osteoclast number. Also one observation made in murine *par2*$^{-/-}$ cultures was the significant change in OC size, which was not measured in human OC cultures, but also not obviously observed in TRAP stain images. Therefore, it may still be worthwhile to investigate the functional activity of human cultures through osteolysis assays and transcript pathway analysis to identify if the regulation of human OCs is driven by a similar adhesion/fusion phenotype as murine cells. Unfortunately, this could not be completed within the time frame available but may still be a valuable area of future investigation.

6.4 Conclusions

As a first study investigating the role of protease signalling via PAR2 in the process of human monocyte differentiation to OCs, this chapter established that PAR2 signalling has a modest impact on human OC formation. The data presented in this chapter indicates that PAR2 signalling regulates OC differentiation in an autocrine manner. Elevated OC numbers with PAR2 inhibitor treatment implies autocrine signals present in M-CSF and RANKL cultures contribute to the regulation of OC differentiation. No effect of PAR2 activating peptides, suggests that this canonical form of PAR2 signalling does not contribute to the regulation of human OC differentiation. And similar to murine cultures, it appears that alternative PAR2 signalling, such as bias, or intracellular signals drive the PAR2 mediated regulation of OC formation. However the exact signals which mediate this response are still not understood in human cell system.

Overall the effect of PAR2 signalling in murine OC differentiation is mirrored in human cultures, albeit with larger levels of variation. The phenotype of human OC with PAR2 activation or inhibition has not been fully explored, in terms of resorptive activity and OC associated gene transcripts. Thus whether the OC enhancement in PAR2 inhibited cultures has a predominant fusion phenotype like the murine cultures is still unknown.

7 General Discussion

This thesis explored the impact of protease dependent signalling in the myeloid/monocyte compartment. Proteases are involved in the catabolic aspect of normal tissue remodelling[402,403]. However, these proteolytic enzymes are also clinically relevant in disease such as arthritis, where their over activity can contribute to tissue destruction[404]. During inflammatory arthritis such as RA, active immune cells such as neutrophils, mast cells, and macrophages are a key source of proteases. It is now understood that in addition to these direct matrix destructive functions, proteases can also drive cell signalling and thus influence cellular behaviour through activation of PARs[405]. Thus, proteases involved in these catabolic tissue remodelling processes may also influence the remodelling activity through their action on cells involved in these processes, such as osteoclasts. Notably, PAR2 is specifically cleaved by proteases highly associated with active immune cells such as mast cell tryptase[232], and has been closely linked to the immune system and immune pathologies such as asthma[299,331], and RA[297,335,406]. Therefore, specifically, this doctoral study focused on the role of protease sensing via PAR2 in directing the differentiation of myeloid cells into bone resorbing osteoclasts. This exploration aimed to understand how proteases may contribute to bone remodelling during homeostasis and bone erosion during inflammatory disease settings via their action of PAR2. Overall, it was postulated that PAR2 was expressed by OCPs / monocytes, and activation of this receptor would impact the capacity for these cells to differentiate into OCs, and thus potentially contribute to bone erosion during articular inflammation.

The previous chapters discussed in detail the results of experiments used to explore my hypothesis and discussed the relevance of these in relation to the current literature. Taken collectively, the results of each chapter culminate to provide a bigger picture of the underlying biology and allow the original hypothesis to be refined.

Before exploring the function of PAR2 in monocytes, confirmation of the expression of this receptor was undertaken. The literature was conflicted in its reporting of PAR2 expression in leukocytes and monocytes, thus a reliable protocol and antibody for the detection of the receptor was optimised in chapter 3. In humans, PAR2 was detected on the surface plasma membrane of

monocytes. In addition, this analysis demonstrated that classical monocytes express the highest level of PAR2 on their surface. Interestingly, work conducted within the lab had previously shown that this population of monocytes has the highest osteoclastogenic potential *in vitro* (personal correspondence; Cecilia Ansalone). Confirmation of PAR2 monocyte expression enabled continuation of this work; elucidation of the function of this receptor in myeloid/monocyte populations. Due to the variable expression of PAR2 across human primary cell samples, initial functional experiments investigating the impact of this receptor in the differentiation process was conducted in murine WT and *par2*$^{-/-}$ animals. Thus, limiting the potential variability associated with human cells and providing a reliable total knockout setting, which has been used extensively in the field.

In chapter 5, *in vitro* OC cell systems were adopted; these identified that PAR2 contributed to the regulation of OC formation and prevented excessive fusion of pre-cursors into giant cells. The increased OC size and number did not have an effect on the activity of these cells; despite a greater surface area of OCs, the *par2*$^{-/-}$ differentiated cells did not result in higher levels of mineral resorption. These initial observations indicated that the presence of PAR2 is important in regulating OC fusion. In order to confirm that this mechanism was driven by active signalling of PAR2 these assays were conducted with PAR2 activating peptides or inhibitors. PAR2 inhibition in WT cells increase the size and number of OC cells to almost comparable levels found in *par2*$^{-/-}$ cells. Firstly, this suggests that endogenous proteases are present within cultures regulating the formation of OCs via PAR2. OCs are highly proteolytically active[287,407] and therefore despite no reported production of PAR2 activating proteases by OCs, there is a high probability that activating proteases are released by these cells. Similar OC assays have been conducted with *par1*$^{-/-}$ murine BM cells[380]. Enhancements in OC formation were observed in these cultures without the addition of exogenous proteases or activating peptides, further supporting the probability of PAR cleaving protease production by OCs or their pre-cursors. Moreover, OCs generated in *par1*$^{-/-}$ cells are also dramatically enhanced in size, similar to those observed in the *par2*$^{-/-}$. The conclusions drawn by the authors of the *par1*$^{-/-}$ OC work are similar to the conclusions reached from *par2*$^{-/-}$ cultures in this study. Endogenous protease signalling appears to limit excessive fusion of pre-cursors without having an impact on other OC driving factors such as NFATc1

expression. The gene expression analysis of OC-associated transcripts conducted in WT and *par2*$^{-/-}$ (chapter 5, see section 5.2.3) demonstrate that there are no significant differences. Overall, this suggests a phenomenon more consistent with altered fusion; potentially via cytoskeletal rearrangement and cell-cell adhesion driving enhanced OC formation.

Interestingly, activating peptide FLIGRL did not further limit the size or number of OC in this assay. This indicated that further canonical stimulation of this receptor had no impact in OC formation. The potential conclusions from this were multi-fold; (a) PAR2 stimulation was at a maximum within this culture and no impact could be observed from additional activation, (b) non-canonical activation of the receptor is driving OC limitation, and/or (c) PAR2 activation is occurring inside the cell, where small molecule inhibitors can gain access but peptides cannot. Which, if any of these hypotheses are correct, has not yet been determined. Furthermore, there is nothing gleaned from prior studies as, for example, the study of *par1*$^{-/-}$ cells did not add any exogenous PAR1 activators to their culture for comparison[380]. However, other potential associations can be inferred from prior studies. For instance, Gα13 signals have been shown to limit OC formation, with RNA-seq highlighting cytoskeletal pathway involvement[375]. Combined with the knowledge that bias signalling of PAR2 via elastase cleavage preferentially drives Gα12/13[408], this may support the suggestion of non-canonical PAR2 signals limiting OC fusion and formation. This hypothesis merits further investigation and may provide insights into the potential pathways which link PAR2 and the excessive fusion phenotype observed. To test this it would be interesting to measure the levels of Gα13 activity in both WT and *par2*$^{-/-}$ cultures to identify if there are any changes in this signalling mechanism.

The OC work discussed above was conducted with NA cells of the murine BM, as defined by their lack of adhesion after overnight culture of the total BM. Even though NA-BM cell assays are the most consistently used in the field they are not without limitations. These cultures are mixed in their cellular content, meaning other immune cells and also stromal cells, which have incidentally been carried over, can influence osteoclastogenesis. Stromal cells and T cells are a key source of OC stimulating factor RANKL and can therefore be highly influential in this assay. In addition, the reliance on cellular adherence in initial overnight cultures

to determine what cells are taken forward can introduce variability before the differentiation process has even begun. This is especially problematic if cellular adhesion is impacted by the loss of PAR2 in knockout cells. In order to try and reduce these limitations a co-culture assay was set up. This had a more precise combination of cell types, with stromal cells intentionally added to the culture and monocytes specifically selected from the BM using negative isolation kits, thus overall limiting the impact of cellular adhesion in the overnight pre-differentiation step.

The data generated in this assay demonstrated that the presence of PAR2 in the stromal OB-like cell was also regulating OC formation. The only observable difference between WT and *par2*$^{-/-}$ OB-like cells, out of all of the parameters analysed, was their production of osteopontin. Interestingly, osteopontin is an extracellular matrix component that OCs depend on for their adhesion to the bone tissue. This further suggests a role for PAR2 signalling in limiting the adhesion of OCPs or OCs, which in turn could limit their fusion potential. Overall, the data presented in this thesis clearly indicates that during homeostatic conditions PAR2 limits the formation of giant OC cells via both direct induction of OC formation and OB-driven OC formation (Figure 7.1). It is suggested but not yet confirmed that this could be driven by adhesion or migratory-associated mechanisms. Taking an unbiased approach to analyse the differences in major pathways between WT and *par2*$^{-/-}$ OCs and stromal-OB, such as RNA-seq, would potentially enable the identification of cellular adhesion / migration and/or cytoskeletal remodelling that are impacted by the absence of this receptor. Moreover, this method could identify other potentially overlooked pathways that PAR2 could influence to regulate the formation of OCs and perhaps point us in the right direction in terms of identifying a mechanism which connects the PAR2 signal and the process of OC formation.

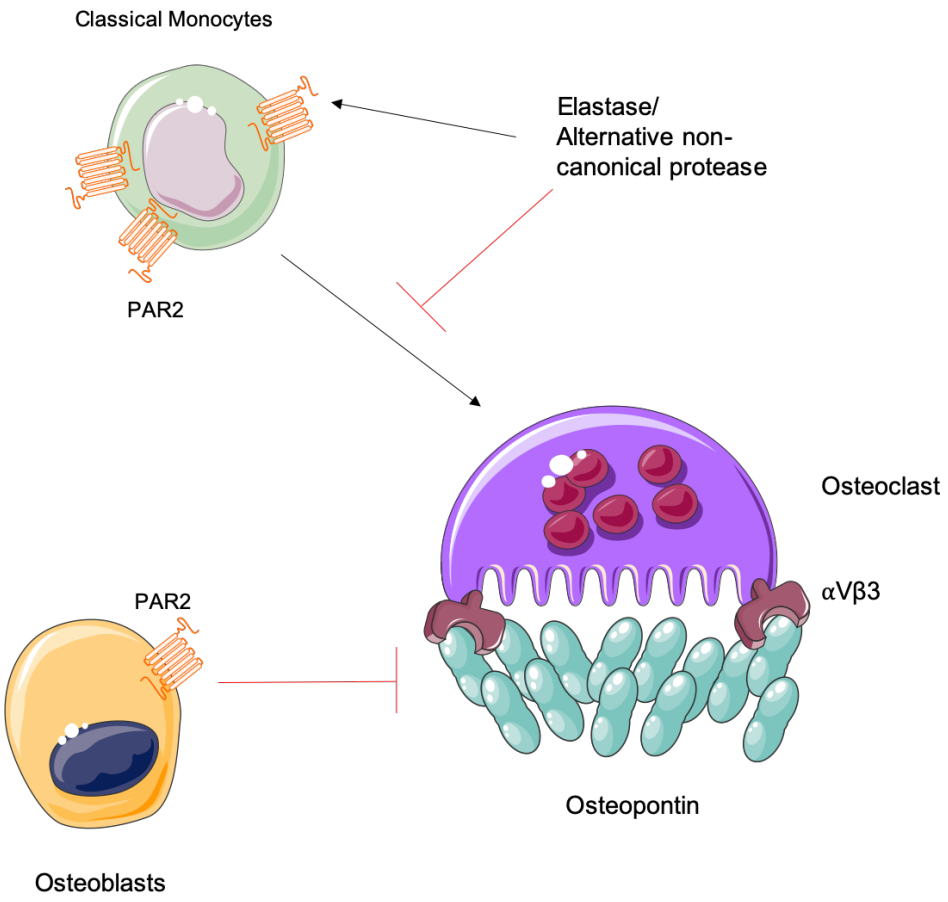

Figure 7.1 PAR2 Limits Osteoclast Formation Through Both Stromal and Hematopoietic Arms of the Bone Remodelling Unit
PAR2 is expressed by monocytes (OCPs) and through non-canonical activation of this receptor the fusion and formation of OC is limited, preventing excessive OC formation. In addition the presence of PAR2 in OB-like stromal cells also limits stromal driven OC formation. One potential mode of action is via the release of osteopontin, a key extracellular matrix component required for OC binding to bone tissue via αVβ3 integrins. PAR2 signalling limits osteopontin production, which regulates the adhesion of OCs and limits the potential ligands for αVβ3 integrin signals.

While PAR2 limits OC formation during homeostasis, its actions are reversed when paired with inflammatory signals such as TNF, where PAR2 appears to drive enhanced OC formation (Figure 7.2). In *par2*$^{-/-}$ cultures, TNF still drives enhancement of OC formation, however, this is limited in comparison with WT cultures, indicating that protease signalling in this instance is driving OC formation. This is where the role of PAR2 in OC formation differs from the role of PAR1. Unlike PAR2 KO BM cells, par1$^{-/-}$ cell cultures have significantly higher OC formation in response to TNF driven inflammatory osteoclastogenesis over their WT counterparts. Therefore, this suggests that PARs are functioning through different mechanisms during TNF-enhanced OC formation. How the role of PAR2 becomes reversed in this environment is unknown, as due to time limitations, this was not explored in any greater detail. It is possible that TNF

signalling influences the action of PAR2 in various ways. For example, TNF may impact the proteases released by OCPs, which instead of driving the same "non-canonical" response proposed previously during homeostasis could drive an alternate PAR2 signal, which supports the OC differentiation process. In addition, the TNF signal could promote or limit the heterodimerisation of PAR2 with other receptors such as PAR1[409], or EPCR[410], all known to dimerise with the receptor and influence its function. Furthermore, it is possible that PAR2 signalling works to enhance TNF signalling. PAR2 has been reported to activate NFkB [398] (see chapter 1, section 1.4.2), so this may act to support the TNF-driven NFkB signal. Overall, due to limited time, the present studies have not identified the mode of action during TNF-driven inflammation that drives an alternate activity of PAR2 to promote OC formation. However, the potential drivers of this change mentioned above should be investigated further in order to fully understand the role of PAR2 in inflammatory-driven OC formation.

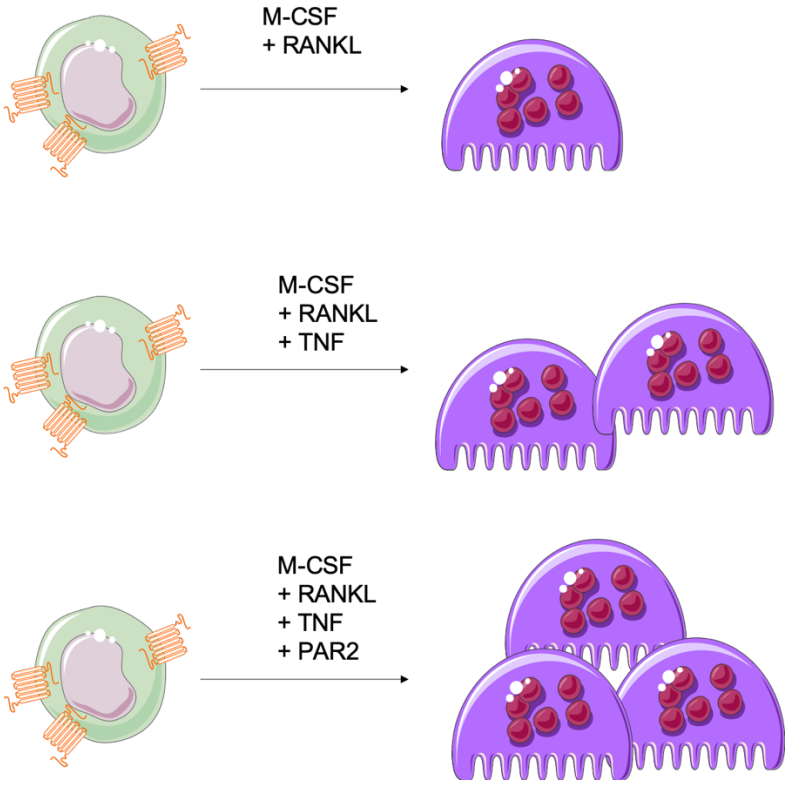

Figure 7.2 PAR2 Further Enhances Inflammatory-driven OC formation
TNF enhances the capacity for OC formation if OCPs are exposed to this cytokine at the right time. The data presented in this thesis indicates that PAR2 activity further enhances the TNF-driven OC formation, resulting in highly excessive OC formation.

Finally, in chapter 6, using human OC cultures paired with PAR2 activating peptides and inhibitors, studies confirmed that the observations made in murine system were translatable to the human system. OC formation was enhanced in AZ8838 treated human homeostatic M-CSF and RANKL alone assays. In turn PAR2 inhibition slightly limited the number of OCs formed during inflammatory TNF OC assays. However, this observation did not reach significance, and reductions over untreated cells were minor but still consistent. Due to the limited reduction in human OC numbers and the high level of variability in the number of OC generated by different human donors, this experiment will require a high sample number to achieve appropriate power. Therefore, it would be valuable to increase the number of human samples in the TNF inflammatory experiment to confirm this finding. However, gaining statistical significance in this observation does not confirm biological relevance. The requirement for high sample number is partially driven by the small impact PAR2 inhibition has on OC number (mean percentage decrease in OC number was 23% with a standard deviation of 3.8. The limited impact *in vitro* of PAR2 inhibition on human OC formation during TNF driven osteoclastogenesis may imply limited biological impact of PAR2 signalling in this process. Despite the influence of PAR2 on OC size in murine cultures, the size of human OCs was not investigated. Human OCs boundaries are not as clearly defined by TRAP stain as the murine OC and therefore cell size is very difficult to analyse. Further exploration of the impact on PAR2 inhibition in human OC differentiation would be valuable. One method to test the migration and fusion capacity of these cells in response to PAR2 stimuli could be to limit the cell number in these cultures and assess the ability of monocytes to form OCs in the presence of PAR2 inhibitors. If the processes of migration and adhesion required for OC formation is impacted by PAR2 activity, there will be a more profound impact on OC number when cell numbers are limited. If precursor cells are not in close proximity, or touching, these cells will be more dependent upon cellular migration in order to fuse, therefore this older technique[59,60] may be valuable as a starting point for human OC assays to assess fusion and migratory capacity influenced by PAR2.

In conclusion, PAR2 signalling does impact OC formation. Across the various chapters of this thesis I have identified that PAR2 limits OC formation during homeostasis and enhances it when paired with inflammatory signals i.e., TNF.

Activity of the receptor is triggered endogenously, through proteases produced by OCPs or OCs themselves, which could potentially drive non-canonical activity of the receptor to regulate OC formation. In addition, I confirmed that human OCPs (monocytes) express high levels of PAR2, and this receptor functions in the same way as the murine receptor. When PAR2 was inhibited, OC formation was significantly increased in homeostatic human OC formation, while a moderate reduction in OC formation was identified during inflammatory TNF-driven OC formation. Further work is required to fully identify the mechanism and pathways that link PAR2 activity and OC formation, but based on the observations made in this thesis, I propose that the influence of PAR2 in cellular adhesion, migration, and cytoskeletal rearrangement and the impact this has on OC formation warrants further investigation. Unfortunately the role of PAR2 during inflammatory-driven OC formation could not be fully explored within this thesis, however, the preliminary data suggesting an alternate role for PAR2 in this environment also warrants further investigation in order to fully understand the role of PAR2 during inflammatory bone erosion.

Appendix – Media, Buffers and Reagents

1X Phosphate Buffered Saline pH 7.4 (PBS): 8g NaCl (Sodium chloride, MW 58.44g/mol), 0.2g KCl (potassium chloride, MW 74.5513 g/mol), 0.2g KH_2PO_4 (Monopotassium phosphate, MW 136.086 g/mol) and 1.74g Na_2HPO_4 (Disodium phosphate, MW 141.96g/mol) in 1L dH_2O.

Protein Lysis buffer: 400µl RIPA buffer (Thermo #89900) supplemented with 4µl HALT Phosphatase and Protease inhibitor cocktail (100x) (Thermo #78440)

Protein Gel Electrophoresis Running buffer: 25ml MOPS SDS Running Buffer (20x) Novex (CAT #NP0001) in 475ml distilled water.

Western Blot Wash buffer (PBST 5%): 5ml Tween-20 in 95ml 1XPBS

Western Blot Blocking Buffer (PBST 5% milk): 5g milk solids in 100ml PBS-T 5%

Antibody Dilution Buffer (PBST 5% BSA): 5g Bovine Serum Albumin (BSA; ThermoFisher; UK) in 100ml PBS-T 5%.

Cell Permeabilising Buffer for IF microscopy: 20µl of Triton X-100 in 10ml 1XPBS (0.2%)

IF Microscopy Blocking Buffer: 48.5ml 1XPBS , 1ml goat serum (5%), 50µl Tween 20 (0.1%)

0.5M EDTA Solution: 168.12g EDTA (Ethylenediaminetetraacetic acid; MW 292.24 g/mol) in 1L dH_20

FACS Buffer: 489.5ml 1XPBS supplemented with 5ml Foetal Bovine Serum (FBS; Life Sciences, UK; 1%), 500µl NaN_3 (0.1%) and 5ml of 0.5M EDTA (5mM).

FACS Buffer for Intracellular Stain: 495ml 1X PBS supplemented with 5ml Foetal Bovine Serum (FBS; Life Sciences, UK; 1%).

RNA lysis buffer: 10ml RLT containing 100µl β-mercaptoethanol (1%).

2% Agarose ethidium bromide gel: 2.6g agarose (Bio-rad; UK) and 2μl ethidium bromide (10mg/ml stock solution, ThermoFisher; UK), 55g of Boric acid (Fisher Scientific, UK), 9.3g ethylenediaminetetraacetic (EDTA, Fisher Scientific, UK), made up to 1L with dH_2O.

Tris-Acetate-EDTA (TAE) pH 8 Buffer: 4.84 g Tris Base, 1.14 ml glacial acetic acid and 0.37 g EDTA in 1L dH_20.

TRAP staining solution: 25μl Fast Garnet GBC Base solution and 25μl $NaNO_2$, mixed for 2 minutes. 4.5 ml warm dH_20 with 50μl Fast Garnet/$NaNO_2$ solution, 50μl Napthol As-Bi Phosphoric acid solution, 200μl Acetate solutions, and 250μl 1M Tartrate solution.

1M Tartrate solution: 2.8g of K-Na Tartrate tetrahidrate (MW 282.23; $C_4H_4KNaO_6*4H_2O$) in 10ml dH_2O.

4% Buffered formalin: For 100ml: 25ml citrate solution (Citric acid, 18 mmol/l, sodium citrate, 9mmol/l, sodium chloride, 12 mmol/l, and surfactant, pH 3.6 ± 0.1), 10ml of 37% formaldehyde and 65ml acetone.

Complete alpha Minimum Essential Media (complete α-MEM): Supplemented with 10% Fetal Bovine Serum (FBS; Life Sciences, UK), 0.02mM L-glutamine, 10U/ml Penicillin, and 0.1μg/ml Streptomycin

Complete DMEM: DMEM (Dulbecco modified essential medium; Life technology, Thermo Fisher Scientific, UK) supplemented with 10% Foetal Bovine Serum (FBS; Life Sciences, UK), 0.02mM L-glutamine, 10U/ml Penicillin, and 0.1μg/ml Streptomycin

Complete RPMI: RPMI 1640 (No glutamine; Life technology, Thermo Fisher Scientific, UK) supplemented with 10% Foetal Bovine Serum (FBS; Life Sciences, UK), 0.02mM L-glutamine, 10U/ml Penicillin, and 0.1μg/ml Streptomycin

Cell separation buffer: 489 ml sterile DPBS (Dulbecco's Phosphate-Buffered Saline; Life Technologies, UK), 5ml Foetal Bovine Serum (1% FBS; Life Sciences, UK) and 1ml 0.5M EDTA (1mM)

Calvarial Digestion Media: 1mg/ml of Collagenase II (Lorne Laboratories Limited, UK) dissolved in FBS free, α-MEM media

Static Adhesion Medium: 500ml RPMI1640 (No glutamine; Life technology, Thermo Fisher Scientific, UK) 0.5g BSA (0.1%), 2.383g HEPES (20mM; pH 7.25), and 95.2mg $MgCl_2$ (2mM)

Static Adhesion Assay Wash Buffer: 2.5L PBS, 476mg $MgCl_2$ (2mM)

Static Adhesion Lysis Buffer: 3mg/ml para-nitrophenyl phosphate (PNP) in 1%TritonX-100/50nM acetate buffer (pH5)

List of References

1. Henderson, R. B., Hobbs, J. A. R., Mathies, M. & Hogg, N. Rapid recruitment of inflammatory monocytes is independent of neutrophil migration. *Blood* **102,** 328–335 (2003).
2. van Furth, R. & Cohn, Z. A. The Origin and Kinetics of Mononuclear Phagocytes. *Journal of Experimental Medicine* **128,** 415–435 (1968).
3. Perdiguero, E. G. *et al*. Tissue-resident macrophages originate from yolk-sac-derived erythro-myeloid progenitors. *Nature* **518,** 547–551 (2015).
4. Hoeffel, G. *et al*. Adult Langerhans cells derive predominantly from embryonic fetal liver monocytes with a minor contribution of yolk sac–derived macrophages. *Journal of Experimental Medicine* **209,** 1167–1181 (2012).
5. Schulz, C. *et al*. A Lineage of Myeloid Cells Independent of Myb and Hematopoietic Stem Cells. *Science* **336,** 86–90 (2012).
6. Guilliams, M. *et al*. Alveolar macrophages develop from fetal monocytes that differentiate into long-lived cells in the first week of life via GM-CSF. *Journal of Experimental Medicine* **210,** 1977–1992 (2013).
7. Mass, E. Delineating the origins, developmental programs and homeostatic functions of tissue-resident macrophages. *International Immunology* **73,** 120 (2018).
8. Lavin, Y., Mortha, A., Rahman, A. & Merad, M. Regulation of macrophage development and function in peripheral tissues. *Nat. Rev. Immunol.* **15,** 731–744 (2015).
9. Ginhoux, F. & Jung, S. Monocytes and macrophages: developmental pathways and tissue homeostasis. *Nat. Rev. Immunol.* **14,** 392–404 (2014).
10. Guilliams, M. *et al*. Dendritic cells, monocytes and macrophages: a unified nomenclature based on ontogeny. *Nat. Rev. Immunol.* **14,** 571–578 (2014).
11. Anderson, K. L. *et al*. Myeloid development is selectively disrupted in PU.1 null mice. *Blood* **91,** 3702–3710 (1998).
12. Lee, J. *et al*. Restricted dendritic cell and monocyte progenitors in human cord blood and bone marrow. *Journal of Experimental Medicine* **212,** 385–399 (2015).
13. Hettinger, J. *et al*. Origin of monocytes and macrophages in a committed progenitor. *Nature Immunology* **14,** 821–830 (2013).
14. Serbina, N. V. & Pamer, E. G. Monocyte emigration from bone marrow during bacterial infection requires signals mediated by chemokine receptor CCR2. *Nature Immunology* **7,** 311–317 (2006).
15. Passlick, B., Flieger, D. & Ziegler-Heitbrock, H. W. Identification and characterization of a novel monocyte subpopulation in human peripheral blood. *Blood* **74,** 2527–2534 (1989).
16. Ziegler-Heitbrock, L. *et al*. Nomenclature of monocytes and dendritic cells in blood. *Blood* **116,** e74–80 (2010).
17. Weber, C. *et al*. Differential chemokine receptor expression and function in human monocyte subpopulations. *J. Leukoc. Biol.* **67,** 699–704 (2000).

18. Lu, B. *et al*. Abnormalities in Monocyte Recruitment and Cytokine Expression in Monocyte Chemoattractant Protein 1–deficient Mice. *Journal of Experimental Medicine* **187,** 601–608 (1998).
19. Kurihara, T., Warr, G., Loy, J. & Bravo, R. Defects in Macrophage Recruitment and Host Defense in Mice Lacking the CCR2 Chemokine Receptor. *Journal of Experimental Medicine* **186,** 1757–1762 (1997).
20. Kuziel, W. A. *et al*. Severe reduction in leukocyte adhesion and monocyte extravasation in mice deficient in CC chemokine receptor 2. *PNAS* **94,** 12053–12058 (1997).
21. Landsman, L. *et al*. CX3CR1 is required for monocyte homeostasis and atherogenesis by promoting cell survival. *Blood* **113,** 963–972 (2009).
22. Strauss-Ayali, D., Conrad, S. M. & Mosser, D. M. Monocyte subpopulations and their differentiation patterns during infection. *J. Leukoc. Biol.* **82,** 244–252 (2007).
23. Belge, K.-U. *et al*. The proinflammatory CD14+CD16+DR++ monocytes are a major source of TNF. *The Journal of Immunology* **168,** 3536–3542 (2002).
24. Narasimhan, P. B., Marcovecchio, P., Hamers, A. A. J. & Hedrick, C. C. Nonclassical Monocytes in Health and Disease. *Annu. Rev. Immunol.* **37,** 439–456 (2019).
25. Auffray, C. *et al*. Monitoring of blood vessels and tissues by a population of monocytes with patrolling behavior. *Science* **317,** 666–670 (2007).
26. Yona, S. *et al*. Fate Mapping Reveals Origins and Dynamics of Monocytes and Tissue Macrophages under Homeostasis. *Immunity* **38,** 79–91 (2013).
27. Geissmann, F., Jung, S. & Littman, D. R. Blood Monocytes Consist of Two Principal Subsets with Distinct Migratory Properties. *Immunity* **19,** 71–82 (2003).
28. Gren, S. T. *et al*. A Single-Cell Gene-Expression Profile Reveals Inter-Cellular Heterogeneity within Human Monocyte Subsets. *PLoS ONE* **10,** e0144351 (2015).
29. Villani, A.-C. *et al*. Single-cell RNA-seq reveals new types of human blood dendritic cells, monocytes, and progenitors. *Science* **356,** eaah4573 (2017).
30. Horton, J. E., Raisz, L. G., Simmons, H. A., Oppenheim, J. J. & Mergenhagen, S. E. Bone Resorbing Activity in Supernatant Fluid from Cultured Human Peripheral Blood Leukocytes. *Science* **177,** 793–795 (1972).
31. Arron, J. R. & Choi, Y. Bone versus immune system. *Nature* **408,** 535–536 (2000).
32. Crotti, T. N., Dharmapatni, A. A. S. S. K., Alias, E. & Haynes, D. R. Osteoimmunology: Major and Costimulatory Pathway Expression Associated with Chronic Inflammatory Induced Bone Loss. *Journal of Immunology Research* **2015,** (2015).
33. Goldring, S. R. *et al*. Bone remodelling in inflammatory arthritis. *Ann. Rheum. Dis.* **72,** ii52–ii55 (2013).
34. Terpos, E., Ntanasis-Stathopoulos, I., Gavriatopoulou, M. & Dimopoulos, M. A. Pathogenesis of bone disease in multiple myeloma: from bench to bedside. *Blood Cancer Journal* **8,** 1–12 (2018).
35. Walker, D. G. Congenital osteopetrosis in mice cured by parabiotic union with normal siblings. *Endocrinology* **91,** 916–920 (1972).

36. Walker, D. G. Bone resorption restored in osteopetrotic mice by transplants of normal bone marrow and spleen cells. *Science* **190,** 784–785 (1975).
37. Walker, D. G. Control of bone resorption by hematopoietic tissue. The induction and reversal of congenital osteopetrosis in mice through use of bone marrow and splenic transplants. *Journal of Experimental Medicine* **142,** 651–663 (1975).
38. Tinkler, S. M., Linder, J. E., Williams, D. M. & Johnson, N. W. Formation of osteoclasts from blood monocytes during 1 alpha-OH Vit D-stimulated bone resorption in mice. *J. Anat.* **133,** 389–396 (1981).
39. Zallone, A. Z., Teti, A. & Primavera, M. V. Monocytes from circulating blood fuse in vitro with purified osteoclasts in primary culture. *J. Cell. Sci.* **66,** 335–342 (1984).
40. Yoshida, H. *et al.* The murine mutation osteopetrosis is in the coding region of the macrophage colony stimulating factor gene. *Nature* **345,** 442–444 (1990).
41. Kong, Y.-Y. *et al.* Activated T cells regulate bone loss and joint destruction in adjuvant arthritis through osteoprotegerin ligand. *Nature* **402,** 304–309 (1999).
42. Kawai, T. *et al.* B and T Lymphocytes Are the Primary Sources of RANKL in the Bone Resorptive Lesion of Periodontal Disease. *Am. J. Pathol.* **169,** 987–998 (2006).
43. Chen, Y. *et al.* Increased RANKL expression in peripheral T cells is associated with decreased bone mineral density in patients with COPD. *Int. J. Mol. Med.* **38,** 585–593 (2016).
44. Kong, Y.-Y. *et al.* OPGL is a key regulator of osteoclastogenesis, lymphocyte development and lymph-node organogenesis. *Nature* **397,** 315–323 (1999).
45. Dougall, W. C. *et al.* RANK is essential for osteoclast and lymph node development. *Genes Dev.* **13,** 2412–2424 (1999).
46. Lam, J. *et al.* TNF-α induces osteoclastogenesis by direct stimulation of macrophages exposed to permissive levels of RANK ligand. *J. Clin. Invest.* **106,** 1481–1488 (2000).
47. Tamura, T. *et al.* Soluble interleukin-6 receptor triggers osteoclast formation by interleukin 6. *PNAS* **90,** 11924–11928 (1993).
48. Yago, T. *et al.* IL-17 induces osteoclastogenesis from human monocytes alone in the absence of osteoblasts, which is potently inhibited by anti-TNF-α antibody: A novel mechanism of osteoclastogenesis by IL-17. *Journal of Cellular Biochemistry* **108,** 947–955 (2009).
49. Takayanagi, H. *et al.* T-cell-mediated regulation of osteoclastogenesis by signalling cross-talk between RANKL and IFN-gamma. *Nature* **408,** 600–605 (2000).
50. Wei, S., Wang, M. W.-H., Teitelbaum, S. L. & Ross, F. P. Interleukin-4 reversibly inhibits osteoclastogenesis via inhibition of NF-kappa B and mitogen-activated protein kinase signaling. *J. Biol. Chem.* **277,** 6622–6630 (2002).
51. Al-Rasheed, A., Scheerens, H., Srivastava, A. K., Rennick, D. M. & Tatakis, D. N. Accelerated alveolar bone loss in mice lacking interleukin-10: late onset. *J. Periodont. Res.* **39,** 194–198 (2004).

52. Horwood, N. J., Elliott, J., Martin, T. J. & Gillespie, M. T. IL-12 alone and in synergy with IL-18 inhibits osteoclast formation in vitro. *The Journal of Immunology* **166,** 4915–4921 (2001).
53. Manicourt, D. H. *et al*. Levels of circulating tumor necrosis factor alpha and interleukin-6 in patients with rheumatoid arthritis. Relationship to serum levels of hyaluronan and antigenic keratan sulfate. *Arthritis Rheum.* **36,** 490–499 (1993).
54. Gilbert, L. *et al*. Inhibition of Osteoblast Differentiation by Tumor Necrosis Factor-α. *Endocrinology* **141,** 3956–3964 (2000).
55. Blin-Wakkach, C., Rouleau, M. & Wakkach, A. Roles of osteoclasts in the control of medullary hematopoietic niches. *Archives of Biochemistry and Biophysics* **561,** 29–37 (2014).
56. Zhang, J. *et al*. Identification of the haematopoietic stem cell niche and control of the niche size. *Nature* **425,** 836–841 (2003).
57. Hess, E. *et al*. RANKL Induces Organized Lymph Node Growth by Stromal Cell Proliferation. *The Journal of Immunology* **188,** 1245–1254 (2012).
58. Jacome-Galarza, C. E., Lee, S. K., Lorenzo, J. A. & Aguila, H. L. Identification, characterization, and isolation of a common progenitor for osteoclasts, macrophages, and dendritic cells from murine bone marrow and periphery. *J. Bone Miner. Res.* **28,** 1203–1213 (2013).
59. Jacquin, C., Gran, D. E., Lee, S. K., Lorenzo, J. A. & Aguila, H. L. Identification of multiple osteoclast precursor populations in murine bone marrow. *J. Bone Miner. Res.* **21,** 67–77 (2006).
60. Arai, F. *et al*. Commitment and differentiation of osteoclast precursor cells by the sequential expression of c-Fms and receptor activator of nuclear factor kappaB (RANK) receptors. *J. Exp. Med.* **190,** 1741–1754 (1999).
61. Fossati-Jimack, L. *et al*. Phagocytosis Is the Main CR3-Mediated Function Affected by the Lupus-Associated Variant of CD11b in Human Myeloid Cells. *PLoS ONE* **8,** e57082 (2013).
62. Min, K. H. P. *et al*. Negative regulation of osteoclast precursor differentiation by CD11b and ß2 integrin-B-cell lymphoma 6 signaling. *J Bone Miner Res* **28,** 135–149 (2013).
63. Charles, J. F. *et al*. Inflammatory arthritis increases mouse osteoclast precursors with myeloid suppressor function. *J. Clin. Invest.* **122,** 4592–4605 (2012).
64. Jacome-Galarza, C. E. *et al*. Developmental origin, functional maintenance and genetic rescue of osteoclasts. *Nature* **568,** 541–545 (2019).
65. Hancox, N. M. Motion picture observations on osteoclasts in vitro. *The Journal of Physiology* **110,** 205 (1949).
66. Hancox, N. M. A method for direct microscopical study of living embryo bone fragments engrafted on the chick chorioallantoic membrane. *The Journal of Physiology* **105,** 39 (1946).
67. Jee, W. S. S. & Nolan, P. D. Origin of Osteoclasts from the Fusion of Phagocytes. *Nature* **200,** 225–226 (1963).
68. Cohen, M. Observation of Formation of Giant Cells in Turtle Blood Cultures. *Am. J. Pathol.* **2,** 431 (1926).
69. Kahn, A. J., Stewart, C. C. & Teitelbaum, S. L. Contact-mediated bone resorption by human monocytes in vitro. *Science* **199,** 988–990 (1978).

70. Ishii, M., Kikuta, J., Shimazu, Y., Meier-Schellersheim, M. & Germain, R. N. Chemorepulsion by blood S1P regulates osteoclast precursor mobilization and bone remodeling in vivo. *Journal of Experimental Medicine* **207,** 2793–2798 (2010).
71. Ishii, M. *et al*. Sphingosine-1-phosphate mobilizes osteoclast precursors and regulates bone homeostasis. *Nature* **458,** 524–528 (2009).
72. Fujikawa, Y., Quinn, J. M., Sabokbar, A., McGee, J. O. & Athanasou, N. A. human osteoclast precursor circulates in the monocyte fraction | Endocrinology | Oxford Academic. *Endocrinology* **137,** 4058–4060 (1996).
73. Massey, H. M. & Flanagan, A. M. Human osteoclasts derive from CD14-positive monocytes. *Br. J. Haematol.* **106,** 167–170 (1999).
74. Sprangers, S., Schoenmaker, T., Cao, Y., Everts, V. & de Vries, T. J. Different Blood-Borne Human Osteoclast Precursors Respond in Distinct Ways to IL-17A. *J. Cell. Physiol.* **231,** 1249–1260 (2016).
75. Smith, R. *et al*. Activation of protease-activated receptor-2 leads to inhibition of osteoclast differentiation. *J. Bone Miner. Res.* **19,** 507–516 (2004).
76. Georgy, S. R. *et al*. Proteinase-activated receptor-2 is required for normal osteoblast and osteoclast differentiation during skeletal growth and repair. *Bone* **50,** 704–712 (2012).
77. Quinn, J. M. W., Whitty, G. A., Byrne, R. J., Gillespie, M. T. & Hamilton, J. A. The generation of highly enriched osteoclast-lineage cell populations. *Bone* **30,** 164–170 (2002).
78. Zach, F., Mueller, A. & Gessner, A. Production and Functional Characterization of Murine Osteoclasts Differentiated from ER-Hoxb8-Immortalized Myeloid Progenitor Cells. *PLoS ONE* **10,** e0142211 (2015).
79. Nevius, E. *et al*. Oxysterols and EBI2 promote osteoclast precursor migration to bone surfaces and regulate bone mass homeostasis. *J. Exp. Med.* **212,** 1931–1946 (2015).
80. Henriksen, K., Karsdal, M. A., Taylor, A., Tosh, D. & Coxon, F. P. in *Bone Research Protocols* 159–175 (Humana Press, Totowa, NJ, 2012). doi:10.1007/978-1-61779-415-5_11
81. BURSTONE, M. S. Histochemical demonstration of acid phosphatase activity in osteoclasts. *J. Histochem. Cytochem.* **7,** 39–41 (1959).
82. Mundy, G. R., VARANI, J., ORR, W., GONDEK, M. D. & WARD, P. A. Resorbing bone is chemotactic for monocytes. *Nature* **275,** 132–135 (1978).
83. Takahashi, N. *et al*. Osteoblastic Cells are Involved in Osteoclast Formation. *Endocrinology* **123,** 2600–2602 (1988).
84. Lagasse, E. & Weissman, I. L. Enforced Expression of Bcl-2 in Monocytes Rescues Macrophages and Partially Reverses Osteopetrosis in op/op Mice. *Cell* **89,** 1021–1031 (1997).
85. Sherr, C. J. *et al*. The c-fms proto-oncogene product is related to the receptor for the mononuclear phagocyte growth factor, CSF 1. *Cell* **41,** 665–676 (1985).
86. Schlessinger, J. Cell Signaling by Receptor Tyrosine Kinases. *Cell* **103,** 211–225 (2000).

87. Faccio, R. *et al*. M-CSF Regulates the Cytoskeleton via Recruitment of a Multimeric Signaling Complex to c-Fms Tyr-559/697/721. *J. Biol. Chem.* **282,** 18991–18999 (2007).
88. Mancini, A. *et al*. Identification of a second Grb2 binding site in the v-Fms tyrosine kinase. *Oncogene* **15,** 1565–1572 (1997).
89. Lee, A. W. M. & States, D. J. Both Src-Dependent and -Independent Mechanisms Mediate Phosphatidylinositol 3-Kinase Regulation of Colony-Stimulating Factor 1-Activated Mitogen-Activated Protein Kinases in Myeloid Progenitors. *Molecular and Cellular Biology* **20,** 6779–6798 (2000).
90. Zhou, P. *et al*. SHIP1 Negatively Regulates Proliferation of Osteoclast Precursors via Akt-Dependent Alterations in D-Type Cyclins and p27. *The Journal of Immunology* **177,** 8777–8784 (2006).
91. Lum, L. *et al*. Evidence for a Role of a Tumor Necrosis Factor-α (TNF-α)-converting Enzyme-like Protease in Shedding of TRANCE, a TNF Family Member Involved in Osteoclastogenesis and Dendritic Cell Survival. *J. Biol. Chem.* **274,** 13613–13618 (1999).
92. Xiong, J. *et al*. Soluble RANKL contributes to osteoclast formation in adult mice but not ovariectomy-induced bone loss. *Nat Commun* **9,** 1–7 (2018).
93. Armstrong, A. P. *et al*. A RANK/TRAF6-dependent Signal Transduction Pathway Is Essential for Osteoclast Cytoskeletal Organization and Resorptive Function. *J. Biol. Chem.* **277,** 44347–44356 (2002).
94. Wada, T. *et al*. The molecular scaffold Gab2 is a crucial component of RANK signaling and osteoclastogenesis. *Nat. Med.* **11,** 394–399 (2005).
95. Park, J. H., Lee, N. K. & Lee, S. Y. Current Understanding of RANK Signaling in Osteoclast Differentiation and Maturation. *Molecules and Cells* **40,** 706–713 (2017).
96. Takayanagi, H. *et al*. Induction and Activation of the Transcription Factor NFATc1 (NFAT2) Integrate RANKL Signaling in Terminal Differentiation of Osteoclasts. *Developmental Cell* **3,** 889–901 (2002).
97. Asagiri, M. *et al*. Autoamplification of NFATc1 expression determines its essential role in bone homeostasis. *Journal of Experimental Medicine* **202,** 1261–1269 (2005).
98. Kim, K., Lee, S. H., Kim, J. H., Choi, Y. & Kim, N. NFATc1 Induces Osteoclast Fusion Via Up-Regulation of Atp6v0d2 and the Dendritic Cell-Specific Transmembrane Protein (DC-STAMP). *Mol Endocrinol* **22,** 176–185 (2008).
99. Crotti, T. N. *et al*. NFATc1 regulation of the human β3 integrin promoter in osteoclast differentiation. *Gene* **372,** 92–102 (2006).
100. Kim, K. *et al*. Nuclear factor of activated T cells c1 induces osteoclast-associated receptor gene expression during tumor necrosis factor-related activation-induced cytokine-mediated osteoclastogenesis. *J. Biol. Chem.* **280,** 35209–35216 (2005).
101. Lacey, D. L. *et al*. Osteoprotegerin Ligand Is a Cytokine that Regulates Osteoclast Differentiation and Activation. *Cell* **93,** 165–176 (1998).
102. Koga, T. *et al*. Costimulatory signals mediated by the ITAM motif cooperate with RANKL for bone homeostasis. *Nature* **428,** 758–763 (2004).

103. Barrow, A. D. *et al*. OSCAR is a collagen receptor that costimulates osteoclastogenesis in DAP12-deficient humans and mice. *J. Clin. Invest*. **121,** 3505–3516 (2011).
104. Sul, O.-J. *et al*. Absence of MCP-1 leads to elevated bone mass via impaired actin ring formation. *J. Cell. Physiol*. **227,** 1619–1627 (2012).
105. Kyriakides, T. R. *et al*. The CC chemokine ligand, CCL2/MCP1, participates in macrophage fusion and foreign body giant cell formation. *Am. J. Pathol*. **165,** 2157–2166 (2004).
106. Fiorino, C. & Harrison, R. E. E-cadherin is important for cell differentiation during osteoclastogenesis. *Bone* **86,** 106–118 (2016).
107. McHugh, K. P. *et al*. Mice lacking beta3 integrins are osteosclerotic because of dysfunctional osteoclasts. *J. Clin. Invest*. **105,** 433–440 (2000).
108. Zou, W. *et al*. Syk, c-Src, the αvβ3 integrin, and ITAM immunoreceptors, in concert, regulate osteoclastic bone resorption. *J. Cell Biol*. **176,** 877–888 (2007).
109. DeFife, K. M., Jenney, C. R., Colton, E. & Anderson, J. M. Disruption of filamentous actin inhibits human macrophage fusion. *FASEB J* **13,** 823–832 (1999).
110. Yagi, M. *et al*. DC-STAMP is essential for cell–cell fusion in osteoclasts and foreign body giant cells. *Journal of Experimental Medicine* **202,** 345–351 (2005).
111. Witwicka, H. *et al*. Studies of OC-STAMP in Osteoclast Fusion: A New Knockout Mouse Model, Rescue of Cell Fusion, and Transmembrane Topology. *PLoS ONE* **10,** e0128275 (2015).
112. Blair, H. C. How the osteoclast degrades bone. *BioEssays* **20,** 837–846 (1998).
113. Blair, H. C., Teitelbaum, S. L., Ghiselli, R. & Gluck, S. Osteoclastic bone resorption by a polarized vacuolar proton pump. *Science* **245,** 855–857 (1989).
114. Bossard, M. J. *et al*. Proteolytic Activity of Human Osteoclast Cathepsin K. *J. Biol. Chem.* **271,** 12517–12524 (1996).
115. Hunt, N. P., Cunningham, S. J., Adnan, N. & Harris, M. The dental, craniofacial, and biochemical features of pyknodysostosis: A report of three new cases. *Journal of Oral and Maxillofacial Surgery* **56,** 497–504 (1998).
116. Frattini, A. *et al*. Defects in TCIRG1 subunit of the vacuolar proton pump are responsible for a subset of human autosomal recessive osteopetrosis. *Nat Genet* **25,** 343–346 (2000).
117. Chabadel, A. *et al*. CD44 and beta3 integrin organize two functionally distinct actin-based domains in osteoclasts. *Mol. Biol. Cell* **18,** 4899–4910 (2007).
118. Saltel, F., Chabadel, A., Bonnelye, E. & Jurdic, P. Actin cytoskeletal organisation in osteoclasts: a model to decipher transmigration and matrix degradation. *Eur. J. Cell Biol*. **87,** 459–468 (2008).
119. Yamamoto, M. *et al*. The Integrin Ligand Echistatin Prevents Bone Loss in Ovariectomized Mice and Rats. *Endocrinology* **139,** 1411–1419 (1998).
120. Murphy, M. G. *et al*. Effect of L-000845704, an alphaVbeta3 integrin antagonist, on markers of bone turnover and bone mineral density in

postmenopausal osteoporotic women. *J. Clin. Endocrinol. Metab.* **90,** 2022–2028 (2005).
121. Engleman, V. W. *et al.* A peptidomimetic antagonist of the alpha(v)beta3 integrin inhibits bone resorption in vitro and prevents osteoporosis in vivo. *J. Clin. Invest.* **99,** 2284–2292 (1997).
122. Sanjay, A. *et al.* Cbl Associates with Pyk2 and Src to Regulate Src Kinase Activity, αvß3 Integrin-Mediated Signaling, Cell Adhesion, and Osteoclast Motility. *J. Cell Biol.* **152,** 181–196 (2001).
123. Faccio, R., Takeshita, S., Zallone, A., Ross, F. P. & Teitelbaum, S. L. c-Fms and the alphavbeta3 integrin collaborate during osteoclast differentiation. *J. Clin. Invest.* **111,** 749–758 (2003).
124. Scott, B. L. & Pease, D. C. Electron microscopy of the epiphyseal apparatus. *The Anatomical Record* **126,** 465–495 (1956).
125. Kirstein, B., Chambers, T. J. & Fuller, K. Secretion of tartrate-resistant acid phosphatase by osteoclasts correlates with resorptive behavior. *Journal of Cellular Biochemistry* **98,** 1085–1094 (2006).
126. Ek-Rylander, B., Flores, M., Wendel, M., Heinegård, D. & Andersson, G. Dephosphorylation of osteopontin and bone sialoprotein by osteoclastic tartrate-resistant acid phosphatase. Modulation of osteoclast adhesion in vitro. *J. Biol. Chem.* **269,** 14853–14856 (1994).
127. Hayman, A. R. *et al.* Mice lacking tartrate-resistant acid phosphatase (Acp 5) have disrupted endochondral ossification and mild osteopetrosis. *Development* **122,** 3151–3162 (1996).
128. Lemma, S. *et al.* Energy metabolism in osteoclast formation and activity. *Int. J. Biochem. Cell Biol.* **79,** 168–180 (2016).
129. Choi, Y., Faccio, R., Teitelbaum, S. L. & Takayanagi, H. in *Osteoimmunology* 41–70 (Academic Press, 2016). doi:10.1016/B978-0-12-800571-2.00004-9
130. Karp, S. J. *et al.* Indian hedgehog coordinates endochondral bone growth and morphogenesis via parathyroid hormone related-protein-dependent and -independent pathways. *Development* **127,** 543–548 (2000).
131. Tu, X. *et al.* Noncanonical Wnt Signaling through G Protein-Linked PKCδ Activation Promotes Bone Formation. *Developmental Cell* **12,** 113–127 (2007).
132. Rutkovskiy, A., Stensløkken, K.-O. & Vaage, I. J. Osteoblast Differentiation at a Glance. *Med Sci Monit Basic Res* **22,** 95–106 (2016).
133. Zhou, X. *et al.* Chondrocytes Transdifferentiate into Osteoblasts in Endochondral Bone during Development, Postnatal Growth and Fracture Healing in Mice. *PLOS Genetics* **10,** e1004820 (2014).
134. Yang, L., Tsang, K. Y., Tang, H. C., Chan, D. & Cheah, K. S. E. Hypertrophic chondrocytes can become osteoblasts and osteocytes in endochondral bone formation. *PNAS* **111,** 12097–12102 (2014).
135. Maes, C. & Kronenberg, H. M. *Chapter 60 – Bone Development and Remodeling. Endocrinology: Adult & Pediatric* 1038–1062.e8 (Elsevier, 2016). doi:10.1016/B978-0-323-18907-1.00060-3
136. Zaidi, M. Skeletal remodeling in health and disease. *Nat. Med.* **13,** 791–801 (2007).
137. Li, X. *et al.* Parathyroid Hormone Stimulates Osteoblastic Expression of MCP-1 to Recruit and Increase the Fusion of Pre/Osteoclasts. *J. Biol. Chem.* **282,** 33098–33106 (2007).

138. Ma, Y. L. *et al*. Catabolic Effects of Continuous Human PTH (1–38) in Vivols Associated with Sustained Stimulation of RANKL and Inhibition of Osteoprotegerin and Gene-Associated Bone Formation. *Endocrinology* **142,** 4047–4054 (2001).
139. Kim, N., Takami, M., Rho, J., Josien, R. & Choi, Y. A Novel Member of the Leukocyte Receptor Complex Regulates Osteoclast Differentiation. *Journal of Experimental Medicine* **195,** 201–209 (2002).
140. Ikeda, K. & Takeshita, S. Factors and Mechanisms Involved in the Coupling from Bone Resorption to Formation: How Osteoclasts Talk to Osteoblasts. *Journal of Bone Metabolism* **21,** 163–167 (2014).
141. Matsuoka, K., Park, K. A., Ito, M., Ikeda, K. & Takeshita, S. Osteoclast-Derived Complement Component 3a Stimulates Osteoblast Differentiation. *J Bone Miner Res* **29,** 1522–1530 (2014).
142. Takeshita, S. *et al*. Osteoclast-secreted CTHRC1 in the coupling of bone resorption to formation. *J. Clin. Invest*. **123,** 3914–3924 (2013).
143. Ryu, J. *et al*. Sphingosine 1-phosphate as a regulator of osteoclast differentiation and osteoclast–osteoblast coupling. *The EMBO Journal* **25,** 5840–5851 (2006).
144. Ikebuchi, Y. *et al*. Coupling of bone resorption and formation by RANKL reverse signalling. *Nature* **561,** 195–200 (2018).
145. Raggatt, L. J. & Partridge, N. C. Cellular and Molecular Mechanisms of Bone Remodeling. *J. Biol. Chem.* **285,** 25103–25108 (2010).
146. Bonewald, L. F. Osteocytes as Dynamic Multifunctional Cells. *Annals of the New York Academy of Sciences* 281–290 (2007).
147. Plotkin, L. I. Apoptotic Osteocytes and the Control of Targeted Bone Resorption. *Curr Osteoporos Rep* **12,** 121–126 (2014).
148. Heino, T. J., Hentunen, T. A. & Väänänen, H. K. Osteocytes inhibit osteoclastic bone resorption through transforming growth factor-ß: Enhancement by estrogen*. *Journal of Cellular Biochemistry* **85,** 185–197 (2002).
149. Swarthout, J. T., D'Alonzo, R. C., Selvamurugan, N. & Partridge, N. C. Parathyroid hormone-dependent signaling pathways regulating genes in bone cells. *Gene* **282,** 1–17 (2002).
150. Jordan, L. A. *et al*. Inhibition of CCL3 abrogated precursor cell fusion and bone erosions in human osteoclast cultures and murine collagen-induced arthritis. *Rheumatology* **57,** 2042–2052 (2018).
151. Tran Van, P., Vignery, A. & Baron, R. An electron-microscopic study of the bone-remodeling sequence in the rat. *Cell Tissue Res.* **225,** 283–292 (1982).
152. Everts, V. *et al*. The bone lining cell: its role in cleaning Howship's lacunae and initiating bone formation. *J. Bone Miner. Res.* **17,** 77–90 (2002).
153. Zhao, C. *et al*. Bidirectional ephrinB2-EphB4 signaling controls bone homeostasis. *Cell Metabolism* **4,** 111–121 (2006).
154. Lerner, U. H., Kindstedt, E. & Lundberg, P. The critical interplay between bone resorbing and bone forming cells. *J. Clin. Periodontol.* **46 Suppl 21,** 33–51 (2019).
155. van Bezooijen, R. L., Papapoulos, S. E. & Löwik, C. W. G. M. Bone morphogenetic proteins and their antagonists: the sclerostin paradigm. *J. Endocrinol. Invest.* **28,** 15–17 (2005).

156. Furuya, M. *et al*. Direct cell-cell contact between mature osteoblasts and osteoclasts dynamically controls their functions in vivo. *Nat Commun* **9,** 300 (2018).
157. Compston, J. E., McClung, M. R. & Leslie, W. D. Osteoporosis. *Lancet* **393,** 364–376 (2019).
158. Reginster, J.-Y. & Burlet, N. Osteoporosis: A still increasing prevalence. *Bone* **38,** 4–9 (2006).
159. Tuck, S. P., Layfield, R., Walker, J., Mekkayil, B. & Francis, R. Adult Paget's disease of bone: a review. *Rheumatology* 2050–2059 doi:10.1093/rheumatology/kew430","keywords":["osteoporosis',"osteitis
160. Drake, M. T., Clarke, B. L. & Khosla, S. Bisphosphonates: mechanism of action and role in clinical practice. *Mayo Clin. Proc.* **83,** 1032–1045 (2008).
161. Tolar, J., Teitelbaum, S. L. & Orchard, P. J. Osteopetrosis. *The New England Journal of Medicine* 2839–2849 (2009). doi:10.1056/NEJMra040952
162. Moscatelli, I. *et al*. Targeting NSG Mice Engrafting Cells with a Clinically Applicable Lentiviral Vector Corrects Osteoclasts in Infantile Malignant Osteopetrosis. *Hum. Gene Ther.* **29,** 938–949 (2018).
163. Moskowitz, R. W. Bone remodeling in osteoarthritis: subchondral and osteophytic responses. *Osteoarthr. Cartil.* **7,** 323–324 (1999).
164. Donell, S. Subchondral bone remodelling in osteoarthritis. *EFORT Open Rev* **4,** 221–229 (2019).
165. Cox, L. G. E., van Rietbergen, B., van Donkelaar, C. C. & Ito, K. Bone structural changes in osteoarthritis as a result of mechanoregulated bone adaptation: a modeling approach. *Osteoarthr. Cartil.* **19,** 676–682 (2011).
166. Symmons, D. *et al*. The prevalence of rheumatoid arthritis in the United Kingdom: new estimates for a new century. *Rheumatology* **41,** 793–800 (2002).
167. McInnes, I. B. & Schett, G. The Pathogenesis of Rheumatoid Arthritis. *The New England Journal of Medicine* **365,** 2205–2219 (2011).
168. McAllister, K., Eyre, S. & Orozco, G. Genetics of rheumatoid arthritis: GWAS and beyond. *Open Access Rheumatol* **3,** 31–46 (2011).
169. Liao, K. P., Alfredsson, L. & Karlson, E. W. Environmental influences on risk for rheumatoid arthritis. *Curr Opin Rheumatol* **21,** 279–283 (2009).
170. Jones, V., Taylor, P. C., Jacoby, R. K. & Wallington, T. B. Synovial synthesis of rheumatoid factors and immune complex constituents in early arthritis. *Ann. Rheum. Dis.* **43,** 235–239 (1984).
171. Schellekens, G. A., de Jong, B. A., van den Hoogen, F. H., van de Putte, L. B. & van Venrooij, W. J. Citrulline is an essential constituent of antigenic determinants recognized by rheumatoid arthritis-specific autoantibodies. *J. Clin. Invest.* **101,** 273–281 (1998).
172. Nielen, M. M. J. *et al*. Specific autoantibodies precede the symptoms of rheumatoid arthritis: a study of serial measurements in blood donors. *Arthritis Rheum.* **50,** 380–386 (2004).
173. McInnes, I. B. & Schett, G. Cytokines in the pathogenesis of rheumatoid arthritis. *Nat. Rev. Immunol.* **7,** 429–442 (2007).
174. Bartok, B. & Firestein, G. S. Fibroblast-like synoviocytes: key effector cells in rheumatoid arthritis. *Immunol. Rev.* **233,** 233–255 (2010).

175. Müller-Ladner, U. *et al.* Synovial fibroblasts of patients with rheumatoid arthritis attach to and invade normal human cartilage when engrafted into SCID mice. *Am. J. Pathol.* **149,** 1607–1615 (1996).
176. Bottini, N. & Firestein, G. S. Duality of fibroblast-like synoviocytes in RA: passive responders and imprinted aggressors. *Nat Rev Rheumatol* **9,** 24–33 (2013).
177. Pettit, A. R., Walsh, N. C., Manning, C., Goldring, S. R. & Gravallese, E. M. RANKL protein is expressed at the pannus-bone interface at sites of articular bone erosion in rheumatoid arthritis. *Rheumatology* **45,** 1068–1076 (2006).
178. Schett, G. Cells of the synovium in rheumatoid arthritis. Osteoclasts. *Arthritis Res. Ther.* **9,** 203 (2007).
179. Behrens, F. *et al.* Imbalance in distribution of functional autologous regulatory T cells in rheumatoid arthritis. *Ann. Rheum. Dis.* **66,** 1151–1156 (2007).
180. Schröder, A. E., Greiner, A., Seyfert, C. & Berek, C. Differentiation of B cells in the nonlymphoid tissue of the synovial membrane of patients with rheumatoid arthritis. *PNAS* **93,** 221–225 (1996).
181. Seyler, T. M. *et al.* BLyS and APRIL in rheumatoid arthritis. *J. Clin. Invest.* **115,** 3083–3092 (2005).
182. Ohata, J. *et al.* Fibroblast-like synoviocytes of mesenchymal origin express functional B cell-activating factor of the TNF family in response to proinflammatory cytokines. *The Journal of Immunology* **174,** 864–870 (2005).
183. Smiljanovic, B. *et al.* The multifaceted balance of TNF-α and type I/II interferon responses in SLE and RA: how monocytes manage the impact of cytokines. *J Mol Med* **90,** 1295–1309 (2012).
184. Stuhlmüller, B. *et al.* CD11c as a transcriptional biomarker to predict response to anti-TNF monotherapy with adalimumab in patients with rheumatoid arthritis. *Clin. Pharmacol. Ther.* **87,** 311–321 (2010).
185. Rossol, M., Kraus, S., Pierer, M., Baerwald, C. & Wagner, U. The CD14(bright) CD16+ monocyte subset is expanded in rheumatoid arthritis and promotes expansion of the Th17 cell population. *Arthritis & Rheumatology* **64,** 671–677 (2012).
186. Smiljanovic, B. *et al.* Monocyte alterations in rheumatoid arthritis are dominated by preterm release from bone marrow and prominent triggering in the joint. *Ann. Rheum. Dis.* **77,** 300–308 (2018).
187. van Staa, T. P., Geusens, P., Bijlsma, J. W. J., Leufkens, H. G. M. & Cooper, C. Clinical assessment of the long-term risk of fracture in patients with rheumatoid arthritis. *Arthritis Rheum.* **54,** 3104–3112 (2006).
188. Dirven, L. *et al.* Changes in hand bone mineral density and the association with the level of disease activity in patients with rheumatoid arthritis: Bone mineral density measurements in a multicenter randomized clinical trial. *Arthritis Care & Research* **63,** 1691–1699 (2011).
189. Gravallese, E. M. *et al.* Identification of cell types responsible for bone resorption in rheumatoid arthritis and juvenile rheumatoid arthritis. *Am. J. Pathol.* **152,** 943–951 (1998).

190. Pettit, A. R. *et al*. TRANCE/RANKL Knockout Mice Are Protected from Bone Erosion in a Serum Transfer Model of Arthritis. *Am. J. Pathol.* **159,** 1689–1699 (2001).
191. Kobayashi, K. *et al*. Tumor Necrosis Factor α Stimulates Osteoclast Differentiation by a Mechanism Independent of the Odf/Rankl–Rank Interaction. *Journal of Experimental Medicine* **191,** 275–286 (2000).
192. Azuma, Y., Kaji, K., Katogi, R., Takeshita, S. & Kudo, A. Tumor necrosis factor-alpha induces differentiation of and bone resorption by osteoclasts. *J. Biol. Chem.* **275,** 4858–4864 (2000).
193. Chakraborty, S., Kloos, B., Harre, U., Schett, G. & Kubatzky, K. F. Pasteurella multocida Toxin Triggers RANKL-Independent Osteoclastogenesis. *Front Immunol* **8,** 185 (2017).
194. Cox, T. R. *et al*. The hypoxic cancer secretome induces pre-metastatic bone lesions through lysyl oxidase. *Nature* **522,** 106–110 (2015).
195. Tsukasaki, M. *et al*. LOX Fails to Substitute for RANKL in Osteoclastogenesis. *J Bone Miner Res* **32,** 434–439 (2017).
196. Tanaka, S. RANKL-Independent Osteoclastogenesis: A Long-Standing Controversy. *J Bone Miner Res* **32,** 431–433 (2017).
197. Lieben, L. Bone: The concept of RANKL-independent osteoclastogenesis refuted. *Nat Rev Rheumatol* **12,** 623–623 (2016).
198. Stolina, M. *et al*. RANKL is a Marker and Mediator of Local and Systemic Bone Loss in Two Rat Models of Inflammatory Arthritis. *J Bone Miner Res* **20,** 1756–1765 (2005).
199. Shigeyama, Y. *et al*. Expression of osteoclast differentiation factor in rheumatoid arthritis. *Arthritis Rheum.* **43,** 2523–2530 (2000).
200. Gravallese, E. M. *et al*. Synovial tissue in rheumatoid arthritis is a source of osteoclast differentiation factor. *Arthritis Rheum.* **43,** 250–258 (2000).
201. Ritchlin, C. T., Haas-Smith, S. A., Li, P., Hicks, D. G. & Schwarz, E. M. Mechanisms of TNF-α– and RANKL-mediated osteoclastogenesis and bone resorption in psoriatic arthritis. *J. Clin. Invest.* **111,** 821–831 (2003).
202. Cohen, S. B. *et al*. Denosumab treatment effects on structural damage, bone mineral density, and bone turnover in rheumatoid arthritis: A twelve-month, multicenter, randomized, double-blind, placebo-controlled, phase II clinical trial. *Arthritis Rheum.* **58,** 1299–1309 (2008).
203. Sato, K. *et al*. Th17 functions as an osteoclastogenic helper T cell subset that links T cell activation and bone destruction. *Journal of Experimental Medicine* **203,** 2673–2682 (2006).
204. Danks, L. *et al*. RANKL expressed on synovial fibroblasts is primarily responsible for bone erosions during joint inflammation. *Ann. Rheum. Dis.* **75,** 1187–1195 (2016).
205. Krishnamurthy, A. *et al*. Identification of a novel chemokine-dependent molecular mechanism underlying rheumatoid arthritis-associated autoantibody-mediated bone loss. *Ann. Rheum. Dis.* **75,** 721–729 (2016).
206. BMJ Publishing Group Ltd & Rheumatism, E. L. A. Correction: Identification of a novel chemokine-dependent molecular mechanism underlying rheumatoid arthritis-associated autoantibody-mediated bone loss. *Ann. Rheum. Dis.* **78,** 866–866 (2019).

207. Baum, R. & Gravallese, E. M. Impact of inflammation on the osteoblast in rheumatic diseases. *Curr Osteoporos Rep* **12,** 9–16 (2014).
208. Vreugdenhil, G., Lowenberg, B., van Eijk, H. G. & Swaak, A. J. G. Tumor necrosis factor alpha is associated with disease activity and the degree of anemia in patients with rheumatoid arthritis. *European Journal of Clinical Investigation* **22,** 488–493 (1992).
209. Tetta, C., Camussi, G., Modena, V., Di Vittorio, C. & Baglioni, C. Tumour necrosis factor in serum and synovial fluid of patients with active and severe rheumatoid arthritis. *Ann. Rheum. Dis.* **49,** 665–667 (1990).
210. Haraoui, B. & Bykerk, V. Etanercept in the treatment of rheumatoid arthritis. *Therapeutics and Clinical Risk Management* **3,** 99–105 (2007).
211. Fliedner, Von, V. *et al.* Production of tumor necrosis factor-α by naive or memory T lymphocytes activated via CD28. *Cell. Immunol.* **139,** 198–207 (1992).
212. Tecchio, C., Micheletti, A. & Cassatella, M. A. Neutrophil-Derived Cytokines: Facts Beyond Expression. *Front Immunol* **5,** 1–7 (2014).
213. Fahey, T. J., Turbeville, T. & McIntyre, K. Differential TNF Secretion by Wound Fibroblasts Compared to Normal Fibroblasts in Response to LPS. *Journal of Surgical Research* **58,** 759–764 (1995).
214. Mohita J Mohan *et al.* The Tumor Necrosis Factor-α Converting Enzyme (TACE): A Unique Metalloproteinase with Highly Defined Substrate Selectivity. *Biochemistry* **41,** 9462–9469 (2002).
215. Ali, T. *et al.* Clinical use of anti-TNF therapy and increased risk of infections. *Drug, Healthcare and Patient Safety* **5,** 79–99 (2013).
216. Keystone, E. C. *et al.* Radiographic, clinical, and functional outcomes of treatment with adalimumab (a human anti–tumor necrosis factor monoclonal antibody) in patients with active rheumatoid arthritis receiving concomitant methotrexate therapy: A randomized, placebo-controlled, 52-week trial. *Arthritis & Rheumatology* **50,** 1400–1411 (2004).
217. Zhao, B., Grimes, S. N., Li, S., Hu, X. & Ivashkiv, L. B. TNF-induced osteoclastogenesis and inflammatory bone resorption are inhibited by transcription factor RBP-J. *J. Exp. Med.* **209,** 319–334 (2012).
218. Li, P. & Schwarz, E. M. The TNF-α transgenic mouse model of inflammatory arthritis. *Springer Semin Immunopathol* **25,** 19–33 (2003).
219. Redlich, K. *et al.* Osteoclasts are essential for TNF-α–mediated joint destruction. *J. Clin. Invest.* **110,** 1419–1427 (2002).
220. Baud, V. & Karin, M. Signal transduction by tumor necrosis factor and its relatives. *Trends Cell Biol.* **11,** 372–377 (2001).
221. Baker, S. J. & Reddy, E. P. Modulation of life and death by the TNF receptor superfamily. *Oncogene* **17,** 3261–3270 (1998).
222. Luo, G., Li, F., Li, X., Wang, Z. G. & Zhang, B. TNF-α and RANKL promote osteoclastogenesis by upregulating RANK via the NF-κB pathway. *Mol Med Rep* **17,** 6605–6611 (2018).
223. Zhang, Y.-H., Heulsmann, A., Tondravi, M. M., Mukherjee, A. & Abu-Amer, Y. Tumor Necrosis Factor-α (TNF) Stimulates RANKL-induced Osteoclastogenesis via Coupling of TNF Type 1 Receptor and RANK Signaling Pathways. *J. Biol. Chem.* **276,** 563–568 (2001).

224. Abu-Amer, Y. *et al*. Tumor Necrosis Factor Receptors Types 1 and 2 Differentially Regulate Osteoclastogenesis. *J. Biol. Chem.* **275,** 27307–27310 (2000).
225. Vu, T.-K. H., Hung, D. T., Wheaton, V. I. & Coughlin, S. R. Molecular cloning of a functional thrombin receptor reveals a novel proteolytic mechanism of receptor activation. *Cell* **64,** 1057–1068 (1991).
226. Nystedt, S., Emilsson, K., Wahlestedt, C. & Sundelin, J. Molecular cloning of a potential proteinase activated receptor. *Proc. Natl. Acad. Sci. U.S.A.* **91,** 9208–9212 (1994).
227. Nystedt, S., Emilsson, K., Larsson, A. K., Strömbeck, B. & Sundelin, J. Molecular cloning and functional expression of the gene encoding the human proteinase-activated receptor 2. *Eur. J. Biochem.* **232,** 84–89 (1995).
228. Ishihara, H. *et al*. Protease-activated receptor 3 is a second thrombin receptor in humans. *Nature* **386,** 502–506 (1997).
229. Xu, W.-F. *et al*. Cloning and characterization of human protease-activated receptor 4. *PNAS* **95,** 6642–6646 (1998).
230. Coughlin, S. R. Thrombin signalling and protease-activated receptors. *Nature* **407,** 258–264 (2000).
231. Belham, C. M. *et al*. Trypsin stimulates proteinase-activated receptor-2-dependent and -independent activation of mitogen-activated protein kinases. *Biochem. J.* **320 (Pt 3),** 939–946 (1996).
232. Molino, M. *et al*. Interactions of Mast Cell Tryptase with Thrombin Receptors and PAR-2. *J. Biol. Chem.* **272,** 4043–4049 (1997).
233. Uehara, A., Muramoto, K., Takada, H. & Sugawara, S. Neutrophil Serine Proteinases Activate Human Nonepithelial Cells to Produce Inflammatory Cytokines Through Protease-Activated Receptor 2. *The Journal of Immunology* **170,** 5690–5696 (2003).
234. Milner, J. M. *et al*. Matriptase is a novel initiator of cartilage matrix degradation in osteoarthritis. *Arthritis Rheum.* **62,** 1955–1966 (2010).
235. Böhm, S. K. *et al*. Molecular cloning, expression and potential functions of the human proteinase-activated receptor-2. *Biochemical Journal* **314,** 1009–1016 (1996).
236. Al-Ani, B., Saifeddine, M., Kawabata, A. & Hollenberg, M. D. Proteinase activated receptor 2: Role of extracellular loop 2 for ligand-mediated activation. *Br. J. Pharmacol.* **128,** 1105–1113 (1999).
237. Marchese, A., Chen, C., Kim, Y.-M. & Benovic, J. L. The ins and outs of G protein-coupled receptor trafficking. *Trends in Biochemical Sciences* **28,** 369–376 (2003).
238. Al-Ani, B., Wijesuriya, S. J. & Hollenberg, M. D. Proteinase-activated receptor 2: differential activation of the receptor by tethered ligand and soluble peptide analogs. *J. Pharmacol. Exp. Ther.* **302,** 1046–1054 (2002).
239. Gardell, L. R. *et al*. Identification and characterization of novel small-molecule protease-activated receptor 2 agonists. *J. Pharmacol. Exp. Ther.* **327,** 799–808 (2008).
240. Seatter, M. J. *et al*. The role of the C-terminal tail in protease-activated receptor-2-mediated Ca2+ signalling, proline-rich tyrosine kinase-2 activation, and mitogen-activated protein kinase activity. *Cell. Signal.* **16,** 21–29 (2004).

241. Kanke, T. *et al*. Proteinase-activated receptor-2-mediated activation of stress-activated protein kinases and inhibitory kappa B kinases in NCTC 2544 keratinocytes. *J. Biol. Chem.* **276,** 31657–31666 (2001).
242. Scott, G. *et al*. The Proteinase-Activated Receptor-2 Mediates Phagocytosis in a Rho-Dependent Manner in Human Keratinocytes. *J Invest Dermatol* **121,** 529–541 (2003).
243. McCoy, K. L., Traynelis, S. F. & Hepler, J. R. PAR1 and PAR2 couple to overlapping and distinct sets of G proteins and linked signaling pathways to differentially regulate cell physiology. *Mol. Pharmacol.* **77,** 1005–1015 (2010).
244. DeFea, K. A. *et al*. beta-arrestin-dependent endocytosis of proteinase-activated receptor 2 is required for intracellular targeting of activated ERK1/2. *J. Cell Biol.* **148,** 1267–1281 (2000).
245. Yagi, Y. *et al*. Involvement of Rho signaling in PAR2-mediated regulation of neutrophil adhesion to lung epithelial cells. *European Journal of Pharmacology* **536,** 19–27 (2006).
246. Böhm, S. K. *et al*. Mechanisms of Desensitization and Resensitization of Proteinase-activated Receptor-2. *J. Biol. Chem.* **271,** 22003–22016 (1996).
247. Ge, L., Ly, Y., Hollenberg, M. & Defea, K. A β-Arrestin-dependent Scaffold Is Associated with Prolonged MAPK Activation in Pseudopodia during Protease-activated Receptor-2-induced Chemotaxis. *J. Biol. Chem.* **278,** 34418–34426 (2003).
248. Stalheim, L. *et al*. Multiple independent functions of arrestins in the regulation of protease-activated receptor-2 signaling and trafficking. *Mol. Pharmacol.* **67,** 78–87 (2005).
249. Ge, L., Shenoy, S. K., Lefkowitz, R. J. & Defea, K. Constitutive Protease-activated Receptor-2-mediated Migration of MDA MB-231 Breast Cancer Cells Requires Both β-Arrestin-1 and -2. *J. Biol. Chem.* **279,** 55419–55424 (2004).
250. Zoudilova, M. *et al*. β-Arrestin-dependent Regulation of the Cofilin Pathway Downstream of Protease-activated Receptor-2. *J. Biol. Chem.* **282,** 20634–20646 (2007).
251. Zoudilova, M. *et al*. β-Arrestins Scaffold Cofilin with Chronophin to Direct Localized Actin Filament Severing and Membrane Protrusions Downstream of Protease-activated Receptor-2. *J. Biol. Chem.* **285,** 14318–14329 (2010).
252. Dulon, S. *et al*. Pseudomonas aeruginosa Elastase Disables Proteinase-Activated Receptor 2 in Respiratory Epithelial Cells. *Am. J. Respir. Cell Mol. Biol.* **32,** 411–419 (2012).
253. Pham, C. T. N. Neutrophil serine proteases fine-tune the inflammatory response. *Int. J. Biochem. Cell Biol.* **40,** 1317–1333 (2008).
254. Pham, C. T. N. Neutrophil serine proteases: specific regulators of inflammation. *Nat. Rev. Immunol.* **6,** 541–550 (2006).
255. Hollenberg, M. D. *et al*. Biased signalling and proteinase-activated receptors (PARs): targeting inflammatory disease. *Br. J. Pharmacol.* **171,** 1180–1194 (2014).
256. Zhao, P. *et al*. Cathepsin S Causes Inflammatory Pain via Biased Agonism of PAR2 and TRPV4. *J. Biol. Chem.* **289,** 27215–27234 (2014).
257. Jiang, Y. *et al*. Biased Signaling by Agonists of Protease Activated Receptor 2. *ACS Chem. Biol.* **12,** 1217–1226 (2017).

258. Nguyen, T. D. *et al*. Trypsin activates pancreatic duct epithelial cell ion channels through proteinase-activated receptor-2. *J. Clin. Invest.* **103,** 261–269 (1999).
259. Fiorucci, S. *et al*. PAR-2 modulates pepsinogen secretion from gastric-isolated chief cells. *Am. J. Physiol. Gastrointest. Liver Physiol.* **285,** G611–G620 (2003).
260. Kawabata, A. *et al*. The protease-activated receptor-2 agonist induces gastric mucus secretion and mucosal cytoprotection. *J. Clin. Invest.* **107,** 1443–1450 (2001).
261. Kawabata, A. *et al*. Activation of Protease-Activated Receptor-2 (PAR-2) Triggers Mucin Secretion in the Rat Sublingual Gland. *Biochem. Biophys. Res. Commun.* **270,** 298–302 (2000).
262. Kawabata, A. *et al*. In vivo evidence that protease-activated receptors 1 and 2 modulate gastrointestinal transit in the mouse. *Br. J. Pharmacol.* **133,** 1213–1218 (2001).
263. Coelho, A.-M., Vergnolle, N., Guiard, B., Fioramonti, J. & Bueno, L. Proteinases and proteinase-activated receptor 2: A possible role to promote visceral hyperalgesia in rats. *Gastroenterology* **122,** 1035–1047 (2002).
264. Lohman, R.-J. *et al*. An antagonist of human protease activated receptor-2 attenuates PAR2 signaling, macrophage activation, mast cell degranulation, and collagen-induced arthritis in rats. *FASEB J* **26,** 2877–2887 (2012).
265. Kawabata, A., Matsunami, M. & Sekiguchi, F. Gastrointestinal roles for proteinase-activated receptors in health and disease. *Br. J. Pharmacol.* **153 Suppl 1,** S230–40 (2008).
266. Nystedt, S., Ramakrishnan, V. & Sundelin, J. The proteinase-activated receptor 2 is induced by inflammatory mediators in human endothelial cells. Comparison with the thrombin receptor. *J. Biol. Chem.* **271,** 14910–14915 (1996).
267. Bolton, S. J., McNulty, C. A., Thomas, R. J., Hewitt, C. R. A. & Wardlaw, A. J. Expression of and functional responses to protease-activated receptors on human eosinophils. *J. Leukoc. Biol.* **74,** 60–68 (2003).
268. Howells, G. L. *et al*. Proteinase-activated receptor-2: expression by human neutrophils. *J. Cell. Sci.* **110 (Pt 7),** 881–887 (1997).
269. Ferrell, R. W., Lockhart, C. J. & Plevin, R. Protease-activated receptor-2 (PAR-2): A potential new target in arthritis. *Drugs of the Future* **33,** 241 (2008).
270. Johansson, U. *et al*. Human peripheral blood monocytes express protease receptor-2 and respond to receptor activation by production of IL-6, IL-8, and IL-1b. *J. Leukoc. Biol.* **78,** 967–975 (2005).
271. Steven, R., Crilly, A., Lockhart, J. C., Ferrell, W. R. & McInnes, I. B. Proteinase-activated receptor-2 modulates human macrophage differentiation and effector function. *Innate Immun* **19,** 663–672 (2013).
272. Colognato, R. *et al*. Differential expression and regulation of protease-activated receptors in human peripheral monocytes and monocyte-derived antigen-presenting cells. *Blood* **102,** 2645–2652 (2003).

273. Shichijo, M. *et al*. PAR-2 deficient CD4+ T cells exhibit downregulation of IL-4 and upregulation of IFN-gamma after antigen challenge in mice. *Allergol Int* **55,** 271–278 (2006).
274. Hou, L., Howells, G. L., Kapas, S. & Macey, M. G. The protease-activated receptors and their cellular expression and function in blood-related cells. *Br. J. Haematol.* **101,** 1–9 (1998).
275. Xue, M. *et al*. Protease-activated receptor 2, rather than protease-activated receptor 1, contributes to the aggressive properties of synovial fibroblasts in rheumatoid arthritis. *Arthritis & Rheumatology* **64,** 88–98 (2012).
276. Ferrell, W. R. *et al*. Essential role for proteinase-activated receptor-2 in arthritis. *J. Clin. Invest.* **111,** 35–41 (2003).
277. Li, T. & He, S. Induction of IL-6 release from human T cells by PAR-1 and PAR-2 agonists. *Immunol. Cell Biol.* **84,** 461–466 (2006).
278. Shpacovitch, V. M. *et al*. Agonists of Proteinase-Activated Receptor 2 Induce Cytokine Release and Activation of Nuclear Transcription Factor κB in Human Dermal Microvascular Endothelial Cells. *J Invest Dermatol* **118,** 380–385 (2002).
279. Houliston, R. A. *et al*. Protease-activated receptors upregulate cyclooxygenase-2 expression in human endothelial cells. *Thromb. Haemost.* **88,** 321–328 (2002).
280. Emilsson, K. *et al*. Vascular effects of proteinase-activated receptor 2 agonist peptide. *J. Vasc. Res.* **34,** 267–272 (1997).
281. Lindner, J. R. *et al*. Delayed onset of inflammation in protease-activated receptor-2-deficient mice. *J. Immunol.* **165,** 6504–6510 (2000).
282. Vergnolle, N. Proteinase-activated receptor-2-activating peptides induce leukocyte rolling, adhesion, and extravasation in vivo. *J. Immunol.* **163,** 5064–5069 (1999).
283. Noorbakhsh, F. *et al*. Proteinase-activated receptor 2 modulates neuroinflammation in experimental autoimmune encephalomyelitis and multiple sclerosis. *J. Exp. Med.* **203,** 425–435 (2006).
284. Kawagoe, J. *et al*. Effect of protease-activated receptor-2 deficiency on allergic dermatitis in the mouse ear. **88,** 77–84 (2002).
285. Abraham, L. A. *et al*. Expression of protease-activated receptor-2 by osteoblasts. *Bone* **26,** 7–14 (2000).
286. López, M. L. *et al*. Expression pattern of protease activated receptors in lymphoid cells. *Cell. Immunol.* **288,** 47–52 (2014).
287. Ochiai, N. *et al*. Murine osteoclasts secrete serine protease HtrA1 capable of degrading osteoprotegerin in the bone microenvironment. *Communications Biology 2019 2:1* **2,** 1–13 (2019).
288. Huesa, C. *et al*. Proteinase-activated receptor 2 modulates OA-related pain, cartilage and bone pathology. *Ann. Rheum. Dis.* **75,** 1–9 (2015).
289. Amiable, N. *et al*. Proteinase-activated receptor (PAR)-2 activation impacts bone resorptive properties of human osteoarthritic subchondral bone osteoblasts. *Bone* **44,** 1143–1150 (2009).
290. Busso, N. *et al*. Evaluation of protease-activated receptor 2 in murine models of arthritis. *Arthritis Rheum.* **56,** 101–107 (2007).
291. Crilly, A. *et al*. Immunomodulatory role of proteinase-activated receptor-2. *Ann. Rheum. Dis.* **71,** 1559–1566 (2012).

292. Palmer, H. S. *et al*. Protease-activated receptor 2 mediates the proinflammatory effects of synovial mast cells. *Arthritis Rheum.* **56,** 3532–3540 (2007).
293. van der Velden, D. *et al*. Mast cell depletion in the preclinical phase of collagen-induced arthritis reduces clinical outcome by lowering the inflammatory cytokine profile. *Arthritis Res. Ther.* **18,** 138 (2016).
294. Shin, K. *et al*. Mast cells contribute to autoimmune inflammatory arthritis via their tryptase/heparin complexes. *J. Immunol.* **182,** 647–656 (2009).
295. Kelso, E. B. *et al*. Expression and proinflammatory role of proteinase-activated receptor 2 in rheumatoid synovium: ex vivo studies using a novel proteinase-activated receptor 2 antagonist. *Arthritis Rheum.* **56,** 765–771 (2007).
296. Godfrey, H. P., Ilardi, C., Engber, W. & Graziano, F. M. Quantitation of human synovial mast cells in rheumatoid arthritis and other rheumatic diseases. *Arthritis Rheum.* **27,** 852–856 (1984).
297. Crilly, A. *et al*. PAR2 expression in peripheral blood monocytes of patients with rheumatoid arthritis. *Ann. Rheum. Dis.* **71,** 1049–1054 (2012).
298. Haringman, J. J. *et al*. Synovial tissue macrophages: a sensitive biomarker for response to treatment in patients with rheumatoid arthritis. *Ann. Rheum. Dis.* **64,** 834–838 (2005).
299. Shrestha Palikhe, N. *et al*. Increased Protease-Activated Receptor-2 (PAR-2) Expression on CD14++CD16+ Peripheral Blood Monocytes of Patients with Severe Asthma. *PLoS ONE* **10,** e0144500 (2015).
300. Adams, M. N., Pagel, C. N., Mackie, E. J. & Hooper, J. D. Evaluation of antibodies directed against human protease-activated receptor-2. *Naunyn-Schmiedeberg's Arch Pharmacol* **385,** 861–873 (2012).
301. Rhodes, K. J. & Trimmer, J. S. Antibodies as valuable neuroscience research tools versus reagents of mass distraction. *J. Neurosci.* **26,** 8017–8020 (2006).
302. Pradidarcheep, W., Labruyère, W. T., Dabhoiwala, N. F. & Lamers, W. H. Lack of specificity of commercially available antisera: better specifications needed. *J. Histochem. Cytochem.* **56,** 1099–1111 (2008).
303. Michel, M. C., Wieland, T. & Tsujimoto, G. How reliable are G-protein-coupled receptor antibodies? *Naunyn-Schmiedeberg's Arch Pharmacol* **379,** 385–388 (2009).
304. Grishina, Z., Ostrowska, E., Halangk, W., Tóth, M. S. & Reiser, G. Activity of recombinant trypsin isoforms on human proteinase-activated receptors (PAR): mesotrypsin cannot activate epithelial PAR-1, -2, but weakly activates brain PAR-1. *Br. J. Pharmacol.* **146,** 990–999 (2005).
305. Blackburn, P. E. *et al*. Purification and biochemical characterization of the D6 chemokine receptor. *Biochem. J.* **379,** 263–272 (2004).
306. Jenkins, A. L., Chinni, C., De Niese, M. R., Blackhart, B. & Mackie, E. J. Expression of protease-activated receptor-2 during embryonic development. *Dev. Dyn.* **218,** 465–471 (2000).
307. Adams, M. N., Christensen, M. E., He, Y., Waterhouse, N. J. & Hooper, J. D. The role of palmitoylation in signalling, cellular trafficking and plasma membrane localization of protease-activated receptor-2. *PLoS ONE* **6,** e28018 (2011).

308. Jacob, C. *et al*. c-Cbl Mediates Ubiquitination, Degradation, and Down-regulation of Human Protease-activated Receptor 2. *J. Biol. Chem.* **280,** 16076–16087 (2005).
309. Ricks, T. K. & Trejo, J. Phosphorylation of protease-activated receptor-2 differentially regulates desensitization and internalization. *J. Biol. Chem.* **284,** 34444–34457 (2009).
310. Horvat, R. & Palade, G. E. The functional thrombin receptor is associated with the plasmalemma and a large endosomal network in cultured human umbilical vein endothelial cells. *J. Cell. Sci.* **108 (Pt 3),** 1155–1164 (1995).
311. Bhosle, V. K., Rivera, J. C. & Chemtob, S. New insights into mechanisms of nuclear translocation of G-protein coupled receptors. *Small GTPases* **139,** 1–10 (2017).
312. Chemtob, S. *et al*. Nuclear Localization of Protease-Activated Receptor 2 Dictates Angiogenesis. *Invest. Ophthalmol. Vis. Sci.* **51,** 4750–4750 (2010).
313. Joyal, J.-S. *et al*. Subcellular localization of coagulation factor II receptor-like 1 in neurons governs angiogenesis. *Nat. Med.* **20,** 1165 (2014).
314. Jung, S.-R. *et al*. Contributions of protein kinases and ß-arrestin to termination of protease-activated receptor 2 signaling. *J. Gen. Physiol.* **147,** 255–271 (2016).
315. Hein, L., Ishii, K., Coughlin, S. R. & Kobilka, B. K. Intracellular targeting and trafficking of thrombin receptors. A novel mechanism for resensitization of a G protein-coupled receptor. *J. Biol. Chem.* **269,** 27719–27726 (1994).
316. Sevigny, L. M. *et al*. Interdicting protease-activated receptor-2-driven inflammation with cell-penetrating pepducins. *Proc. Natl. Acad. Sci. U.S.A.* **108,** 8491–8496 (2011).
317. Madhusudhan, T. *et al*. Cytoprotective signaling by activated protein C requires protease-activated receptor-3 in podocytes. *Blood* **119,** 874–883 (2012).
318. Cunningham, M. R. *et al*. Novel Role for Proteinase-activated Receptor 2 (PAR2) in Membrane Trafficking of Proteinase-activated Receptor 4 (PAR4). *J. Biol. Chem.* **287,** 16656–16669 (2012).
319. Batliwalla, F. M. *et al*. Peripheral blood gene expression profiling in rheumatoid arthritis. *Genes & Immunity 2005 6:5* **6,** 388 (2005).
320. Chara, L. *et al*. The number of circulating monocytes as biomarkers of the clinical response to methotrexate in untreated patients with rheumatoid arthritis. *Journal of Translational Medicine 2011 9:2* **13,** 2 (2015).
321. Chara, L. *et al*. Monocyte populations as markers of response to adalimumab plus MTX in rheumatoid arthritis. *Arthritis Res. Ther.* **14,** R175 (2012).
322. Hyun, E., Andrade-Gordon, P., Steinhoff, M. & Vergnolle, N. Protease-activated receptor-2 activation: a major actor in intestinal inflammation. *Gut* **57,** 1222–1229 (2008).
323. Jones, S. M. *et al*. PAR2 (Protease-Activated Receptor 2) Deficiency Attenuates Atherosclerosis in Mice. *Arterioscler. Thromb. Vasc. Biol.* (2018). doi:10.1161/ATVBAHA.117.310082
324. Kandel, S. H., Radwan, W. M., Esaily, H. A. & Al-mahmoudy, S. F. Proteinase-activated receptor 2 expression on peripheral blood

monocytes and T-cells in patients with rheumatoid arthritis. *The Egyptian Rheumatologist* **38,** 91–98 (2016).
325. Tsuchiya, S. *et al*. Establishment and characterization of a human acute monocytic leukemia cell line (THP-1). *Int. J. Cancer* **26,** 171–176 (1980).
326. Li, Z. H. *et al*. High-dose PMA with RANKL and MCSF induces THP-1 cell differentiation into human functional osteoclasts in vitro. *Mol Med Rep* **16,** 8380–8384 (2017).
327. Autissier, P., Soulas, C., Burdo, T. H. & Williams, K. C. Evaluation of a 12-color flow cytometry panel to study lymphocyte, monocyte, and dendritic cell subsets in humans. *Cytometry A* **77,** 410–419 (2010).
328. Wang, Y. *et al*. M-CSF Induces Monocyte Survival by Activating NF-κB p65 Phosphorylation at Ser276 via Protein Kinase C. *PLoS ONE* **6,** e28081 (2011).
329. Kelley, T. W. *et al*. Macrophage Colony-stimulating Factor Promotes Cell Survival through Akt/Protein Kinase B. *J. Biol. Chem.* **274,** 26393–26398 (1999).
330. Mackie, E. J. *et al*. Protease-activated receptors in the musculoskeletal system. *Int. J. Biochem. Cell Biol.* **40,** 1169–1184 (2008).
331. Asaduzzaman, M. *et al*. Protease-Activated Receptor-2 blockade inhibits changes seen in a chronic murine asthma model. *Allergy* (2017). doi:10.1111/all.13313
332. Dekita, M. *et al*. Cathepsin S Is Involved in Th17 Differentiation Through the Upregulation of IL-6 by Activating PAR-2 after Systemic Exposure to Lipopolysaccharide from Porphyromonas gingivalis. *Front Pharmacol* **8,** 470 (2017).
333. Asaduzzaman, M. *et al*. Functional inhibition of PAR2 alleviates allergen-induced airway hyperresponsiveness and inflammation. *Clin. Exp. Allergy* **45,** 1844–1855 (2015).
334. Boileau, C. *et al*. Activation of proteinase-activated receptor 2 in human osteoarthritic cartilage upregulates catabolic and proinflammatory pathways capable of inducing cartilage degradation: a basic science study. *Arthritis Res. Ther.* **9,** R121 (2007).
335. Kelso, E. B. *et al*. Therapeutic promise of proteinase-activated receptor-2 antagonism in joint inflammation. *J. Pharmacol. Exp. Ther.* **316,** 1017–1024 (2006).
336. Hansen, K. K. *et al*. A major role for proteolytic activity and proteinase-activated receptor-2 in the pathogenesis of infectious colitis. *Proc. Natl. Acad. Sci. U.S.A.* **102,** 8363–8368 (2005).
337. Vergnolle, N., Hollenberg, M. D., Sharkey, K. A. & Wallace, J. L. Characterization of the inflammatory response to proteinase-activated receptor-2 (PAR2)-activating peptides in the rat paw. *Br. J. Pharmacol.* **127,** 1083–1090 (1999).
338. Jiang, B. *et al*. The role of proteinase 3 (PR3) and the protease-activated receptor-2 (PAR-2) pathway in dendritic cell (DC) maturation of human-DC-like monocytes and murine DC
. *Clin. Exp. Rheumatol.* **28,** S56–S61 (2010).
339. Qian, N. *et al*. Tryptase promotes breast cancer angiogenesis through PAR-2 mediated endothelial progenitor cell activation. *Oncology Letters* **16,** 1513–1520 (2018).

340. Sun, L. *et al*. Proteinase-activated receptor 2 promotes tumor cell proliferation and metastasis by inducing epithelial-mesenchymal transition and predicts poor prognosis in hepatocellular carcinoma. *World Journal of Gastroenterology* **24,** 1120–1133 (2018).
341. Bosshart, H. & Heinzelmann, M. THP-1 cells as a model for human monocytes. *Annals of Translational Medicine* **4,** 438–438 (2016).
342. Kang, C. S. *et al*. Protease-activated receptor 2 is associated with activation of human macrophage cell line THP-1. *Immune Netw* **5,** 193–198 (2005).
343. Ben-David, U. *et al*. Genetic and transcriptional evolution alters cancer cell line drug response. *Nature* **560,** 325 (2018).
344. Tindell, A. G. *et al*. Correlation of protease-activated receptor-2 expression and synovitis in rheumatoid and osteoarthritis. *Rheumatol. Int.* **32,** 3077–3086 (2012).
345. Yamaguchi, R. *et al*. Mechanism of interleukin-13 production by granulocyte-macrophage colony-stimulating factor-dependent macrophages via protease-activated receptor-2. *Blood Cells Mol. Dis.* **55,** 21–26 (2015).
346. Huesa, C. *et al*. PAR2 response in fluid flow-stimulated chondrocytes. *Bone Research Society Abstracts* (2015). doi:10.3389/978-2-88919-659-3
347. Liuzzo, J. P., Petanceska, S. S., Moscatelli, D. & Devi, L. A. Inflammatory mediators regulate cathepsin S in macrophages and microglia: A role in attenuating heparan sulfate interactions. *Mol. Med.* **5,** 320–333 (1999).
348. Lindahl, C. *et al*. Increased levels of macrophage-secreted cathepsin S during prostate cancer progression in TRAMP mice and patients. *Cancer Genomics Proteomics* **6,** 149–159 (2009).
349. Andrade, S. S. *et al*. Cathepsin K induces platelet dysfunction and affects cell signaling in breast cancer - molecularly distinct behavior of cathepsin K in breast cancer. *BMC Cancer* **16,** 173 (2016).
350. Reddy, V. B., Shimada, S. G., Sikand, P., LaMotte, R. H. & Lerner, E. A. Cathepsin S elicits itch and signals via protease-activated receptors. *J Invest Dermatol* **130,** 1468–1470 (2010).
351. Chao, H.-H. *et al*. Lipopolysaccharide pretreatment increases protease-activated receptor-2 expression and monocyte chemoattractant protein-1 secretion in vascular endothelial cells. *Journal of Biomedical Science 2011 18:1* **24,** 85 (2017).
352. Chi, L. *et al*. Interleukin-6 Production by Endothelial Cells via Stimulation of Protease-Activated Receptors Is Amplified by Endotoxin and Tumor Necrosis Factor-α. *Journal of Interferon and Cytokine Research* 231–240 (2001). doi:10.1089/107999001750169871
353. Zhou, B. *et al*. Activation of PAR2 or/and TLR4 promotes SW620 cell proliferation and migration via phosphorylation of ERK1/2. *Oncology Reports* **25,** 503–511 (2011).
354. Ostrowska, E., Sokolova, E. & Reiser, G. PAR-2 activation and LPS synergistically enhance inflammatory signaling in airway epithelial cells by raising PAR expression level and interleukin-8 release. *Am. J. Physiol. Lung Cell Mol. Physiol.* **293,** L1208–L1218 (2007).
355. Rallabhandi, P. *et al*. Analysis of Proteinase-activated Receptor 2 and TLR4 Signal Transduction A NOVEL PARADIGM FOR RECEPTOR COOPERATIVITY. *J. Biol. Chem.* **283,** 24314–24325 (2008).

356. Kagan, J. C. *et al*. TRAM couples endocytosis of Toll-like receptor 4 to the induction of interferon-β. *Nature Immunology* **9,** 361 (2008).
357. Tsukamoto, H. *et al*. Lipopolysaccharide (LPS)-binding protein stimulates CD14-dependent Toll-like receptor 4 internalization and LPS-induced TBK1–IKKε–IRF3 axis activation. *J. Biol. Chem.* **293,** 10186–10201 (2018).
358. Wong, K. L. *et al*. Gene expression profiling reveals the defining features of the classical, intermediate, and nonclassical human monocyte subsets. *Blood* **118,** e16–31 (2011).
359. Patarroyo, M., Prieto, J., Beatty, P. G., Clark, E. A. & Gahmberg, C. G. Adhesion-mediating molecules of human monocytes. *Cell. Immunol.* **113,** 278–289 (1988).
360. Siggelkow, H. *et al*. Cytokines, Osteoprotegerin, and RANKL In Vitro and Histomorphometric Indices of Bone Turnover in Patients With Different Bone Diseases. *J Bone Miner Res* **18,** 529–538 (2003).
361. Marotte, H. *et al*. A 1-year case-control study in patients with rheumatoid arthritis indicates prevention of loss of bone mineral density in both responders and nonresponders to infliximab. *Arthritis Res. Ther.* **9,** R61 (2007).
362. Woodside, D. G., Liu, S. & Ginsberg, M. H. Integrin Activation. *Thromb. Haemost.* **86,** 316–323 (2017).
363. Liu, X. *et al*. Induction of Mast Cell Accumulation by Tryptase via a Protease Activated Receptor-2 and ICAM-1 Dependent Mechanism. *Mediators Inflamm.* **2016,** 1–10 (2016).
364. Russell, F. A., Schuelert, N., Veldhoen, V. E., Hollenberg, M. D. & McDougall, J. J. Activation of PAR 2receptors sensitizes primary afferents and causes leukocyte rolling and adherence in the rat knee joint. *Br. J. Pharmacol.* **167,** 1665–1678 (2012).
365. Shpacovitch, V. M. *et al*. Agonists of proteinase-activated receptor-2 modulate human neutrophil cytokine secretion, expression of cell adhesion molecules, and migration within 3-D collagen lattices. *J. Leukoc. Biol.* **76,** 388–398 (2004).
366. Miyata, S., Koshikawa, N., Yasumitsu, H. & Miyazaki, K. Trypsin Stimulates Integrin α5β1-dependent Adhesion to Fibronectin and Proliferation of Human Gastric Carcinoma Cells through Activation of Proteinase-activated Receptor-2. *J. Biol. Chem.* **275,** 4592–4598 (2000).
367. Yang, L. *et al*. Proteinase-activated Receptor 2 Promotes Cancer Cell Migration through RNA Methylation-mediated Repression of miR-125b. *J. Biol. Chem.* **290,** 26627–26637 (2015).
368. Morris, D. R. *et al*. Protease-Activated Receptor-2 Is Essential for Factor VIIa and Xa–Induced Signaling, Migration, and Invasion of Breast Cancer Cells. *Cancer Res.* **66,** 307–314 (2006).
369. McGuire, J. J., Saifeddine, M., Triggle, C. R., Sun, K. & Hollenberg, M. D. 2-furoyl-LIGRLO-amide: a potent and selective proteinase-activated receptor 2 agonist. *J. Pharmacol. Exp. Ther.* **309,** 1124–1131 (2004).
370. Kawabata, A. *et al*. Potent and metabolically stable agonists for protease-activated receptor-2: evaluation of activity in multiple assay systems in vitro and in vivo. *J. Pharmacol. Exp. Ther.* **309,** 1098–1107 (2004).

371. Georgy, S. R. *et al*. Proteinase-activated receptor-2 (PAR2) and mouse osteoblasts: regulation of cell function and lack of specificity of PAR2-activating peptides. *Clin. Exp. Pharmacol. Physiol.* **37,** 328–336 (2010).
372. Suen, J. Y. *et al*. Pathway-selective antagonism of proteinase activated receptor 2. *Br. J. Pharmacol.* **171,** 4112–4124 (2014).
373. Cheng, R. K. Y. *et al*. Structural insight into allosteric modulation of protease-activated receptor 2. *Nature* **545,** 112–115 (2017).
374. Mihara, K. *et al*. Thrombin-mediated direct activation of proteinase-activated receptor-2 (PAR2): another target for thrombin signaling. *Mol. Pharmacol.* **89,** 606–614 (2016).
375. Nakano, S. *et al*. G-protein Gα 13 functions as a cytoskeletal and mitochondrial regulator to restrain osteoclast function. *Sci. Rep.* **9,** 4236 (2019).
376. Wang, W., Qiao, Y. & Li, Z. New Insights into Modes of GPCR Activation. *Trends Pharmacol. Sci.* **39,** 367–386 (2018).
377. Bénard, G. *et al*. Mitochondrial CB1 receptors regulate neuronal energy metabolism. *Nature Neuroscience 2012 15:4* **15,** 558 (2012).
378. Revankar, C. M., Cimino, D. F., Sklar, L. A., Arterburn, J. B. & Prossnitz, E. R. A Transmembrane Intracellular Estrogen Receptor Mediates Rapid Cell Signaling. *Science* **307,** 1625–1630 (2005).
379. Rozenfeld, R. & Devi, L. A. Regulation of CB 1cannabinoid receptor trafficking by the adaptor protein AP-3. *FASEB J* **22,** 2311–2322 (2008).
380. Jastrzebski, S. *et al*. Protease-Activated Receptor 1 Deletion Causes Enhanced Osteoclastogenesis in Response to Inflammatory Signals through a Notch2-Dependent Mechanism. *J. Immunol.* ji1801032 (2019). doi:10.4049/jimmunol.1801032
381. Reinholt, F. P., Hultenby, K., Oldberg, A. & Heinegård, D. Osteopontin--a possible anchor of osteoclasts to bone. *PNAS* **87,** 4473–4475 (1990).
382. Ek-Rylander, B. & Andersson, G. Osteoclast migration on phosphorylated osteopontin is regulated by endogenous tartrate-resistant acid phosphatase. *Experimental Cell Research* **316,** 443–451 (2010).
383. Green, P. M., Ludbrook, S. B., Miller, D. D., Horgan, C. M. T. & Barry, S. T. Structural elements of the osteopontin SVVYGLR motif important for the interaction with α4 integrins. *FEBS Letters* **503,** 75–79 (2001).
384. Oh, Y., Oh, I., Morimoto, J., Uede, T. & Morimoto, A. Osteopontin has a crucial role in osteoclast-like multinucleated giant cell formation. *Journal of Cellular Biochemistry* **115,** 585–595 (2014).
385. Darmoul, D., Gratio, V., Devaud, H. & Laburthe, M. Protease-activated Receptor 2 in Colon Cancer TRYPSIN-INDUCED MAPK PHOSPHORYLATION AND CELL PROLIFERATION ARE MEDIATED BY EPIDERMAL GROWTH FACTOR RECEPTOR TRANSACTIVATION. *J. Biol. Chem.* **279,** 20927–20934 (2004).
386. Koo, B. H., Chung, K. H., Hwang, K. C. & (null), D. K. Factor Xa induces mitogenesis of coronary artery smooth muscle cell via activation of PAR-2. *FEBS* **523,** 85–89 (2002).

387. Sabri, A. *et al*. Signaling Properties and Functions of Two Distinct Cardiomyocyte Protease-Activated Receptors. *Circ. Res.* (2000). doi:10.1161/01.RES.86.10.1054
388. Bakele, M. *et al*. An Interactive Network of Elastase, Secretases, and PAR-2 Protein Regulates CXCR1 Receptor Surface Expression on Neutrophils. *J. Biol. Chem.* **289,** 20516–20525 (2014).
389. Tennant, G. M., Wadsworth, R. M. & Kennedy, S. PAR-2 mediates increased inflammatory cell adhesion and neointima formation following vascular injury in the mouse. *Atherosclerosis* **198,** 57–64 (2008).
390. Winter, M. C., Shasby, S. S., Ries, D. R. & Shasby, D. M. PAR2 activation interrupts E-cadherin adhesion and compromises the airway epithelial barrier: protective effect of beta-agonists. *Am. J. Physiol. Lung Cell Mol. Physiol.* **291,** L628–35 (2006).
391. Podolnikova, N. P., Podolnikov, A. V., Haas, T. A., Lishko, V. K. & Ugarova, T. P. Ligand recognition specificity of leukocyte integrin αMß2 (Mac-1, CD11b/CD18) and its functional consequences. *Biochemistry* **54,** 1408–1420 (2015).
392. Kudo, O. *et al*. Proinflammatory cytokine (TNFα/IL-1α) induction of human osteoclast formation. *J Pathol* **198,** 220–227 (2002).
393. Seo, J. H., Lim, J. W., Yoon, J.-H. & Kim, H. Proteinase-activated receptor-2 mediates the expression of integrin alpha5 and beta1 in Helicobacter pylori-infected gastric epithelial AGS cells. *Digestion* **80,** 40–49 (2009).
394. Lim, S. Y., Tennant, G. M., Kennedy, S., Wainwright, C. L. & Kane, K. A. Activation of mouse protease-activated receptor-2 induces lymphocyte adhesion and generation of reactive oxygen species. *Br. J. Pharmacol.* **149,** 591–599 (2006).
395. Fyfe, M., Bergström, M., Aspengren, S. & Peterson, A. PAR-2 activation in intestinal epithelial cells potentiates interleukin-1beta-induced chemokine secretion via MAP kinase signaling pathways. *Cytokine* **31,** 358–367 (2005).
396. Kanke, T. *et al*. Novel antagonists for proteinase-activated receptor 2: inhibition of cellular and vascular responses in vitro and in vivo. *Br. J. Pharmacol.* **158,** 361–371 (2009).
397. Tripathi, T., Abdi, M. & Alizadeh, H. Protease-activated receptor 2 (PAR2) is upregulated by Acanthamoeba plasminogen activator (aPA) and induces proinflammatory cytokine in human corneal epithelial cells. *Invest. Ophthalmol. Vis. Sci.* **55,** 3912–3921 (2014).
398. Sriwai, W., Mahavadi, S., Al-Shboul, O., Grider, J. R. & Murthy, K. S. Distinctive G Protein-Dependent Signaling by Protease-Activated Receptor 2 (PAR2) in Smooth Muscle: Feedback Inhibition of RhoA by cAMP-Independent PKA. *PLoS ONE* **8,** e66743 (2013).
399. Shen, B., Delaney, M. K. & Du, X. Inside-out, outside-in, and inside-outside-in: G protein signaling in integrin-mediated cell adhesion, spreading, and retraction. *Current Opinion in Cell Biology* **24,** 600–606 (2012).
400. Nakamura, I., Le T Duong, Rodan, S. B. & Rodan, G. A. Involvement of αvß3 integrins in osteoclast function. *J Bone Miner Metab* **25,** 337–344 (2007).

401. Francis, N. *et al*. Keratinocyte-specific ablation of protease-activated receptor 2 prevents gingival inflammation and bone loss in a mouse model of periodontal disease. *Cell. Microbiol*. **20,** e12891 (2018).
402. Georges, S. *et al*. Proteases and bone remodelling. *Cytokine Growth Factor Rev.* **20,** 29–41 (2009).
403. Green, K. A. & Lund, L. R. ECM degrading proteases and tissue remodelling in the mammary gland. *BioEssays* **27,** 894–903 (2005).
404. Rengel, Y., Ospelt, C. & Gay, S. Proteinases in the joint: clinical relevance of proteinases in joint destruction. *Arthritis Res. Ther*. **9,** 221 (2007).
405. Hollenberg, M. D. Proteinase-mediated signaling: Proteinase-activated receptors (PARs) and much more. *Life Sciences* **74,** 237–246 (2003).
406. McCulloch, K. *et al*. Rheumatic Disease: Protease-Activated Receptor-2 in Synovial Joint Pathobiology. *Front. Endocrinol*. **9,** 257 (2018).
407. Everts, V. *et al*. Osteoclastic bone degradation and the role of different cysteine proteinases and matrix metalloproteinases: differences between calvaria and long bone. *J. Bone Miner. Res.* **21,** 1399–1408 (2006).
408. Ramachandran, R. *et al*. Neutrophil Elastase Acts as a Biased Agonist for Proteinase-activated Receptor-2 (PAR2). *J. Biol. Chem.* **286,** 24638–24648 (2011).
409. Lin, H. & Trejo, J. Transactivation of the PAR1-PAR2 heterodimer by thrombin elicits ß-arrestin-mediated endosomal signaling. *J. Biol. Chem.* **288,** 11203–11215 (2013).
410. Liang, H. P. H. *et al*. EPCR-dependent PAR2 activation by the blood coagulation initiation complex regulates LPS-triggered interferon responses in mice. *Blood* **125,** 2845–2854 (2015).